

Uniwersytet Gdański

1. Wydział Chemii

Katedra Chemii Fizycznej

2. Wydział Matematyki, Fizyki i Informatyki,

Instytut Fizyki Doświadczalnej

Vladyslav Ievtukhov

Synteza, badania spektroskopowe

**i poszukiwanie zastosowań heterocyklicznych układów
molekularnych wykazujących zjawiska foto- i chemiluminescencji**

Rozprawa doktorska

Promotor:

dr hab. Karol Krzemiński, prof. UG

Promotor pomocniczy:

dr hab. Illia E. Serdiuk, prof. UG

Gdańsk 2025

University of Gdańsk

1. Faculty of Chemistry ,

Chair of Physical Chemistry

2. Faculty of Mathematics, Physics and Informatics

Institute of Experimental Physics

Vladyslav Ievtukhov

**Synthesis, spectroscopic analysis, and exploration of applications for
heterocyclic molecular systems exhibiting photo and
chemiluminescence phenomena**

The doctoral dissertation

Prepared under the supervision of:

dr hab. Karol Krzemiński, prof. UG

Co-supervisor:

dr hab. Illia E. Serdiuk, prof. UG

Gdansk 2025

Acknowledgments

First and foremost, I would like to express my deepest gratitude to my supervisor, **dr hab. Karol Krzymiński, prof. UG**, for his continuous guidance, valuable advices during my research work, and support throughout the preparation of this PhD thesis. His expertise, great patience, and constructive feedback were crucial at every stage of my scientific carrier.

I also wish to sincerely thank my co-supervisor and friend **dr hab. Illia E. Serdiuk, prof. UG**, whose active involvement, valuable discussions, and ongoing support contributed a lot to the progress and completion of this work.

I am grateful to **prof. Piotr Bojarski**, head of the Institute of Experimental Physics at the Faculty of Mathematics, Physics and Informatics, for his support and for providing excellent research conditions.

I owe my deepest thanks to my family, especially my parents, for their constant spiritual support, endless patience, and for constant support for me at all stages of my scientific and professional career.

My appreciation also goes to all my colleagues from both the Faculty of Chemistry, and the Faculty of Mathematics, Physics and Informatics, Institute of Experimental Physics, for their collaboration, helpful discussions, and the inspiring, friendly atmosphere that made daily work such a pleasure.

Special thanks go to **Alina Kovtun**, for her belief in my abilities, for every warm word and motivation boost when I needed it most, especially in moments of doubt.

TABLE OF CONTENTS

<i>Acknowledgments</i>	3
List of abbreviations and symbols used	5
Publications included in the dissertation.....	7
Streszczenie.....	9
Abstract	11
Thematic area I. Chemiluminescent systems	15
Thematic area II. TADF systems	19
Research hypotheses	22
Work objectives	23
Part I. Acridinium salts as indicators in luminescence studies	24
Measurements of chemiluminescence	25
Part Ia. Aromatic acridinium thioesters as new chemiluminogenic substrates in the analysis of some biological antioxidants	26
Computational studies	30
UV-Vis absorption spectroscopy studies on the formation of ATE-AO adducts	32
Part Ib. 9-CMA as a potential acridinium indicator for the quantitative identification of biologically relevant sulphur nucleophiles.	34
Experimental part	35
Computational studies	37
Conclusions	39
Part II. Spectroscopic and computational studies of the TADF mechanism of the TMCz-BO compound as a promising deep-blue emitter for OLED technology	41
Experimental part	42
PL properties	43
TADF mechanism in various media.	44
Rotational isomerism and excited-state mixing	46
Conclusions of the PhD thesis.....	50
Literature cited	52

List of abbreviations and symbols used

- CL – Chemiluminescence
- ECL – Enhanced chemiluminescence
- 9-CMA – 9-Cyano-10-methyl acridinium
- NAC – N-acetyl-L-cysteine
- GSH – Glutathione
- DPA – D-penicillamine
- ATC – Acetylthiocholine chloride
- UV-Vis – Ultraviolet–visible
- TAC – Total antioxidant capacity
- LOD – Limit of detection, M
- LOQ – Limit of quantification, M
- TD DFT – Time-dependent density functional theory
- RLU – Relative light unit
- RSH – Sulphur-containing nucleophilic substances
- AO – Antioxidants
- ATE – Acridinium thioesters
- DTT – Dithiothreitol
- GT – Glutathione
- QR – Quercetin
- CYS – Cysteine
- MET – Methionine
- OLED – Organic light-emitting diode
- EQE – External quantum efficiency
- TADF – Thermally activated delayed fluorescence
- PF – Prompt Fluorescence
- DF – Delay Fluorescence
- k_{ISC} – Intersystem crossing, s^{-1}
- k_{rISC} – Reverse intersystem crossing, s^{-1}
- k_{r} – Rate constant, s^{-1}
- ^1CT – Excited singlet state formed by a charge transfer transition
- ^3CT – Excited triplet state formed by a charge transfer transition
- $^1\text{LE}_\text{A}$ – Locally excited state singlet state localised on the acceptor fragment
- $^3\text{LE}_\text{A}$ – Locally excited triplet state localised on the acceptor fragment
- $^3\text{LE}_\text{D}$ – Locally excited triplet state localised on the donor fragment
- PL – Photoluminescence
- S_1 – First electron excited singlet state
- T_1 – First electron excited triplet state
- S^* – Excited singlet state

- T^* – Excited triplet state
- ΔE_{ST} – Energy gap between the state T^* and S^*
- SOC – Spin-orbit coupling, eV or cm^{-1}
- V – Spin-orbit coupling constant, eV or cm^{-1}
- HOMO – Highest occupied molecular orbitals, eV
- LUMO – Lowest unoccupied molecular orbitals, eV
- PLQY – Photoluminescence quantum yield, %
- k_B – Boltzmann constant, $\approx 1.38 \times 10^{-23}$ J/K
- \hbar – Reduced Planck's constant, $\approx 1.0545718 \times 10^{-34}$ J·s
- A – Pre-exposure constant, s^{-1}
- T – Temperature, K
- λ – Reorganisation energy, eV or J/mol
- f – Oscillator strength
- ε – Molar extinction coefficient, $\text{L} \cdot \text{mol}^{-1} \cdot \text{cm}^{-1}$
- TD-DFT – Time-dependent density-functional theory
- TMCz-BO – 9-[1,4]Benzoxaborino[2,3,4-kl]phenoxaborin-7-yl-1,3,6,8- tetramethyl-9H-carbazole
- DPEPO – Bis[2-(diphenylphosphine)phenyl] ether oxide
- PMMA – polymethyl methacrylate
- ZNX – Zeonex

Publications included in the dissertation

[P1] V. Ievtukhov, B. Zadykiewicz, M. Ye. Blazheyevski and K. Krzysiński, New luminometric method for quantification of biological sulphur nucleophiles with the participation of 9-cyano-10-methylacridinium salt, *Luminescence*, 2021, 32, 208–219. DOI: 10.1002/bio.4162.

[P2] V. Ievtukhov, A. Romanowska, M. Pieńkos, K. Żamojć, B. Zadykiewicz and K. Krzysiński, Aromatic acridinium thioesters as new chemiluminogenic substrates in the analysis of some biological antioxidants, *Journal of Luminescence*, 2024, 275, 120745. DOI: 10.1016/j.jlumin.2024.120745.

[P3] V. Ievtukhov, M. Mońka, O. Ciupak, I. Bylińska, P. Bojarski, K. Krzysiński, I. E. Serdiuk, Experimental evidence of the excited-state mixing in the blue emitter for organic light-emitting diodes, *Journal of Materials Chemistry C*, 2025, 13, 68–80. DOI: 10.1039/D4TC03925D.

Conference papers:

International:

- SPIE Optics and Photonics Conference – 2022, San Diego, USA
- 28th CSCM (Croatian–Slovenian Crystallographic Meeting) – 2022, Poreč, Croatia
- RSC (Royal Society of Chemistry) Conference – 2023, Dublin, Ireland
- 6th International Caparica Conference on Chromogenic and Emissive Materials – 2024, Caparica, Portugal (best shotgun award)

Domestic:

- National Interdisciplinary Conference “OMNIBUS Part III” – 2020 (online conference)
- 3rd Pomeranian Chemical Symposium of Students – 2021 (online)
- 14th Copernican Doctoral Seminar – 2021, Nicolaus Copernicus University in Toruń
- 9th Łódź Symposium of Chemistry Doctoral Students – 2021, University of Łódź
- 7th IWASOM (International Workshop on Advanced Spectroscopy and Materials) – 2022, University of Gdańsk
- VII IWASOM (Międzynarodowe Warsztaty Zaawansowanej Spektroskopii i Materiałów) – 2022, Uniwersytet Gdański

Other works:

Polish patent application P.448129 [WIPO ST 10/C: PL448129]

V. Ievtukhov, A. Prlj, O. Ciupak, M. Mońka, I. E. Serdiuk, Pursuing the Holy Grail of Thermally Activated Delayed Fluorescence Emitters: A Molecular Strategy for Reducing Energy Gap and Enhancing Spin-Orbit Coupling. *Chemical Science* 2025, DOI: 10.1039/D5SC00954E IF 7.6

Acknowledgements

The doctoral thesis was prepared within the framework of the Doctoral School of Natural Sciences at the University of Gdańsk (2019-2025)

The research presented as a doctoral dissertation was financially supported by:

- The National Science Centre (NCN) within the Sonata 16 grant (Nr UMO-2020/39/D/ST5/03094)
- Project UG Badania Młodych Naukowców 2020 (Nr 539-T080-B486-20),
- Project UG Badania Młodych Naukowców 2021 (Nr 539-T080-B885-21)
- Project UG Badania Młodych Naukowców 2023 (Nr 539-T080-B991-23)
- Fundusz Działalności Statutowej (DS) Pracowni Badań Luminescencyjnych (PBL) w latach 2019-2024
- Fundusz Działalności Statutowej (DS) Instytut Fizyki Doświadczalnej (IFD) w latach 2022-2025
- Quantum-chemical calculations were performed on the Wrocław Centre for Networking and Supercomputing (WCSS) computers.

Streszczenie

Heterocykliczne układy molekularne odgrywają jedną z kluczowych ról w opracowywaniu zaawansowanych materiałów dla dzisiejszych technologii. Tego typu układy, charakteryzujące się strukturami cyklicznymi zawierającymi co najmniej jeden atom inny niż węgiel, wykazują unikalne właściwości elektroniczne i optyczne. Tematyka niniejszej rozprawy koncentruje się wokół problematyki syntezy, analizy spektroskopowej i potencjalnych zastosowań nowych związków, reprezentujących dwie klasy heterocyklicznych związków aromatycznych, zawierających atom azotu znajdujący się w różnych stanach elektronowych: N^+ – kationowe sole akrydyniowe (z niedoborem elektronów) i N^0 – donory elektronów, np. pochodne karbazolu. Związki reprezentujące obie klasy połączeń otrzymano i zbadano w ramach niniejszej pracy pod kątem szeroko rozumianych zjawisk luminescencji, w tym procesów fotochemicznych i fotofizycznych, odpowiedzialnych za emisję światła, które mogą znaleźć zastosowania praktyczne w nowoczesnej analityce biomedycznej i środowiskowej oraz optoelektronice.

Głównym celem przedłożonej pracy było zaprojektowanie, otrzymanie i wyizolowanie w stanie chemicznie czystym kilku nowych połączeń chemicznych z w/w grup oraz zbadanie parametrów i mechanizmów emisji światła w reprezentatywnych układach molekularnych. Układy do badań zaprojektowano pod kątem potencjalnych zastosowań w nowoczesnych i szybko rozwijanych technologiach, takich jak analityka oparta o procesy chemi- lub elektrochemiluminescencji i organiczne diody elektroluminescencyjne (OLED). W szczególności, badania skupione były na fotofizycznych i fotochemicznych aspektach zachowania luminescencyjnych układów w stanach wzbudzonych oraz na mechanizmach generowania promieniowania w różnych środowiskach. Z punktu widzenia fotochemicznego nacisk położono na optymalizację wydajności, kinetyki i mechanizmu procesów utleniania, które stanowią źródła chemiluminescencji. Z perspektywy fotofizyki badania dotyczyły mechanizmu generowania termicznie aktywowanej opóźnionej fluorescencji (TADF), szybkości dezaktywacji stanów wzbudzonych i przejść zabronionych spinowo, wraz z wpływem różnych parametrów na te procesy.

Pierwsza część pracy poświęcona została badaniom układów molekularnych na bazie pochodnych akrydyny – związku o trójcyklicznej strukturze będącym podstawą strukturalną wielu leków, barwników i wielu połączeń chemicznych o zastosowaniach praktycznych. W szczególności poświęcono ją badaniom różnego typu soli akrydyniowych. Związki tego typu zawierają zwykle podstawnik na endocyklicznym atomie azotu (najczęściej grupę alkilową lub jej pochodną), co przyczynia się do ich ciekawych i obiecujących z użytkowego punktu widzenia właściwości fotofizycznych, takich jak zdolność do wydajnej chemiluminescencji i fluorescencji. Właściwości te sprawiają, że sole akrydyniowe są dobrymi kandydatami do zastosowań analitycznych - w szczególności do wykrywania i ilościowego określania zawartości biologicznie istotnych cząsteczek gdy są stosowane w charakterze znaczników i indykatorów luminescencyjnych.

Część niniejszej rozprawy, dotycząca procesów chemiluminescencji składa się z dwóch podczęści, A i B, z których każda koncentruje się na odrębnych i oryginalnych zastosowaniach pochodnych soli akrydyniowych.

Podczęść Ia koncentruje się na opracowaniu nowej luminometrycznej metody ilościowego oznaczania biologicznych nukleofilów zawierających atom(y) siarki. W badaniach wykorzystano sole (azotan(V) i chlorek) 9-cyjano-10-metyloakrydyniowy jako substraty luminogenne (indykatory CL). Badane z ich udziałem biologiczne nukleofile zawierające atom siarki, takie jak N-acetylo-L-cysteina (NAC), glutation (GSH), D-penicylamina (DPA) i chlorek acetylotiocholiny (ATC), odgrywają istotną rolę w procesach biochemicznych ludzi i zwierząt, w tym detoksykacji, sygnalizacji komórkowej i w reakcjach enzymatycznych. Oznaczanie tego typu nukleofilów ma kluczowe znaczenie dla zrozumienia ich funkcji biologicznych i potencjalnych ról terapeutycznych. Podczęść **Ia** opisuje syntezę soli akrydyniowych, opracowanie testu chemiluminometrycznego z jej udziałem oraz analityczną walidację tej metody, oferując oryginalne podejście do wykrywania i ilościowego oznaczania tych ważnych biologicznie cząsteczek. Szczegóły tego obszaru badań opisano w publikacji [P1], stanowiącej część niniejszej rozprawy.

W ramach podczęści **Ib** zbadano rolę aromatycznych tioestrów akrydyniowych jako wskaźników (indykatorów) chemiluminescencyjnych w analizie biologicznych przeciwutleniaczy. Antyoksydanty, takie jak takie jak ditiotretol (DTT), glutation (GT), kwercetyna (QR), cysteina (CYS) i metionina (MET) odgrywają kluczową rolę w ochronie komórek przed uszkodzeniami oksydacyjnymi poprzez neutralizację wolnych rodników i reaktywnych form tlenu. Związki te odgrywają ważną rolę w zachowaniu homeostazy komórkowej i zapobieganiu chorobom mniej lub bardziej związanym ze stresem oksydacyjnym, takimi jak rak, zaburzenia neurodegeneracyjne i choroby układu krążenia. Dokładne i czułe wykrywanie tego typu antyoksydantów ma kluczowe znaczenie dla badań w obszarze diagnostyki klinicznej. Pełny opis można znaleźć w badaniu, a wyniki i ich szczegółową analizę przedstawiono w artykule [P2].

Druga część rozprawy koncentruje się na badaniach fotofizycznych związków heterocyklicznych wykazujących TADF - zjawisko, które zwiększa wydajność układów typu OLED poprzez wykorzystanie całkowitej energii wzbudzenia elektronowego. Technologia OLED stanowi obecnie znaczący postęp w obszarach technik wyświetlania i oświetlenia, oferując wysoką wydajność, elastyczność i doskonałą jakość kolorów. Niniejsza rozprawa opisuje badania spektroskopowe i obliczenia kwantowo-chemiczne oryginalnego związku o kodzie TMCz-BO (patrz tabela skrótów, str. 1). Związek ten jest uznawany za obiecujący emiter o czystej i stabilnej barwie niebieskiej - parametry które są szczególnie trudne do osiągnięcia w technologii OLED i są kluczowe dla wyświetlaczy o wysokiej wydajności i energooszczędnego oświetlenia. Wykonane w ramach niniejszej rozprawy badania charakteryzują właściwości fotofizyczne tego związku i proponują nowy mechanizm procesu TADF, który może być pomocny w projektowaniu zaawansowanych materiałów wykazujących zjawisko TADF. W artykule [P3] przedstawione są kompleksowe wyniki badań w tym obszarze i szczegółowa ich analiza.

Abstract

Heterocyclic molecular systems play a key role in developing advanced materials for today's technologies. Such systems, characterised by cyclic structures, containing at least one heteroatom, express unique electronic and optical properties. This dissertation explores the synthesis, spectroscopic analysis, and potential applications of two classes of nitrogen-containing heterocyclic aromatic compounds with different electronic states of the nitrogen heteroatom: N^+ – electron-deficient cationic acridinium salts – and N^0 – electron-releasing carbazole derivatives. Both groups of compounds were studied in this work to gain a comprehensive understanding of luminescence phenomena, including photochemical and photophysical processes responsible for light emission, which may have practical applications in modern luminescence analytics and optoelectronics.

This work aimed to investigate the mechanisms of light emission in such selected molecular systems with potential applications in modern technologies, such as chemiluminescence-based analysis and organic light-emitting diodes (OLEDs). Specifically, the study focused on the photophysical and photochemical behaviour of organic molecules in their excited states. From a photochemical perspective, the emphasis was placed on enhancing the rate and efficiency of oxidation reactions that serve as sources of chemiluminescence. From the standpoint of photophysics, the research explored the mechanism of thermally activated delayed fluorescence (TADF), rates of radiative deactivation and spin-forbidden transitions, along with the influence of various parameters on such processes.

The **first part** of this work is dedicated to the study of acridine-based molecular systems. In this thesis, acridinium salts are employed as chemiluminescent indicators; a detailed background is provided in Thematic Area I, while this section focuses on the specific assays and validation results.

Part Ia focuses on developing a new luminometric method for quantifying biological sulphur nucleophiles. The study utilises 9-cyano-10-methylacridinium salts as a core component in this method. Biological sulphur nucleophiles, including N-acetyl-L-cysteine (NAC), glutathione (GSH), D-penicillamine (DPA), and acetylthiocholine chloride (ATC), play vital roles in various biochemical processes, including detoxification, cellular signalling, and enzymatic reactions. Accurate quantification of these nucleophiles is critical for understanding their biological functions and potential therapeutic roles. This subpart details the synthesis of the acridinium salts, the development of luminometric assays with their participation, and the analytical validation of the method, offering an original approach to detect and quantify these essential molecules.

Part Ib investigates the role of aromatic acridinium thioesters as chemiluminescent indicators for biological antioxidants. Antioxidants such as dithiothreitol (DTT), glutathione (GT), quercetin (QR), cysteine (CYS), and methionine (MET) play critical roles in protecting cells from oxidative damage by neutralising free radicals and reactive oxygen species. These compounds play a crucial role in maintaining cellular homeostasis and preventing diseases associated with oxidative stress, including cancer, neurodegenerative

disorders, and cardiovascular diseases. Accurate and sensitive detection of these antioxidants is vital for research and clinical diagnostics. A complete description can be found in the research, and the results are presented in publication **P2**.

The **second part** of the dissertation focuses on mechanistic studies of heterocyclic compounds exhibiting TADF, a phenomenon that enhances the efficiency of OLEDs by utilising the total energy of electrical excitation. OLED technology represents a significant advancement in display and lighting technologies, offering high efficiency, flexibility, and superior colour quality. This thesis describes the spectroscopic studies and theoretical calculations of the developed initially TMCz-BO TADF compound. This compound was reported as a promising deep blue emitter, a colour that is particularly challenging to achieve high efficiency in OLED technology. The deep blue emission is crucial for high displays and energy-efficient lighting. This study characterises the photophysical properties of this molecular system and proposes a mechanism for the TADF process, mentioned above, which can be helpful in designing future TADF materials. The paper **P3** provides an in-depth account of the study and presents its results in detail.

Introduction

The luminescence phenomenon encompasses photo-, electro-, and chemiluminescence (abbreviated as PL, EL, and CL, respectively), which are of particular importance for current applications. Due to their specific features, including high efficiency, adjustable emission range, photophysical stability, and relative simplicity, organic heterocyclic systems based on nitrogen-containing heterocycles, like acridine, carbazole, and their derivatives have found applications in rapidly developing modern techniques, such as luminescence analytics and optoelectronics. Thus, molecular systems based on CL and TADF are currently intensively investigated in many laboratories worldwide. Due to the relatively efficient occupation of excited states along both excitation paths, these phenomena enable applications in organic light-emitting diodes (OLEDs), time-resolved fluorescence imaging, chemiluminescent probes for drug detection, and sensors for biologically active compounds, such as antigens and antibodies and other specific proteins, hormones, vitamins, oxygen peroxide, and other bioactive substrates, including sulphur-containing ones, investigated in this thesis.

Chemiluminescence is the emission of light resulting from a chemical reaction, typically involving the oxidation of a luminogenic substrate (e.g. luminol, lucigenin, acridinium salts, and others) [1,2,3,4,5,6,7]. Unlike fluorescence, CL does not require external light excitation, eliminating background noise caused by scattered light and autofluorescence, and does not require a sophisticated optical system. This makes CL a perfect solution for ultra-sensitive assays, including CLIA (*Chemiluminescence Immunoassays*). ECLIA (*Electrochemiluminescence Immunoassays*), ELISA (*Enzyme-linked Immunosorbent assays*), real-time monitoring of reactive oxygen species (ROS), and detecting trace amounts of biomolecules (e.g.). Indicators and labels based on acridinium salts have garnered considerable attention lately due to their relatively high CL quantum yield efficiency, which ranges from 5% to 10%, depending on environmental factors and stability, making them robust tools for developing new solutions in modern analytics.

Photoluminescence, in turn, involves the absorption of photons at a specific wavelength and the subsequent emission of light at a longer wavelength [8]. PL techniques are extensively applied in diagnostics and bioimaging, where fluorophores label particular molecules. Advanced fluorescence methods, such as time-resolved fluorescence (TRF) and Fluorescence Resonance Energy Transfer (FRET)-based techniques, enable the study of dynamic molecular interactions and cellular processes. [9]. PL complements CL by allowing the spatial and temporal visualisation of target molecules and providing quantitative fluorescence intensity or lifetime analysis. While fluorescence-based techniques offer powerful visualisation and analytical capabilities, chemiluminescence (CL) presents distinct advantages, particularly in terms of reducing background signal and enhancing sensitivity. In aqueous media, acridinium-based systems are preferred due to their higher emission efficiency and tunable kinetics compared with luminol-based approaches [10-12, 15].

In the research work described here, I investigated how structurally close fragments can exhibit various luminescence properties. Nitrogen-containing heterocycles were selected with differently charged nitrogen atoms:

- 1) N^+ – electron-deficient cationic acridinium salts
- 2) N^0 – electron-releasing carbazole derivatives.

The presence of N^+ creates a deficit of electron density on the acridine core, especially at the C9 atom (Fig. 1). Such an acridinium moiety serves usually as an acceptor in electron transfer reactions or transitions. Specifically, N^+ enables the effective nucleophilic attack on the C9 position and initiation of the CL process.

In the case of N^0 electron-releasing analogues, namely carbazole derivatives, which are typically engaged in electrophilic reactions, they exhibit high stability in both the singlet (S_1) and triplet (T_1) excited states. In charge-transfer systems, such moieties often function as strong electron donors, with the highest occupied molecular orbital (HOMO) predominantly localised on these fragments. Due to the above reasons, nitrogen in the N^0 configuration is a key element in the molecular design of emitters that exhibit thermally activated delayed fluorescence (TADF) and can be used in electroluminescence applications. Accordingly to the different features of the abovementioned compounds, the present research focuses on two main thematic areas:

1. Research on novel chemiluminescent indicators based on acridinium salts and corresponding luminometric methods;
2. The investigation of the TADF mechanism of the efficient carbazole-based blue emitter to advance applications in optoelectronic materials and devices.

Thematic area I. Chemiluminescent systems

N-substituted 9-(phenoxycarbonyl) acridinium salts, also known as acridinium esters (AEs, Fig. 1), have garnered significant attention due to their exceptional chemiluminescent properties [10,11,12,13,14]. Each structural fragment of AE plays an important role influencing its CL features. In many previous studies, research was conducted based on modifications to the phenyl ring. Such modifications have demonstrated the effect of substituent groups' chemiluminogenic and physicochemical properties, which have influenced their stability, emission intensity, and overall analytical performance.

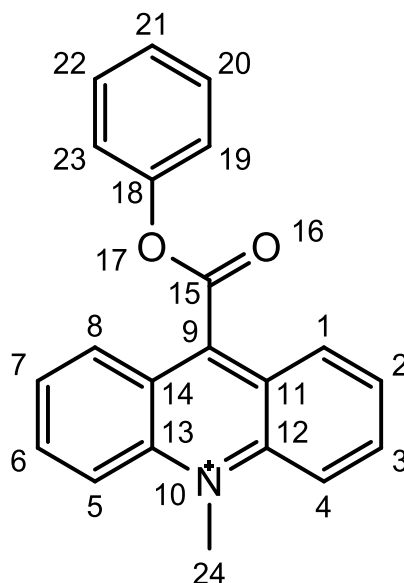


Fig. 1. Structural formula of the cation of N-methyl-9-(phenoxycarbonyl) acridinium ester (AE) [21].

The findings described in the work of K. Krzymiński, A. Ozóg et al. [14] highlight the importance of the "usefulness" parameter, a composite metric that reflects the chemiluminescence quantum yield of AEe in conjunction with its susceptibility to hydrolysis. This parameter can be employed to evaluate a compound's performance in analytical applications, including biomedical assays and tests such as those mentioned above, including CLIA, Western Blot, and ELISA tests [15,16,17]. The observed relationship between this parameter and the cavity volume of the molecular fragment released during oxidation (chemiluminogenic reaction) offers a possible path and measure for the strategic design of new chemiluminescent 10-methyl-9-(phenoxycarbonyl)acridinium cations of potential practical use. Here I only summarise the essentials; comprehensive literature details are discussed in [P1] and [P2], and proceed directly to the structures investigated in this thesis.

The substituent type and its position within acridine-benzene ring systems of AEs strongly influence their chemiluminogenic properties as well as the "usefulness" parameter, mentioned above. The key position, which is crucial for the performance of a given acridinium derivative, includes the 9-position (where nucleophilic attack of oxidiser (typically hydroperoxyl anion, OOH^-) takes place) as well as the phenol

fragment's (ortho and/or meta and/or *para* positions of the benzene ring). Substitutions at these fragments affect the electronic properties of the given AE, stability, and reactivity. The 9-position is particularly important, as it directly affects the CL efficiency of emission and reaction kinetics. At the 9-position, nucleophilic attack by OOH^- initiates the transformation path leading to CL. Substituents at this site predominantly modulate reaction efficiency, whereas substituents on the phenoxy fragment tune both leaving-group ability and, consequently, emission kinetics.

Substituents introduced into the acridinium rings typically alter the charge transfer processes, affecting the light emission intensity and wavelength of the resulting oxidation product, which is responsible for the light emission, specifically the 9(10*H*)-acridone derivative. Electron-donating groups such as: $-\text{OH}$, $-\text{OCH}_3$, $-\text{NH}_2$ increase electron density in the acridinium core, decreasing the energy of the excited state and potentially lowering the energy gap between excited (S_1) and ground states (S_0). This typically causes a bathochromic shift in the emitted light and sometimes increases chemiluminescent efficiency by enhancing charge transfer. On the other hand, electron-withdrawing groups such as $-\text{NO}_2$, $-\text{CF}_3$, $-\text{CN}$, and $-\text{COOH}$ typically reduce electron density in the acridinium ring system, decreasing the energy of the S_1 excited state, causing a hypsochromic shift and - in some cases - reducing the CL efficiency.

Oxidative reaction kinetics is a complex parameter influenced by substituents at different positions that can either stabilise or destabilise reactive intermediates. Substituents in the phenol fragment (*at ortho, meta, and para* locations) influence the oxidation rate through both electronic and steric effects. Altering the acidity of the phenolic group modulates the effectiveness of the leaving group. The knowledge of such structure-property relationships facilitates rational use of the acridinium salts as sensitive indicators and labels for automated clinical diagnostic assays. An analysis of the research study conducted by Wang et al. [18] confirmed that the substitution at the 9-position in acridinium salts esters leads to faster emission kinetics, improves stability, and reduces non-specific binding to magnetic microparticles with diverse surface properties. AEs have been well-characterised regarding their chemiluminescent properties, serving as efficient light-emitting substrates in various detection systems. Their established reactivity with peroxides and nucleophiles makes them reliable candidates for oxidative chemiluminescent reactions.

Topicality of the 1st problem. Although the behaviour of AEs is relatively well understood, they may not provide the selectivity or sensitivity required for specific biological applications, particularly in distinguishing between sulphur-based antioxidants. The need to identify these nucleophiles stems from their critical involvement in key biochemical processes, including enzymatic activity, detoxification, and redox regulation, highlighting the importance of sensitive and specific chemiluminescent indicators in diagnostic and analytical contexts [19]. Traditional detection techniques often struggle with sensitivity, specificity, or operational simplicity. Methods such as spectroscopy, chromatography, and calorimetric assays may lack the sensitivity to detect low concentrations of analytes or the specificity to differentiate closely related compounds. Additionally, techniques such as mass spectrometry (MS) or nuclear magnetic resonance (NMR), while highly specific, can be complex, time-consuming, and require sophisticated equipment.

These limitations underscore the need for advancements in detection methods that strike a balance between precision and practicality.

The **primary objective of our research** was to develop a method for identifying biologically active sulphur-containing nucleophiles. To achieve this goal, new thioesters were developed that improve the sensitivity of the analytical method (**Fig. 2**).

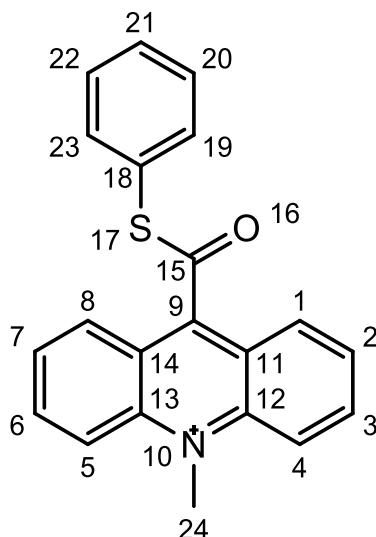


Fig. 2. Structural formula of exemplary N-methyl-9-(phenylthiocarbonyl)acridinium ester cation.

By comparing esters and thioesters, one can determine that the emission efficiencies of both groups of chemiluminescent salts are quite similar, despite exhibiting distinct CL profile characteristics. Regardless of the functional group attached to the benzene ring, thioesters typically produce flash-type emissions, leading to relatively high peak CL intensities but moderate to low area under the curve (AUC) values. In contrast, AEs generally display the opposite trend, particularly when an electron-donating group (such as an alkyl or alkoxy group) is present in the phenoxy moiety, which serves as the leaving group [20,21]. The findings demonstrate that thioester-based chemiluminescent systems provide faster emission characteristics, making them promising candidates for detecting sulfur-containing antioxidants. Integrating acridinium salt derivatives into these methodologies enhances sensitivity and specificity, paving the way for improved analytical and diagnostic applications.

The second problem addressed in this thesis is the methodological complexity associated with using hydrogen peroxide (H_2O_2) as an oxidising agent. H_2O_2 is a reactive compound of low stability that requires strict control over concentration, temperature, and storage conditions. Its decomposition is exothermic, and in the presence of specific catalysts or impurities, it can generate reactive oxygen species (ROS), posing significant safety hazards such as chemical burns, oxidative damage to biological materials, and the risk of pressure buildup or explosion in closed systems. Despite these challenges, reliable evaluation of antioxidant activity remains essential. Among the available analytical approaches, spectroscopic methods are particularly valued for their precision and ease of use. These include the 2,2-

Diphenyl-1-picrylhydrazyl (DPPH) Free Radical Scavenging Assay, which monitors the reduction of the DPPH radical via colour change; the 2,2'-azino-bis(3-ethylbenzothiazoline-6-sulfonic acid) (ABTS) Radical Cation Decolorization Assay, which measures the capacity of antioxidants to neutralise ABTS radicals; and the Ferric Reducing Antioxidant Power (FRAP) Assay, which assesses reducing power based on the conversion of Fe^{3+} to Fe^{2+} . As an alternative to AE, another acridinium salt, 9-CMA⁺ (9-cyano-10-methylacridinium salt), can be applied as an indicator for the identification of -SH-containing nucleophiles. The presence of the -SH functional group makes these compounds strong nucleophiles that are easily deprotonated and susceptible to oxidation. This chemical behaviour influences their selective interactions with other components in the system, particularly electron-deficient molecules. As a result, they exhibit significant biological activity and can be either naturally synthesised by living organisms or applied externally as pharmaceutical agents.

The cyano (-CN) group at the 9-position plays a critical role in modulating the electronic properties of the acridinium core. As a strong electron-withdrawing substituent, the -CN group stabilises the acridinium system by lowering the electron density on the aromatic ring, thereby influencing the redox potential and enhancing the molecule's susceptibility to nucleophilic attack. This modification facilitates more efficient oxidation reactions with molecular oxygen. Additionally, the presence of the cyano group can impact the chemiluminescence quantum yield by affecting the energy levels of the excited states involved in the light-emitting process.

The oxidation with molecular oxygen in the presence of sulphur-containing nucleophiles (RSH) was previously described in the works [22,23]. It was proposed that under strongly alkaline conditions, the anionic forms of the nucleophiles (RS^-) could interact with molecular oxygen, leading to the formation of superoxide radicals (O_2^-). Based on the biradical character of O_2 , this hypothesis allowed the authors to suggest an alternative reaction pathway for the chemiluminogenic oxidation of 9-CMA⁺.

The 9-CMA salt was also previously characterised in the research conducted by Wroblewska A. and Huta O. [24,25], highlighting its unique chemiluminescent properties and potential applications for detecting N-, O-, and S-containing nucleophiles.

Topicality. Although various methods exist for detecting biologically active sulphur-containing nucleophiles, many of these methods rely on additional oxidation. A chemiluminogenic indicator with the cyano group in the 9th position was used. Such modification eliminates the need for H_2O_2 as a necessary agent for oxidation, instead allowing oxidation to occur with molecular oxygen only. This luminometric method described in this work offers a significant advancement by obviating the need for hydrogen peroxide, simplifying the experimental procedure, and enhancing the detection sensitivity. These findings open the way for broader applications for determining N-, O-, and S-S-containing nucleophiles.

Thematic area II. TADF systems

The second thematic area of this dissertation addresses the potential of heterocyclic compounds exhibiting thermally activated delayed Fluorescence (TADF) phenomena for applications in organic light-emitting diode (OLED) technology. This research encompasses a comprehensive spectroscopic study and computational analysis of the TADF mechanism that leads to light generation. The 9-[1,4]benzoxaborino[2,3,4-kl]phenoxaborin-7-yl-1,3,6,8-tetramethyl-9H-carbazole (TMCz-BO) compound was reported previously as a deep blue emitter [26] that was investigated in various media and temperatures. To explain the origin of TADF and fast rISC, which enable rather unique triplet harvesting abilities of TMCz-BO, this study identifies an advanced mechanism of TADF, offering insights into optimising materials for OLED applications.

The primary response of this research lies in the urgent need for highly efficient, stable, emissive materials for OLED technology. These materials, which exhibit bright, intense, and highly saturated light emission, are crucial for achieving high colour purity, intense luminance, and efficient light emission in OLED displays and lighting applications. Among the various colours required for high-performance OLED displays, deep-blue emitters present one of the most significant challenges due to their demanding photophysical requirements. Blue emitters represent a key challenge in current research, as achieving efficient deep blue emission is essential for high colour purity and energy-efficient light generation. This makes developing novel blue-emitting materials a top priority in the field.

The primary challenge with all-organic emitters, particularly those emitting blue light, is addressing the issue of triplet harvesting. Traditional OLEDs often suffer from the inefficiency of triplet exciton harvesting, where, due to spin statistics, 75% of the generated excitons are in a triplet state, which do not directly contribute to light emission. One of the most promising strategies for effective triplet harvesting and achieving blue emission in OLEDs is through TADF. TADF materials use singlet and triplet excitons for light emission, thus enabling nearly 100% internal quantum efficiency without relying on expensive heavy metals like iridium or platinum, which are typically used in phosphorescent OLEDs [27,28,29]. The TADF mechanism depends on the reverse intersystem crossing (rISC) process, where triplet excitons are converted to singlet states, leading to delayed fluorescence (DF) [30] (**Fig. 3**). When other parameters are constant, the faster rISC rate and the shorter DF lifetime result in higher TADF efficiency and OLED stability.

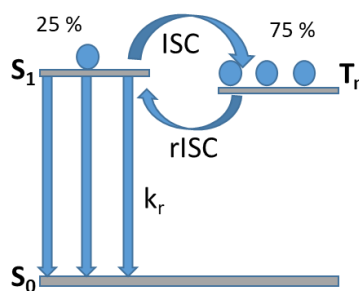


Fig. 3 General simplified scheme of the TADF mechanism

TADF OLED emitters are characterised by the following parameters: [31,32]

PL_{max} - Photoluminescence maximum that shows the emission colour of the emitter – for blue emitters, PL_{max} should be in the range of 450-460 nm.

PLQY - Photoluminescence quantum yield, indicating light emission efficiency after photon absorption—ideal value: near 100% (≥90%). High PLQY ensures maximum light output and minimal energy loss.

It is defined as the ratio of the number of emitted photons to the number of absorbed photons. PLQY is one of the key values influencing the external quantum efficiency of the OLED, which characterises the percentage of electrical input energy converted into emitted photons.

ΔE_{ST} - singlet-triplet energy gap. The ideal value should be close to 0 eV (typically <0.2 eV). Small ΔE_{ST} enables high rISC values, which are essential for high-efficiency TADF.

τ_{PF} – represents the prompt fluorescence lifetime, when a molecule remains in its excited singlet state (S₁) before emitting a photon via fluorescence.

τ_{DF} – delayed fluorescence lifetime, which refers to the time a molecule remains in an excited state before emitting a photon through thermally activated delayed fluorescence—ideal value: < 10 μs. A short τ_{DF} prevents exciton quenching, efficiency losses, and roll-off. A shorter τ_{DF} indicates that triplet excitons are quickly converted to singlets and then to photons, due to a faster rISC process. This improves the overall radiative efficiency and light output.

k_r – Key parameter that defines the probability of an excited state returning to the ground state (S₁ → S₀) by emitting a photon. Ideal value: >10⁸ s⁻¹. A high k_r ensures efficient light emission.

k_{ISC} – Intersystem rate constant, represents the probability per unit time that an excited molecule undergoes intersystem crossing (ISC), a non-radiative transition from the singlet excited state (S₁) to the triplet state (T₁).

k_{rISC} – Reverse intersystem rate constant describes the probability per unit time that an excited molecule transitions from the triplet state back to the singlet excited state. The ideal value should be ≥10⁶ s⁻¹. A high k_{rISC} value ensures fast TADF, preventing triplet loss mechanisms such as non-radiative decay. We specifically focused on the rISC mechanism and factors which enhance it. The rISC rate constant can be described by the Marcus-Hush equation [33]

$$k_{\text{rISC}} = \frac{V^2}{\hbar} \sqrt{\frac{\pi}{k_B T \lambda}} \exp \left[-\frac{(\Delta E_{\text{ST}} + \lambda)^2}{4k_B T \lambda} \right],$$

where:

V is the SOC constant,

λ is the sum of internal and external reorganisation energies for the respective transition,

k_B is the Boltzmann constant,

ħ is the reduced Planck's constant,

T is the temperature.

Spin-orbit coupling is one of the key parameters defining rISC. It is an interaction between an electron's spin and its orbital motion within an atom or molecule. Higher SOC leads to faster rISC, improving OLED efficiency [34]. SOC values should selectively be as high as possible between the T_1 and S_1 states, as strong SOC facilitates rISC without promoting undesired pathways.

In general, rISC is a spin-forbidden process that occurs in the (milli)second range, too slow for OLED applications. The most effective molecular design strategy for effective rISC combines the electron donor (D) and acceptor (A) fragments in an orthogonal arrangement. This separation of HOMO and LUMO creates charge-transfer singlet and triplet states of charge-transfer character (1CT and 3CT), thereby reducing the energy difference between the excited states (ΔE_{ST}). The origin of relatively high SOC in such DA molecules is still debated.

Currently, two fundamental concepts explain the nonzero SOC and the rISC mechanism in general. Within the classic quantum model, SOC between 1CT and 3CT states of the same character is zero. Therefore, the first, three-state rISC model relies on an additional nearby triplet state with a nature that is different from that of S_1 (1CT). More commonly, it is a locally excited state formed via redistribution of electronic density on a donor (3LE_D) or acceptor (3LE_A) fragment. This model predicts the highest rISC rate when the 3LE state(s) aligns both energetically [35,36,37] and vibronically [32] with the 1CT state. The key distinction between CT and LE states lies in their dipole moments: CT states, with very large dipole moments, are susceptible to medium polarity, unlike weakly polarised LE states. Therefore, under static quantum models, the ΔE_{CT-LE} gap can be modulated by medium polarity, allowing for insights into the role of the $3LE-1CT$ channel in the rISC mechanism [40]. Furthermore, differing geometries between CT and LE states affect reorganisation energy, a key element of Marcus theory. Smaller λ values facilitate electronic transitions, including ISC and rISC.

Moving beyond the understanding of electronic transitions occurring within the energy minima, it was found that molecular vibrations can play an essential role for SOC in D-A emitters. Such a vibrational activation of SOC lies at the basis of a second concept – the two-state rISC model. In emitters with stabilised CT states, the $^3CT \rightarrow ^1CT$ transition becomes efficient, driven by molecular motions that modulate the dihedral angle (θ) between D and A fragments. Such torsions causing considerable distribution of θ from 60-120° at room temperature cause a drastic increase of SOC from 0.00 cm^{-1} (90°) to 0.20 (60° or 120°) [40]. With $\Delta E_{1CT-3CT}$ and $\lambda_{1CT-3CT}$ values of just a few meV, this allows fast rISC in polar media [15] or strong D-A emitters [38] where CT states are effectively stabilised.

The most challenging aspect is understanding the photophysics of DA emitters, with the rISC mechanism falling between the two- and three-state models. The attempts to design the most demanded deep-blue emitters rely on the systems with weakened D and A fragments [41] and low-polarity environments. Under such conditions, $\Delta E_{1CT-3CT}$ and $\lambda_{1CT-3CT}$ increase sharply, and various $^3LE \rightarrow ^1CT$ transitions can be as efficient as the $^3CT \rightarrow ^1CT$ one.

Some recently developed molecular design strategies enable rISC within micro- and even sub-microsecond time frames [39,40,41]. However, most efforts are expected to focus on blue TADF emitters, with less success. Work [42] reported two emitters (PhCz-TOSBA and TPA-TOSBA) with PL_{max} at 454 and 467 nm,

τ_{DF} of 47 μs and 140 μs , and k_{rISC} values of $4 \times 10^4 \text{ s}^{-1}$ and $1.9 \times 10^4 \text{ s}^{-1}$, achieving EQE_{max} below 17%. Niu et al. [43] developed 1-MeCz-TRZ using a sterically hindered 1-methylcarbazole donor and a triphenyl-s-triazine acceptor, yielding a PL_{max} of 449 nm, a τ_{DF} of 24.8 μs , and an EQE_{max} of 13.1%. Another study [44] introduced indenocarbazole derivatives (e.g., InCz34DPhTz) with PL_{max} at 475 nm, high PLQY (97.9%), τ_{DF} of 70.3 μs , and k_{rISC} of $1.6 \times 10^4 \text{ s}^{-1}$, achieving an EQE_{max} of 25.9% but with significant roll-off at higher luminance. These examples highlight a common challenge for blue TADF emitters: weaker CT strength for deep-blue emission results in longer DF lifetimes, lower EQE, and reduced OLED stability due to slower rISC.

In comparison to the emitters mentioned above, TMCz-BO exhibits excellent parameters. The authors [69] reported a short τ_{DF} lifetime of 0.75 μs , a high k_{rISC} value of $1.9 \times 10^6 \text{ s}^{-1}$, and an EQE_{max} of 20.7%. The key improvement is the low efficiency roll-off of the OLED device, which remains below 3.5% even at a high luminance of 1000 cd m^{-2} .

Considering the exceptional TADF properties of TMCz-BO emitter, the next aim of this study was to understand the mechanism of enhanced rISC in TMCz-BO and how it helps to improve blue OLED technology. We closely examined its photophysics in various media and temperatures. Our findings reveal that the rISC rate in TMCz-BO increases significantly with higher polarity in both liquid and amorphous solid states, and is also strongly influenced by medium viscosity. The complex photophysical behaviour, caused by the strong interaction of two singlet and three triplet excited states, sets TMCz-BO apart from typical DA emitters, which usually involve two or three key excited states. Studies conducted within this thesis suggest that the TADF mechanism in TMCz-BO goes beyond the conventional three-state rISC model. An advanced quantum model was introduced to address this, accounting for the intense mixing of excited states.

Overall, this dissertation contributes to advancing analytical techniques and optoelectronic materials by introducing innovative methods and new paradigms for the mechanisms of photophysical and photochemical properties of emissive materials. The research is supported by three scientific articles, each addressing different aspects of the study and contributing to the broader understanding of photo- and chemiluminescent phenomena in heterocyclic systems.

Research hypotheses

1. Development and optimisation of original analytical systems based on the chemiluminescence process.
2. Experimental verification of the applicability of the systems above to determine detection limits for sulphur-containing biological compounds (DTT, GSH, etc.).
3. Application of various types of chemiluminogenic salts and instrumentation to compare and obtain optimal analytical parameters such as linearity ranges, correlation coefficients, LOD/LOQ, and repeatability.
4. Experimental verification of the mechanisms leading to chemically generated chemiluminescence of acridinium salts in the presence or absence of antioxidant substances.
5. Spectroscopic characterisation of the TMCz-BO in media of different polarity and viscosity, aimed at determining parameters such as k_{ISC} , k_{rISC} , kr , PLQY, etc.

- Investigation of the TADF mechanism at the TD-DFT level to explain experimental findings related to heterocyclic donor–acceptor (D–A) type molecular systems.

Work objectives

The research objectives of this PhD thesis were addressed through the following tasks:

Part I: Aromatic acridinium thioesters as new chemiluminogenic substrates in the analysis of some biological antioxidants

- Conduct CL tests for a series of thioesters and select the optimal substrate for further research based on its CL emission intensity;
- Identify the most effective solvent for maximising CL signal generation.
- Investigate the reaction mechanism using DFT calculations;
- Conduct spectroscopic investigations to confirm the formation of different adducts during the reaction.

Part Ib 9-CMA as a potential acridinium salt indicator for the quantitative identification of biologically relevant sulphur nucleophiles

- Purify the 9-CMA compound for subsequent experiments using liquid chromatography (LC);
- Optimise conditions for a chemiluminometric method without the addition of H₂O₂ and apply it for the quantitative determination of sulfur-containing biological compounds;
- Analyse the mechanism of CL applying DFT calculations;

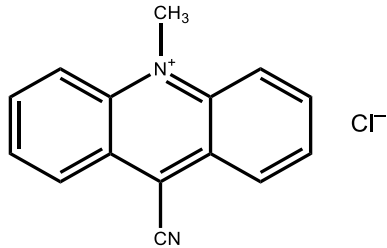
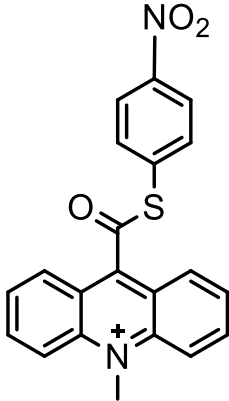
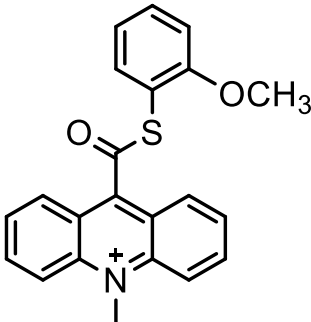
Part II: Spectroscopic and computational studies of the TADF mechanism of the TMCz-BO compound as a promising deep-blue emitter for OLED technology

- Perform steady-state and time-resolved PL measurements for TMCz-BO in solutions and films under various temperatures to reveal trends of rISC, ISC, and other photophysical processes;
- Analyse the effect of medium and temperature on TADF;
- Perform calculations of ¹CT, ³CT, ¹LE_A, ³LE_A, ³LE_D states at the DFT/TD-DFT level of theory to reveal electronic properties of TMCz-BO in various excited states, analyse molecular orbitals, gaps, and reorganisation energies for each electronic transition;
- Perform a comprehensive analysis of experimental and computational data to explain the TADF mechanism.

Part I. Acridinium salts as indicators in luminescence studies

In the research work, CL indicators such as 9-CMA, 4NO₂-ATE, and 2MeO-ATE were developed as substrates for the quantitative determination of biologically active compounds (Table 1).

Table 1: Substrates for the quantitative determination of biologically active compounds

Substrate		
 <p>9-cyano-10-methylacridinium chloride (9-CMA⁺)</p>	 <p>10-methyl-9-(((4-nitrophenyl)thio)carbonyl)acridinium trifluoromethanesulphonate (4-NO₂-ATE)</p>	 <p>9-(((2-methoxyphenyl)thio)carbonyl)-10-methylacridinium trifluoromethanesulphonate (2-MeO-ATE)</p>

4NO₂-ATE and 2MeO-ATE were used for the quantitative determination of antioxidants, including dithiothreitol (DTT), glutathione (GSH), and quercetin (QR). The above CL indicators were chosen due to their unique structure, which features the presence of an S atom instead of an O atom to enhance the emissive properties of the esters, as sulphur has greater electrophilicity and lower electronegativity compared to oxygen (0.88 vs. 0.48). Dr Anna Romanowska obtained the thioesters mentioned above, and my role was to check their purity and/or chemical identity.

The biological antioxidants (p.a., Sigma-Aldrich) were selected for investigations, because they are well-characterised and often employed in scientific research to serve as reference compounds for evaluating new analytical approaches [45,46,47].

9-CMA was used as a luminogenic substrate for the quantitative determination of sulphur-containing nucleophiles, such as N-acetyl-L-cysteine (NAC), glutathione (GT), D-penicillamine (DPA), and acetylthiocholine chloride (ATC). Such an indicator was chosen as the research substrate due to its known spectral properties, making it a promising reagent for the detection of a wide range of sulphur-containing nucleophiles [24]. The structure of this acridinium salt enables the efficient generation of electronically excited states during oxidation, resulting in strong light emission without the need for additional oxidants, such as hydrogen peroxide. This simplifies the analytical setup, improving safety and reproducibility. All biologically active sulphur-containing nucleophiles mentioned above were chosen because they play essential roles in maintaining redox balance and cellular defence mechanisms. NAC serves as both a direct

antioxidant and a precursor to GSH, making it vital in clinical settings, particularly for treating acetaminophen poisoning and respiratory conditions [48]. DPA is used therapeutically in the management of Wilson's disease and rheumatoid arthritis due to its metal-chelating and immunomodulatory properties [49]. ATC, while primarily known as a cholinergic agent, is also used in neurochemical studies to understand enzyme activities and neurotransmission [50]. More detailed research is provided below.

Measurements of chemiluminescence

Chemiluminescence measurements were performed using a Lumat3 LB 9508 tube luminometer (Berthold, Germany) and a Fluoroskan Ascent FL plate luminometer (Labsystems-Thermo, Finland, USA). Lumat3 LB 9508 is equipped with an ultrasensitive photon detector. All experiments were conducted under consistent conditions using freshly prepared solutions. Light emission intensity was recorded in relative luminescence units (RLUs) over time, typically with a resolution of 0.15 seconds per measurement. Chemiluminescent emission was triggered using reaction mixtures containing ATE and hydrogen peroxide in alkaline solutions (KOH). In experiments involving the 9-CMA-based substrate, CL generation required incubation in alkaline conditions (KOH) followed by specific mixing procedures. For antioxidants or analytes, signal intensities and regions under the emission curves (AUC) were used to build calibration plots and assess the analytical performance of the investigated systems, with selected ones employing lucigenin as a reference indicator for comparison purposes.

The crude 9-CMA (the base) was purified chromatographically (LC) using silica gel (40–63 mesh, Merck) as the solid phase and cyclohexane-ethyl acetate mixture (2/1 v/v) as the mobile phase. The purity of the final product was assessed using reverse-phase high-performance liquid chromatography (RP-HPLC). All the investigated substances were originally in the form of crystal powders. NAC, glutathione, and D-penicillamine were supplied by Ambeed (USA), and ATC was provided by Sigma-Aldrich (USA). Their purity was established using RP-HPLC in the setup described above before proceeding to further experiments.

ATE's chemical identity was confirmed by spectroscopic analyses (MALDI-QTOF mass spectra, ^1H and ^{13}C NMR spectra and FT-IR spectra).

Computational studies were performed using DFT [51] at $\omega\text{B97XD/}$ level of theory [52] using the 6-31G(d,p) basis set [53] and TD-DFT [54] methods for ground and excited states, respectively. The chosen approach, supported by previous studies [55,56,57], provides reliable qualitative insights into the chemiluminescence mechanisms. Vibrational frequency and IRC [58] analyses confirmed stationary points and reaction pathways. Calculations were performed in aqueous solution using the PCM model with the Gaussian16 program [59], and visualisation was performed in ChemCraft [60].

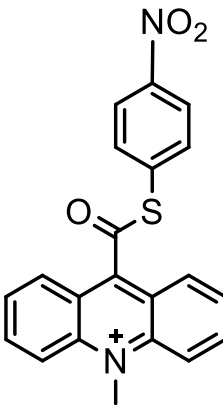
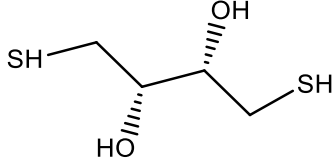
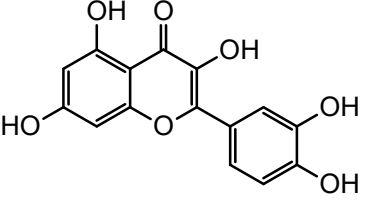
Part Ia. Aromatic acridinium thioesters as new chemiluminogenic substrates in the analysis of some biological antioxidants

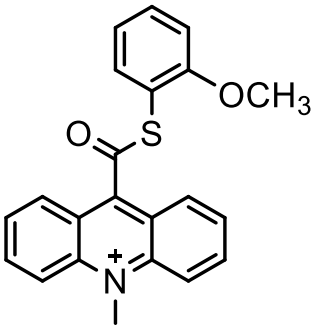
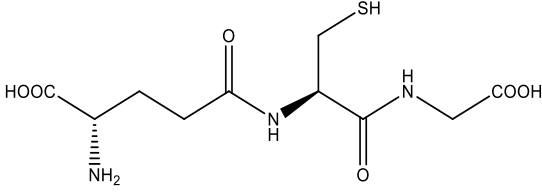
A key feature of certain N-substituted acridinium salts is their ability to emit light as a result of chemical reactions, a process known as chemiluminescence (CL) [1, 2, 3,61]. This phenomenon has been widely applied in fields such as medicine [62], pharmaceuticals [63], biochemistry [64], food science [65], and environmental monitoring [66]. In CL analysis, the intensity of the emitted light can be quantified to determine the concentration of specific biomolecules, including antigens [67], antibodies [68,69,70], hormones [71,72], enzymes [73], and antioxidants [74,75], often at extremely low concentrations (down to 10^{-16} to 10^{-19} M in some immunoassays [76]). Among these, acridinium esters (AEs) offer several advantages over traditional luminometric standards, such as luminol and its derivatives [27,37,43]. These advantages include relatively high quantum yields, rapid and easily controllable emission dynamics, and low background signals due to the absence of catalysts required to initiate CL [24,41].

The luminescent properties and strong chemical reactivity of chemiluminogenic acridinium thioesters motivated us to investigate the use of these esters as indicators for detecting antioxidants (AOs) (**Table 2**)

Research objects

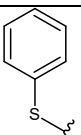
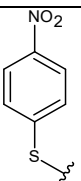
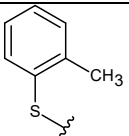
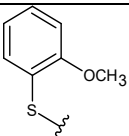
Table 2 Structural formulas of the ATEs and biologically active compounds investigated in this work.

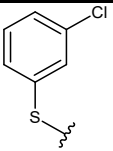
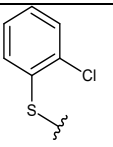
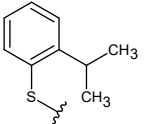
Substrate	Biologically active compounds
 <p>10-methyl-9-(((4-nitrophenyl)thio)carbonyl)acridin-10-ium trifluoromethanesulphonate</p>	 <p>Dithiothreitol (DTT) (2<i>S</i>,3<i>S</i>)-1,4-Bis(sulfanyl)butane-2,3-diol</p>
	 <p>Quercetin (QR) 3,3',4',5,7-PentahydroxyPLavone</p>

 <p>9-(((2-methoxyphenyl)thio)carbonyl)-10-methylacridin-10-ium trifluoromethanesulphonate</p>	 <p>Glutathione (GSH) (2S)-2-Amino-5-({(2R)-1-[(carboxymethyl)amino]-1-oxo-3-sulfanylpropan-2-yl}amino)-5-oxopentanoic acid</p>
---	--

Six different acridinium thioesters (**ATEs**) containing 4-nitro-, 2-methoxy- and 2-isopropyl groups, attached in the benzene ring (compounds encoded as 4NO₂-ATE, 2MeO-ATE, 2iPr-ATE) were investigated in this work (**Table 3**). All these ATEs were obtained starting from 9-(chlorocarbonyl) acridinium hydrochloride (prepared from commercial acridinyl-9-carboxylic acid chloride (Sigma-Aldrich, USA)) by reacting it with thionyl chloride [25,77]. Detailed descriptions of syntheses and the chemical identity of the studied acridinium thioesters are provided in the **P2**. For each compound, spectroscopic analyses (MALDI-QTOF mass spectra, ¹H and ¹³C NMR spectra and FT-IR spectra) are provided with experimental details.

Table 3 Names, formulas and abbreviations of acridinium thioesters (ATEs) investigated in this work.

Abbreviation	R ¹	Systematic name
H-ATE		10-methyl-9-((phenylthio)carbonyl)acridin-10-ium trifluoromethanesulphonate
4NO₂-ATE		10-methyl-9-(((4-nitrophenyl)thio)carbonyl)acridin-10-ium trifluoromethanesulphonate
2Me-ATE		10-methyl-9-(((2-methylphenyl)thio)carbonyl)acridin-10-ium trifluoromethanesulphonate
2MeO-ATE		9-(((2-methoxyphenyl)thio)carbonyl)-10-methylacridin-10-ium trifluoromethanesulphonate

3Cl-ATE		9-(((3-chlorophenyl)thio)carbonyl)-10-methylacridin-10-ium trifluoromethanesulphonate
2Cl-ATE		9-(((2-chlorophenyl)thio)carbonyl)-10-methylacridin-10-ium trifluoromethanesulphonate
2iPr-ATE		9-(((2-isopropylphenyl)thio)carbonyl)-10-methylacridin-10-ium trifluoromethanesulphonate

Based on the results of the screening experiments with all 7 ATE compounds (Fig. 4), the two best candidates were selected as chemiluminogenic indicators: 2MeO-ATE and 4NO₂-ATE. These compounds showed the maximal CL intensity (I_{CL}^{max} , orange bars) and integral emission (blue bars). Light emission was initiated by sequential addition of 50 μ L of 0.1% H₂O₂ and 50 μ L of 0.1 M KOH. CL intensities were recorded ($n = 5$) until signal completion, and areas under the curves (AUCs, in RLU²) were calculated individually.

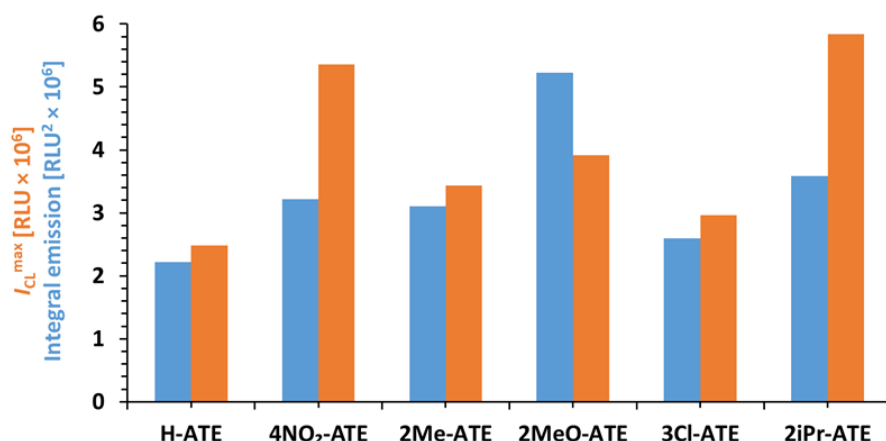


Fig. 4 Emissive efficiencies of acridinium thioesters (ATEs, **Table 4**) in aqueous environment ($c = 1.0 \times 10^{-10}$ M), measured as maximum (I_{CL}^{max}) and integral intensity (AUC) of CL, using H₂O₂/KOH triggering system. For details, see the Materials and Methods section of **P2**.

Table 4. Kinetic parameters of chemiluminescence obtained by plate luminometry for selected acridinium thioesters (ATEs) in various liquid phases. The concentration of ATEs was 1.0×10^{-10} M, triggering solution: H₂O₂/KOH. For details, see the Materials and Methods section **P2**

Abbreviation (Table 1)	Solvent	CL decay rate constant (k_{CL} , s ⁻¹)	Correlation coefficient (R^2)	Halftime ($t_{1/2}$, sec.)	Time of maximal emission (t_{max} , s)	Intercept (b)
4NO ₂ -ATE	H ₂ O	1.103	0.971	0.628	0.30	13.02
2MeO-ATE		1.026	0.954	0.675		12.69
4NO ₂ -ATE	EtOH	0.756	0.847	0.916		12.76
2MeO-ATE		1.238	0.982	0.560		14.45
4NO ₂ -ATE	DMSO	1.064	0.914	0.651		13.65

2MeO-ATE		1.28	0.921	0.541		13.85
-----------------	--	------	-------	-------	--	-------

A detailed examination of the data in **Table 4** reveals specific patterns and variations. Generally, organic solvents appear to have a greater effect on differentiating kinetic constants than aqueous environments, with ethanol showing a more pronounced impact than DMSO. Specifically, for the salts 2MeO-ATE and 4NO₂-ATE, nearly identical CL decay rate constants of 1.0–1.1 s⁻¹ were observed in water. In ethanol, these values ranged from approximately 0.8 to 1.2 s⁻¹, while in DMSO, they varied between 1.1 and 1.3 s⁻¹. The calculated half-lives ($t_{1/2}$), based on first-order kinetic constants [59], also showed similar trends. The enhanced CL intensity in more polar solvents results from their greater ability to stabilise excited states and reactive intermediates compared to water, which reduces quenching interactions and consequently increases the emission quantum yield.

Fig. 5 summarises the trends in emissive properties for selected acridinium thioesters (4NO₂-ATE and 2MeO-ATE).

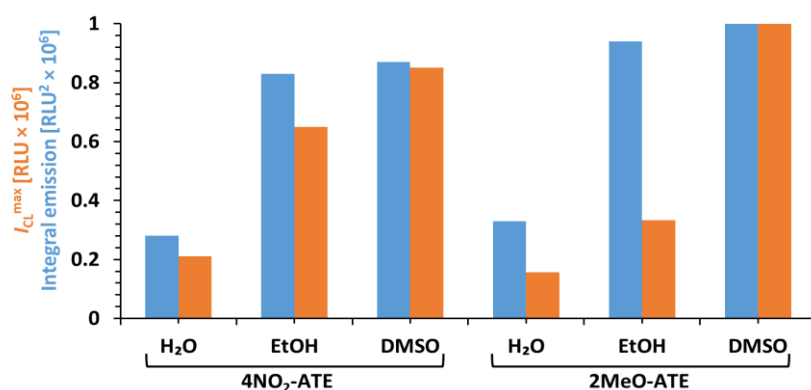


Fig. 5 Emissive efficiency of acridinium thioesters selected for analytical studies in various liquid environments, measured as maximum (I_{CL}^{max}) and AUC using H₂O₂/KOH triggering system. For details, see the Materials and Methods section. **P2**

Among the three solvents used for triggering, while maintaining consistent experimental conditions, in water, compounds consistently show the lowest emission intensity for both I_{CL}^{max} and AUC . When comparing the ethanol medium, distinct differences in maximal emissions are observed between 4NO₂-ATE and 2MeO-ATE. Specifically, the I_{CL}^{max} values (orange bars) increase progressively across the H₂O-EtOH-DMSO series, with relative values of I_{CL}^{max} being 1:3:3.5 for 4NO₂-ATE and 1:2.5:5.5 for 2MeO-ATE. This indicates that the chemiluminescence efficiency of these salts improves as solvent polarity decreases in the series H₂O-EtOH-DMSO, with their relative polarities being 1.0, 0.65, and 0.44, respectively. For practical reasons (biocompatibility, stability, low viscosity and lack of eventual side reactions), water and water-ethanol media were selected as solvents for the CL assays of AOs, described in this work.

The antioxidant activity of three biologically significant antioxidants—dithiothreitol (DTT), glutathione (GT), and quercetin (QR)—was examined. The primary aim of these experiments was to observe and measure alterations in CL emission parameters.

The graphs presenting the intensity of CL emission (I_{CL}^{max}) and AUC vs. concentration of the antioxidant containing systems are presented in **Fig. 6**.

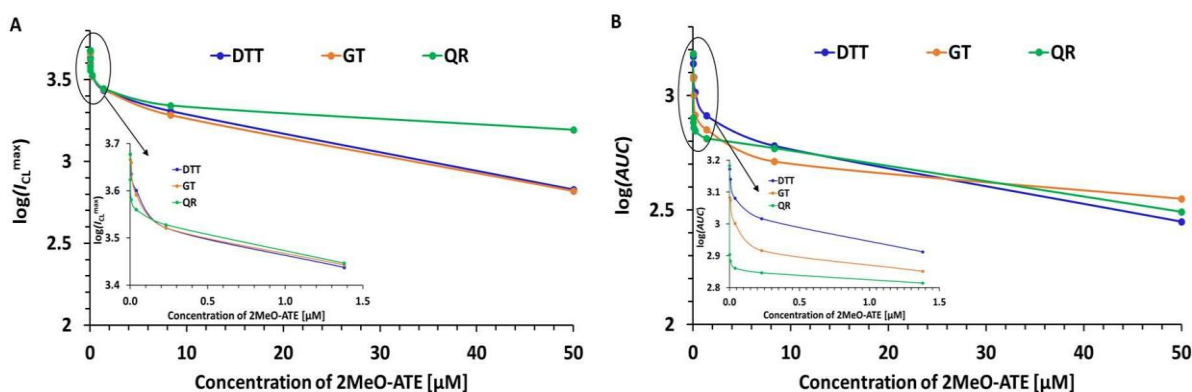


Fig. 6 Graph presenting dependence of log (maximal CL intensity) against AO concentration (A) and log(area under curve) against AO concentration (B), using 2MeO-ATE as CL indicator ($c = 1.25 \times 10^{-7}$ M) in aqueous-ethanolic solution and H_2O_2/KOH triggering system. For details, see the Materials and Methods section, **P2**.

Glutathione showed the highest antioxidant activity, indicated by the most significant reduction in emission parameters when 2MeO-ATE was used as the chemiluminescent indicator. Specifically, the I_{CL}^{max} value for 2MeO-ATE dropped approximately 5.2-fold with GT, compared to a 2.8-fold decrease with either dithiothreitol (DTT) or quercetin (QR) (**Fig. 6A**). Similarly, the area under the curve (AUC) values decreased about 10.6-fold for GT, 5.1-fold for DTT, and 2.1-fold for QR (**Fig. 6B**). These results indicate that GT has the highest antioxidant activity among the tested substances. Similar trends were observed using 4NO₂-ATE as the CL indicator, although the data were more variable, likely due to its lower hydrolytic stability compared to 2MeO-ATE.

The obtained data clearly demonstrate that all the investigated systems exhibit a flash-type emission, reaching peak intensity at around 0.3 seconds, regardless of the substituent type in the leaving group or the surrounding environment. This indicates that the sulphur atom in the thioester leaving group primarily influences the kinetics of CL decay among the studied ATEs.

Computational studies

Theoretical calculations were performed in collaboration with Dr. Beata Zadykiewicz. My role was based on further comparison of the data obtained from theoretical calculations and actual experimental data.

To predict and understand the transformation mechanisms within the studied complex systems, computational methods were applied. Our aim was to clarify the mechanism of interactions between ATEs and AOs and to identify the reasons behind the reduction in emission intensity. The mechanism below is explained on the example of 4NO₂-ATE as a CL indicator and DTT, with analysis of the Gibbs free energy changes for each step in the aqueous phase.

Our investigations suggest that reaction starts with the formation of the AO's anion and OOH^- ($\Delta_{r,298}G^0 = -63.7$ kcal/mol). Next, there are two possible reaction pathways: reaction of $\text{DTT}^-(\text{AO}^-)$ and $4\text{NO}_2\text{-ATE}$ (II) that leads to the formation of $4\text{-NO}_2\text{-ATE-AO}$ ($\Delta_{r,298}G^0 = -23.4$ kcal/mol) and reaction of OOH^- and $4\text{NO}_2\text{-ATE}$ (III) that leads to the formation of $4\text{-NO}_2\text{-ATE-OOH}$ ($\Delta_{r,298}G^0 = -52.5$ kcal/mol). A comparison of the potential reaction pathways **II** and **III** indicates that pathway **III**, involving a nucleophilic attack at the carbon atom in position 9 of the acridinium salts moiety, is -29.1 kJ/mol more favourable than **II** (Table 3). In the next step, the OOH^- anion replaces the AO^- ion in binding to ATE (step **IV**) ($\Delta_{r,298}G^0 = -29.1$ kcal/mol). Therefore, both pathways—steps **II** + **IV** versus step **III**—can co-occur and compete with each other. Both paths lead to the formation of the ATE-OOH , which next detaches thiophenyl anion, forming a high-energy cyclic intermediate $[\text{ATE-OO}]$ ($\Delta_{r,298}G^0 = -71.4$ kcal/mol) (Fig. 6, step **V**), which then decarboxylates to produce the excited CL product, 10-methyl-acridan-9-one ($\Delta_{r,298}G^0 = -19.0$ kcal/mol) (step **VI**). These two steps are thermodynamically favourable with a sum of $\Delta_{r,298}G^0 = -90.4$ kJ/mol (Table 5). Comparing the substituent effect, step **V** is most favourable for the $4\text{NO}_2\text{-ATE}$ derivative, while H-ATE and 2MeO-ATE show similar energy values. It correlates with the experimental trend, where $4\text{NO}_2\text{-ATE}$ shows the highest $I_{\text{CL}}^{\text{max}}$ intensity.

The CL pathway from the reaction of acridinium thioesters with antioxidants, is presented in Fig. 7

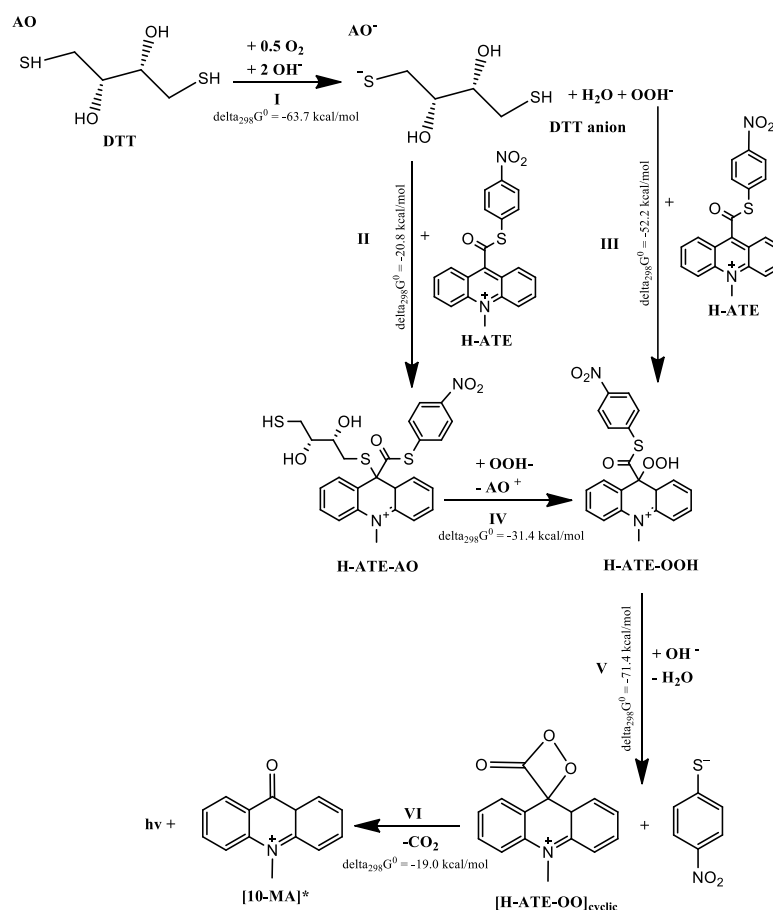


Fig. 7 The mechanism (DFT level of theory), presenting elementary steps occurring during chemiluminogenic transformations of representative acridinium thioesters (H-ATE , $4\text{-NO}_2\text{-ATE}$, 2MeO-ATE , Table 1) in the presence of DTT (Fig. 1). For details, see Materials and Methods section, **P2**.

Table 5: Thermodynamic data related to the elementary steps of chemiluminogenic transformations of ATEs cations in alkaline environments with D-penicillamine

Step No.	Nucleophile (DTT)	aqueous phase
		$\Delta_{r,298}G^0$
I	$\text{DTT} + \frac{1}{2}\text{O}_2 + 2\text{OH}^- \rightarrow \text{DTT}^- + \text{OOH}^- + \text{H}_2\text{O}$	-63.7
4NO₂-ATE		
II	$\text{DTT}^- + 4\text{NO}_2\text{-ATE} \rightarrow 4\text{NO}_2\text{-ATE-DTT}$	-20.8
III	$4\text{NO}_2\text{-ATE} + \text{OOH}^- \rightarrow 4\text{NO}_2\text{-ATE-OOH}$	-52.2
IV	$4\text{NO}_2\text{-ATE-AO} + \text{OOH}^- \rightarrow 4\text{NO}_2\text{-ATE-OOH} + \text{DTT}^+$	-31.4
V	$4\text{NO}_2\text{-ATE-OOH} + \text{OH}^- \rightarrow [\text{H-ATE-OO}] \text{ (cyclic form)} + \text{H}_2\text{O} + \text{PhS}^-$	-71.4
VI	$[\text{H-ATE-OO}] \text{ (cyclic form)} \rightarrow [10\text{-MA}]^* + h\nu$	-19.0

$\Delta_{r,298}H^0$ and $\Delta_{r,298}G^0$ (both in kcal mol^{-1}), respectively, represent the enthalpy and Gibbs' free energy (gaseous phase) or free energy (aqueous phase) of the corresponding process at standard temperature and pressure.

Thermodynamic and kinetic data obtained for the selected luminogenic systems containing antioxidants Can be found in the “Computational studies on formation of ATE-AO adducts” section in **P2**.

UV-Vis absorption spectroscopy studies on the formation of ATE-AO adducts

To validate the mechanism proposed by DFT level theory, we conducted spectrophotometric experiments. **Figure 8** shows the differential UV-Vis spectra for 4NO₂-ATE in the presence of DTT, a representative antioxidant (AO).

The observation that both an increase and a decrease in absorbance for the two investigated ATEs occur at the same wavelengths under the influence of two structurally distinct antioxidants aligns well with theoretical calculations, which clearly suggest the formation of the same type of species for the studied system.

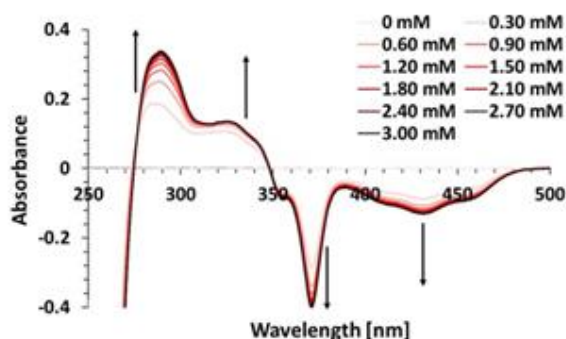


Fig. 8 Differential UV-Vis spectra recorded for the selected 4NO₂-ATE/DTT system in aqueous-ethanolic solutions. (pH = 3.5). The concentration of 4NO₂-ATE was equal to 1.0×10^{-4} M.

To sum up, in this part, new acridinium salts were successfully used as chemiluminescence indicators to detect biological antioxidants (dithiothreitol, glutathione, quercetin) with favourable analytical parameters (LOD/LOQ: $0.7\text{--}2.7 \times 10^{-6}$ M).

One of the three core parts of this research was the experimental investigation of the chemiluminescent properties of selected ATEs, which I conducted. This section made a significant contribution to the overall study, providing essential data for evaluating the analytical potential of these compounds. I performed comparative emission studies of several ATE derivatives and identified 4NO₂-ATE and 2MeO-ATE as the most promising candidates for further analysis based on their emission efficiency ($I_{\text{CL}}^{\text{max}}$ and AUC).

These compounds were tested in different solvent environments (water, ethanol, and DMSO) under identical conditions. The results revealed a strong solvent-dependent effect on emission efficiency, while the emission kinetics remained stable. This indicates the robustness of ATEs across different situations and highlights their potential for reliable use in luminescence-based analytical methods. Additionally, our group conducted quantum-chemical calculations at the DFT and TD-DFT levels and confirmed the preferred formation of adducts between ATEs and antioxidant anions, thereby enhancing the chemiluminescence reaction by generating OOH^- ions and improving the efficiency of electronically excited product formation, specifically 10-methylacridan-9-one.

Further validation was provided by dr Krzysztof Żamojć by UV-Vis absorption spectroscopy, which showed distinct differences in the absorption spectra of ATE-AO adducts compared to the sum of the pure components, confirming the interaction between ATEs and antioxidants.

Part Ib. 9-CMA as a potential acridinium indicator for the quantitative identification of biologically relevant sulphur nucleophiles

Biologically active sulphur-containing nucleophiles, such as N-acetyl-L-cysteine (NAC), glutathione (GSH), D-penicillamine (DPA), and acetylthiocholine chloride (ATC), possess notable nucleophilicity, easy deprotonation, and a propensity for oxidation. These properties dictate their specific interactions, especially with electron-deficient molecules, and underlie their significant biological activity, whether generated within the body or delivered as therapeutic agents. The more detailed overview of these nucleophiles is provided in the ESI of the **P1** publication.

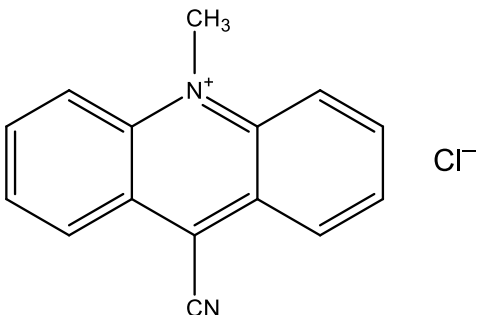
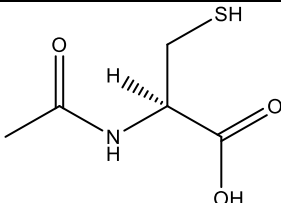
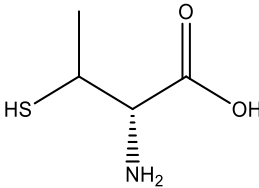
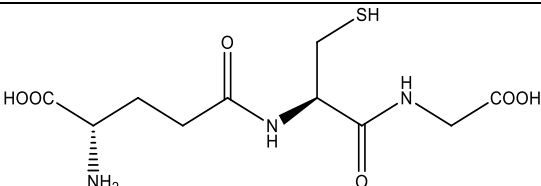
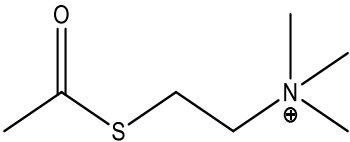
Given their crucial roles, there is a pressing need for precise, reliable, and sensitive methods to quantify these compounds in biomedical research. Historically, initial quantification methods for thiol drugs included redox titrations with reagents such as iodine solutions, silver nitrate (V), and copper (II) salts [78,79]. Over time, more advanced techniques have been developed to analyse these substances in various matrices. Modern methods often incorporate derivatisation steps to produce derivatives amenable to detection through ultraviolet-visible (UV-vis) spectrophotometry, fluorimetry, and various chromatographic techniques, including tandem methods. These advancements enhance the detection sensitivity and specificity for such compounds in complex biological systems.

In our work, we chose the luminescence method due to its advantages. The luminescent method generally does not require lengthy separations or costly equipment, such as chromatographic systems (HPLC, LC–MS) or FIA/sequential injection (SI) techniques. Additionally, it often offers greater sensitivity compared to other methods. Traditional CL approaches, including those employing standard luminol [80], have been utilised alongside spectrophotometric techniques [5] for the analysis of biological thiols. A rapid titration method for N-acetyl-L-cysteine (NAC) involving hypochlorite ions (ClO⁻) and CL measurements using standard luminol [81,82].

Experimental part

Biologically active sulphur-containing nucleophiles that were chosen as research objects are presented in **Table 6**

Table 6. Structural formulas of the substrate and biologically active compounds containing a thiol moiety are investigated in this work.

Substrate	Biologically active compounds
 <p>9-cyano-10-methylacridinium chloride (9-CMA⁺)</p>	 <p>N-acetyl-L-cysteine (NAC) (2R)-2-acetamido-3-sulfanylpropanoic acid</p>
	 <p>D-penicillamine (DPA) (2S)-2-amino-3-methyl-3-sulfanylbutanoic acid</p>
	 <p>Glutathione (GSH) (2S)-2-Amino-5-((2R)-1-[(carboxymethyl)amino]-1-oxo-3-sulfanylpropan-2-yl)amino)-5-oxopentanoic acid</p>
	 <p>Acetylthiocholine (ATC) 2-(Acetylsulfanyl)-N,N,N-trimethyl-ethan-1-aminium chloride</p>

Before conducting quantitative analyses, the optimal experimental conditions were determined. Preincubation studies of the analytes (RSHs) in an alkaline environment with molecular oxygen (and vigorous mixing) allowed us to establish the best duration for generating sufficiently high signals from their

reaction with 9-CMA⁺ and RS⁻. The results from these optimisation experiments were: 4 minutes for NAC, 5 minutes for GSH, 6 minutes for DPA, and 7 minutes for ATC.

Fig. 9 presents the time profiles of emission from the substrate used for CL (9-CMA⁺) under optimal conditions, in the presence of the studied sulfur-containing biological substances.

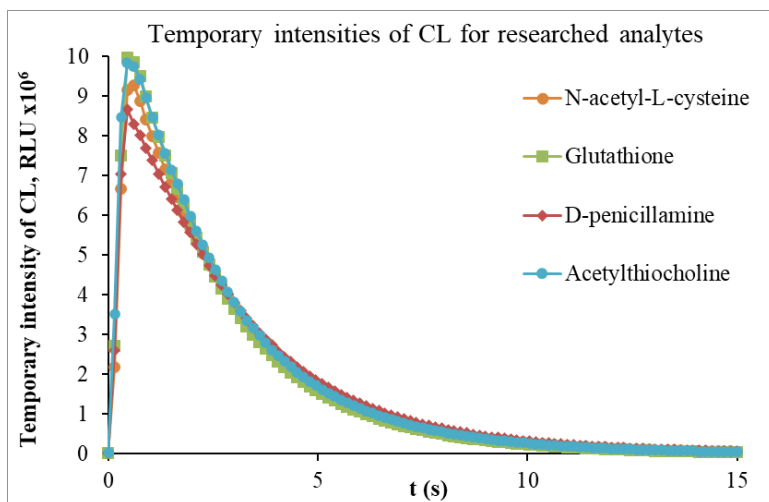


Fig. 9 Temporary intensities of chemiluminescence of 9-CMA⁺ in alkaline medium in various concentrations of thiol-containing compounds (the analytes). C(9-CMA⁺) = 2.5×10^{-5} M, 0.5 M KOH. The concentration range of researched analytes was in the range of $1-10 \times 10^{-6}$ M.

Measurements of CL with the use of 10,10'-dimethyl-9,9'-biacridinium nitrate (lucigenin) as the indicator [83,84, 85] were also performed in the presence of investigated analytes to obtain the comparison data.

The experiments showed that lucigenin, used as the reference compound, was a less effective luminogenic substrate for assaying the studied analytes compared to the 9-CMA salt. In this scenario, the CL emission intensity produced by 9-CMA⁺ under optimal assay conditions was significantly higher than that of lucigenin (**Table 7**).

Table 7. A comparison of the efficiency of CL emission from 9-CMA⁺ and Lucigenin was conducted based on the net areas under the emission curves ($\Delta(\text{AUC})$) within a 25-second timeframe. The final concentrations of the reagents were $c(\text{RSHs}) = 1.0 \times 10^{-5}$ M and $c(9 \text{ CMACl}) = 2.5 \times 10^{-5}$ M.

Name of substance	$\Delta(\text{AUC})$ for 9-CMA ⁺ $\times 10^7 (\text{RLU}^2)$	$\Delta(\text{AUC})$ for Lucigenin $\times 10^5 (\text{RLU}^2)$
D-penicillamine	2.81	8.02
Glutathione	2.82	9.88
Acetylthiocholine	2.94	6.21
N-acetyl-L-cysteine	2.90	9.99

Utilising lucigenin as a CL indicator resulted in a less favourable reaction profile (**Fig. 10**), requiring more time to achieve effective emission (characterised by glow-type kinetic curves).

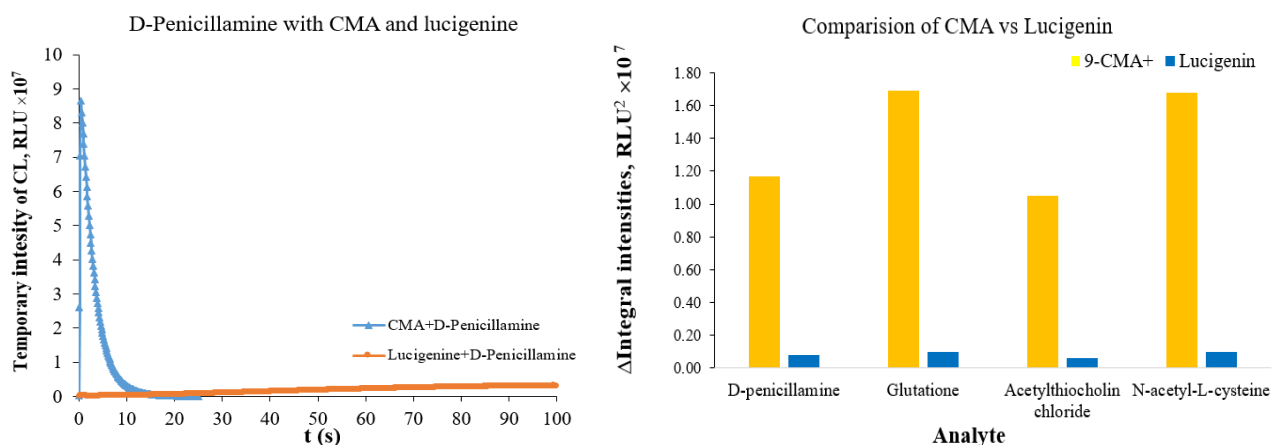


Fig. 10 (a) Comparison of kinetic profiles denoting temporary CL intensities against time for 9-CMA⁺ ($c = 2.5 \times 10^{-5}$ M) and lucigenin ($c = 2.5 \times 10^{-5}$ M) in the presence of an exemplary analyte, D-penicillamine ($c = 1.0 \times 10^{-5}$ M) in 0.5 M KOH. (b) Comparison of the areas under CL curves within a time span of 25 sec (AUC) for 9-CMA⁺ and for lucigenin in the presence of the studied substances under optimal conditions.

Based on this comparison, the 9-CMA⁺ was chosen as the chemiluminogenic indicator for the assays. The results of the chemiluminometric tests are shown in Figure 11.

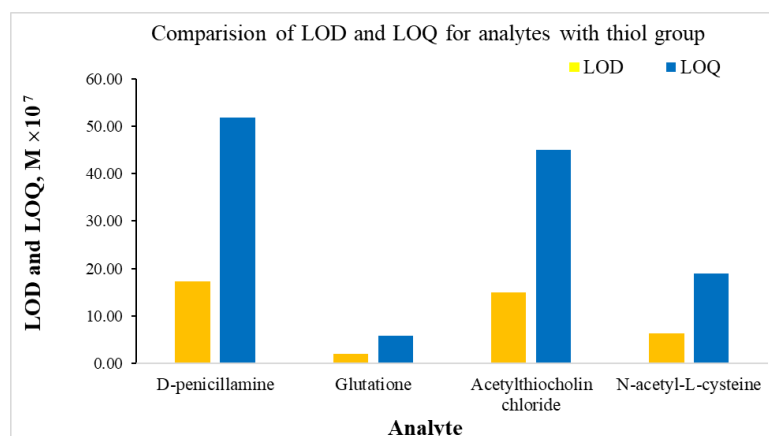


Fig. 11 Resulting LOD and LOQ of the quantification of biologically active analytes containing a thiol group.

Computational studies

Theoretical calculations for 9-CMA⁺ were also performed in collaboration with Dr. Beata Zadykowicz. My role, as in the previous work, was to compare the data obtained from theoretical calculations with experimental data. In addition, to conduct a detailed analysis of the differences in mechanisms for ATEs and 9-CMA based on $\Delta_{r,298}G^0$ values for key steps in CL generation.

The mechanism for 9-CMA (Fig. 11) is similar to that for ATEs described above. The main differences are: -it starts with O₂ as oxidising agent instead of H₂O₂. There is no need for H₂O₂ as the oxidising agent for the first step of the reaction, where RSH's anion forms ($\Delta_{r,298}G^0 = -40.8$ kcal/mol).

- ΔG for cyclisation ($\Delta_{r,298}G^0 = -32.9$ kcal/mol) is more positive than for ATEs.

For this mechanism, there are two alternative routes for the formation of 9-CMA-OOH.

First path (step II) leads to the formation of the 9-CMA-SR intermediate ($\Delta_{r,298}G^0 = -12.4$ kcal/mol) with further substitution of RS^- by OOH^- ($\Delta_{r,298}G^0 = -37.0$ kcal/mol) (step III). Second alternative path (IV) leads to the formation of 9-CMA-OOH and is more preferable due to the lowest $\Delta_{r,298}G^0 = -49.4$ kcal/mol. Both paths lead to 9-CMA-OO⁻ anion formation (step V) ($\Delta_{r,298}G^0 = -33.7$ kcal/mol). The bottleneck of this reaction is the VIth step of the reaction, where 9-CMA-OO⁻ (cyclic form) forms ($\Delta_{r,298}G^0 = 3.8$ kcal/mol). This step leads to the formation of the unstable transitional product, which, upon further decomposition, leads to the formation of acridone [10-MA⁺] and CL generation. But as compared to ATEs, the formation of [10-MA]^{*} is more favourable owing to the lowest ($\Delta_{r,298}G^0 = -83.0$ kcal/mol).

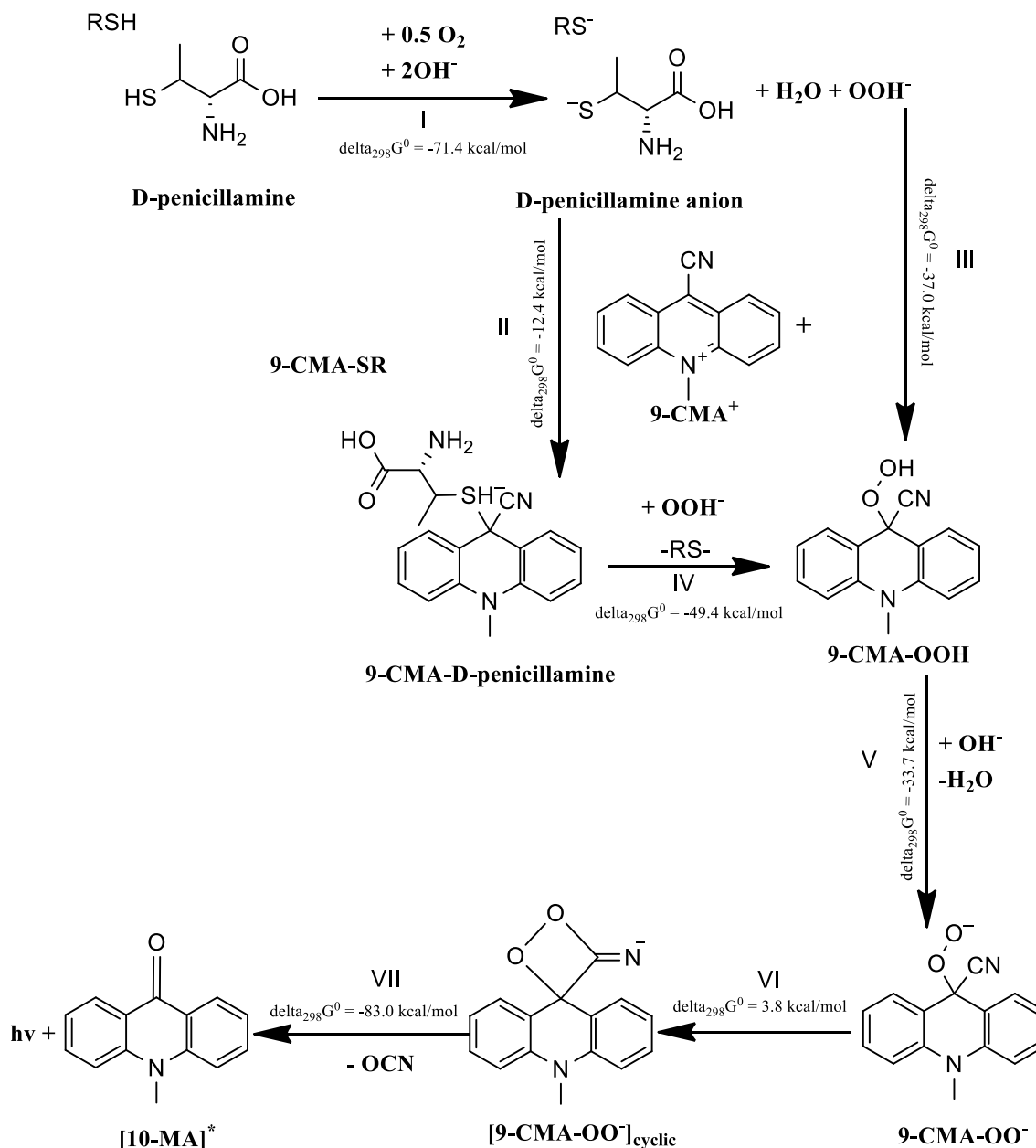


Fig. 12 Transformation pathways resulting in the chemiluminescence of 9-CMA⁺ in an alkaline medium, involving D-penicillamine as the studied analyte (RSHs) and molecular oxygen, based on DFT calculations.

Table 8: Thermodynamic data related to the elementary steps of chemiluminogenic transformations of 9-CMA⁺ cations in alkaline environments with D-penicillamine

No.	Process	aqueous phase
		$\Delta_{r,298}G^0$
I	$\text{RSH} + \frac{1}{2}\text{O}_2 + 2\text{OH}^- \rightarrow \text{RS}^- + \text{OOH}^- + \text{H}_2\text{O}$	-40.8
II	$9\text{-CMA}^+ + \text{OOH}^- \rightarrow 9\text{-CMA-OOH}$	-49.4
III	$9\text{-CMA}^+ + \text{RS}^- \rightarrow 9\text{-CMA-SR}$	-12.4
IV	$9\text{-CMA-SR} + \text{OOH}^- \rightarrow 9\text{-CMA-OOH} + \text{RS}^-$	-37.0
V	$9\text{-CMA-OOH} + \text{OH}^- \rightarrow 9\text{-CMA-OO}^- + \text{H}_2\text{O}$	-33.7
VI	$9\text{-CMA-OO}^- \rightarrow 9\text{-CMA-OO (cyclic form)}$	3.8
VII	$9\text{-CMA-OO (cyclic)} \rightarrow 10\text{-Me-9-acridone}^* + \text{OCN}^-$	-32.9
VIII	$10\text{-Me-9-acridone}^* \rightarrow 10\text{-Me-9-acridone} + h\nu$	-83.0

$\Delta_{r,298}H^0$ and $\Delta_{r,298}G^0$ (both in kcal mol^{-1}), respectively, represent the enthalpy and Gibbs' free energy (gaseous phase) or free energy (aqueous phase) of the corresponding process at standard temperature and pressure.

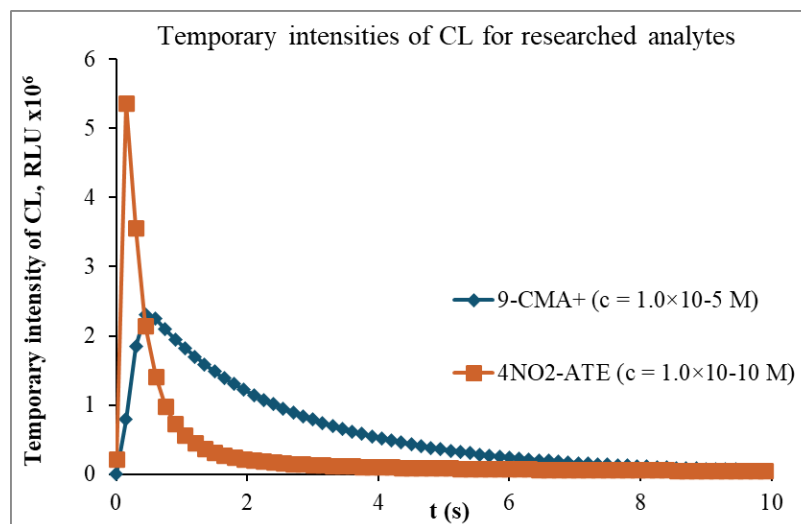
Conclusions

In the research of acridinium derivatives, novel chemiluminescent systems were developed and successfully applied for the sensitive detection of biologically relevant antioxidants (dithiothreitol, glutathione, quercetin) with favourable analytical parameters (LOD/LOQ: $0.7\text{--}2.7 \times 10^{-6}$ M). Two complementary approaches were explored: the use of newly synthesised acridinium thioesters (ATEs) and high-purity 9-cyano-10-methylacridinium salts (9-CMA), both of which demonstrated strong analytical potential.

Experimental investigations of selected ATE derivatives revealed significant solvent-dependent effects on emission efficiency, with 4NO₂-ATE and 2MeO-ATE emerging as the most promising indicators. These findings were supported by quantum-chemical DFT and TD-DFT calculations, which indicated favourable adduct formation between ATEs and antioxidant anions, facilitating the generation of hydroperoxy ions (OOH⁻) and enhancing the chemiluminescence process. UV-Vis spectroscopy further confirmed these interactions through distinctive absorption changes.

In parallel, a new luminometric method based on 9-CMA was developed for the quantification of thiol-containing compounds, including NAC, glutathione, D-penicillamine, and ATC. This method benefits from a simple setup, does not require hydrogen peroxide, and achieves excellent sensitivity (LOD: 0.19–1.73 μM , LOQ: 0.59–5.19 μM), with glutathione yielding the lowest detection limits. The necessity of using highly pure 9-CMA ($\geq 99.9\%$) for accurate results was emphasised, and its purity can be reliably monitored via RP-HPLC with Fluorescence detection.

Quantum-chemical modelling demonstrated possible mechanisms of CL generation involving 9-CMA and ATE in the presence of organosulfur compounds, which appear to be similar in the sense that it is possible to generate the OOH⁻ anion without the addition of hydrogen peroxide. This means that both systems can generate chemiluminescence under these conditions. However, my experimental studies have shown that emission in the ATE systems does not occur without the addition of H₂O₂, unlike the systems containing 9-CMA. This is likely due to the substantially increased electron deficiency caused by the presence of the cyano group. Another experimentally observed difference in the CL measurements is much lower emission efficiency of the 9-CMA-based systems (**Fig. 12**) (2.1×10^6 RLU for 9-CMA⁺ ($c = 1.0 \times 10^{-5}$ M) and 5.4×10^6 RLU for 4NO₂-ATE ($c = 1.0 \times 10^{-10}$ M), which is probably related to the low probability of forming a dioxetane intermediate (ΔG is slightly positive). The key role of molecular oxygen in the oxidation



mechanism supports a revised pathway for chemiluminogenic oxidation under alkaline conditions for both substrates.

Fig. 12 Comparison of CL temporary intensities for 4NO₂-ATE derivative vs 9-CMA for organosulfur compounds determination 9-CMA⁺ ($c = 1.0 \times 10^{-5}$ M) and 4NO₂-ATE ($c = 1.0 \times 10^{-10}$ M)

Together, these studies demonstrate the versatility and robustness of acridinium-based chemiluminescent systems, offering powerful tools for the analytical detection of biologically active substances with high sensitivity, selectivity, and mechanistic insight.

Part II. Spectroscopic and computational studies of the TADF mechanism of the TMCz-BO compound as a promising deep-blue emitter for OLED technology

In this research, we focus on the spectroscopic properties and TADF mechanism of the TMCz-BO compound (**Figure 13**). This compound is of particular interest due to its unique molecular design, which combines a boron-containing moiety with a carbazole backbone [86]. The inclusion of boron in the molecular structure influences the electronic properties and enhances the TADF characteristics, making it a promising candidate for deep blue emission. As was mentioned in the Introduction, minimal roll-off of the TMCz-BO-based devices suggests excellent stability and strong potential for commercialisation in blue OLEDs. Considering the exceptional TADF properties of the TMCz-BO emitter and the importance of understanding the enhanced rISC mechanism for further progress in blue OLED technology, we investigated the photophysics of this emitter in various environments.

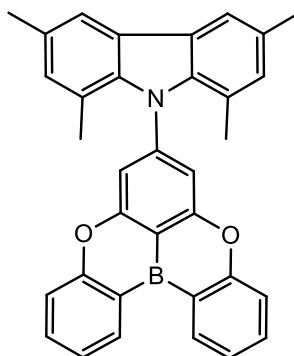


Fig. 13. Structure of the TMCz-BO molecule

Within this research project, we aimed to elucidate the complex photophysical behaviour of the TMCz-BO emitter, which is characterised by the coexistence of two singlet and three triplet excited states, setting it apart from more conventional DA emitters, which typically involve two or three key excited states. Our findings suggest that the TADF mechanism in TMCz-BO extends well beyond the two- or three-state rISC model, and even foundational principles of the static quantum model may need to be revised to account for the intense mixing of the excited states.

The study is divided into two main parts: experimental spectroscopic studies and quantum chemical calculations. The experimental work involves detailed photophysical characterisation, including absorption, emission, and time-resolved spectroscopy, to investigate the TADF properties and overall emission behaviour of the compound. These studies are complemented by quantum chemical calculations, which provide insights into the electronic structure, excited state dynamics, and the factors influencing the rISC process in this molecule.

Experimental part

Sample preparation, measurements, and calculations

TMCz-BO was synthesised following the preparation protocol outlined in [87]. The results of the analyses confirmed both the identification and purity of the compound. Spectroscopic-grade solvents were utilised for solvatochromic measurements, and all reagents were obtained and used without additional purification.

Films were prepared on quartz glass using a solution-processing technique, specifically through spin-coating from CHCl_3 solutions containing the emitter and a suitable host. If necessary, an ultrasonic bath, ULTRON, was used before spin-coating to enhance solubility.

Steady-state PL spectra were acquired using an FS5 spectrofluorometer (Edinburgh Instruments, UK) in the front-face excitation geometry, with a spectral resolution of 1 nm. Absolute PLQY were determined using an integrating sphere integrated into the Quantaurus-QY Absolute PL Quantum Yield Spectrometer. Steady-state phosphorescence spectra in solution were recorded at 77 K in a liquid nitrogen-cooled quartz dewar, using a Varian spectrofluorometer with a delay time of 50 ms and a time gate of 0.5 s.

Time-resolved PL measurements were conducted using a custom setup comprising a pulsed Nd: YAG laser (PL2251A, EKSPLA) coupled with an optical parametric generator (PG 401/SH) as the excitation source, and a 2501S grating spectrometer (Bruker Optics) combined with a streak camera (C4334-01, Hamamatsu) for detection. The system included a double-stage high-vacuum pump (T-Station 85, Edwards). To minimise scattering, reflections, and second-order artefacts, high-performance optical filters were employed in the excitation path, including a 325/50 bandpass (BP) filter and a 375 nm longpass (LP) filter (Edmund Optics) [88]. Streak camera images were integrated over a defined wavelength range to generate PL intensity decay curves. Phosphorescence spectra in films were collected using a closed-cycle helium cryostat (APD DE-202) and a temperature controller (LakeShore 336).

Quantum chemical calculations were conducted at the DFT/TD-DFT level of theory using the Gaussian 16 program package [89]. The B3LYP [90] functional was used with cc-pvdz basis set [91] for geometry optimizations in different electronic states were performed, and spin-orbit coupling (SOC) constants were calculated using the ORCA 4.2 software package [92] with B3LYP functional and DEF2-TZVP [93] basis set with included relativistic zero-order regular approximation (ZORA) [94].

Steady-state absorption and PL in liquid solutions

Stationary and time-resolved spectroscopies investigated the nature and relative alignment of electronic states. In methylcyclohexane (MCH), TMCz-BO shows a narrow, intense long-wavelength absorption band with a molar extinction coefficient of $15,100 \text{ M}^{-1} \text{ cm}^{-1}$ at 378 nm (**Fig. 14A**). This is unusual for D-A type TADF emitters, which typically exhibit broad, low-intensity CT bands and have much lower ϵ below 2000 cm^{-1} [95]. Instead, TMCz-BO's absorption resembles that of the isolated BO acceptor, indicating a locally excited $S_0 \rightarrow S_1$ transition ($S_0 \rightarrow {}^1\text{LE}_A$). The slightly broadened blue edge most likely shows a higher-energy

$S_0 \rightarrow {}^1CT$ transition that overlaps with the $S_0 \rightarrow {}^1LE_A$ transition. Identical spectra in various solvents, including polar DMSO, confirm the absence of solvatochromism, indicating that the $S_0 \rightarrow S_1$ transition forms a singlet locally excited state 1LE_A on the acceptor fragment independently of the medium. At 77 K, increasing solvent polarity shifts the Fluorescence maximum from 385 nm in MCH to 445 nm in DMSO (Fig. 14B). While the emission remains structured in less polar solvents, it becomes broad and featureless in highly polar ones, indicating a growing 1CT character in the S_1 state, dominant in DMSO.

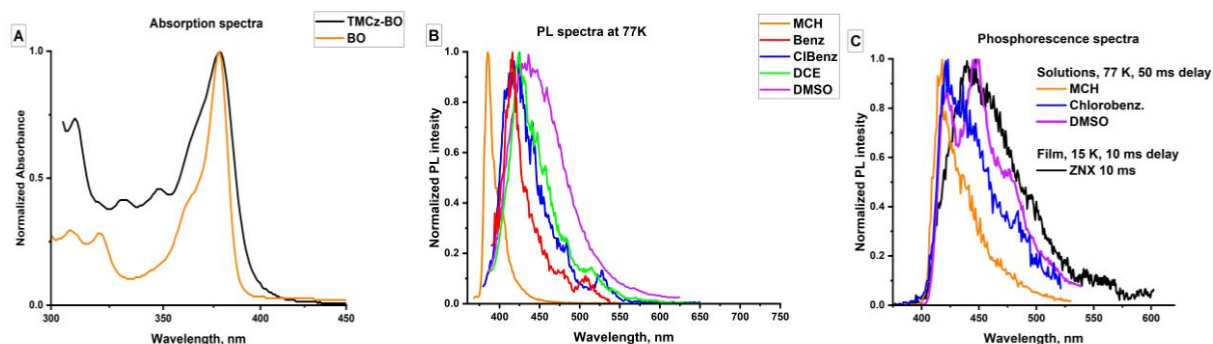


Figure 14. Absorption spectra of TMCz-BO and the isolated acceptor (BO) in MCH (A). Emission spectra of TMCz-BO in various solvents: PL at 77K (B) and phosphorescence at 77K (C). For details, see the Results and discussion section in **P3**.

PL properties

The temperature-dependent solvatofluorochromic studies suggest that at room temperature, the S_1 state of TMCz-BO exhibits a dual nature. Depending on the medium, either the 1LE_A or 1CT character may dominate, or both may contribute. These conclusions have significant consequences for the TADF mechanism. Namely, as was mentioned above, rISC usually occurs from the triplet state (T_1) to the singlet state (S_1) due to the small energy gap (ΔE_{ST}) between these states. rISC from the triplet state to the singlet excited state S_2 is generally not common because the S_2 state, especially of LE nature, is usually energetically much higher.

The triplet state nature was analysed using phosphorescence spectra at 77K. In MCH, the phosphorescence spectra of TMCz-BO and BO are similar (SI section of **P3**), indicating a 3LE_A character for T_1 . As polarity increases in solvents like benzene, chlorobenzene, and DCE, the spectra shift and broaden, suggesting a growing 3CT contribution (**Figure 14C**). In DMSO, TMCz-BO unexpectedly exhibits phosphorescence resembling that of the donor fragment TMCz (SI section of **P3**), possibly due to DMSO's high nucleophilicity, which stabilises the triplet state on the donor (3LE_D). Therefore, at least three triplet states can take part in photophysical processes.

Figure 15 presents a qualitative alignment of the lowest excited states at 77K, according to a static quantum model that assumes no mixing of electronic states. The energies of the 1CT and 1LE_A states were determined by deconvoluting PL spectra in a benzene solution of TMCz-BO at 77K. In contrast, the triplet states 3LE_A , 3CT , and 3LE_D were estimated from phosphorescence spectra in MCH, benzene, and DMSO solutions,

respectively. At room temperature, variations in polarity, solvent relaxation, and specific medium effects can alter this state alignment.

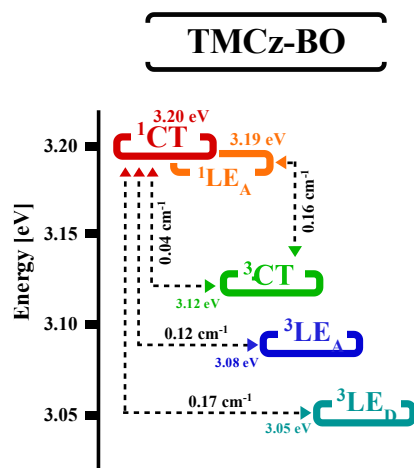


Fig. 15. Energy diagram of the lowest excited states of TMCz-BO at 77K with TDDFT-predicted SOC values

There are thus at least five excited states of close energy: $^1\text{LE}_\text{A}$, ^1CT , $^3\text{LE}_\text{A}$, ^3CT , and $^3\text{LE}_\text{B}$, which can participate in photophysical processes.

TADF mechanism in various media.

We compared the impacts of different viscosity and polarity media on the TMCz-BO TADF behaviour. For our research, we used liquid solutions with varying polarities as media with low viscosity, and various types of polymers or solid matrixes with different polarities as media with high viscosity, namely, nonpolar Zeonex® (ZNX), polar bis[2-(diphenylphosphino)phenyl]ether oxide (DPEPO), and polymethyl methacrylate (PMMA) with medium polarity.

Table 9. Photophysical properties in liquid solutions and amorphous films

Medium	PL _{max}	PL _{onset} / E _{S1}		k _{ISC}	k _{rISC}
	[nm]	[nm / eV]		[10 ⁶ s ⁻¹]	
Solutions					
MCH	405	386	3.21	-	-
Tol.-hex. 1/3 (v/v)	424	389	3.19	2.4	2.3
Benzene	450	408	3.04	4.5	2.7
Chlorobenzene	482	415	2.99	9.5	2.9
DCE	519	434	2.86	12	3.5
DMSO	557	451	2.75	14	3.7
Films					
ZNX	411	377	3.31	73	1.8×10 ⁻²
PMMA	430	381	3.25	21	3.1×10 ⁻²
DPEPO	459	411	3.02	10	0.14

Only MCH solutions lack TADF. Both Fluorescence and phosphorescence originated from LE_A states.

Under these low-viscosity, low-polarity conditions, TMCz-BO behaves as an LE emitter rather than a CT one. We noted that the significant role of the 1LE_A character in the S_1 state leads to slower ISC via the $^1LE_A \rightarrow T_n$ transition mechanism.

In the ZNX film, where polarity remains low and viscosity increases sharply, fluorescence remains the same, but phosphorescence at 15K shows a marked difference from that in MCH frozen glass. While both exhibit similar onset values, the ZNX phosphorescence no longer resembles pure 3LE_A emission in shape. Furthermore, despite having identical E_{S1} values for ZNX and MCH, TMCz-BO serves as a rare example of UV-blue TADF with a reasonable rISC rate and a microsecond-range DF lifetime. Within this medium, the substantial contribution of the 1LE state supports narrow-band emission. Meanwhile, the viscosity effect ensures that both the S_1 and T_1 states exhibit **significant CT character**, allowing them to act as intermediaries for rISC. This represents an unconventional case of an inverted three-state rISC mechanism following the pathway $^3LE_i \rightleftharpoons ^3CT \rightleftharpoons ^1CT \rightleftharpoons ^1LE_A$. In contrast, typical D-A emitters leverage the 3LE state as the mediator for the $^3CT \rightleftharpoons ^1CT$ transition, operating via the $^3CT \rightleftharpoons ^3LE_i \rightleftharpoons ^1CT$ mechanism, as was mentioned in the introduction.

Based on spectroscopic analysis at low temperatures and room temperature, we can conclude that in more polar media, fluorescence becomes broader, which indicates higher stability of the CT states. Under those conditions, the CT-CT channel becomes essential for the rISC mechanism. Moreover, in high-viscosity media, **regardless of polarity, tMCzBO behaves more as a CT emitter**. That leads to higher values of ISC and rISC rate constants. In polar environments, the stabilised $^1CT \rightarrow T_n$ mechanism results in higher ISC rates.

In different polarity media, the mechanism of rISC can be explained by a two-state $T_1 \rightarrow S_1$ model. The linear dependence of $\ln(k_{rISC})$ on E_{S1} in Fig. 16 confirms this assumption. To explain the experimental dependency, we modelled rISC rates using 3CT - 1CT transition SOC values and with a higher constant SOC value (0.44 cm^{-1}). Those models were unable to describe the exact rISC dependence on polarity, which is why we concluded that SOC is also dependent on polarity. This model is introduced in Figure 16, marked in red.

Numerical solutions of k_{rISC} equations using $\Delta E_{3CT \rightarrow 1CT}$ yielded varying SOC constants, from 0.051 cm^{-1} (toluene-hexane mixture) to 0.038 cm^{-1} (DMSO) (**Fig. 16**). This provides the conclusion that SOC depends on the energy of the excited state. Notably, **it indicates that the nature of S_1 and T_1 depends on the polarity of the medium.**

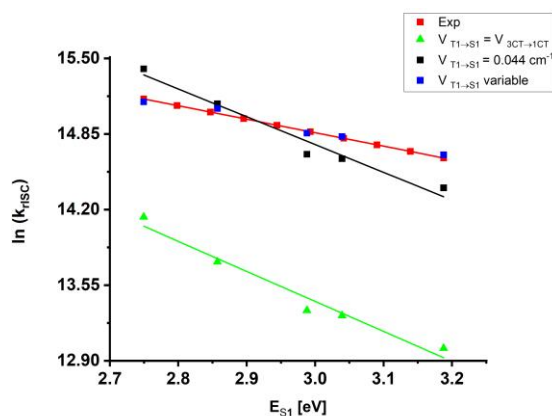


Fig. 16. Comparison of k_{rISC} calculations using different approaches with experimental values.

To explain such a peculiarity, we calculated SOC values for various possible S-T transitions. Considering that ISC and rISC values have a strong dependence on media viscosity, we assumed that molecular vibrations influenced them. That's why we researched how molecular vibrations impact SOC values for various possible S-T transitions.

Rotational isomerism and excited-state mixing

From the perspective of the TADF mechanism, molecular vibrations that alter the dihedral angle (θ) between the donor (D) and acceptor (A) are crucial (**Fig. 17**). Such θ -rotations have the most substantial effect on the $^1\text{CT} \rightleftharpoons ^3\text{CT}$ transition in TMCz-BO, affording SOC increase. The SOC value for the $^1\text{CT} \rightleftharpoons ^3\text{CT}$ increases from 0 cm^{-1} in the $\theta = 90^\circ$ isomer to 0.11 cm^{-1} in the $\theta = 60^\circ$ isomer (see “Dependence of electronic parameters on the dihedral angle between donor and acceptor fragments (θ)” section in the SI of the **P3**).

For the $^1\text{CT} \rightleftharpoons ^3\text{LE}_A$, $^3\text{LE}_D$ transitions, SOC values were calculated, and those transitions have the highest SOC values (0.12 cm^{-1} for $^1\text{CT} \rightleftharpoons ^3\text{LE}_A$ and 0.17 cm^{-1} for $^1\text{CT} \rightleftharpoons ^3\text{LE}_D$), but these transitions are weakly affected by the change of θ . Despite being weakly influenced by changes in θ , these high SOC values facilitate efficient reverse intersystem crossing (rISC), distinguishing this system from others.

Transitions, namely $^1\text{LE}_A \rightleftharpoons ^3\text{LE}_A$ and $^1\text{LE}_A \rightleftharpoons ^3\text{LE}_D$, are almost completely forbidden. This leads to an important conclusion that **the contribution of $^1\text{LE}_A$ should thus decrease the total SOC constant of $\text{S}_1 \rightleftharpoons \text{T}_1$ transitions. That's why in non-polar media such as MCH and ZNX, the rISC constant values are low.**

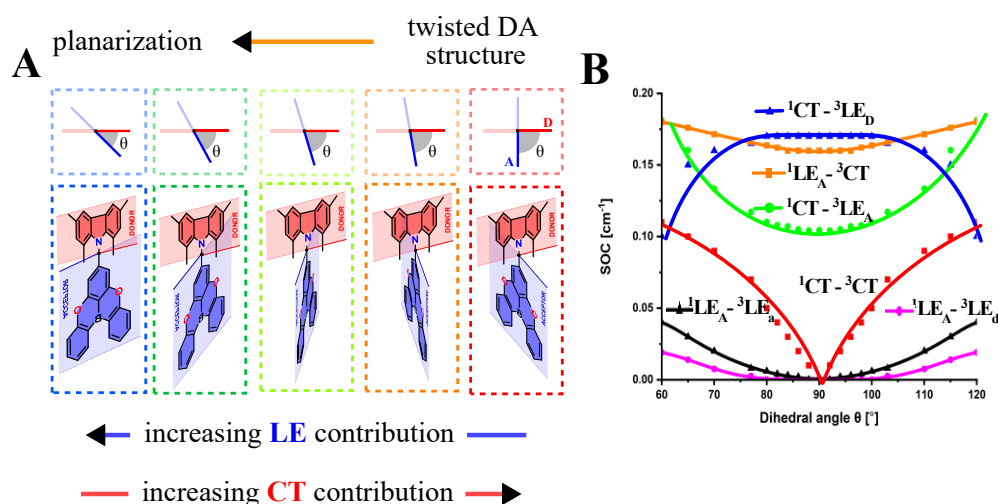


Fig. 17 Distribution of the θ values for rotamers at room temperature (A). Dependences of the electronic state energy from SOC values (B).

Therefore, the following observations can be made based on the experimental observations:

- The S_1 and T_1 states of TMCz-BO exhibit a multifaceted nature in low-viscosity media at room temperature, where molecular vibrations and solvent relaxation show minimal or negligible energetic barriers.
- In solutions, the rISC mechanism is described using a two-state T_1 - S_1 model.
- However, SOC values depend on the solvent polarity which cannot be described with a two-state model.

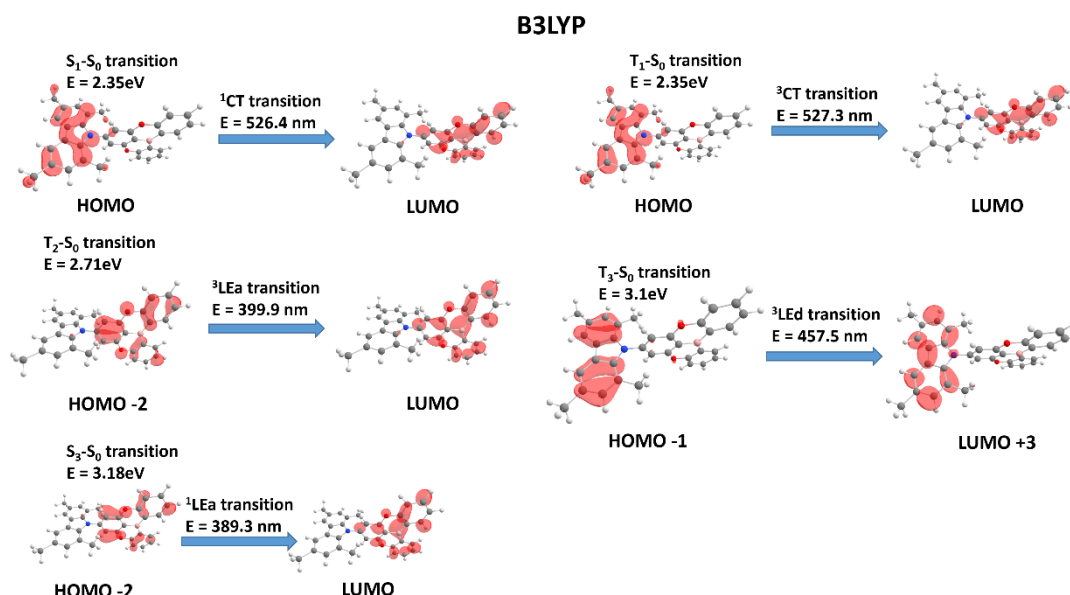


Fig. 18 Profiles of molecular orbitals calculated using the B3LYP method

Computational studies at various levels of theory are in alignment with the experimentally observed 5 excited states of different nature and multiplicity. While the predicted energy of a given state varies depending on the computational method, analysis of the transition molecular orbitals confirms the

coexistence of the five lowest excited states (**Fig. 18**). The singlet state localised on the TMCz donor, $^1\text{LE}^D$, lies above 3.8 eV and is not involved in photophysical processes.

However, the calculated SOC values predicted for various pairs of excited S and T states do not explain the dependence of SOC on medium properties. For this reason, for liquid solutions, we proposed the concept of **dynamic excited-state mixing (DESM)** (**Fig. 19C**). Such an electronic effect implies dual ^1CT – $^1\text{LE}_A$ nature of the S_1 state and triple ^3CT – $^3\text{LE}_A$ – $^3\text{LE}_D$ nature of the T_1 state (**Fig. 19A**). To assess the scale of DESM and its solvent-dependent evolution, we estimated spin-flip transition contributions by fitting empirical SOC constants to TD-DFT-predicted $V_{Tn \rightarrow Sn}$ values (**Fig. 19B**). Considering the reduced LE character in higher polarity and assuming equal contributions from $^3\text{LE}_A$ and $^3\text{LE}_D$ states, the rotationally activated $^3\text{CT} \rightarrow ^1\text{CT}$ channel dominates across all media, increasing from 50% to over 85% with polarity. Transitions involving $^1\text{LE}_A$ are significant in low-to-medium polarity solvents ($E_{SI} < 3.0$ eV) but diminish in more polar media, where $^3\text{LE}_A \rightarrow ^1\text{CT}$ and $^3\text{LE}_D \rightarrow ^1\text{CT}$ account for 15–20% of rISC. These estimates depend on $\Delta E_{3\text{CT} \rightarrow 1\text{CT}}$ and may vary with higher ΔE_{T1-S1} gaps.

For the amorphous film media, where solvent and structural relaxation, as well as some of the molecular vibrations, are inhibited, **static excited-state mixing (SESM)** was introduced (**Fig. 19C**). Vibrations that facilitate SESM take place within local energy minima specific to each individual, or θ -rotamer. In this scenario, for a set of rotamers sharing the same θ value, processes like emission, ISC, and rISC follow distinct mechanisms unique to that rotamer. The differences in the θ -rotamer distribution and occurrence of DESM or SESM explain the different behaviour of TMCz-BO in film and solutions. However, the presence of numerous emitting species in amorphous solid media makes the modelling of SESM very challenging.

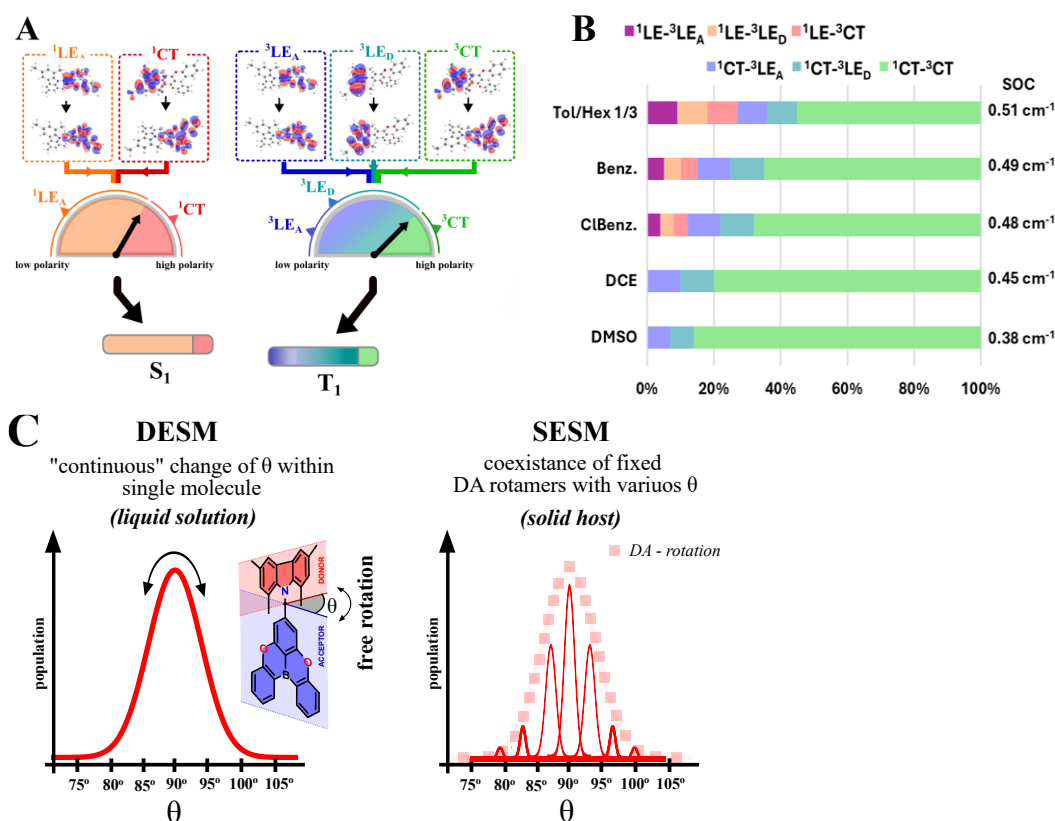


Fig. 19 The resulting dual and triple characters of S1 and T1 states (A), contributions of various electronic transitions in rISC values in various solutions estimated from empirical SOC (B), Differences in the θ -rotamer distribution for the DESM and SESM mechanisms in liquid solution and solid host, respectively (C).

Conclusions of the PhD thesis

In this PhD work, I explored the photophysical behaviour and applications of two essential classes of luminescent compounds: acridinium salts and a carbazole derivative. Both classes of compounds share a common structural feature: they are nitrogen-containing heterocyclic organic molecules with pronounced luminescent properties. The photoluminescence and chemiluminescence light emission from both types of those compounds relies on a series of electron transfer processes, mainly or partly due to the key role of the nitrogen atom.

In Part I of my research work, novel acridinium-based chemiluminescent systems, acridinium thioester derivatives, and 9-CMA were developed and applied to determine antioxidant activity and detect thiol-containing compounds.

During the experimental studies, I identified two acridinium thioester derivatives — 4NO₂-ATE and 2MeO-ATE—as the most promising candidates, based on their chemiluminescence emission profiles. Additionally, I established optimal conditions for chemiluminescence generation using acridinium thioesters as substrates, guided by the observed solvent-dependent variations in emission efficiency. The developed chemiluminescent systems for antioxidant detection demonstrate low detection limits (LOD/LOQ: 0.7–2.7×10⁻⁶ M).

Regarding the method containing 9-CMA, I focused on evaluating the optimal conditions for the detection procedure. This original method was applied for the identification of thiol-containing compounds, such as N-acetyl-L-cysteine, D-penicillamine, glutathione, and acetylthiocholine chloride. I achieved a sensitivity range of LOD: 0.19–1.73 μM, and the precision did not exceed 10% RSD, with glutathione as the most detectable analyte. The purity of 9-CMA (≥99.9%) proved critical and was monitored via RP-HPLC with Fluorescence detection.

The chemiluminescence mechanisms in studied compounds were confirmed by quantum-chemical DFT and TD-DFT calculations. In contrast to ATEs, it was revealed that in 9-CMA, molecular oxygen is sufficient to initiate the reaction as an oxidant, with no need for H₂O₂ as a common oxidising agent. The calculations also supported favourable intermediate products (HATE-OOH, 9-CMA-OOH) that lead to the chemiluminescence process. UV-Vis spectroscopy confirmed these interactions through characteristic absorption changes.

The primary purpose of Part II was to understand and explain the excellent performance of TMCz-BO as an OLED emitter. During our research work, which combined fluorescence and phosphorescence spectroscopies with DFT calculations, I successfully elucidated the mechanism of triplet harvesting and light emission in this emitter.

Unlike conventional D-A emitters, TMCz-BO shows a complex photophysical behaviour characterised by:

- five coexisting excited states of close energy,

- SOC values are dependent on the solvent polarity,
- molecular vibrations that influence strongly the electronic parameters and as a result rISC rate. The most critical vibrations change the dihedral angle between the donor and acceptor.

On the example of TMCz-BO, the current understanding of the TADF mechanism in solutions is enriched by a dynamic excited states mixing model, which implies a dual $^1\text{CT}-^1\text{LE}_\text{A}$ nature of the S_1 state and a triple $^3\text{CT}-^3\text{LE}_\text{A}-^3\text{LE}_\text{D}$ nature of the T_1 state. For the amorphous films, we concluded that the best way to describe state mixing would be the SESM model, which considers inhibited structural relaxation and molecular vibrations under high viscosity. While these findings also correlate with the results for different emitters, they put further demands for developing of experimental and modelling techniques to investigate complex systems for advanced stable and efficient deep-blue emitters.

Literature cited

- ¹ K. D. Gundermann, F. McCapra, *Springer: Berlin-Heidelberg*, 1987, 23.
- ² A. Roda, P. Pasini, M. Guardigli, M. Baraldini, M. Musiani, M. Mirasoli, *Fresenius J. Anal. Chem.*, 2000, 366, 752. <https://doi.org/10.1007/s002160051569>
- ³ M. Nakazono, S. Nanbu, T. Akita, K. Hamase, *Dyes Pigment.*, 2019, 170, 107628. <https://doi.org/10.1016/j.dyepig.2019.107628>
- ⁴ L. Ren, H. Cui, *Luminescence*, 2014, 29, 929–932. <https://doi.org/10.1002/bio.2643>
- ⁵ K. Smith, Z. Ahmed, J.S. Woodhead, G.A. El-Hiti, *J. Oleo Sci.* 2023, 460, 447–460. <https://doi.org/10.5650/jos.ess22327>
- ⁶ Y. Lan, F. Yuan, T. H. Fereja, C. Wang, B. Lou, J. Li, G. Xu, *Anal. Chem.*, 2019, 91, 2135. <https://doi.org/10.1021/acs.analchem.8b04670>
- ⁷ L. A. Montano, J. D. Ingle, *Anal. Chem.*, 1979, 51, 919. <https://doi.org/10.1021/ac50043a032>
- ⁸ H. H. Wang, *Semiconductor Nanomaterials for PLEXible Technologies*, 2009, 247–273. <https://doi.org/10.1016/B978-1-4377-7823-6.00009-X>
- ⁹ K. Kamino, N. Kadakia, F. Avgidis, Z. X. Liu, K. Aoki, T. S. Shimizu, T. Emonet, *Proc. Natl. Acad. Sci. U.S.A.*, 2023, 120, <https://doi.org/10.1073/pnas.2211807120>
- ¹⁰ F. McCapra, *Acc. Chem. Res.*, 1976, 9, 201. <https://doi.org/10.1021/ar50102a001>
- ¹¹ G. Zomer, J. F. C. Stavenuiter, R. H. Van den Berg, E. H. J. M. Jansen, *Pract. Spectrosc.*, 1991, 12, 505.
- ¹² C. Dodeigne, L. Thunus, R. Lejeune, *Talanta*, 2000, 51, 415. [https://doi.org/10.1016/s0039-9140\(99\)00294-5](https://doi.org/10.1016/s0039-9140(99)00294-5)
- ¹³ G. Zomer, M. Jacquemijns, A.M. Garcia-Campana, *W.R.G. Baeyens, eds.*, 2001, 529–49.
- ¹⁴ K. Krzysiński, A. Ożóg, P. Malecha, A. D. Roshal, A. Wróblewska, B. Zadykiewicz, J. Błażejowski, *J. Organomet. Chem.*, 2011, 76, 1072. <https://doi.org/10.1002/bio.4162>
- ¹⁵ "Overview of ELISA." *Thermo Fisher Scientific*, www.thermofisher.com/pl/en/home/life-science/protein-biology/protein-biology-learning-center/protein-biology-resource-library/pierce-protein-methods/overview-elisa.html. Accessed 26 Apr. 2025.
- ¹⁶ L. Cinquanta, D. E. Fontana, N. Bizzaro, *Auto-Immun. Highlights*, 2017, 8(1), 9. <https://doi.org/10.1007/s13317-017-0097-2>
- ¹⁷ T. Mahmood & C. Yang, (2012). *N. Am. J. Med. Sci.*, 4(9), 429. <https://doi.org/10.4103/1947-2714.100998>
- ¹⁸ A. Natrajan, D. Wen, *Org. Biomol. Chem.*, 2015, 13(5), 1503–1509. <https://doi.org/10.1039/c4ob02528h>
- ¹⁹ W. L. Hinze, T. E. Riehl, H. N. Singh, Y. Baba, *Anal. Chem.*, 1984, 56 (12), 2180. <https://doi.org/10.1021/ac00276a046>
- ²⁰ B. Zadykiewicz, J. Czechowska, A. Ożóg, A. Renkevich, K. Krzysiński, *Org. Biomol. Chem.*, 14, 2016, 652–668. <https://doi.org/10.1039/C5OB01798J>
- ²¹ K. Krzysiński, A.D. Roshal, B. Zadykiewicz, A. Białk-Bielińska, A. Sieradzan, *J. Phys. Chem. A*, 2010, 114, 10550–10562. <https://doi.org/10.1021/jp104253f>

-
- ²² J. Darkwa, C. Mundoma, R. H. Simoyi, *J. Chem. Soc., Faraday Trans.* 1998, 94(14), 1971.
<https://doi.org/10.1039/a708863i>
- ²³ M. Y. Blazheevskiy, N. Y. Bondarenko, *Methods Objects Chem. Anal.* 2011, 6, 124.
- ²⁴ A. Wróblewska, O. M. Huta, I. O. Patsay, R. S. Petryshyn, J. Błażejowski, *J. Therm. Anal. Calorim.*, 2003, 507(2), 229-236. <https://doi:10.1016/j.aca.2003.11.032>
- ²⁵ A. Wróblewska, O. M. Huta, S. V. Midyanyj, I. O. Patsay, J. Rak, and J. Błażejowski, *J. Org. Chem.*, 2004, 69, 5, 1607–1614 <https://doi.org/10.1021/ja00251a024>
- ²⁶ J. U. Kim, I. S. Park, C.-Y. Chan, M. Tanaka, Y. Tsuchiya, H. Nakanotani, and C. Adachi, *Nat. Commun.*, 2020, 11, 1765. <https://doi.org/10.1038/s41467-020-15558-5>
- ²⁷ B. Minaev, G. Baryshnikov, H. Agren, *Phys. Chem. Chem. Phys.*, 2014, 16, 1719-1758.
<https://doi.org/10.1039/C3CP53806K>
- ²⁸ J. Jayabharathi, V. Thanikachalam, S. Thilagavathy, *Coord. Chem. Rev.*, 2023, 483, 215100.
<https://doi.org/10.1016/j.ccr.2023.215100>
- ²⁹ T. Zhang, J. Miao, M. U. Ali, M. Shi, Y. He, T. Fu, H. Meng, *Dyes and Pigments*, 2020, 180, 108477.
<https://doi.org/10.1016/j.dyepig.2020.108477>
- ³⁰ P. K. Samanta, D. Kim, V. Coropceanu, J. L. Brédas, *J. Am. Chem. Soc.*, 2017, 139, 4042–4051.
<https://doi.org/10.1021/jacs.6b12124>
- ³¹ Y. Tao, K. Yuan, T. Chen, P. Xu, H. Li, R. Chen, C. Zheng, L. Zhang, W. Huang, *Adv. Mater.*, 2014, 26, 7931–7958. <https://doi.org/10.1002/adma.201401502>
- ³² I. E. Serdiuk, M. Monka, K. Kozakiewicz, B. Liberek, P. Bojarski, S. Y. Park, *J. Phys. Chem. B*, 2021, 125, 10, 2696–2706. <https://doi.org/10.1021/acs.jpccb.0c10605>
- ³³ H. Uoyama, K. Goushi, K. Shizu, H. Nomura, C. Adachi, *Nature*, 2012, 492, 234.
<https://doi.org/10.1038/nature11687>.
- ³⁴ Z. Wang, X. Jiang, J. Xiong, B. Xiao, Y. Wang, X. Zhou, R. Pan, X. Tang, *J. Phys. Chem. Lett.*, 2024, 15, 9630–9636. <https://doi.org/10.1021/acs.jpclett.4c02311>
- ³⁵ A. Endo, M. Ogasawara, A. Takahashi, D. Yokoyama, Y. Kato and C. Adachi, *Adv. Mater.*, 2009, 21, 4802-4806. <https://doi.org/10.1002/adma.200900983>
- ³⁶ A. Endo, K. Sato, K. Yoshimura, T. Kai, A. Kawada, H. Miyazak, C. Adachi, *Appl. Phys. Lett.*, 2011, 98, 083302. <https://doi.org/10.1063/1.3558906>
- ³⁷ T. Penfold, F. Dias, & A. Monkman, *Chem. Commun.*, 2018, 54(32), 3926-3935. <https://doi.org/10.1039/C7CC09612G>
- ³⁸ J. Ochi, Y. Yamasaki, K. Tanaka, Y. Kondo, K. Isayama, S. Oda, M. Kondo, T. Hatakeyama, *Nat. Commun.*, 2024, 15, 2361. <https://doi.org/10.1038/s41467-024-46619-8>
- ³⁹ Y., X. Hu, J. Miao, T. Hua, et al. *Nat. Photon.*, 2022, 16, 803–810. <https://doi.org/10.1038/s41566-022-01083-y>
- ⁴⁰ L. S. Cui, A. J. Gillett, S. F. Zhang, et al. *Nat. Photon.*, 2020, 14, 636–642. <https://doi.org/10.1038/s41566-020-0668-z>
- ⁴¹ Y. Wada, H. Nakagawa, S. Matsumoto, et al. *Nat. Photon.*, 2020, 14, 643–649.
<https://doi.org/10.1038/s41566-020-0667-0>

-
- ⁴² H. Gao, S. Shen, Y. Qin, G. Liu, T. Gao, X. Dong, Z. Pang, X. Xie, P. Wang, and Y. Wang, *J. Phys. Chem. Lett.*, 2022, 13, 32, 7561–7567. <https://doi.org/10.1021/acs.jpclett.2c01745>
- ⁴³ R. Niu, J. Li, D. Liu, R. Dong, W. Wei, H. Tian, C. Shi, *Dyes and Pigments*, 2021, 194, 109581. <https://doi.org/10.1016/j.dyepig.2021.109581>
- ⁴⁴ X. Lv, R. Huang, S. Sun, Q. Zhang, S. Xiang, S. Ye, P. Leng, F. B. Dias, and L. Wang, *ACS Appl. Mater. Interfaces*, 2019, 11, 10758–10767. <https://doi.org/10.1021/acsami.8b20699>
- ⁴⁵ D. Xu, M. J. Hu, Y. Q. Wang and Y. L. Cui, *Molecules*, 2019, 24, 1123. <https://doi.org/10.3390/molecules24061123>.
- ⁴⁶ D. A. Averill-Bates, *Vitam. Horm.*, 2023, **121**, 109–141. <https://doi.org/10.1016/bs.vh.2022.09.002>.
- ⁴⁷ M. M. de Mecca, G. D. Castro, and J. A. Castro, *Arch. Toxicol.*, 1993, **67**(8), 547–551. <https://doi.org/10.1007/BF01969267>
- ⁴⁸ S. A. Sahasrabudhe, M. R. Terluk, and R. V. Kartha, *Antioxidants (Basel)*, 2023, **12**(7), 1316. <https://doi.org/10.3390/antiox12071316>.
- ⁴⁹ M. Pugliese, V. Biondi, E. Gugliandolo, P. Licata, A. F. Peritore, R. Crupi, and A. Passantino, *Antibiotics (Basel)*, 2021, **10**(6), 648. <https://doi.org/10.3390/antibiotics10060648>
- ⁵⁰ F. J. Dowd, *Pharmacology and Therapeutics for Dentistry*, 7th ed., 2017, pp. 82–97. <https://doi.org/10.1016/B978-0-323-39307-2.00006-0>
- ⁵¹ J.K. Labanowski, J.W. Andzelm, *Density Functional Methods in Chemistry*, Springer, New York, 1991.
- ⁵² J.-D. Chai, M. Head-Gordon, *Phys. Chem. Chem. Phys.* 10 (2008) 6615–6620. <https://doi.org/10.1039/B810189B>.
- ⁵³ P.C. Hariharan, J.A. Pople, *Theoret. Chim. Acta* 28 (1973) 213–222. <https://doi.org/10.1007/BF00533485>.
- ⁵⁴ G. Scalmani, M.J. Frisch, B. Mennucci, J. Tomasi, R. Cammi, V. Barone, *J. Chem. Phys.*, 124 (2006) 094107. <https://doi.org/10.1063/1.2173258>.
- ⁵⁵ J. M. Lourenço, J. C. G. Esteves da Silva, L. Pinto da Silva, *J. Luminescence* 194 (2018) 139–145. <https://doi.org/10.1016/j.jlumin.2017.10.025>.
- ⁵⁶ L. Pinto da Silva, C. M. Magalhães, *Int. J. Quantum Chem.* 119 (2019) e25881. <https://doi.org/10.1002/qua.25881>.
- ⁵⁷ C. M. Magalhães, P. González-Berdullas, J. C. G. Esteves da Silva, L. Pinto da Silva, *New J. Chem.* 45 (2021) 18518–18527. <https://doi.org/10.1039/D1NJ03440E>.
- ⁵⁸ K. Fukui, *Acc. Chem. Res.*, 14 (1981) 363–368. <https://doi.org/10.1021/ar00072a001>.
- ⁵⁹ M. J. Frisch, G. W. Trucks, H. B. Schlegel, G. E. Scuseria, M. A. Robb, J. R. Cheeseman, G.; Barone, V. Scalmani, G. A. Petersson, H. Nakatsuji, et al. Gaussian 16, Revision C.01 Gaussian, Inc.: Wallingford, CT, 2016.
- ⁶⁰ G.A. Zhurko, *Chemcraft*, 2005, <https://chemcraftprog.com>.
- ⁶¹ V. Ievtukhov, B. Zadykiewicz, M.Y. Blazheyevskiy, K. Krzysiński, *Luminescence*, 2022, 37, 208–219. <https://doi.org/10.1002/bio.4162>.
- ⁶² A. Natrajan, D. Wen, *Org. Biomol. Chem.*, 2015, 13, 2622–2633. <https://doi.org/10.1039/C4OB02528H>.
- ⁶³ J. F. Huertas-Pérez, D. Moreno-González, D. Airado-Rodríguez, F.J. Lara, A.M. García-Campaña, *Trends Anal. Chem.*, 2016, 75, 35–48. <https://doi.org/10.1016/j.trac.2015.07.004>.

-
- ⁶⁴ D. L. Giokas, A. G. Vlessidis, G. Z. Tsogas, N. P. Evmiridis, *Trends Anal. Chem.*, 2010, 29, 1113–1126. <https://doi.org/10.1016/j.trac.2010.07.001>.
- ⁶⁵ L. Gámiz-Gracia, A. M. García-Campaña, J. F. Huertas-Pérez, F. J. Lara, *Anal. Chim. Acta*, 2009, 640, 7–28. <https://doi.org/10.1016/j.aca.2009.03.017>.
- ⁶⁶ M. R. Jones, K. Lee, *Microchem. J.*, 2019, 147, 1021–1027. <https://doi.org/10.1016/j.microc.2019.04.027>.
- ⁶⁷ A. P. Richardson, J. B. Kim, G. J. Barnard, W. P. Collins, F. McCapra, *Clin. Chem.*, 1985, 31, 1664–1668. <https://doi.org/10.1093/clinchem/31.10.1664>.
- ⁶⁸ L. Zhao, L. Sun, X. Chu, *Trends Anal. Chem.*, 2009, 28, 404–415. <https://doi.org/10.1016/j.trac.2008.12.006>.
- ⁶⁹ I.Y. Goryacheva, P. Lenain, S. De Saeger, *Trends Anal. Chem.*, 2013, 46, 30–43. <https://doi.org/10.1016/j.trac.2013.01.013>.
- ⁷⁰ L. Holec-Gąsior, B. Ferra, J. Czechowska, I.E. Serdiuk, K. Krzyminiński, J. Kur, *Diagn. Microbiol. Infect. Dis.*, 2016, 85, 422–425. <https://doi.org/10.1016/j.diagmicrobio.2016.05.013>.
- ⁷¹ A. Roda, M. Guardigli, *Anal. Bioanal. Chem.*, 2012, 402, 69–76. <https://doi.org/10.1007/s00216-011-5455-8>.
- ⁷² H. Arakawa, K. Tsuruoka, K. I. Ohno, N. Tajima, H. Nagano, *Luminescence*, 2014, 29, 374–377. <https://doi.org/10.1002/bio.2555>.
- ⁷³ J. Zhang, P. Cheng, K. Pu, *Bioconjugate Chem.*, 2019, 30, 2089–2101. <https://doi.org/10.1021/acs.bioconjchem.9b00391>.
- ⁷⁴ A. Ogawa, H. Arai, H. Tanizawa, T. Miyahara, T. Toyo'oka, *Anal. Chim. Acta*, 1999, 383, 221–230. [https://doi.org/10.1016/S0003-2670\(98\)00747-8](https://doi.org/10.1016/S0003-2670(98)00747-8).
- ⁷⁵ K. Krzyminiński, A. D. Roshal, P. B. Rudnicki-Velasquez, K. Żamojć, *Luminescence*, 2019, 34, 512–519. <https://doi.org/10.1002/bio.3629>.
- ⁷⁶ A. Roda, P. Pasini, M. Mirasoli, E. Michelini, M. Guardigli, *Trends Biotechnol.*, 2004, 22, 295–303. <https://doi.org/10.1016/j.tibtech.2004.03.011>.
- ⁷⁷ J. Czechowska, A. Kawecka, A. Romanowska, M. Marczak, P. Wityk, K. Krzyminiński, B. Zadykowicz, *J. Luminescence*, 2017, 187, 102–112. <https://doi.org/10.1016/j.jlumin.2017.02.068>.
- ⁷⁸ M. D. Mashkovsky, *Medicines*, 1997, 1, 350.
- ⁷⁹ The State Pharmacopoeia of Ukraine, The Ukrainian Scientific Pharmacopoeial Center for Quality of Medicines, 1st ed. State Enterprise "Ukrainian Scientific Pharmacopoeial Center for Drug Quality", Ukraine, 2001, 556.
- ⁸⁰ N. Costa, M. Mirjana, *Acta Pol. Pharm.*, 1988, 45, 418.
- ⁸¹ T. S. Jovanović, B. S. Stanković, *Analyst*, 1989, 114, 401. <https://doi.org/10.1039/AN9891400401>
- ⁸² I. López García, P. Viñas, J. A. Martínez Gil, *Fresenius' J. Anal. Chem.*, 1993, 345 (11), 723. <https://doi.org/10.1007/bf00325843>.
- ⁸³ A. A. Al-Warthan, S. A. Al-Tamrah, A. A. Al-Akel, *Anal. Sci.*, 1994, 10 (3), 449. <https://doi.org/10.2116/analsci.10.449>
- ⁸⁴ A. Larena, J. Martinez-Urreaga, *J. Mol. Struct.*, 1986, 143, 521. [https://doi.org/10.1016/0022-2860\(86\)85315-7](https://doi.org/10.1016/0022-2860(86)85315-7)

-
- ⁸⁵ W. L. Hinze, T. E. Riehl, H. N. Singh, Y. Baba, *Anal. Chem.*, 1984, 56 (12), 2180.
<https://doi.org/10.1021/ac00276a046>
- ⁸⁶ Kim, J. U., Park, I. S., Chan, C.-Y., Tanaka, M., Tsuchiya, Y., Nakanotani, H., & Adachi, C. *Nature Commun.*, 2020, 1765. <https://doi.org/10.1038/s41467-020-15558-5>
- ⁸⁷ J. U. Kim, I. S. Park, C.-Y. Chan, M. Tanaka, Y. Tsuchiya, H. Nakanotani, & C. Adachi, *Nat. Commun.*, 2020, 1765. <https://doi.org/10.1038/s41467-020-15558-5>
- ⁸⁸ A. A. Kubicki, P. Bojarski, M. Grinberg, M. Sadownik and B. Kukliński, *Opt. Commun.* 2006, 269, 275–280.
- ⁸⁹ M. J. Frisch, G. W. Trucks, H. B. Schlegel, G. E. Scuseria, M. A. Robb, J. R. Cheeseman, G.; Barone, V. Scalmani, G. A. Petersson, H. Nakatsuji, et al. Gaussian 16, Revision C.01 Gaussian, Inc.: Wallingford, CT, 2016.
- ⁹⁰ A. D. Becke, *J. Chem. Phys.*, 1993, 98, 1372–1377. <https://doi.org/10.1063/1.464304>
- ⁹¹ T. H. Dunning Jr., *J. Chem. Phys.*, 1989, 90, 1007-23. <https://doi.org/10.1063/1.456153>
- ⁹² F. Neese, *Wiley Interdiscip. Rev.: Comput. Mol. Sci.*, 2012, 2, 73–78. <http://dx.doi.org/10.1002/wcms.81>
- ⁹³ F. Weigend and R. Ahlrichs, *Phys. Chem. Chem. Phys.*, 2005, 7, 3297-305.
<https://doi.org/10.1039/b508541a>
- ⁹⁴ E. van Lenthe, J. G. Snijders, and E. J. Baerends, *J. Chem. Phys.*, 1996, 105.
<https://doi.org/10.1063/1.472460>
- ⁹⁵ I. E. Serdiuk, C. H. Ryoo, K. Kozakiewicz, M. Mońka, B. Liberek, S. Y. Park, *J. Mater. Chem. C*, 2020, 8, 6052-6062. <https://doi.org/10.1039/C9TC07102D>

Publications included in the thesis

[P1] V. Ievtukhov, A. Romanowska, M. Pieńkos, K. Żamojć, B. Zadykiewicz, K. Krzysiński, Aromatic acridinium thioesters—a new class of chemiluminogenic compounds and their interactions with some biological antioxidants, *Journal of Luminescence* 275 (2024), 120745. DOI: 10.1016/j.jlumin.2024.120745



Full Length Article

Aromatic acridinium thioesters—a new class of chemiluminogenic compounds and their interactions with some biological antioxidants

Vladyslav Ievtukhov, Anna Romanowska, Milena Pieńkos, Krzysztof Żamojć, Beata Zadykowicz^{*,*}, Karol Krzyński^{*}

Faculty of Chemistry, University of Gdansk, Wita Stwosza 63, 80-308, Gdansk, Poland

ARTICLE INFO

Keywords:

Acridinium thioesters
Chemiluminescence
DFT calculations
Reaction mechanism
Antioxidants
Luminescence analytics
UV-Vis spectrophotometry

ABSTRACT

This study introduces a novel group of acridinium salts, specifically 10-methyl-9-((phenylthio)carbonyl)acridin-10-ium trifluoromethanesulphonates (ATEs), which are the sulphur analogues of widely used acridinium esters in bioanalytics. We conducted comprehensive experimental and theoretical studies on the chemiluminescence (CL) properties of these ATEs, including emission efficiency and kinetics in various liquid environments. These findings provide insights into the unique chemiluminescence behaviour of ATEs and pave the way for their potential applications in luminometric assays.

All ATE compounds, regardless of the type and location of the substituent, exhibit an effective flash-type emission. The 2-methoxy and 4-nitro-substituted derivatives demonstrated the highest effectiveness in an organic environment (dimethylsulfoxide, ethanol). We further evaluated the analytical usefulness of selected ATEs by studying their interactions with biological antioxidants (AOs) in aqueous systems. These interactions were found to reduce the emission capability of CL in proportion to the AO concentration in the system. The linearity ranges of AO analyses were within the range 10^{-9} – 10^{-6} M, with detection limits at the level of 10^{-7} M. Quantum chemical (DFT) calculations on the thermodynamics and kinetics of ATE chemiluminescence disclosed that they are highly susceptible to nucleophilic addition of the OOH^- ion, initiating the CL process. They also demonstrated the thermodynamic feasibility of producing specific adducts of the ATE-AO type. The above results were supported by differential UV-Vis spectroscopy measurements, which revealed the formation of new bands around 370 nm, attributed to the formation of the adducts mentioned above.

The presented work describes the first characteristics of chemiluminogenic acridinium thioesters and draws perspectives on their practical uses in the analytics of biological substances. These findings also contribute to our understanding of the reactivity of ATEs in solutions accompanied by light emission.

1. Introduction

Acridines, the aza-analogues of anthracene [1–3], make a group of heterocyclic compounds that express many biological activities, such as anti-inflammatory, antimalarial, antiparasitic, antiviral, fungicidal ones [1,4–6]. They also possess interesting physicochemical features, among them the capability for various types of luminescence [1,7–11]. As a result, some acridines (e.g. *Acridine Orange*) have been employed in luminescence analytics and laser technologies [12,13] as fluorescent dyes for the visualisation of tissues or cells [10].

Some of the N-substituted acridinium salts can effectively emit light from the chemical reaction, exhibiting chemiluminescence (CL)

[14–16]. The latter phenomenon has found numerous applications – in medical/pharmaceutical [17,18], analytical [19], biochemical [20], food and environmental [21] sciences, and even in cosmetics [22]. In CL analysis, assessment of the intensity of generated light enables, after calibration, the determination of various types of molecules (e.g. antigens and antibodies [23–26], hormones [27,28], enzymes [29], antioxidants [30,31]) at deficient concentration levels (typically 10^{-16} – 10^{-19} M) [32]. Acridinium chemiluminogenic salts are widely employed in modern bioanalytics as CL labels (in bound form) [17,33,34], or as CL indicators [16,35] – if they are used in the free form [36]. Mainly, the acridinium esters (AEs) express many advantages over luminometric standard luminol (5-amino-2,3-dihydrophthalazine-1,

* Corresponding author.

** Corresponding author.

E-mail addresses: beata.zadykowicz@ug.edu.pl (B. Zadykowicz), karol.krzymski@ug.edu.pl (K. Krzyński).

<https://doi.org/10.1016/j.jlumin.2024.120745>

Received 26 March 2024; Received in revised form 23 May 2024; Accepted 9 June 2024

Available online 10 June 2024

0022-2313/© 2024 Elsevier B.V. All rights are reserved, including those for text and data mining, AI training, and similar technologies.

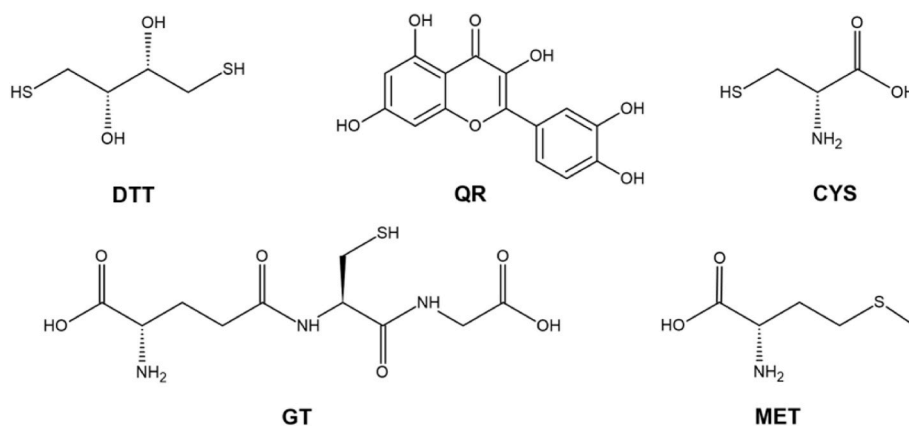


Fig. 1. Structural formulas of biological antioxidants investigated in this work: dithiothreitol (DTT), glutathione (GT), quercetin (QR), cysteine (CYS) and methionine (MET).

4-dione) and its derivatives [17,27,33]. Among them are relatively high quantum yields, fast and easy controllable emission dynamics and low background signal, resulting from no need for a catalyst to trigger light emission [14,31].

The other aspect of this work is natural compounds exhibiting antioxidant properties essential in biological systems. Exemplary, in animals and humans, they neutralise the effects of oxidative stress by capturing the free radicals, causative factors for many diseases (e.g. diabetes, high blood pressure, atherosclerosis, acute renal failure, Alzheimer's and Parkinson's [37–40]). Numerous studies [41–44] revealed that antioxidants are essential in maintaining human health and preventing diseases because they inhibit or eliminate oxidative processes [37,39,40]. Thus, determining various substances' total antioxidant capacity (TAC) seems significant in modern analytics. Many approaches have been developed in that context, but no universal one can be applied to various classes of antioxidants [45]. They utilise different types of transformations, such as H atom transfer (e.g. Oxygen Radical Absorption Capacity test, ORAC), electron transfer (e.g. Cupric Reducing Antioxidant Power test, CUPRAC), or both processes (e.g. 2,2'-azino-bis(3-ethylbenzothiazoline)-6-sulfonic acid, diammonium salt – ABTS test). Most such assays employ UV–Vis spectroscopy, but electrochemical and luminometric approaches are also known, offering generally higher sensitivity and simplicity of use [22]. Exemplary, in the work by Kőszegi et al. [46], the authors proposed the TAC assay, based on the luminol/4-iodophenol/H₂O₂/peroxidase system, capable of generating enhanced chemiluminescence (ECL). The latter method is characterised by superior sensitivity and precision but is relatively expensive and sometimes problematic because of the need for the use of enzymes. In the work of Said et al. [47], the ECL method was compared with the one based UV–Vis absorption measurements in the TAC assays of human seminal plasma, giving superior analytical parameters, such as high correlation coefficients ($r = 0.99$) and low inter-assay coefficients of variation ($CV = 4.7\%$). In one of our former works [31], we applied original acridinium esters (AE) to assess the antioxidant capacity of some dietary supplements, such as quercetin and vitamin C. The authors have determined second-order kinetic constants for systems containing variable amounts of antioxidants, which were assumed to be a measure of their antioxidant activity. The proposed approach was advantageous if compared to luminol-based assays in terms of sensitivity, time of measurements, and the ability to analyse coloured and turbid samples.

The chemiluminogenic properties of substituted AEs were investigated in aqueous and non-aqueous environments (aliphatic alcohols, dimethyl sulfoxide and acetonitrile) [48]. It turned out that the substituents in the benzene ring mainly determine the reaction dynamics. On the other hand, the presence of electron-donating substituent (e.g. OCH₃) in position 2 of the acridine ring is manifested by a bathochromic shift of the CL spectrum. It was demonstrated that the dynamics of

emission are related both to the properties of solvent (its polarity and nucleophilicity), as well as the type and concentration of base (KOH, TBAOH, 1,8-diazabicyclo[5.4.0]undec-7-ene, DBU) employed for triggering the emission of light.

In this work, we propose a new group of chemiluminogenic salts, 10-methyl-9-((phenylthio)carbonyl)acridin-10-ium trifluoromethanesulphonates (acridinium thioesters, ATEs), substituted in the benzene ring with groups/atoms of various electronic and steric properties [15,49]. The concept of replacing O with S atom in known acridinium esters is based on differences between these two atoms, which would manifest in beneficial emissive properties of resulting derivatives. The larger size of the S atom generally allows a broader charge distribution around the molecular skeleton [50]. At the same time, its lower electronegativity is manifested by a weaker tendency to H-bonding compared to respective O analogues. The latter feature, and the fact that a more significant negative charge deficit characterises the acyl carbon atom in thioesters than in esters, may facilitate their higher susceptibility to nucleophilic attack and, thus, more efficient transformation to the electronically excited product(s). Adding to the above, as the S atom can form many types of chemical bonds, it opens up opportunities to be engaged in various transformations/interactions with guest molecules present in the system, where the high-energy thioester bond can act as a donor.

Our recent computational studies at the DFT level of theory on ATEs revealed their high thermodynamic susceptibility towards nucleophilic attack and – resulting from it – high emission kinetics constants, compared to typical acridinium esters [51]. The expected acridinium thioesters' high reactivity may create perspectives for their potential utility in the analytics of various nucleophilic substrates. In this work, we demonstrate their potential usefulness in quantitative analytics of exemplary antioxidants of biological importance (AOs, Fig. 1).

2. Materials and methods

2.1. Synthesis and chemical identity of acridinium thioesters (ATEs)

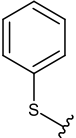
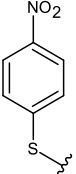
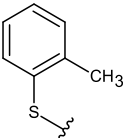
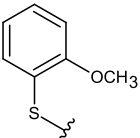
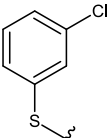
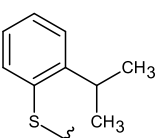
To obtain compounds investigated in this work (ATEs, Table 1), known synthetic procedures for AE were adopted, starting from 9-(chlorocarbonyl)acridin-10-ium chloride and appropriate thiophenol [15,49,52]. Comprehensive spectroscopic analyses (MALDI-QTOF mass spectra, ¹H and ¹³C NMR and FT-IR spectra) were performed. Copies of the spectra are given in the Electronic Supplementary Information section (ESI). The general scheme of synthesis of ATEs is presented in Scheme 1.

Detailed procedures for the synthesis of ATEs and their precursors are provided below.

9-(Phenylthio)carbonyl)acridines (PTCAcrs). 9-(Chlorocarbonyl)acridin-10-ium chloride (1.07 mmol) was added to a stirred solution of

Table 1

The names, formulas and abbreviations of the acridinium thioesters (ATEs) are investigated in this work.

Abbreviation	R ¹	Systematic name
H-ATE		10-methyl-9-((phenylthio)carbonyl)acridin-10-ium trifluoromethanesulphonate
4NO ₂ -ATE		10-methyl-9-(((4-nitrophenyl)thio)carbonyl)acridin-10-ium trifluoromethanesulphonate
2Me-ATE		10-methyl-9-(((2-methylphenyl)thio)carbonyl)acridin-10-ium trifluoromethanesulphonate
2MeO-ATE		9-(((2-methoxyphenyl)thio)carbonyl)-10-methylacridin-10-ium trifluoromethanesulphonate
3Cl-ATE		9-(((3-chlorophenyl)thio)carbonyl)-10-methylacridin-10-ium trifluoromethanesulphonate
2iPr-ATE		9-(((2-isopropylphenyl)thio)carbonyl)-10-methylacridin-10-ium trifluoromethanesulphonate

thiophenol (0.97 mmol), triethylamine (1.07 mmol), 4-(dimethylamine) pyridine in dry dichloromethane and the reaction mixture was stirred for 24 h in room temperature. The resulting solution was then evaporated. The pure product was obtained by column chromatography on silica gel (40–60 µm, Normasil 60, VWR/BDH Chemicals) using cyclohexane – chloroform mixture (1/1 v/v) as mobile phase. Analyses:

9-((Phenylthio)carbonyl)acridine (H-PTCAcr): Yield: 0.145 g (51 %); yellow solid. ¹H NMR (CD₃Cl, 700 MHz): δ 8.17 (H1/8, d, J = 1.00), 7.67 (H2/7, t, J = 1.74), 7.83 (H3/6, t, J = 0.64), 8.28 (H4/5, d, J = 1.35), 7.65 (H19/20; H22/23, m, J = 1.74), 7.48 (H21, t, J = 1.21). ¹³C NMR (CD₃Cl, 700 MHz): δ 121.41 (C1/8), 125.16 (C2/7), 130.23 (C3/6), 129.95 (C4/5), 134.60 (C9), 124.74 (C11/14), 148.55 (C12/13), 193.97 (C15), 129.92 (C16), 130.54 (C17/21), 126.80 (C18/20), 127.27

(C19). HRMS (ESI-QTOF): *m/z* [M + H⁺] calcd for C₂₀H₁₃NOS: 316.07; found: 316.13. FT-IR (KBr, cm⁻¹): 3434.83, 1686.89, 1514.20, 1437.81, 1055.34, 881.72, 798.59, 774.02, 748.25, 687.96, 608.4.

9-(((4-Nitrophenyl)thio)carbonyl)acridine (4NO₂-PTCAcr): Yield: 0.281 g (88 %); yellow solid. ¹H NMR (CD₃Cl, 700 MHz): δ = 8.14 (H1/8, d, J = 6.12), 7.90 (H2/7, t, J = 2.78), 7.71 (H3/6, t, J = 8.54), 8.21 (H4/5, d, J = 0.14), 7.92 (H17/21, d, J = 2.78), 8.41 (H18/20, d, J = 1.00). ¹³C NMR (CD₃Cl, 700 MHz): δ 124.39 (C1/8), 127.74 (C2/7), 130.05 (C3/6), 128.18 (C4/5), 134.88 (C9), 126.40 (C11/14), 148.70 (C12/13), 191.56 (C15), 130.77 (C16/17/21), 121.21 (C18/20), 135.11 (C19). ESI-QTOF: *m/z* [M + H⁺] calcd for C₂₀H₁₂N₂O₃S: 360.39; found: 361.12. IR (film, cm⁻¹): 2923.84, 2853.35, 1521.32, 1459.52, 1342.67, 847.98, 781.23.

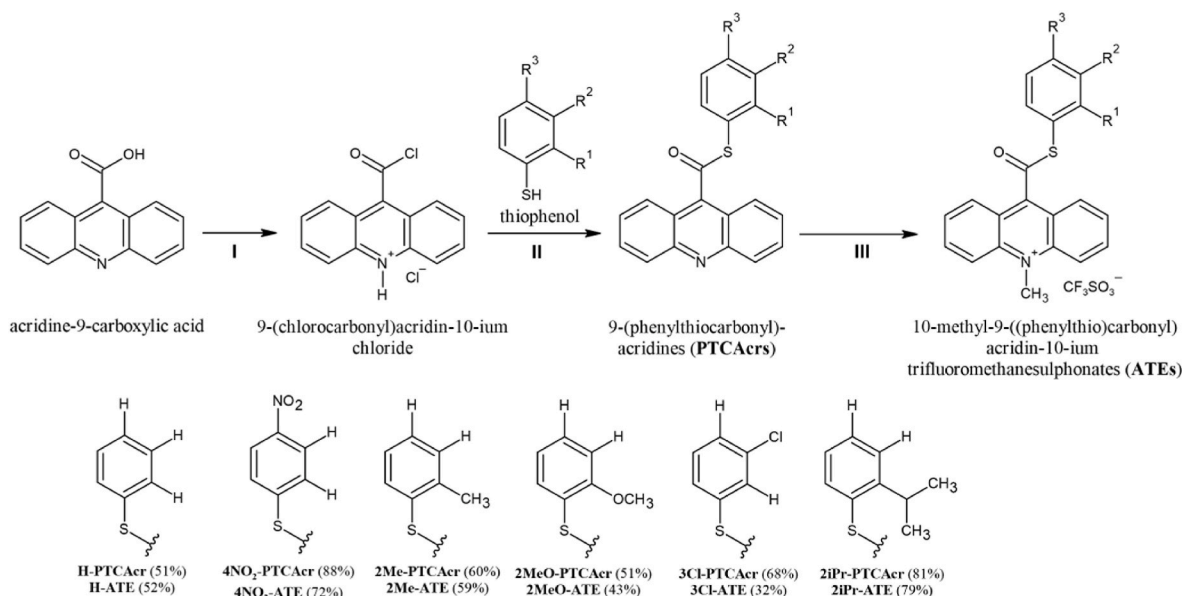
9-(((2-Methylphenyl)thio)carbonyl)-acridine (2Me-PTCAcr): Yield: 0.175 g (60 %); yellow solid. ¹H NMR (CD₃Cl, 700 MHz): δ = 8.10 (H1/8, d, J = 0.50), 7.60 (H2/7, t, J = 0.44), 7.78 (H3/6, t, J = 0.30), 8.22 (H4/5, d, J = 1.00), 7.39 (H17, d, J = 0.63), 7.29 (H18/19, m, J = 0.18), 7.58 (H20, t, J = 0.31), 2.58 (H23, s). ¹³C NMR (CD₃Cl, 700 MHz): δ 121.60 (C1/8), 127.28 (C2/7), 130.56 (C3/6), 129.94 (C4/5), 136.09 (C9), 124.68 (C11/14), 148.56 (C12/13), 193.12 (C15), 127.28 (C16), 142.31 (C17), 130.94 (C18), 125.12 (C19), 126.22 (C20), 131.25 (C21), 21.23 (C23). ESI-QTOF: *m/z* [M + H⁺] calcd for C₂₁H₁₅NOS: 330.41; found: 330.14. FT-IR (film, cm⁻¹): 1686.14, 1513.41, 1459.11, 1436.59, 1065.79, 1053.67, 881.25, 798.97, 775.10, 752.37, 709.19, 610.42.

9-(((2-Methoxyphenyl)thio)carbonyl)-acridine (2MeO-PTCAcr): Yield: 0.216 g (51 %); yellow solid. ¹H NMR (CD₃Cl, 700 MHz): δ = 8.27 (H1/8, d, J = 4.10), 7.87 (H2/7, t, J = 1.36), 8.01 (H3/6, t, J = 0.17), 8.50 (H4/5, d, J = 1.00), 6.99 (H17, d, J = 1.47), 7.44 (H18, t, J = 0.75), 7.51 (H19/20, d, J = 0.80), 7.65 (H21, t, J = 1.43), 3.92 (H23, s). ¹³C NMR (CD₃Cl, 700 MHz): δ 121.88 (C1/8), 125.37 (C2/7), 128.19 (C3/6), 127.65 (C4/5), 136.51 (C9), 121.98 (C11/14), 145.87 (C12/13), 192.32 (C15), 114.22 (C16), 159.48 (C17), 111.88 (C18), 122.40 (C19), 121.50 (C20), 132.84 (C21), 56.13 (C23). ESI-QTOF: *m/z* [M + H⁺] calcd for C₂₁H₁₅NO₂S: 346.41; found: 346.15. FT-IR (film, cm⁻¹): 1684.48, 1513.70, 1476.62, 1435.36, 1276.97, 1057.37, 1022.41, 883.59, 801.83, 778.00, 756.87, 745.75, 612.21.

9-(((3-Chlorophenyl)thio)carbonyl)-acridine (3Cl-PTCAcr): Yield: 0.141 g (68 %); yellow solid. ¹H NMR (CD₃Cl, 700 MHz): δ = 8.23 (H1/8, d, J = 1.00), 7.60 (H2/7, t, J = 1.54), 7.78 (H3/6, t, J = 0.67), 8.06 (H4/5, d, J = 0.74), 7.40 (H17, d, J = 1.21), 7.37 (H19, m, J = 0.72), 7.39 (H20, t, J = 0.72), 7.48 (H21, d, J = 0.15). ¹³C NMR (CD₃Cl, 700 MHz): δ 121.32 (C1/8), 124.55 (C2/7), 130.46 (C3/6/20), 128.43 (C4/5), 134.26 (C9), 122.36 (C11/14), 148.45 (C12/13), 193.02 (C15), 132.68 (C16), 129.91 (C17), 135.21 (C18), 125.15 (C19), 127.48 (C21). ESI-QTOF: *m/z* [M + H⁺] calcd for C₂₀H₁₂ClNOS: 350.83; found: 350.09. FT-IR (film, cm⁻¹): 2924.21, 1695.11, 1566.56, 1460.35, 1055.26, 876.01, 791.60, 772.80, 747.52, 680.58, 645.74.

9-(((2-Isopropylphenyl)thio)carbonyl)-acridine (2iPr-PTCAcr): Yield: 0.188 g (81 %); yellow solid. ¹H NMR (CD₃Cl, 700 MHz): δ = 8.09 (H1/8, d, J = 0.74), 7.59 (H2/7, t, J = 0.55), 7.78 (H3/6, t, J = 0.51), 8.22 (H4/5, d, J = 1.00), 7.46 (H17, t, J = 1.44), 7.30 (H19/20, dt, J = 0.21), 7.65 (H18, d, J = 0.44), 3.53 (H21, m, J = 0.48), 1.30 (H23, d, J = 4.92). ¹³C NMR (CD₃Cl, 700 MHz): δ 121.56 (C1/8), 125.03 (C2/7), 130.53 (C3/6), 129.97 (C4/5), 136.57 (C9), 124.68 (C11/14), 148.60 (C12/13), 193.56 (C15), 127.14 (C16), 152.19 (C17), 126.76 (C18), 127.27 (C19), 126.95 (C20), 131.25 (C21), 31.68 (C23), 23.88 (C24). ESI-QTOF: *m/z* [M + H⁺] calcd for C₂₃H₁₉NOS: 358.47; found: 358.18. FT-IR (film, cm⁻¹): 2964.78, 1682.59, 1513.86, 1472.93, 1458.93, 1436.74, 1149.59, 1057.12, 1043.74, 1010.24, 880.75, 860.54, 801.46, 775.84, 760.97, 743.06, 611.70.

10-Methyl-9-((phenylthio)carbonyl)acridinium-10-ium trifluoromethanesulphonates (triflates) (ATEs) (Table 1). Ten-fold molar excess of fresh methyl trifluoromethanesulphonate (Sigma Aldrich) was added to a solution of chromatographically purified 9-(phenylthio)carbonyl)acridines (PTCAcrs) in dry dichloromethane and a small amount (10–20 mg) of polymer-bound 2,6-di-*tert*-butylpyridine was



Scheme 1. Synthesis steps, structural formulas, names and chemical yields of acridinium thioesters (ATEs) studied in this work (ATEs, Table 1).

added to the flask. The reaction mixture was stirred for 2 h at r.t. under Ar, slightly diluted with acetonitrile and filtered with a PTFE syringe filter (0.22 μ m). The acridinium salts, ATEs, were precipitated by adding an excess of dry diethyl ether to the filtrate and cooling down the mixture (overnight, -20°C). The yellow powders of pure products, the acridinium thioesters, were isolated by filtration and were washed with dry diethyl ether. Analyses:

10-Methyl-9-((phenylthio)carbonyl)acridine-10-ium triflate (H-ATE): Yield: 0.030 g (52 %); yellow solid. ^1H NMR (CD_3CN , 700 MHz): δ 8.57 (H1/8, d, J = 7.53), 8.09 (H2/7, t, J = 10.63), 8.47 (H3/6, t, J = 4.21), 8.64 (H4/5, d, J = 1.00), 7.79 (H17/21, d, J = 0.86), 7.61 (H18/19/20, dd, J = 12.65), 4.82 (H22, s). ^{13}C NMR (CD_3CN , 700 MHz): δ 119.75 (C1/8), 140.16 (C2/7), 123.14 (C3/6), 130.06 (C4/5), 154.32 (C9), 128.32 (C11/14), 142.79 (C12/13), 192.67 (C15), 135.76 (C16), 131.81 (C17/21), 130.64 (C18/20), 125.30 (C19), 40.04 (C22). ESI-QTOF: m/z [$\text{M} + \text{H}^+$] calcd for $\text{C}_{21}\text{H}_{16}\text{NOS}$: 330.42; found: 330.16. FT-IR (film, cm^{-1}): 1674.20, 1460.55, 1263.05, 1222.62, 1159.11, 1145.86, 1063.56, 1029.91, 871.68, 842.32, 763.22, 637.39, 517.29.

10-Methyl-9-(((4-nitrophenyl)thio)carbonyl)acridin-10-ium triflate (4NO₂-ATE): Yield: 0.050 g (72 %); yellow solid. ^1H NMR (CD_3CN , 700 MHz): δ 8.60 (H1/8, d, J = 9.45), 8.14 (H2/7, t, J = 5.73), 8.51 (H3/6, t, J = 4.85), 8.68 (H4/5, d, J = 1.00), 8.09 (H17/21, d, J = 3.05), 8.45 (H18/20, d, J = 2.82), 4.87 (H22, s). ^{13}C NMR (CD_3CN , 700 MHz): δ 130.22 (C1/8), 125.20 (C2/7), 136.59 (C3/6), 119.85 (C4/5), 153.29 (C9), 128.17 (C12/13), 140.24 (C11/14), 190.96 (C15), 40.17 (C22), 142.87 (C16), 133.18 (C17/21), 123.15 (C18/20), 150.12 (C19). ESI-QTOF: m/z [$\text{M} + \text{H}^+$] calcd for $\text{C}_{21}\text{H}_{15}\text{N}_2\text{O}_3\text{S}$: 375.41; found: 375.14. FT-IR (film, cm^{-1}): 1691.86, 1604.83, 1552.31, 1524.63, 1372.62, 1346.25, 1261.46, 1222.43, 1177.78, 1148.98, 1059.22, 1029.35, 1008.43, 853.58, 835.37, 766.90, 745.31, 636.69, 516.37.

10-Methyl-9-(((2-methylphenyl)thio)carbonyl)acridin-10-ium triflate (2Me-ATE): Yield: 0.035 g (59 %); yellow solid. ^1H NMR (CD_3CN , 700 MHz): δ = 8.55 (H1/8, d, J = 0.58), 8.14 (H2/7, t, J = 0.27), 8.51 (H3/6, t, J = 0.29), 8.69 (H4/5, d, J = 1.00), 7.80 (H19, d, J = 0.60), 7.48 (H18/20, m, J = 0.40), 7.60 (H21, d, J = 0.60), 4.86 (H22, s), 2.68 (H23, s). ^{13}C NMR (CD_3CN , 700 MHz): δ 128.10 (C1/8), 119.81 (C2/7), 137.04 (C3/6), 119.81 (C4/5), 154.50 (C9), 124.96 (C11/14), 140.16 (C12/13), 191.79 (C15), 142.84 (C16), 143.47 (C17), 132.41 (C18), 123.29 (C19), 130.13 (C20), 132.10 (C21), 20.99 (C22) 40.07 (C23). ESI-QTOF: m/z [$\text{M} + \text{H}^+$] calcd for $\text{C}_{22}\text{H}_{18}\text{NOS}$: 344.45; found: 344.17. FT-IR (film, cm^{-1}): 1672.83, 1263.15, 1224.03, 1148.63,

1030.97, 840.20, 764.85, 749.85, 638.59.

9-(((2-Methoxyphenyl)thio)carbonyl)-10-methylacridin-10-ium trifluorometanosulphonate (2MeO-ATE): Yield: 0.030 g (43 %); yellow solid. ^1H NMR (CD_3CN , 700 MHz): δ = 8.14 (H1/8, d, J = 0.50), 8.50 (H2/7, t, J = 0.31), 8.66 (H3/6, t, J = 1.00), 8.64 (H4/5, d, J = 1.00), 7.16 (H18, d, J = 0.31), 7.70 (H19, t, J = 0.24), 7.27 (H20, t, J = 0.39), 7.65 (H21, d, J = 0.26) 4.05 (H23, s) 4.82 (H22, s). ^{13}C NMR (CD_3CN , 700 MHz): δ 123.36 (C1/8), 119.67 (C2/7), 140.15 (C3/6), 113.03 (C4/5), 154.97 (C9), 122.24 (C11/14), 142.73 (C12/13), 191.65 (C15), 137.28 (C16), 160.33 (C17), 129.87 (C18), 134.27 (C19), 113.03 (C20), 128.34 (C21), 56.77 (C23), 49.95 (C22). ESI-QTOF: m/z [$\text{M} + \text{H}^+$] calcd for $\text{C}_{22}\text{H}_{18}\text{NO}_2\text{S}$: 361.45; found: 360.16. FT-IR (film, cm^{-1}): 3484.85, 3306.93, 3236.70, 1712.42, 1673.40, 1610.57, 1556.94, 1434.24, 1409.20, 1357.63, 1260.70, 1172.9, 1035.49, 838.74, 757.42, 638.17.

9-(((3-Chlorophenyl)thio)carbonyl)-10-methylacridin-10-ium trifluorometanosulphonate (3Cl-ATE): Yield: 0.027 g (38 %); yellow solid. ^1H NMR (CD_3CN , 700 MHz): δ 8.59 (H1/8, d, J = 4.29), 8.12 (H2/7, t, J = 4.56), 8.51 (H3/6, t, J = 2.22), 8.6 (H4/5, d, J = 1.00), 7.93 (H17, s), 7.68 (H19, d, J = 0.45), 7.63 (H20, t, J = 4.64), 7.77 (H21, d, J = 0.99), 4.86 (H22, s). ^{13}C NMR (CD_3CN , 700 MHz): δ 127.09 (C1/8), 135.29 (C2/7), 140.05 (C3/6), 119.78 (C4/5), 142.82 (C9), 123.15 (C11/14), 153.80 (C12/13), 191.91 (C15), 135.47 (C16), 134.24 (C17), 140.21 (C18), 128.29 (C19), 130.12 (C20), 131.97 (C21), 40.10 (C22). ESI-QTOF: m/z [$\text{M} + \text{H}^+$] calcd for $\text{C}_{21}\text{H}_{15}\text{ClNOS}$: 364.86; found: 364.12. FT-IR (film, cm^{-1}): 3417.37, 1682.01, 1623.63, 1607.54, 1459.30, 1268.60, 1254.92, 1227.35, 1157.46, 1030.04, 838.03, 770.78, 756.67, 639.71, 517.08.

9-(((2-Isopropylphenyl)thio)carbonyl)-10-methylacridin-10-ium trifluorometanosulphonate (2iPr-ATE): Yield: 0.049 g (79 %); yellow solid. ^1H NMR (CD_3CN , 700 MHz): δ = 8.53 (H1/8, d, J = 1.36), 8.15 (H2/7, t, J = 0.30), 8.51 (H3/6, t, J = 1.36), 8.68 (H4/5, d, J = 1.00), 7.67 (H18/20, d, J = 0.44), 7.48 (H19, m, J = 0.12), 7.85 (H21, d, J = 0.35), 3.59 (H22, m, J = 0.22), 4.87 (H22, s), 1.39 (H23, d, J = 2.49). ^{13}C NMR (CD_3CN , 700 MHz): δ 128.0 (C1/8), 123.25 (C2/7), 140.15 (C3/6), 119.86 (C4/5), 153.37 (C9), 127.88 (C11/14), 142.85 (C12/13), 192.34 (C15), 154.54 (C16), 137.44 (C17), 130.15 (C18), 123.72 (C19), 128.01 (C20), 132.78 (C21), 40.1 (C22), 32.40 (C23), 23.67 (C24). ESI-QTOF: m/z [$\text{M} + \text{H}^+$] calcd for $\text{C}_{24}\text{H}_{22}\text{NOS}$: 372.50; found: 372.21. FT-IR (film, cm^{-1}): 1264.33, 1156.07, 1030.24, 758.30, 637.61.

2.2. Measurements of chemiluminescence

The stock solutions (5.0×10^{-3} M) of ATEs (Table 1) were prepared by dissolving the salts in anhydrous dimethylsulfoxide (DMSO, 99.9 %, Sigma-Aldrich, USA) or in anhydrous ethanol (EtOH, p.a., POCH, Poland). Promptly before measurements, the above solutions were diluted with 1.0×10^{-3} M HCl (Hempur, Poland) to obtain concentrations of ATE of 4.0×10^{-5} M and pH of about 4.5.

Preliminary measurements of CL were conducted to select optimally performing systems, employing a Lumat3 LB 9508 luminometer (Berthold Technologies, Germany) equipped with an ultrasensitive detector. The light emission intensity was measured in relative light units (RLUs) with a total measurement time of 10 s and a resolution of 0.15 s per point. The above solutions were further diluted with 1.0×10^{-3} M HCl to obtain a final concentration of ATEs of 3.0×10^{-8} M. Next, to 10 μ L of ATE solution was added 790 μ L of solvent (DMSO, EtOH, ultra-pure water (UP H₂O)). Then 100 μ L of 0.1 % H₂O₂ and 100 μ L of 0.1 M KOH were sequentially injected into the tube, and temporary CL intensities were recorded until a complete reaction profile was obtained.

The experiments with the participation of antioxidants (AOs, Fig. 1) were performed employing a plate luminometer, Fluoroskan Ascent FL (Labsystems, Finland). Ascent FL software ver. 2.4.2 was employed to collect and process the data. The measurements were conducted using two optimal substrates employed as CL indicators (2MeO-ATE and 4NO₂-ATE). The settings optimised for this type of measurement were as follows: time of acquisition: 4–5 s, integration time: 2.0×10^{-2} s, measure counts: 100, PMT: 1000 V (maximal value). Measurements were taken at 298 K, using a standard 96-well white polystyrene plate (Thermo Fisher Scientific Inc., USA). Solutions of ATEs were diluted before measurements with 1.0×10^{-3} M HCl to obtain a concentration of 5.0×10^{-7} M. To assess emission temporary intensities (I_{CL} , in RLU), 50 μ L of the latter solutions of ATEs were added to each well, followed by 50 μ L of 5.0×10^{-5} M in an aqueous/alcoholic solution of AOs and shaking for 1 min. To trigger the emission of light, 50 μ L of 0.1 % H₂O₂ and 50 μ L of 0.1 M KOH were sequentially injected into each well and readings of CL temporary intensities ($n = 5$) were carried out until signal completion. The areas under curves (AUCs, in RLU²) were calculated for completed reaction profiles.

2.3. Computational methods

Ground-state optimised geometry of the studied compounds (Table 1) was performed employing DFT [53] at ω B97XD [54] level of theory in conjunction with the 6-31G(d,p) [55] basis sets. The quantum-chemical calculations for 10-methyl-acridan-9-one ([10-MA] *) in the electronically excited state (S_1) were performed using the time-dependent density functional theory (TD DFT) [56] method with the same functional and basis set. Selecting the technique and the function to study emissive transformations, we considered other investigations [57–59], which demonstrated that the chosen method could provide accurate qualitative results for the mechanism of chemiluminescence of the investigated group of molecules. The harmonic vibrational frequencies, characterising the stationary points, were evaluated to ensure that the obtained structures correspond to true minima or transition state (TS) on the potential energy surface. Intrinsic reaction coordinate (IRC) [60] calculations were also performed at the same level of theory to obtain the minimum energy paths. Calculations have been achieved in the selected solvent (aqueous phase) by applying the polarisable continuum model (PCM) [61,62] with the Gaussian16 program [63], and the output files were visualised using the ChemCraft program package [64].

2.4. UV–Vis electronic absorption measurements

UV–Vis spectrophotometric measurements were carried out in 1:1 (v/v) water:ethanol mixture at room temperature, employing a Lambda 650

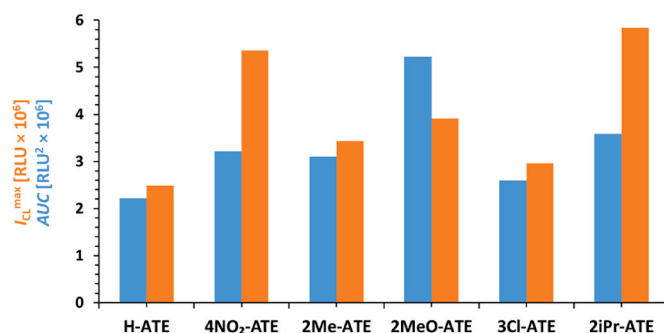


Fig. 2. Emissive efficiencies of acridinium thioesters (Table 1) in an aqueous environment ($c = 1.0 \times 10^{-10}$ M), measured as maximum (I_{CL}^{max}) and integral emission intensity (AUC) of CL, triggered by H₂O₂/KOH system. For details, see the Materials and Methods section.

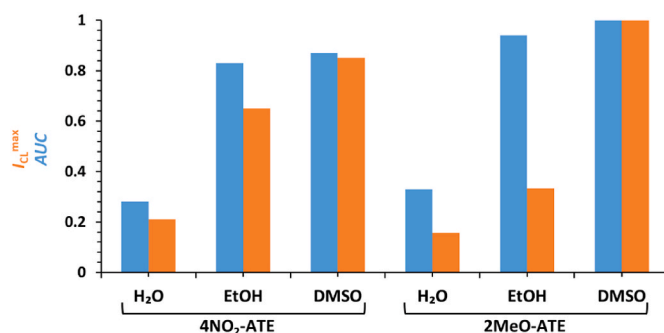


Fig. 3. Emissive efficiencies (normalized values) of acridinium thioesters selected for analytical studies in various liquid environments, measured as maximum (I_{CL}^{max}) and integral CL intensities (AUC) using H₂O₂/KOH triggering system. For details, see the Materials and Methods section.

(PerkinElmer, Waltham, MA, USA) UV/Vis spectrophotometer. The UV–Vis absorption spectra of ATEs were recorded in the range of 250–550 nm in the absence and presence of increasing amounts of dithiothreitol (DTT), glutathione (GT) and quercetin (QR). In the spectrophotometric titrations, 2 mL of 4NO₂-ATE and 2MeO-ATE at a fixed concentration equal to 1.0×10^{-4} M were treated with 5 μ L aliquots of each AO solution. The concentration of AOs varied and depended on the solubility in the given system ($c_{DTT} = 0.12$ M; $c_{QR} = 6.0 \times 10^{-3}$ M; $c_{GT} = 0.10$ M). Analogous titrations were performed using a pure solvent to obtain differential UV–Vis spectra.

3. Results and discussion

3.1. Synthesis and spectroscopy of acridinium thioesters (ATEs)

The title compounds, 10-methyl-9-((phenylthio)carbonyl)acridin-10-ium trifluoromethanesulphonates (ATEs, Table 1), were synthesised applying a three-step reaction path, which enabled reaction yields in the range of 32–79 % (Scheme 1). Experiments were planned based on literature reports available for related compounds, acridinium oxo-esters (AEs) [15,49,65], by modifying reaction conditions (time, temperature).

The obtained bases (PTCAcrs) were purified using gravitational column chromatography (LC). Their purity was assessed by thin-layer chromatography (TLC) on SiO₂ with fluorescence detection at 254/365 nm. A single spot was obtained for each compound after purification.

The chemical identity of the final products, ATEs (Table 1), was confirmed using elemental analyses, nuclear magnetic resonance spectra (¹H and ¹³C NMR), and high-resolution mass spectra (HR MS, ESI-

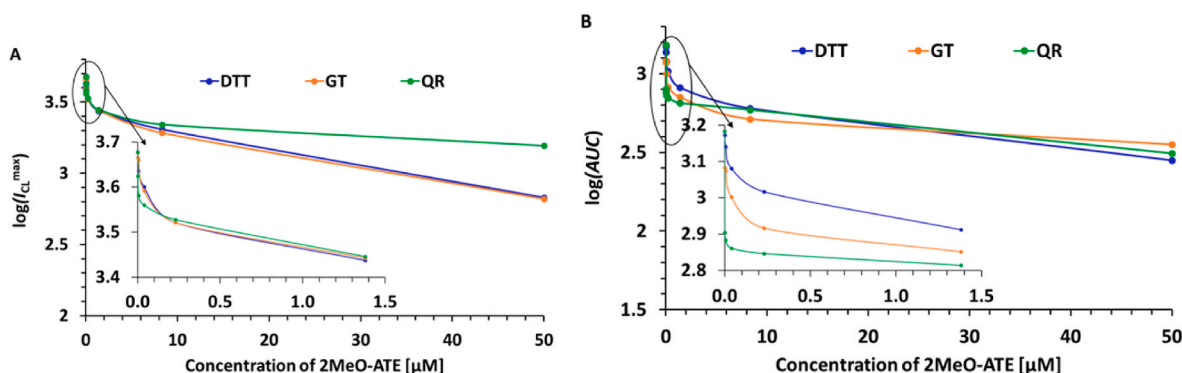


Fig. 4. Graph presenting dependence of $\log(\text{maximal CL intensity})$ against AO concentration (A) and $\log(\text{area under the curve})$ against AO concentration (B), using 2MeO-ATE as CL indicator ($c = 1.25 \times 10^{-7} \text{ M}$) in aqueous-ethanolic solution and $\text{H}_2\text{O}_2/\text{KOH}$ triggering system. For details, see the Materials and Methods section.

QTOF), supported by vibrational spectroscopy (FT-IR). The respective data are provided in ESI (Fig. 1S–4S).

The crucial stage of the synthesis routes was the methylation of the endocyclic nitrogen in the 9-(phenylthio)carbonyl)acridines (PTCAcrs), being the immediate precursors of investigated chemiluminogenic salts. As the thioester moiety in position 9 of the acridine ring suppresses the susceptibility of the N atom to electrophilic attack, a potent methylating agent, such as methyl trifluoromethanesulphonate ($\text{CF}_3\text{SO}_2\text{OCH}_3$), which is ca. 10^4 more effective than typical reagent – methyl iodide, was employed [66]. However, the mentioned reagent is prone to hydrolysis, which can cause unwanted side-reactions that result in the blockage of the acridine N atom for alkyl substitution. Accordingly, the final synthesis step was carried out in the presence of polymer-bound 2, 6-di-*tert*-butylpyridine, acting as a “proton sponge”, in freshly purified solvent and under inert atmosphere.

^1H and ^{13}C NMR and ESI-QTOF HR MS spectroscopy were the main techniques employed to confirm the chemical identity of the obtained compounds. High-resolution measurements at frequencies of 700 MHz (for ^1H) and 125 MHz (for ^{13}C), supported by theoretical predictions (ChemOffice, Cambridge), allowed the assignment of signals (Fig. 2S and 3S in ESI). Our previous research on related compounds, acridinium esters, facilitated the proper assignment of recorded signals to ^1H and ^{13}C nuclides [67]. Signals corresponding to H4 and H5 atoms near the acridine N atom appear at lower fields than the other signals in each case (Fig. 2S, ESI). A similar situation occurs in the case of H atoms in the acridine's positions 1 and 8 – in the latter case, likely due to the proximity of the S atom from the thioester group. These effects are related to the decrease in electron density in the mentioned positions, caused by the de-shielding influence of the N and S atoms on their spatial proximity [67].

The FT-IR vibrational spectra of the investigated compounds (Table 1) were recorded in KBr pellets and are presented in Fig. 4S in ESI. Generally, they show the two spectral areas in which characteristic signals appear: the absorption of the carbonyl groups ($1730\text{--}1780 \text{ cm}^{-1}$) and the thioester group ($1020\text{--}1250 \text{ cm}^{-1}$). The assignments of bands in the FT-IR spectra were based on physicochemical tables [68]; they represent a qualitative level, supporting the results derived from NMR and MS spectra.

3.2. Chemiluminogenic features of acridinium thioesters

A series of original compounds synthesised for this work, acridinium thioesters (ATEs, Table 1), were subjected to preliminary measurements of CL to assess their ability to generate light in various liquid environments. Experiments were carried out mainly in aqueous environments regarding their potential employment in bioanalytics. For the related chemiluminogenic salts, aromatic acridinium esters (AEs), extensive knowledge of their physicochemistry has been collected [15,48,49]. Solubility of reagents used in measurements, minimisation of eventual

side-reaction, and compatibility of solvent(s) with plastic parts of apparatus were also addressed when designing optimal experimental setup for measurements of CL.

The emission time profiles of the ATEs are presented in Fig. 5S (ESI). Obtained curves, temporary intensities (I_{CL}) and the areas under CL curves (AUCs) allowed us to construct the graph, in which their emissive properties are compared (Fig. 2). The latter relationships indicate that the efficiency of CL (expressed as $I_{\text{CL}}^{\text{max}}$ or AUC) of the three compounds is beneficial in comparison to others, which make them promising substrates for analytical purposes. These are ATEs containing 4-nitro-, 2-methoxy- and 2-isopropyl groups, attached in the benzene ring (compounds 4NO₂-ATE, 2MeO-ATE, 2iPr-ATE, respectively, Table 1). Two of them were selected for further investigations, namely 4NO₂-ATE and 2MeO-ATE, as they differed in terms of character and location of the substituent, which may influence possible interactions that may occur among ATE (the CL indicator) and AO (the analyte). They somewhat differ in terms of the shape of the CL profile in an aqueous environment. According to that, 4NO₂-ATE is characterised by the highest maximal temporary emission ($I_{\text{CL}}^{\text{max}}$), making the essential parameter employed in luminescence analysis. Its high-value results from the strong electron-acceptor properties of the NO₂ group, as is the case among typical AEs [49]. However, the compound 4NO₂-ATE, due to the narrowest emission profile among investigated ones, is at the same time characterised by the only moderate value of integral emission (AUC) (Fig. 2).

In the case of 2MeO-ATE, quite the opposite feature is observed, as it is characterised by the highest AUC and moderate values of $I_{\text{CL}}^{\text{max}}$ among researched acridinium salts. The latter parameter is preferably employed in luminescence analytics, as it reflects the signal's intensity in the entire spectral range. However, integrating algorithms must be implemented for assessment, which are not always available in routine work devices.

Discussing the usefulness of new chemiluminogenic reagents and comparing the emission effectiveness of representative acridinium thio- vs. oxo-esters at the same experimental conditions seems beneficial. In general, the emission efficiencies of both groups of chemiluminogenic salts are quite comparable, although they present different types of CL profiles. The thioesters, regardless of the functional group present in the benzene ring, are characterised by flash-time emission, resulting in generally high $I_{\text{CL}}^{\text{max}}$ values and, at the same time, moderate to low AUC values. Among AEs, the opposite situation typically occurs – especially if the electron-donating group (e.g. alkyl, alkoxy group, etc.) is introduced into the phenoxy moiety (the leaving group) [15,48,49]. Fig. 6S (ESI) presents an exemplary diagram illustrating such a relationship – in which one of the most efficiently emitting AE, 9-(3-methyl phenoxy carbonyl)-10-methyl acridinium triflate [15] (encoded here as 3Me-AE), and one of ATEs of the highest efficiency of emission, 2iPr-ATE (Table 1) are presented. However, it should be noted that after a specified period (1 month, 4 °C, aqueous environment, pH = 3), a substantial loss of emissive capability was observed in the case of all ATEs (loss of emission

Table 2

Kinetic parameters of CL obtained by plate luminometry for selected acridinium thioesters (ATEs, Table 1) in various liquid environments. The concentration of ATEs was 1.0×10^{-10} M, triggering solution: $\text{H}_2\text{O}_2/\text{KOH}$; for details, see the Materials and Methods section.

Cpd code (Table 1)	Solvent	CL decay rate constant (k_{CL} , s^{-1})	Correlation coefficient (R^2)	Half-life ^a ($t_{1/2}$, sec.)	Time of max. CL intensity (t_{max} , s)	Intercept
4NO ₂ -ATE	Water	1.10	0.97	0.63	0.30	13.0
2MeO-ATE		1.03	0.95	0.68		12.7
4NO ₂ -ATE	Ethanol	0.76	0.85	0.92		12.8
2MeO-ATE		1.24	0.98	0.56		14.5
4NO ₂ -ATE	DMSO	1.06	0.91	0.65		13.6
2MeO-ATE		1.28	0.92	0.54		13.8

^a Half-life values were calculated on the basis on CL time profiles and reflect the times required for a quantity of ATE to reduce to half of its initial amount [50].

in the range of ca. 50–75 %, depending, data not shown) – which reveals that ATEs are somewhat more prone to hydrolysis than their O-analogues. However, this does not exclude them from analytical uses if work solutions of ATEs are prepared freshly before planned experiments.

To investigate the influence of the environment on the emissive properties of selected compounds (4NO₂-ATE and 2MeO-ATE), their emission efficiencies were assessed in various environments (water, ethanol and dimethylsulfoxide) under identical experimental conditions (Fig. 7S). The graphs indicate that the solvent type significantly impacts the emission efficiencies of ATEs (both $I_{\text{CL}}^{\text{max}}$ and AUC). However, the kinetics of CL decay does not change substantially, as indicated by comparable shapes of reaction profiles and experimentally assessed kinetic constants (Table 2). This makes another difference if one compares the emissive properties of ATEs vs. AEs. Considering emissive features, the latter chemiluminogenic substrates seem more environment-dependent, as indicated by our former studies [48].

Fig. 3 indicates that the trends in emissive properties for selected acridinium thioesters (4NO₂-ATE and 2MeO-ATE) are essentially similar in various environments. Among three solvents used as triggering mediums and keeping experimental settings constant, the lowest emission intensity is always observed in water (as referred to in both $I_{\text{CL}}^{\text{max}}$ and AUC). Similar to maximal emissions, quite distinct differences are observed in ethanol when comparing two selected salts, 4NO₂-ATE and 2MeO-ATE. Accordingly, $I_{\text{CL}}^{\text{max}}$ values (orange bars) increase monotonically in H₂O–EtOH–DMSO series for both emitters (relative values of $I_{\text{CL}}^{\text{max}}$ are ca. 1.0:3.0:3.5 for 4NO₂-ATE and 1.0:2.5:5.5 for 2MeO-ATE). It can be suggested that the CL efficiency of these acridinium salts increases with a decrease in solvent polarity in H₂O–EtOH–DMSO series (their relative polarities are 1.0, 0.65 and 0.44, respectively [48]).

Among the investigated systems, the highest intensity of CL emission is observed in DMSO (Fig. 3). It should be noted that the efficiency of CL emission is generally enhanced in polar and aprotic solvents, such as in the above one, as in the case of standard luminol, where its CL yield increases from ca. 1.2–5.0 % [69] when the medium is changed from water to DMSO, respectively. When analysing emissive properties of AEs in organic environments, similar behaviour is observed, although the changes are less distinct [48].

For practical reasons (biocompatibility, stability, low viscosity, and lack of eventual side reactions), water and water-ethanol systems were selected for the CL measurements in the presence of biological antioxidants chosen for this work (AOs). Three AOs were investigated in the context of luminometric assays, namely dithiothreitol (DTT), glutathione (GT) and quercetin (QR) (Fig. 1). The main assumption of undertaken experiments was to monitor and quantitate changes in emission parameters (CL intensity and decay kinetics and range of UV–Vis absorption), resulting from interactions/reactions between AOs and ATEs. We hoped that such experiments would enable the development of a new variant of a sensitive assay for quantitative determinations of antioxidants using acridinium CL, with perspectives for its further development.

The graphs, presenting the intensity of CL emission $I_{\text{CL}}^{\text{max}}$ and AUC vs AO content in the system (calibration graphs), are presented in Fig. 4. The relationships were obtained based on emission profiles in the

presence of constant amounts of investigated antioxidants, or a variable amount of an antioxidant added to the reacting system (Fig. 8S in ESI). Fig. 4 presents a non-linear relationship of CL intensities of 2MeO-ATE, selected in this experiment as CL indicator vs AOs concentration in the range of $1.0 \times 10^{-8} - 9.0 \times 10^{-6}$ M.

Significant changes in the intensity of CL emission are observed in the low concentration range of analytes ($10^{-8} - 10^{-7}$ M), which suggests various processes in the system, dependent on the proportion among reactants. Distinct signal variabilities are observed in the case of glutathione (GT) and dithiothreitol (DTT), which contain (reactive) thiol groups in their structures. On the other hand, the lowest variability of CL signal as a function of AO concentration is observed in the case of polyphenol quercetin (QR).

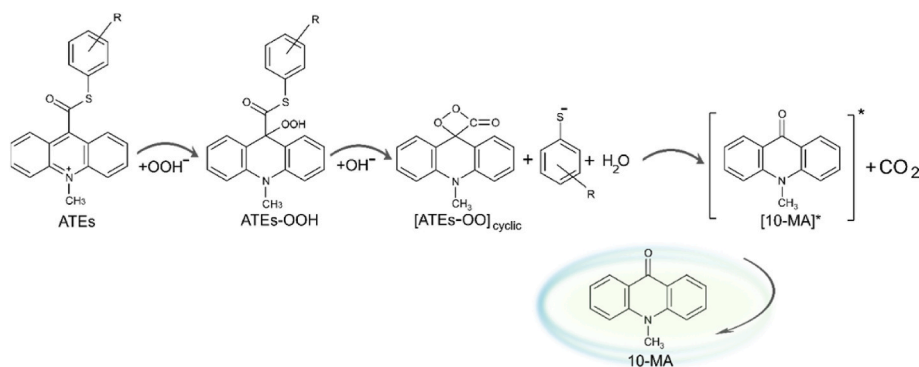
In general, glutathione (GT) seems to be the most effective antioxidant among those investigated, as was revealed by the highest decrease of both emission parameters if 2MeO-ATE was employed as a CL indicator. According to that, the $I_{\text{CL}}^{\text{max}}$ value for 2MeO-ATE decreased about 5.2 times for GT and about 2.8 times if dithiothreitol (DTT) or quercetin (QR) were present in the system (Fig. 4A). Similar situation occurs when AUC values are taken into consideration the latter parameter decreased ca. 10.6 times in the case of GT, while 5.1 times for DTT and 2.1 times for QR (Fig. 4B). Basing on the above observations and used methodology, it can be stated, that GT expresses the highest antioxidant activity among the investigated analytes. Similar results were obtained when 4NO₂-ATE was employed as a CL indicator. Still, the data was more scattered, likely because of its lower chemical stability in aqueous solution, than that of 2MeO-ATE.

The above interdependences were logarithmic, resulting in linear relationships presented in Fig. 9S in ESI. After assessing the regression parameters, LOD/LOQ values were derived. These values fall in the 0.65–0.79/1.9–2.4 μM range, using I_{CLmax} as a measurement parameter and 0.75–0.90/2.2–2.7 μM if AUC values were included in calculations (Table 1S in ESI). Obtained values for investigated compounds reflect their antioxidant activities (TAC) in the given system, comparable for GT and DTT and distinctly lower for QR.

It can be concluded that described here, a new variant of luminescence analysis utilising CL of ATEs enables us to obtain better or comparable sensitivities as the most sensitive assays described for analyses of antioxidant compounds, including the enhanced chemiluminescence method (ECL).

According to issues concerning emission kinetics, respective data obtained for the selected acridinium thioesters, namely 2MeO-ATE and 4NO₂-ATE (Table 1) in various environments is gathered in Table 2. The values of the pseudo-first-order rate constants (k_{CL}) were determined graphically by performing the linearisation of the time profiles of CL in each case (regression coefficients were in the range of 0.85–0.98) [50]. Emission profiles, recorded for investigated ATEs in a typical aqueous environment, are presented in Fig. 5S (ESI). On the other hand, Fig. 7S in ESI illustrates the CL profiles in various solvents recorded for both optimally performing substrates selected for quantitative analyses of AOs (4NO₂-ATE and 2MeO-ATE).

The data presented here clearly indicate that, regardless of the substituent introduced in the leaving group and the environment, the flash-type emission characterises all the investigated systems, reaching a



Scheme 2. A simplified scheme of transformations leading to ATE chemiluminescence is proposed at the DFT level of theory [51].

maximum intensity value of around 0.3 s. It suggests that the S atom in the thioester “leaving” group primarily determines the kinetics of CL decay among researched acridinium salts. This feature distinguishes the group of ATEs from typical acridinium esters (AEs), where the influence of the substituent in the benzene ring on the emission kinetics is distinct, changing rate constants even several times, depending on their type and location [15,48].

A closer look at the data collected in Table 2 indicates some differences and regularities. Generally, the organic environment seems to differentiate kinetic constants slightly more than the aqueous one, and this effect is more pronounced in the case of ethanol than DMSO. According to that, for the two selected salts, 2MeO-ATE and 4NO₂-ATE, almost identical rate constants of 1.0–1.1 s⁻¹ were obtained in water, while in ethanol, these values fall in the range of ca. 0.8–1.2 s⁻¹ and

DMSO – between 1.1 and 1.3 s⁻¹. The CL half-life times ($t_{1/2}$), calculated based on first-order kinetic constants [50], vary similarly, consistently assuming values below 1 s.

3.3. Computational studies on the formation of ATE-AO adducts

Our former investigations [51] revealed that forming an electronically excited product upon chemiluminogenic oxidation of acridinium thioesters occurs in two steps – contrary to the multistep process, characterising their O-analogues [15,70]. These steps include the transformation of the ATE into a cyclic intermediate ([ATE-OO]_{cyclic}, Scheme 2) after the concerted elimination of the thiophenyl anion, and in the second – the cyclic intermediate (dioxanone) is decarbonated to produce the electronically excited product – 10-methyl-acridan-9-one

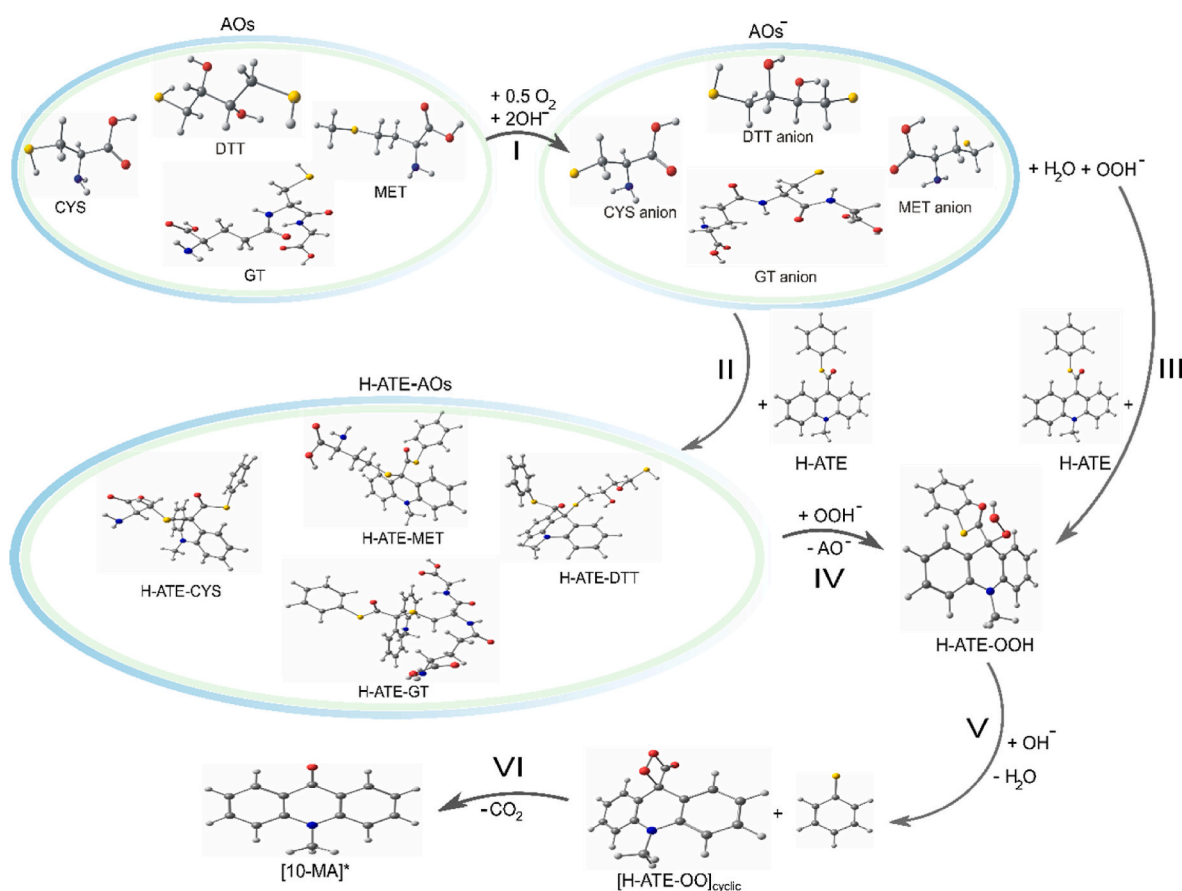


Fig. 5. The mechanism (DFT level of theory), presenting elementary steps occurring during chemiluminogenic transformations of representative acridinium thioester (H-ATE, Table 1) in the presence of selected AOs (Fig. 1). For details, see Materials and Methods section.

Table 3

Thermodynamic and kinetic data were obtained for the selected luminogenic systems containing antioxidants (ATEs + AOs) generated by quantum chemical calculations at the DFT level of theory.

THERMODYNAMIC CHARACTERISTIC					
Step no. (Fig. 5)	Nucleophile (AO)	Gaseous phase		Aqueous phase	
		$\Delta_{r,298}H^0$ <i>a</i>	$\Delta_{r,298}G^0$ <i>a</i>	$\Delta_{r,298}H^0$ <i>a</i>	$\Delta_{r,298}G^0$ <i>a</i>
I	DTT	−107.5	−104.1	−67.3	−63.7
	GT	−116.1	−113.2	−73.1	−70.5
VI	−	−6.9	−18.7	−7.5	−19.0
H-ATE					
II	DTT	−117.7	−104.3	−36.5	−23.4
	GT	−114.1	−97.6	−30.6	−13.4
III	−	−176.4	−162.3	−65.7	−52.5
IV	DTT	−58.6	−58.0	−29.2	−29.1
	GT	−62.3	−64.7	−35.1	−38.7
V	−	−73.3	−85.5	−51.1	−63.0
4NO ₂ -ATE					
II	DTT	−122.9	−109.8	−33.8	−20.8
	GT	−119.1	−103.3	−31.6	−14.5
III	−	−181.3	−167.5	−66.4	−52.2
IV	DTT	−58.3	−57.7	−32.7	−31.4
	GT	−62.1	−64.2	−34.9	−37.7
V	−	−92.9	−105.4	−59.1	−71.4
2MeO-ATE					
II	DTT	−113.8	−101.0	−33.6	−19.2
	GT	−110.4	−94.1	−32.5	−14.7
III	−	−168.9	−155.3	−61.7	−47.7
IV	DTT	−55.2	−54.4	−28.1	−28.5
	GT	−58.5	−61.2	−29.3	−33.1
V	−	−75.6	−89.3	−49.6	−63.8

KINETIC CHARACTERISTICS					
Step no. (Fig. 5)	Nucleophile (AO)	Gaseous phase		Aqueous phase	
		$\Delta_{a,298}H^0$ <i>a</i>	$\Delta_{a,298}G^{0\ a}$ $_{298}k^0$ ($_{298}\tau_{99}$) <i>b</i>	$\Delta_{a,298}H^0$ <i>a</i>	$\Delta_{a,298}G^0$ <i>a</i>
H-ATE					
TS-IV	DTT	23.5	42.1	65.5	83.8
			8.42×10^{-19} (5.47 $\times 10^{18}$)		
TS-VI	−	18.3	18.0	18.3	19.3
			4.01×10^{-1} (1.15 $\times 10^1$)		

^a $\Delta_{r,298}H^0$, $\Delta_{r,298}G^0$ and $\Delta_{a,298}H^0$, $\Delta_{a,298}G^0$ (all in kcal mol^{−1}), respectively, represent the enthalpy and Gibbs' free energy (gaseous phase) or free energy (aqueous phase) of the reaction (r) and activation (a) corresponding to a given step number (Fig. 5) at standard temperature and pressure.

^b $_{298}k^0$ (in s^{−1}) and $_{298}\tau_{99}$ (in seconds), respectively, denote the rate constant and the time after which the reaction is 99 % complete.

([10-MA]*, Scheme 2). However, computations revealed that ATEs are transformed more efficiently into the excited product. Still, at the same time – they are also more prone to hydrolysis than acridinium oxo-esters investigated so far [51]. Calculations were performed on the CL reaction mechanism in environments of different polarities to examine the possibility of reducing the last effect of ATEs [71]. They revealed that in nonpolar solvents (e.g. n-hexane), the CL reaction is characterised by more favourable thermodynamic and kinetic characteristics than in aqueous media or polar solvents (such as DMSO or alcoholic environment).

Our former studies [15,49–51,70] on the mechanism of CL of acridinium esters suggest that, as a primary result of oxidation in alkaline media, cyclic, high-energetic intermediates are formed by the elimination of respective phenoxy or carbonate anions (the leaving groups, mentioned above), leading to the formation of electronically excited molecules of N-substituted acridin-9-ones. Studies revealed that the type of the leaving group primarily determines the kinetics, chemical stability, and – to some extent – the efficiency of the emission [15,49–51,

65].

The LCAO coefficient of the p_z LUMO orbital on the carbon atom in position 9 of the acridinium moiety is only slightly lower in acridinium thioesters than in acridinium esters (0.315 vs. 0.325, respectively) [15, 51]. This indicates that both chemiluminogenic salts are characterised by comparable susceptibility to the nucleophilic attack of OOH[−], starting the chemiluminogenic oxidation.

Computational methods were applied to predict and understand the mechanism of transformations in the investigated complex systems. We wanted to know how the ATEs react to AOs and the cause of the decrease in emission intensity. Three structures of ATEs (H-ATE, 4NO₂-ATE and 2MeO-ATE) and four AOs (DTT, CYS, MET and GT) were selected for computations. Based on our previous theoretical studies [51,71], we have postulated the CL pathway, resulting from the reaction of acridinium thioesters with antioxidants, presented in Fig. 5. Tables 3 and 2S in ESI summarise the results of quantum-chemical calculations of investigated reaction steps (Fig. 5) for all derivatives selected to computational studies. Fig. 6 shows PES profile against reaction progress of the investigated chemiluminescence reaction for the combination of unsubstituted acridinium thioester (H-ATE) with the one of the investigated antioxidants – DTT. Additionally, the density functional theory (DFT) optimised geometries of all considered molecules (lowest energy and transition state structures), along with their cartesian coordinates, are shown in Table 3S in ESI.

As previously confirmed experimentally and computationally [15, 49,51,52,71], acridinium derivatives readily undergo oxidation in an alkaline environment. A nucleophilic attack of an anionic form of an oxidant (e.g. OOH[−], formed in an alkaline media according to the reaction: H₂O₂ + OH[−] → OOH[−] + H₂O) on the carbon atom in position 9 of acridine moiety initiates the CL reaction. In the next step, an energy-rich cyclic intermediate is formed, which can create an electronically excited product – N-substituted-acridan-9-one, resulting from decomposition. This excited product, returning to the ground state, gives off part of the excess energy in the form of visible light. However, our previous study [16] showed that some sulphur nucleophilic drugs can initiate the formation of OOH[−] ions when reacted with oxygen in an alkaline environment. Based on them, we proposed a mechanism for forming electronically excited products due to the reaction of biological antioxidants selected for this work, with acridinium thioesters, shown in Fig. 5.

The results of computational studies reveal that forming OOH[−] ions in the reaction of sulphur antioxidants with oxygen in an alkaline environment (step I, Figs. 5 and 6) is possible. The enthalpy and free energy values in the gaseous and aqueous phases indicate the thermodynamically preferred formation of peroxyhydrogen ions in the case of all studied antioxidants (Table 3, step I). In the next step, we checked which nucleophilic attack on the carbon atom at position 9 of acridine moiety (preferred position of the nucleophile addition [51,71]) would be more energetically favourable – the antioxidant anion (AOs[−]), formed in step I, or OOH[−] ion (Figs. 5 and 6, step II and III, respectively). The values of enthalpy and free energy in the gaseous and aqueous phases show that both additions of the nucleophilic anions are possible. Still, the addition of peroxyhydrogen ions seems to be more thermodynamically preferable. However, in the next step, we checked whether it is possible to exchange AO[−] anion bound to ATE for OOH[−] ion (Fig. 5, step IV). The results (Table 3 and Fig. 6) indicate that such an exchange will be thermodynamically possible. It can, therefore, be assumed that both pathways will compete with each other (steps II and IV with step III). Kinetic factors likely determine which pathway reaction will be directed. For this reason, we checked the activation barrier for the reaction of AO[−] to OOH[−] ion exchange in the reaction with DTT (step IV, Figs. 5 and 6). The activation barrier for step IV was determined only in the case of one reactant (DTT) due to the elevated difficulty and time-consuming nature of the computations and obtaining results comparable to our previous studies, concerning 9-cyano-10-methylacridinium cation and sulphur nucleophiles [16]. The activation barriers are

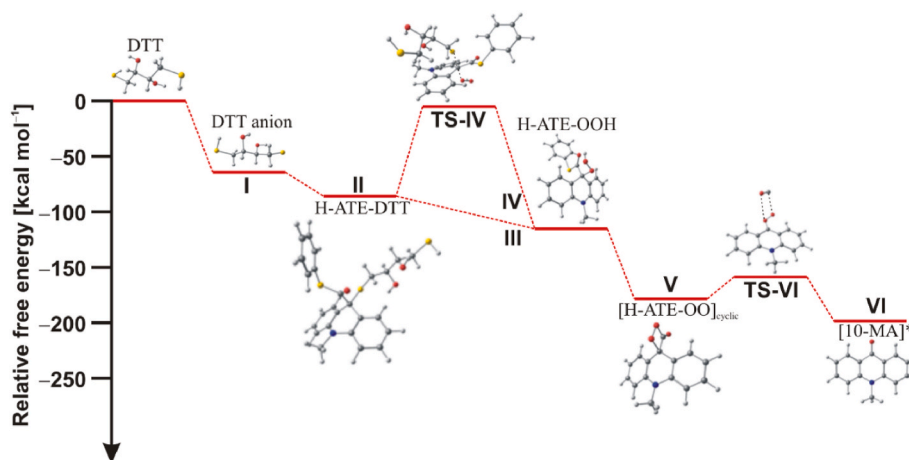


Fig. 6. The diagram of relative free energy in the aqueous phase of the reaction of chemiluminogenic transformation of representative acridinium thioester (H-ATE) in the presence of representative antioxidant (DTT) (see Fig. 5).

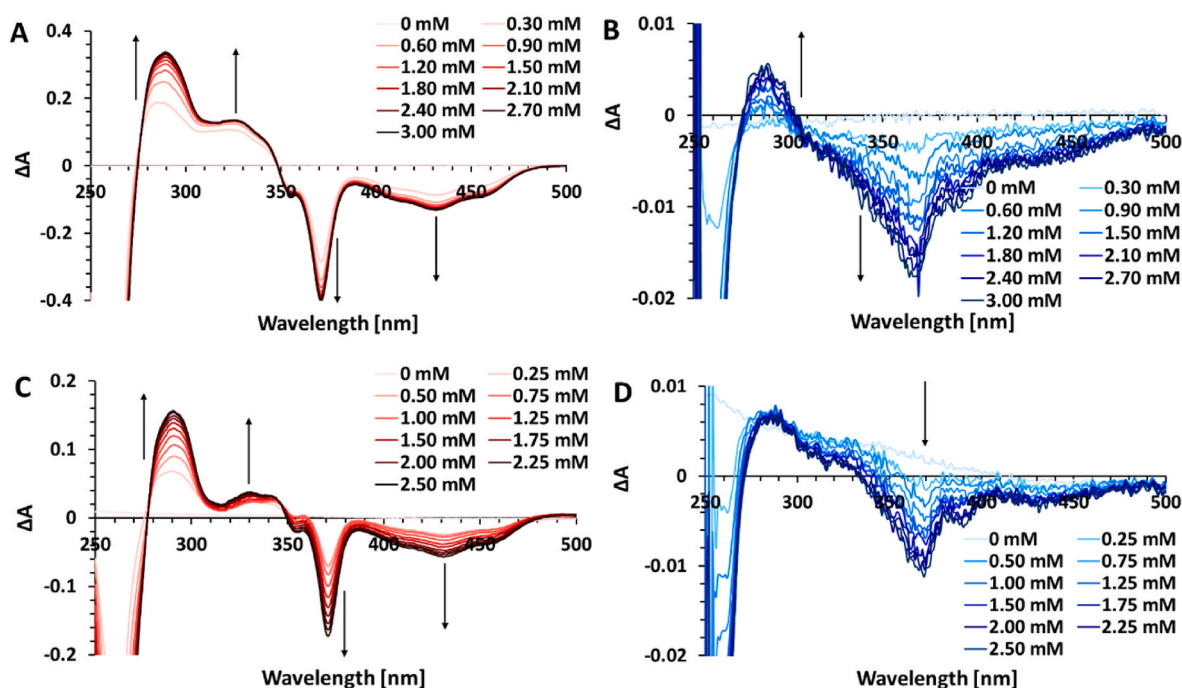


Fig. 7. Differential UV-Vis spectra recorded for selected ATE-AO systems in aqueous-ethanolic solutions (pH = 3.5). 4NO₂-ATE/DTT (A), 2MeO-ATE/DTT (B), 4NO₂-ATE/GT (C), 2MeO-ATE/GT (D). The concentration of 4NO₂-ATE and 2MeO-ATE was constant in all experiments and equal to 1.0×10^{-4} M.

very high both in the gaseous and aqueous phases (the values of Gibbs free energy (gaseous phase) and free energy (aqueous phase) are 42.1 and 83.8 kcal mol⁻¹, respectively). The results of kinetic characteristics of step IV may exclude steps II and IV (Figs. 5 and 6). On the other hand, the simultaneous occurrence of both reactions (the path with steps I, II and IV, and the path with steps I and III) may be a determinant of the participation of antioxidants in the analytical approach, proposed in this work.

The next step takes place in an alkaline media, in which the thiophenyl anion is detached and an energy-rich cyclic intermediate – [ATE-OO]_{cyclic} – is formed (Fig. 5, step V), which, undergoing decarboxylation, forms an electronically excited product of CL reaction – 10-methyl-acridan-9-one ([10-MA]*, Fig. 5, step VI). Both steps are thermodynamically favourable in the gaseous and aqueous phases. The results of computational studies show that step V is thermodynamically most favoured in the case of the 4NO₂-ATE derivative. At this step, the

other two investigated derivatives (H-ATE and 2MeO-ATE) have similar enthalpy and free energy values in the gaseous and aqueous phases. Step VI will be decisive for the reaction rate due to the activation barrier accompanying the decomposition of the cyclic intermediate ([ATE-OO]_{cyclic}) and the formation of the electronically excited product – 10-methyl-acridan-9-one ([10-MA]*). The activation barrier presented in Table 3 for this step is relatively low (not exceeding 20 kcal mol⁻¹).

3.3.1. UV-Vis absorption spectroscopy studies on the formation of ATE-AO adducts

We performed spectrophotometric experiments to confirm the mechanism postulated by the DFT level theory. Fig. 7 presents differential UV-Vis spectra for selected substrates, 4NO₂-ATE and 2MeO-ATE, in the absence and presence of DTT and GT as exemplary AOs. These spectra were obtained based on spectrophotometric titrations performed for all studied systems (appropriate UV-Vis spectra are shown in

Fig. 10S in ESI). The stability of 4NO₂-ATE and 2MeO-ATE within 8 h has been checked and confirmed spectrophotometrically (**Fig. 11S** in ESI). It can be observed that under the action of DTT and GT, the absorption at wavelengths shorter than 350 nm increases (with maxima at approximately 290, 330 and 340 nm). In contrast, the opposite effect can be observed at wavelengths longer than 350 nm (with clear minima at approximately 370 and 430 nm). The observed changes are more significant for 4NO₂-ATE when compared with 2MeO-ATE, proving that a new chemical entity is formed due to the reaction between ATEs and AOs. The increase and decrease of absorbance for both investigated ATEs under the action of two structurally different antioxidants observed at the same wavelengths are in good agreement with theoretical calculations, which indicate the formation of the same type of individuals in all studied systems.

4. Conclusions

Six original compounds capable of chemiluminescence, namely 10-methyl-9-((phenylthio)carbonyl)acridin-10-ium trifluoromethanesulphonates (ATEs), were obtained in three-step syntheses with moderate to high overall yields (average value 56 %) by adopting and optimising known procedures. The above S-containing acridinium salts were isolated in chemically pure form, applying classical preparation techniques (extraction, precipitation and crystallisation, TLC and LC chromatography). The purity of the investigated compounds – the CL indicators were assessed by RP-HPLC (>99 % in all cases), and their chemical identity was confirmed by high-resolution spectroscopic techniques, such as ESI-QTOF MS and ¹H + ¹³C NMR and FT-IR spectra.

10-Methyl-9-((phenylthio)carbonyl)acridin-10-ium cations effectively react with hydrogen peroxide in an alkaline medium (hydroperoxyl anions, OOH⁻), which causes flash-type emissions, regardless of the substituent introduced in the benzene ring. The latter feature distinguishes the investigated group of compounds from typical acridinium aromatic esters (AEs), in which the type and location of the substituent in this moiety primarily determine the emission kinetics [15,49]. The CL yields of 10-methyl-9-((phenylthio)carbonyl)acridin-10-ium cations and their O-analogues, 10-methyl-9-(phenoxy)carbonyl)acridinium cations, turned out to be comparable, which indicates their high reactivity, giving perspectives for their practical uses. However, the resistance to hydrolysis of ATEs in aqueous environments seems somewhat lower than that of AEs, but it does not exclude their practical applications.

An example of utilisation of the acridinium thioesters is given, as they were employed as CL indicators in determining some biological antioxidants (AOs), which are dithiothreitol, glutathione and quercetin. Favourable analytical parameters, including detection/determination limits (LOD/LOQ) for AOs in the range of 0.7–2.7 × 10⁻⁶ M) were obtained, which opens up the perspectives for their uses as new types of CL indicators and fragments of labels.

Quantum-chemical calculations at the DFT and TD-DFT levels of theory have proven that the formation of adducts of acridinium thioesters and anions of mentioned-above antioxidants is preferred. Additionally, it was confirmed that the presence of AOs affects the chemiluminogenic transformation of ATEs by forming OOH⁻ ions in the reaction of sulphur antioxidants with oxygen in an alkaline environment and improving the efficiency of the formation of the electronically excited product, that is, 10-methyl-acridan-9-one.

UV–Vis absorption spectroscopy further proved the formation of adducts between the chemiluminogenic substrates and antioxidants proposed here. These studies revealed that the absorption of formed ATE-AO adducts differs more or less within the wavelength range 275–500 nm compared to the sum of the absorptions of pure individuals (ATEs and AOs) undergoing reaction.

CCRediT authorship contribution statement

Vladyslav Ievtukhov: Visualization, Investigation, Formal analysis,

Data curation, Writing – original draft. **Anna Romanowska:** Investigation, Funding acquisition, Formal analysis, Data curation. **Milena Pienkos:** Visualization, Investigation, Formal analysis, Data curation. **Krzysztof Zamojć:** Writing – original draft, Visualization, Methodology, Investigation. **Beata Zadykiewicz:** Writing – review & editing, Writing – original draft, Visualization, Supervision, Methodology, Investigation, Funding acquisition, Conceptualization. **Karol Krzysiński:** Writing – review & editing, Writing – original draft, Supervision, Methodology, Funding acquisition, Conceptualization.

Declaration of competing interest

The authors declare that they have no known competing financial interests or personal relationships that could have appeared to influence the work reported in this paper.

Data availability

Data will be made available on request.

Acknowledgements

This research was funded by the Polish Ministry of Science and Higher Education within grants BMN 538-8226-B738-15 (B.Z.), 538-8226-B413-16, 538-8226-B413-17 (A.R.) and Statutory Activity grant (DS) No. 531-T080-D742-23 (K.K.). The purchase of the tube luminometer (Lumat3 LB 9508) manufactured by Berthold Technologies was possible as a result of financial support from the National Scientific Centre (NCN) through Grant No. 2011/03/D/ST4/02419 (Contract No. UMO-2011/03/D/ST4/02419). Calculations were carried out on the computers of the Wrocław Centre for Networking and Supercomputing (WCSS) (Grant No. 215).

Appendix A. Supplementary data

Supplementary data to this article can be found online at <https://doi.org/10.1016/j.jlumin.2024.120745>.

References

- [1] A. Albert, *The Acridines: Their Preparation, Physical, Chemical and Biological Properties and Use*, Edward Arnold & Co, London, 1951.
- [2] M.A.P. Martins, C.P. Frizzo, D.N. Moreira, L. Buriol, P. Machado, Solvent-free heterocyclic synthesis, *Chem. Rev.* 109 (2009) 4140–4182, <https://doi.org/10.1021/cr9001098>.
- [3] A. Kellmann, Intersystem crossing and internal conversion quantum yields of acridine in polar and nonpolar solvents, *J. Phys. Chem.* 81 (1977) 1195–1198, <https://doi.org/10.1021/j100527a014>.
- [4] W.A. Denny, Acridine derivatives as chemotherapeutic agents, *Curr. Med. Chem.* 9 (2002) 1655–1665, <https://doi.org/10.2174/0929867023369277>.
- [5] M. Małachowska-Ugarte, G. Cholewiński, K. Dzierzbicka, P. Trzonkowski, Synthesis and biological activity of novel mycophenolic acid conjugates containing nitro-acridine/acridone derivatives, *Eur. J. Med. Chem.* 54 (2012) 197–201, <https://doi.org/10.1016/j.ejmech.2012.04.040>.
- [6] M. Gensicka-Kowalewska, G. Cholewiński, K. Dzierzbicka, Recent developments in the synthesis and biological activity of acridine/acridone analogues, *RSC Adv.* 7 (2017) 15776–15804, <https://doi.org/10.1039/C7RA01026E>.
- [7] T. Matsuno, T. Hirano, M. Ohashi, Mass spectrometric investigation of structures of intermediates in acridine chemiluminescence, *J. Mass Spectrom. Soc. Jpn.* 44 (1996) 175–181, <https://doi.org/10.5702/masspec.44.175>.
- [8] M. Nakazono, S. Nanbu, T. Akita, K. Hamase, Acridinium ester chemiluminescence: methyl substitution on the acridine moiety, *J. Oleo Sci.* 70 (2021) 1677–1684, <https://doi.org/10.5650/jos.ess21186>.
- [9] J.C. Fister III, J.M. Harris, D. Rank, W. Wacholtz, Molecular photophysics of Acridine Yellow studied by phosphorescence and delayed fluorescence: an undergraduate physical chemistry experiment, *J. Chem. Educ.* 74 (1997) 1208–1212, <https://doi.org/10.1021/ed074p1208>.
- [10] C.D. Geddes, Optical thin film polymeric sensors for the determination of aqueous chloride, bromide and iodide ions at high pH, based on the quenching of fluorescence of two acridinium dyes, *Dyes Pigments* 45 (2000) 243–251, [https://doi.org/10.1016/S0143-7208\(00\)00025-5](https://doi.org/10.1016/S0143-7208(00)00025-5).
- [11] S. Majeed, W. Gao, Y. Zholudov, K. Muzyka, G. Xu, Electrochemiluminescence of acridines, *Electroanalysis* 28 (2016) 2672–2679, <https://doi.org/10.1002/elan.201600209>.

- [12] M.G. Palmgren, Acridine orange as a probe for measuring pH gradients across membranes: mechanism and limitations, *Anal. Biochem.* 192 (1991) 316–321, [https://doi.org/10.1016/0003-2697\(91\)90542-2](https://doi.org/10.1016/0003-2697(91)90542-2).
- [13] V.A. Byval'tsev, L.A. Bardanova, N.R. Onaka, R.A. Polkin, S.V. Ochkal, V. V. Shepelev, M.A. Aliyev, A.A. Potapov, Acridine Orange: a review of novel applications for surgical cancer imaging and therapy, *Front. Oncol.* 9 (2019) 925, <https://doi.org/10.3389/fonc.2019.00925>.
- [14] K. Smith, X. Mu, Z. Li, A.M. Holland, J.S. Woodhead, G.A. El-Hiti, Synthesis, structure elucidation, and chemiluminescent activity of new 9-substituted 10-(ω-(succinimidylloxycarbonyl)alkyl)acridinium esters, *Luminescence* 38 (2023) 487–496, <https://doi.org/10.1002/bio.4474>.
- [15] K. Krzyminiński, A. Ożóg, P. Malecha, A.D. Roshal, A. Wróblewska, B. Zadykiewicz, J. Błażejowski, Chemiluminogenic features of 10-methyl-9-(phenoxy carbonyl) acridinium trifluoromethanesulfonates alkyl substituted at the benzene ring in aqueous media, *J. Org. Chem.* 76 (2011) 1072–1085, <https://doi.org/10.1021/jo120882>.
- [16] V. Ievtukhov, B. Zadykiewicz, M.Y. Blazheyevskiy, K. Krzyminiński, New luminometric method for quantification of biological sulfur nucleophiles with the participation of 9-cyano-10-methylacridinium salt, *Luminescence* 37 (2022) 208–219, <https://doi.org/10.1002/bio.4162>.
- [17] L.J. Kricka, Clinical applications of chemiluminescence, *Anal. Chim. Acta* 500 (2003) 279–286, [https://doi.org/10.1016/S0003-2670\(03\)00809-2](https://doi.org/10.1016/S0003-2670(03)00809-2).
- [18] M. Yang, J. Huang, J. Fan, J. Du, K. Pu, X. Peng, Chemiluminescence for bioimaging and therapeutics: recent advances and challenges, *Chem. Soc. Rev.* 49 (2020) 6800–6815.
- [19] J.F. Huertas-Pérez, D. Moreno-González, D. Airado-Rodríguez, F.J. Lara, A. M. García-Campaña, Advances in the application of chemiluminescence detection in liquid chromatography, *Trends Anal. Chem.* 75 (2016) 35–48, <https://doi.org/10.1016/j.trac.2015.07.004>.
- [20] D.L. Giokas, A.G. Vlessidis, G.Z. Tsogas, N.P. Evmiridis, Nanoparticle-assisted chemiluminescence and its applications in analytical chemistry, *Trends Anal. Chem.* 29 (2010) 1113–1126, <https://doi.org/10.1016/j.trac.2010.07.001>.
- [21] L. Gámiz-Gracia, A.M. García-Campaña, J.F. Huertas-Pérez, F.J. Lara, Chemiluminescence detection in liquid chromatography: applications to clinical, pharmaceutical, environmental and food analysis – a review, *Anal. Chim. Acta* 640 (2009) 7–28, <https://doi.org/10.1016/j.aca.2009.03.017>.
- [22] S.R.S. Pour, D. Calabria, A. Nascetti, D. Caputo, G. De Cesare, M. Guardigli, M. Zangheri, M. Mirasoli, Easy-to-Use chemiluminescent-based assay for a rapid and low-cost evaluation of the antioxidant activity of cosmetic products, *Chemosensors* 12 (2024) 25–41, <https://doi.org/10.3390/chemosensors12020025>.
- [23] A.P. Richardson, J.B. Kim, G.J. Barnard, W.P. Collins, F. McCapra, Chemiluminescence immunoassay of plasma progesterone, with progesterone-acridinium ester used as the labelled antigen, *Clin. Chem.* 31 (1985) 1664–1668, <https://doi.org/10.1093/clinchem/31.10.1664>.
- [24] L. Zhao, L. Sun, X. Chu, Chemiluminescence immunoassay, *Trends Anal. Chem.* 28 (2009) 404–415, <https://doi.org/10.1016/j.trac.2008.12.006>.
- [25] I.Y. Goryacheva, P. Lenain, S. De Saeger, Nanosized labels for rapid immunotests, *Trends Anal. Chem.* 46 (2013) 30–43, <https://doi.org/10.1016/j.trac.2013.01.013>.
- [26] L. Holec-Gąsior, B. Ferra, J. Czechowska, I.E. Serdiuk, K. Krzyminiński, J. Kur, *Diagn. Microbiol. Infect. Dis.* 85 (2016) 422–425, <https://doi.org/10.1016/j.diagmicrobio.2016.05.013>.
- [27] A. Roda, M. Guardigli, Analytical chemiluminescence and bioluminescence: latest achievements and new horizons, *Anal. Bioanal. Chem.* 402 (2012) 69–76, <https://doi.org/10.1007/s00216-011-5455-8>.
- [28] H. Arakawa, K. Tsuruoka, K.I. Ohno, N. Tajima, H. Nagano, Development of a highly sensitive chemiluminescent assay for hydrogen peroxide under neutral conditions using acridinium ester and its application to an enzyme immunoassay, *Luminescence* 29 (2014) 374–377, <https://doi.org/10.1002/bio.2555>.
- [29] J. Zhang, P. Cheng, K. Pu, Recent advances of molecular optical probes in imaging of β-galactosidase, *Bioconjugate Chem.* 30 (2019) 2089–2101, <https://doi.org/10.1021/acs.bioconjchem.9b00391>.
- [30] A. Ogawa, H. Arai, H. Tanizawa, T. Miyahara, T. Toyō'oka, On-line screening method for antioxidants by liquid chromatography with chemiluminescence detection, *Anal. Chim. Acta* 383 (1999) 221–230, [https://doi.org/10.1016/S0003-2670\(98\)00747-8](https://doi.org/10.1016/S0003-2670(98)00747-8).
- [31] K. Krzyminiński, A.D. Roshal, P.B. Rudnicki-Velasquez, K. Żamojć, On the use of acridinium indicators for the chemiluminescent determination of the total antioxidant capacity of dietary supplements, *Luminescence* 34 (2019) 512–519, <https://doi.org/10.1002/bio.3629>.
- [32] A. Roda, P. Pasini, M. Mirasoli, E. Michelini, M. Guardigli, Biotechnological applications of bioluminescence and chemiluminescence, *Trends Biotechnol.* 22 (2004) 295–303, <https://doi.org/10.1016/j.tibtech.2004.03.011>.
- [33] C. Dodeigne, L. Thunus, R. Lejeune, Chemiluminescence as a diagnostic tool. A review, *Talanta* 501 (2000) 415–439, [https://doi.org/10.1016/S0039-9140\(99\)00294-5](https://doi.org/10.1016/S0039-9140(99)00294-5).
- [34] Z. Wang, J. Huang, J. Huang, B. Yu, K. Pu, F.J. Xu, Chemiluminescence: from mechanism to applications in biological imaging and therapy, *Aggregate* 2 (2021) e140, <https://doi.org/10.1002/agt2.140>.
- [35] A. Wróblewska, O.M. Huta, I.O. Patsay, R.S. Petryshyn, J. Błażejowski, Addition of nucleophiles to the 9-cyano-10-methylacridinium cation: utilization in their chemiluminescent assay, *Anal. Chim. Acta* 507 (2004) 229–236, <https://doi.org/10.1016/j.aca.2003.11.032>.
- [36] H. Akhavan-Tafti, Chemiluminescent detection of horseradish peroxidase by the enzymatic generation of acridinium esters, *Clin. Chem.* 41 (1995) 1368–1369, <https://doi.org/10.1093/clinchem/41.9.1368>.
- [37] J.D. Lambeth, Nox enzymes, ROS, and chronic disease: an example of antagonistic pleiotropy, *Free Rad. Biol. Med.* 43 (2007) 332–347, <https://doi.org/10.1016/j.freeradbiomed.2007.03.027>.
- [38] M. Valko, K. Jomova, C.J. Rhodes, K. Kuča, K. Musilek, Redox- and non-redox-metal-induced formation of free radicals and their role in human disease, *Arch. Toxicol.* 90 (2016) 1–37, <https://doi.org/10.1007/s00204-015-1579-5>.
- [39] T.S. Leyane, S.W. Jere, N.N. Hourel, Oxidative stress in ageing and chronic degenerative pathologies: molecular mechanisms involved in counteracting oxidative stress and chronic inflammation, *Int. J. Mol. Sci.* 23 (2022) 7273, <https://doi.org/10.3390/ijms23137273>.
- [40] I.Z. Sadiq, Free radicals and oxidative stress: signalling mechanisms, redox basis for human diseases, and cell cycle regulation, *Curr. Mol. Med.* 23 (2023) 13–35, <https://doi.org/10.2174/1566524022666211222161637>.
- [41] B. Halliwell, Antioxidants in human health and disease, *Annu. Rev. Nutr.* 16 (1996) 33–50, <https://doi.org/10.1146/annurev.nu.16.070196.000341>.
- [42] C.S. Yang, C.-T. Ho, J. Zhang, X. Wan, K. Zhang, J. Lim, Antioxidants: differing meanings in food science and health science, *J. Agric. Food Chem.* 66 (2018) 3063–3068, <https://doi.org/10.1021/acs.jafc.7b05830>.
- [43] A.A. Adwas, A.S.I. Elsayed, A.E. Azab, F.A. Quwaydir, Oxidative stress and antioxidant mechanisms in the human body, *J. Appl. Biotechnol. Bioeng.* 6 (2019) 43–47, <https://doi.org/10.15406/jabb.2019.06.00173>.
- [44] A. Rana, M. Samtiya, T. Dhewa, V. Mishra, R.E. Aluko, Health benefits of polyphenols: a concise review, *J. Food Biochem.* 46 (2022) e14264, <https://doi.org/10.1111/jfbc.14264>.
- [45] I.G. Munteanu, C. Apetrei, Analytical methods used in determining antioxidant activity: a review, *Int. J. Mol. Sci.* 22 (2021) 3380, <https://doi.org/10.3390/ijms22073380>.
- [46] T. Köszegi, N. Sali, M. Raknić, Z. Horváth-Szalai, R. Csepregi, M. Zovko Končić, N. Papp, M. Poór, A novel luminol-based enhanced chemiluminescence antioxidant capacity microplate assay for use in different biological matrices, *J. Pharmacol. Toxicol. Methods* 88 (2017) 153–159, <https://doi.org/10.1016/j.vascn.2017.09.256>.
- [47] T.M. Said, N. Kattal, R.K. Sharma, S.C. Sikka, A.J. Thomas Jr., E. Mascha, A. Agarwal, Enhanced chemiluminescence assay vs colorimetric assay for measurement of the total antioxidant capacity of human seminal plasma, *J. Androl.* 24 (2003) 676–680, <https://doi.org/10.1002/j.1939-4640.2003.tb02726.x>.
- [48] K. Krzyminiński, A.D. Roshal, B. Zadykiewicz, A. Białk-Bielińska, A. Sieradzka, Chemiluminogenic properties of 10-methyl-9-(phenoxy carbonyl)acridinium cations in organic environments, *J. Phys. Chem. A* 114 (2010) 10550–10562, <https://doi.org/10.1021/jp104253f>.
- [49] B. Zadykiewicz, J. Czechowska, A. Ożóg, A. Renkevich, K. Krzyminiński, Effective chemiluminogenic systems based on acridinium esters bearing substituents of various electronic and steric properties, *Org. Biomol. Chem.* 14 (2016) 652–668, <https://doi.org/10.1039/C5OB01798J>.
- [50] P.W. Atkins, J. De Paula, J. Keeler, *Atkins' Physical Chemistry*, Oxford University Press, Oxford, 2017.
- [51] M. Piękos, B. Zadykiewicz, Computational insights on the mechanism of the chemiluminescence reaction of a new group of chemiluminogens – 10-methyl-9-thiophenoxy carbonyl acridinium cations, *Int. J. Mol. Sci.* 21 (2020) 4417, <https://doi.org/10.3390/ijms21124417>.
- [52] J. Czechowska, A. Kawecka, A. Romanowska, M. Marczak, P. Wityk, K. Krzyminiński, B. Zadykiewicz, Chemiluminogenic acridinium salts: a comparison study. Detection of intermediate entities appearing upon light generation, *J. Lumin.* 187 (2017) 102–112, <https://doi.org/10.1016/j.jlumin.2017.02.068>.
- [53] J.K. Labanowski, J.W. Andzelm, *Density Functional Methods in Chemistry*, Springer, New York, NY, USA, 1991.
- [54] J.D. Chai, M. Head-Gordon, Long-range corrected hybrid density functionals with damped atom-atom dispersion corrections, *Phys. Chem. Chem. Phys.* 10 (2008) 6615–6620, <https://doi.org/10.1039/B810189B>.
- [55] P.C. Hariharan, J.A. Pople, The influence of polarisation functions on molecular orbital hydrogenation energies, *Theoret. Chim. Acta* 28 (1973) 213–222, <https://doi.org/10.1007/BF00533485>.
- [56] G. Scalmani, M.J. Frisch, B. Mennucci, J. Tomasi, R. Cammi, V. Barone, Geometries and properties of excited states in the gas phase and solution: theory and application of a time-dependent Density Functional Theory Polarizable Continuum Model, *J. Chem. Phys.* 124 (2006) 094107, <https://doi.org/10.1063/1.2173258>.
- [57] J.M. Lourenço, J.C.G. Esteves da Silva, L. Pinto da Silva, Combined experimental and theoretical study of Coelenterazine chemiluminescence in aqueous solution, *J. Lumin.* 194 (2018) 139–145, <https://doi.org/10.1016/j.jlumin.2017.10.025>.
- [58] L. Pinto da Silva, C.M. Magalhães, Mechanistic insights into the efficient intramolecular chemiexcitation of dioxetanones from TD-DFT and multireference calculations, *Int. J. Quant. Chem.* 119 (2019) e25881, <https://doi.org/10.1002/qua.25881>.
- [59] C.M. Magalhães, P. González-Berdullas, J.C.G. Esteves da Silva, L. Pinto da Silva, Elucidating the chemiexcitation of dioxetanones by replacing the peroxide bond with S–S, N–N and C–C bonds, *New J. Chem.* 45 (2021) 18518–18527, <https://doi.org/10.1039/D1NJ03440E>.
- [60] K. Fukui, The path of chemical reactions – the IRC approach, *Acc. Chem. Res.* 14 (1981) 363–368, <https://doi.org/10.1021/ar00072a001>.
- [61] J. Tomasi, M. Persico, Molecular interactions in solution: an overview of methods based on continuous distributions of the solvent, *Chem. Rev.* 94 (1994) 2027–2094, <https://doi.org/10.1021/cr00031a013>.
- [62] V. Barone, M. Cossi, J. Tomasi, A new definition of cavities for the computation of solvation free energies by the polarizable continuum model, *J. Chem. Phys.* 107 (1997) 3210–3221, <https://doi.org/10.1063/1.474671>.

- [63] M.J. Frisch, G.W. Trucks, H.B. Schlegel, G.E. Scuseria, M.A. Robb, J.R. Cheeseman, G. Scalmani, V. Barone, G.A. Petersson, H. Nakatsuji, X. Li, M. Caricato, A. V. Marenich, J. Bloino, B.G. Janesko, R. Gomperts, B. Mennucci, H.P. Hratchian, J. V. Ortiz, A.F. Izmaylov, J.L. Sonnenberg, D. Williams-Young, F. Ding, F. Lipparini, F. Egidi, J. Goings, B. Peng, A. Petrone, T. Henderson, D. Ranasinghe, V. G. Zakrzewski, J. Gao, N. Rega, G. Zheng, W. Liang, M. Hada, M. Ehara, K. Toyota, R. Fukuda, J. Hasegawa, M. Ishida, T. Nakajima, Y. Honda, O. Kitao, H. Nakai, T. Vreven, K. Throssell, J.A. Montgomery Jr., J.E. Peralta, F. Ogliaro, M. J. Bearpark, J.J. Heyd, E.N. Brothers, K.N. Kudin, V.N. Staroverov, T.A. Keith, R. Kobayashi, J. Normand, K. Raghavachari, A.P. Rendell, J.C. Burant, S.S. Iyengar, J. Tomasi, M. Cossi, J.M. Millam, M. Klene, C. Adamo, R. Cammi, J.W. Ochterski, R.L. Martin, K. Morokuma, O. Farkas, J.B. Foresman, D.J. Fox, Gaussian 16, Revision C.01, Gaussian, Inc., Wallingford CT, 2019.
- [64] G.A. Zhurko, Chemcraft - Graphical program for visualization of quantum chemistry computations, Available online: Ivanovo, Russia 2005, <https://chemcraftprog.com>. (Accessed 18 May 2023).
- [65] K. Smith, X. Mu, Z. Li, A.M. Holland, J.S. Woodhead, G.A. El-Hiti, Synthesis, structure elucidation, and chemiluminescent activity of new 9-substituted 10-(ω -(succinimidylloxycarbonyl)alkyl)acridinium esters, *Luminescence* 38 (2023) 487–496, <https://doi.org/10.1002/bio.4474>.
- [66] M.G. Ahmed, R.W. Alder, G.H. James, M.L. Sinnott, M.C. Whiting, Alkylations with methyl and ethyl fluorosulphonates, *Chem. Commun.* (1968) 1533–1534, <https://doi.org/10.1039/C19680001533>.
- [67] K. Krzemiński, P. Malecha, B. Zadykiewicz, A. Wróblewska, J. Błażejowski, ^1H and ^{13}C NMR spectra, structure and physicochemical features of phenyl acridine-9-carboxylates and 10-methyl-9-(phenoxycarbonyl)acridinium trifluoromethanesulphonates – alkyl substituted in the phenyl fragment, *Spectrochim. Acta: Mol. Biomol. Spectrosc.* 78 (2011) 401–409, <https://doi.org/10.1016/j.saa.2010.10.029>.
- [68] R.M. Silverstein, F.X. Webster, D.J. Kiemle, *Spectroscopic Identification of Organic Compounds*, John Wiley & Sons, Inc., New York, USA, 2005.
- [69] G. Zomer, The nature of chemiluminescence reactions, in: A. Roda (Ed.), *Chemiluminescence and Bioluminescence: Past, Present and Future*, The Royal Society of Chemistry, Cambridge, UK, 2010, pp. 51–90.
- [70] J. Rak, P. Skurski, J. Błażejowski, Towards an understanding of the chemiluminescence accompanying the reaction of 9-carboxy-10-methylacridinium phenyl ester with hydrogen peroxide, *J. Org. Chem.* 64 (1999) 3002–3008, <https://doi.org/10.1021/jo980566u>.
- [71] M. Pieńkos, B. Zadykiewicz, Solvent effect on the chemiluminescence of acridinium thioester: a computational study, *ChemPhysChem* 23 (2022) e202200166, <https://doi.org/10.1002/cphc.202200166>.

Electronic Supplementary Information

Aromatic acridinium thioesters as new chemiluminescence indicators in the analysis of biological antioxidants

Vladyslav Ievtukhov, Anna Romanowska, Milena Pieńkos, Krzysztof Żamojć,
Beata Zadykowicz* and Karol Krzyminiński*

Faculty of Chemistry, University of Gdansk, Wita Stwosza 63, 80-308 Gdansk, Poland

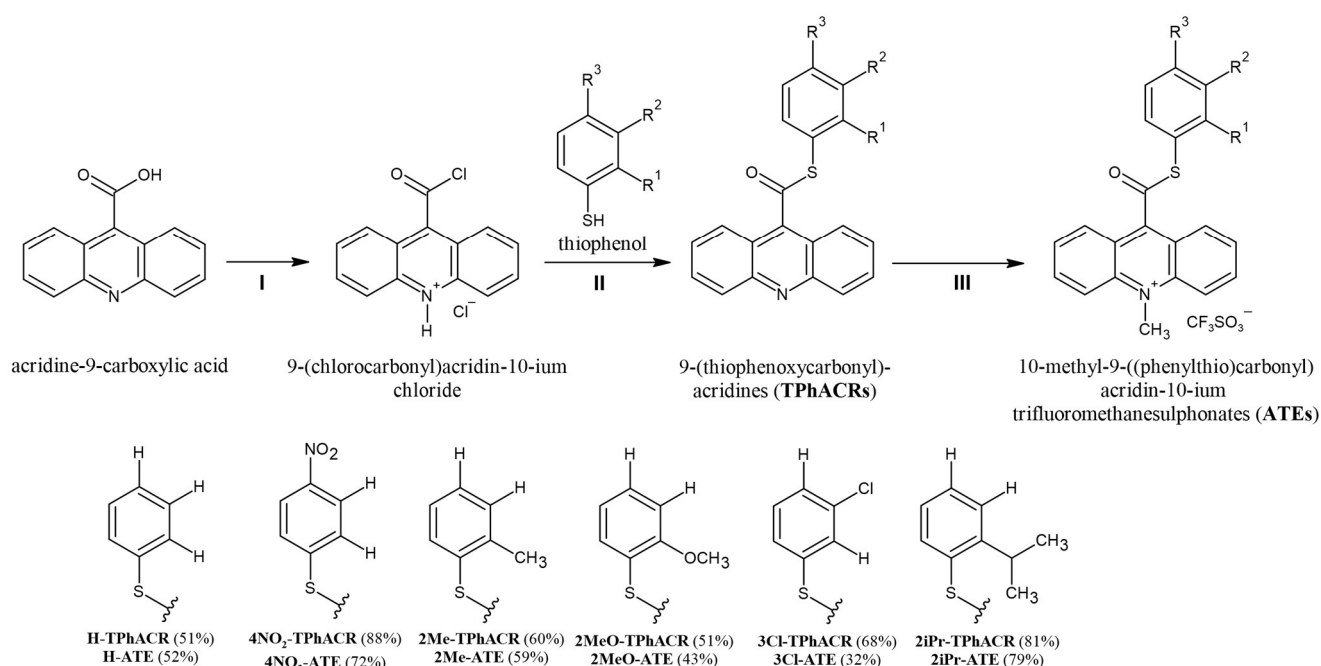
* Corresponding authors.

E-mail addresses: beata.zadykowicz@ug.edu.pl (B. Zadykowicz),
karol.krzyminski@ug.edu.pl (K. Krzyminiński).

Contents

1. Synthetic procedures	2
2. Analyses	3
3. Mass spectra	6
4. ¹ H NMR spectra	8
5. ¹³ C NMR spectra	10
6. IR spectra	12
7. Chemiluminogenic properties of acridinium thioesters (ATEs)	14
8. UV-Vis electronic absorption of ATE-AO systems	17
9. Computational data	18

1. Synthetic procedures



Scheme 1S. Synthesis steps, structural formulas, names and chemical yields of group of acridinium thioesters studied in this work (ATEs, Table 1).

9-(Chlorocarbonyl)acridin-10-ium chloride

Three-fold molar excess of thionyl chloride was added to dried acridine-9-carboxylic acid (4.5 mmol, Sigma-Aldrich) and reaction mixture was stirred under reflux for 3 h at 90–95°C. The resulting solution was then evaporated under reduced pressure with added benzene and crude acridinium salt was precipitated, filtered and washed with dry ethyl ether.

9-(Thiophenoxycarbonyl)acridines

9-Carbonylacridinium chloride (above step, 1.07 mmol) was added to a stirred solution of thiophenol (0.97 mmol), triethylamine (1.07 mmol), 4-(dimethylamino)pyridine in dry dichloromethane and reaction mixture was stirred for 24 h in room temperature. The resulting solution was then evaporated. The pure product was obtained by column chromatography on silica gel (40–60 μm , Normasil 60, VWR/BDH Chemicals) using cyclohexane – chloroform mixture (1/1 v/v) as mobile phase.

10-Methyl-9-(thiophenoxycarbonyl)acridinium trifluoromethanesulfonates (ATEs)

10-fold molar excess of fresh methyl trifluoromethanesulphonate (from ampule, Sigma Aldrich) was added to a solution of chromatographically purified 9-(thiophenoxycarbonyl)-acridine in dry dichloromethane and small amount (10–20 mg) of polymer-bound 2,6-di-*tert*-butylpyridine was added

to the flask. Reaction mixture was stirred for 2h at room temperature under inert gas (Ar), slightly diluted with acetonitrile and filtered with PTFE syringe filter (0.22 μm). The acridinium salts, ATEs, were precipitated by adding an excess of dry diethyl ether to the filtrate and cooling down the mixture (overnight, -20°C). The yellow powders of pure products, the acridinium thioesters, were isolated by filtration, and were washed with dry diethyl ether.

2. Analyses

9-(Thiophenoxycarbonyl)acridines

9-(Thiophenoxycarbonyl)acridine

Yield: 0,145 g (51%); yellow solid;

^1H NMR (CD_3Cl , 700 MHz): δ 8.17 (H1/8, d, $J = 1.00$), 7.67 (H2/7, t, $J = 1.74$), 7.83 (H3/6, t, $J = 0.64$), 8.28 (H4/5, d, $J = 1.35$), 7.65 (H19/20; H22/23, m, $J = 1.74$), 7.48 (H21, t, $J = 1.21$);

^{13}C NMR (CD_3Cl , 700 MHz): δ 121.41 (C1/8), 125.16 (C2/7), 130.23 (C3/6), 129.95 (C4/5), 134.60 (C9), 124.74 (C11/14), 148.55 (C12/13), 193.97 (C15), 129.92 (C16), 130.54 (C17/21), 126.80 (C18/20), 127.27 (C19);

HRMS (ESI-QTOF): m/z [$\text{M} + \text{H}^+$] calcd for $\text{C}_{20}\text{H}_{13}\text{NOS}$: 316.07; found: 316.13;

IR (KBr, cm^{-1}): 3434.83, 1686.89, 1514.20, 1437.81, 1055.34, 881.72, 798.59, 774.02, 748.25, 687.96, 608.4.

9-((2-Methyl)-thiophenoxycarbonyl)acridine

Yield: 0,175 g (60%); yellow solid;

^1H NMR (CD_3Cl , 700 MHz): δ = 8.10 (H1/8, d, $J = 0.50$), 7.60 (H2/7, t, $J = 0.44$), 7.78 (H3/6, t, $J = 0.30$), 8.22 (H4/5, d, $J = 1.00$), 7.39 (H17, d, $J = 0.63$), 7.29 (H18/19, m, $J = 0.18$), 7.58 (H20, t, $J = 0.31$), 2.58 (H23, s);

^{13}C NMR (CD_3Cl , 700 MHz): δ 121.60 (C1/8), 127.28 (C2/7), 130.56 (C3/6), 129.94 (C4/5), 136.09 (C9), 124.68 (C11/14), 148.56 (C12/13), 193.12 (C15), 127.28 (C16), 142.31 (C17), 130.94 (C18), 125.12 (C19), 126.22 (C20), 131.25 (C21), 21.23 (C23);

HRMS (ESI-QTOF): m/z [$\text{M} + \text{H}^+$] calcd for $\text{C}_{21}\text{H}_{15}\text{NOS}$: 330.41; found: 330.14;

IR (film, cm^{-1}): 1686.14, 1513.41, 1459.11, 1436.59, 1065.79, 1053.67, 881.25, 798.97, 775.10, 752.37, 709.19, 610.42.

9-((2-Methoxy)-thiophenoxycarbonyl)acridine

Yield: 0.216 g (51%); yellow solid;

^1H NMR (CD_3Cl , 700 MHz): δ = 8.27 (H1/8, d, $J = 4.10$), 7.87 (H2/7, t, $J = 1.36$), 8.01 (H3/6, t, $J = 0.17$), 8.50 (H4/5, d, $J = 1.00$), 6.99 (H17, d, $J = 1.47$), 7.44 (H18, t, $J = 0.75$), 7.51 (H19/20, d, $J = 0.80$), 7.65 (H21, t, $J = 1.43$), 3.92 (H23, s);

^{13}C NMR (CD_3Cl , 700 MHz): δ 121.88 (C1/8), 125.37 (C2/7), 128.19 (C3/6), 127.65 (C4/5), 136.51 (C9), 121.98 (C11/14), 145.87 (C12/13), 192.32 (C15), 114.22 (C16), 159.48 (C17), 111.88 (C18), 122.40 (C19), 121.50 (C20), 132.84 (C21), 56.13 (C23);

HRMS (ESI-QTOF): m/z [$\text{M} + \text{H}^+$] calcd for $\text{C}_{21}\text{H}_{15}\text{NO}_2\text{S}$: 346.41; found: 346.15;

IR (film, cm^{-1}): 1684.48, 1513.70, 1476.62, 1435.36, 1276.97, 1057.37, 1022.41, 883.59, 801.83, 778.00, 756.87, 745.75, 612.21.

9-((2-Isopropyl)-thiophenoxycarbonyl)acridine

Yield: 0.188 g (81%); yellow solid;

^1H NMR (CD_3Cl , 700 MHz): δ = 8.09 (H1/8, d, J = 0.74), 7.59 (H2/7, t, J = 0.55), 7.78 (H3/6, t, J = 0.51), 8.22 (H4/5, d, J = 1.00), 7.46 (H17, t, J = 1.44), 7.30 (H19/20, dt, J = 0.21), 7.65 (H18, d, J = 0.44), 3.53 (H21, m, J = 0.48), 1.30 (H23, d, J = 4.92);

^{13}C NMR (CD_3Cl , 700 MHz): δ 121.56 (C1/8), 125.03 (C2/7), 130.53 (C3/6), 129.97 (C4/5), 136.57 (C9), 124.68 (C11/14), 148.60 (C12/13), 193.56 (C15), 127.14 (C16), 152.19 (C17), 126.76 (C18), 127.27 (C19), 126.95 (C20), 131.25 (C21), 31.68 (C23), 23.88 (C24);

HRMS (ESI-QTOF): m/z [$M + H^+$] calcd for $\text{C}_{23}\text{H}_{19}\text{NOS}$: 358.47; found: 358.18;

IR (film, cm^{-1}): 2964.78, 1682.59, 1513.86, 1472.93, 1458.93, 1436.74, 1149.59, 1057.12, 1043.74, 1010.24, 880.75, 860.54, 801.46, 775.84, 760.97, 743.06, 611.70.

9-((3-Chloro)-thiophenoxycarbonyl)acridine

Yield: 0.141 g (68%); yellow solid;

^1H NMR (CD_3Cl , 700 MHz): δ = 8.23 (H1/8, d, J = 1.00), 7.60 (H2/7, t, J = 1.54), 7.78 (H3/6, t, J = 0.67), 8.06 (H4/5, d, J = 0.74), 7.40 (H17, d, J = 1.21), 7.37 (H19, m, J = 0.72), 7.39 (H20, t, J = 0.72), 7.48 (H21, d, J = 0.15);

^{13}C NMR (CD_3Cl , 700 MHz): δ 121.32 (C1/8), 124.55 (C2/7), 130.46 (C3/6/20), 128.43 (C4/5), 134.26 (C9), 122.36 (C11/14), 148.45 (C12/13), 193.02 (C15), 132.68 (C16), 129.91 (C17), 135.21 (C18), 125.15 (C19), 127.48 (C21);

HRMS (ESI-QTOF): m/z [$M + H^+$] calcd for $\text{C}_{20}\text{H}_{12}\text{ClNOS}$: 350.83; found: 350.09;

IR (film, cm^{-1}): 2924.21, 1695.11, 1566.56, 1460.35, 1055.26, 876.01, 791.60, 772.80, 747.52, 680.58, 645.74.

9-((4-Nitro)-thiophenoxycarbonyl)acridine

Yield: 0.281 g (88%); yellow solid;

^1H NMR (CD_3Cl , 700 MHz): δ = 8.14 (H1/8, d, J = 6.12), 7.90 (H2/7, t, J = 2.78), 7.71 (H3/6, t, J = 8.54), 8.21 (H4/5, d, J = 0.14), 7.92 (H17/21, d, J = 2.78), 8.41 (H18/20, d, J = 1.00);

^{13}C NMR (CD_3Cl , 700 MHz): δ 124.39 (C1/8), 127.74 (C2/7), 130.05 (C3/6), 128.18 (C4/5), 134.88 (C9), 126.40 (C11/14), 148.70 (C12/13), 191.56 (C15), 130.77 (C16/17/21), 121.21 (C18/20), 135.11 (C19);

HRMS (ESI-QTOF): m/z [$M + H^+$] calcd for $\text{C}_{20}\text{H}_{12}\text{N}_2\text{O}_3\text{S}$: 360.39; found: 361.12;

IR (film, cm^{-1}): 2923.84, 2853.35, 1521.32, 1459.52, 1342.67, 847.98, 781.23.

10-Methyl-9-((phenylthio)carbonyl)acridin-10-ium trifluorometanosulphonates (ATEs)

10-Methyl-9-((phenylthio)carbonyl)acridin-10-ium trifluorometanosulphonate (H-ATE)

Yield: 0.030 g (52%); yellow solid;

^1H NMR (CD_3CN , 700 MHz): δ 8.57 (H1/8, d, J = 7.53), 8.09 (H2/7, t, J = 10.63), 8.47 (H3/6, t, J = 4.21), 8.64 (H4/5, d, J = 1.00), 7.79 (H17/21, d, J = 0.86), 7.61 (H18/19/20, dd, J = 12.65), 4.82 (H22, s);

^{13}C NMR (CD_3CN , 700 MHz): δ 119.75 (C1/8), 140.16 (C2/7), 123.14 (C3/6), 130.06 (C4/5), 154.32 (C9), 128.32 (C11/14), 142.79 (C12/13), 192.67 (C15), 135.76 (C16), 131.81 (C17/21), 130.64 (C18/20), 125.30 (C19), 40.04 (C22);

HRMS (ESI-QTOF): m/z [$M + H^+$] calcd for $\text{C}_{21}\text{H}_{16}\text{NOS}$: 330.42; found: 330.16;

IR (film, cm^{-1}): 1674.20, 1460.55, 1263.05, 1222.62, 1159.11, 1145.86, 1063.56, 1029.91, 871.68, 842.32, 763.22, 637.39, 517.29.

10-Methyl-9-(((4-nitrophenyl)thio)carbonyl)acridin-10-ium trifluorometanosulphonate (4NO₂-ATE)

Yield: 0,050 g (72%); yellow solid;

¹H NMR (CD₃CN, 700 MHz): δ 8.60 (H1/8, d, J = 9.45), 8.14 (H2/7, t, J = 5.73), 8.51 (H3/6, t, J = 4.85), 8.68 (H4/5, d, J = 1.00), 8.09 (H17/21, d, J = 3.05), 8.45 (H18/20, d, J = 2.82), 4.87 (H22, s);

¹³C NMR (CD₃CN, 700 MHz): δ 130.22 (C1/8), 125.20 (C2/7), 136.59 (C3/6), 119.85 (C4/5), 153.29 (C9), 128.17 (C12/13), 140.24 (C11/14), 190.96 (C15), 40.17 (C22), 142.87 (C16), 133.18 (C17/21), 123.15 (C18/20), 150.12 (C19);

HRMS (ESI-QTOF): m/z [M + H⁺] calcd for C₂₁H₁₅N₂O₃S: 375.41; found: 375.14;

IR (film, cm⁻¹): 1691.86, 1604.83, 1552.31, 1524.63, 1372.62, 1346.25, 1261.46, 1222.43, 1177.78, 1148.98, 1059.22, 1029.35, 1008.43, 853.58, 835.37, 766.90, 745.31, 636.69, 516.37.

10-methyl-9-(((2-methylphenyl)thio)carbonyl)acridin-10-ium trifluorometanosulphonate (2Me-ATE)

Yield: 0,035 g (59%); yellow solid;

¹H NMR (CD₃CN, 700 MHz): δ = 8.55 (H1/8, d, J = 0.58), 8.14 (H2/7, t, J = 0.27), 8.51 (H3/6, t, J = 0.29), 8.69 (H4/5, d, J = 1.00), 7.80 (H19, d, J = 0.60), 7.48 (H18/20, m, J = 0.40), 7.60 (H21, d, J = 0.60), 4.86 (H22, s), 2.68 (H23, s);

¹³C NMR (CD₃CN, 700 MHz): δ 128.10 (C1/8), 119.81 (C2/7), 137.04 (C3/6), 119.81 (C4/5), 154.50 (C9), 124.96 (C11/14), 140.16 (C12/13), 191.79 (C15), 142.84 (C16), 143.47 (C17), 132.41 (C18), 123.29 (C19), 130.13 (C20), 132.10 (C21), 20.99 (C22) 40.07 (C23);

HRMS (ESI-QTOF): m/z [M + H⁺] calcd for C₂₂H₁₈NOS: 344.45; found: 344.17;

IR (film, cm⁻¹): 1672.83, 1263.15, 1224.03, 1148.63, 1030.97, 840.20, 764.85, 749.85, 638.59.

9-(((2-Methoxyphenyl)thio)carbonyl)-10-methylacridin-10-ium trifluorometanosulphonate (2MeO-ATE)

Yield: 0,030 g (43%); yellow solid;

¹H NMR (CD₃CN, 700 MHz): δ = 8.14 (H1/8, d, J = 0.50), 8.50 (H2/7, t, J = 0.31), 8.66 (H3/6, t, J = 1.00), 8.64 (H4/5, d, J = 1.00), 7.16 (H18, d, J = 0.31), 7.70 (H19, t, J = 0.24), 7.27 (H20, t, J = 0.39), 7.65 (H21, d, J = 0.26) 4.05 (H23, s) 4.82 (H22, s);

¹³C NMR (CD₃CN, 700 MHz): δ 123.36 (C1/8), 119.67 (C2/7), 140.15 (C3/6), 113.03 (C4/5), 154.97 (C9), 122.24 (C11/14), 142.73 (C12/13), 191.65 (C15), 137.28 (C16), 160.33 (C17), 129.87 (C18), 134.27 (C19), 113.03 (C20), 128.34 (C21), 56.77 (C23), 49.95 (C22);

HRMS (ESI-QTOF): m/z [M + H⁺] calcd for C₂₂H₁₈NO₂S: 361.45; found: 360.16;

IR (film, cm⁻¹): 3484.85, 3306.93, 3236.70, 1712.42, 1673.40, 1610.57, 1556.94, 1434.24, 1409.20, 1357.63, 1260.70, 1172.9, 1035.49, 838.74, 757.42, 638.17.

9-(((3-Chlorophenyl)thio)carbonyl)-10-methylacridin-10-ium trifluorometanosulphonate (3Cl-ATE)

Yield: 0,027 g (38%); yellow solid;

¹H NMR (CD₃CN, 700 MHz): δ 8.59 (H1/8, d, J = 4.29), 8.12 (H2/7, t, J = 4.56), 8.51 (H3/6, t, J = 2.22), 8.6 (H4/5, d, J = 1.00), 7.93 (H17, s), 7.68 (H19, d J = 0.45), 7.63 (H20, t, J = 4.64), 7.77 (H21, d, J = 0.99), 4.86 (H22, s);

¹³C NMR (CD₃CN, 700 MHz): δ 127.09 (C1/8), 135.29 (C2/7), 140.05 (C3/6), 119.78 (C4/5), 142.82 (C9), 123.15 (C11/14), 153.80 (C12/13), 191.91 (C15), 135.47 (C16), 134.24 (C17), 140.21 (C18), 128.29 (C19), 130.12 (C20), 131.97 (C21), 40.10 (C22);

HRMS (ESI-QTOF): m/z [M + H⁺] calcd for C₂₁H₁₅ClNOS: 364.86; found: 364.12;

IR (film, cm^{-1}): 3417.37, 1682.01, 1623.63, 1607.54, 1459.30, 1268.60, 1254.92, 1227.35, 1157.46, 1030.04, 838.03, 770.78, 756.67, 639.71, 517.08.

9-(((2-Isopropylphenyl)thio)carbonyl)10-methylacridin-10-ium trifluorometanosulphonate (2iPr-ATE)

Yield: 0,049 g (79%); yellow solid;

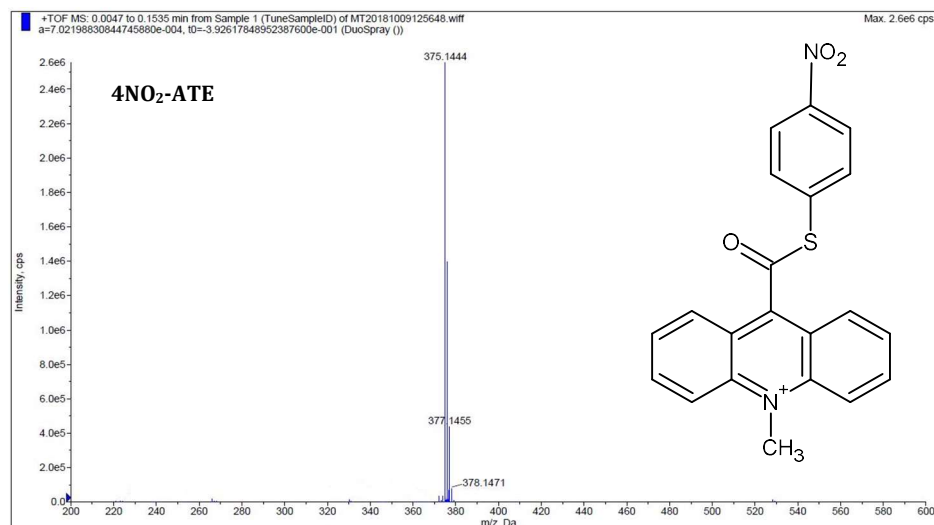
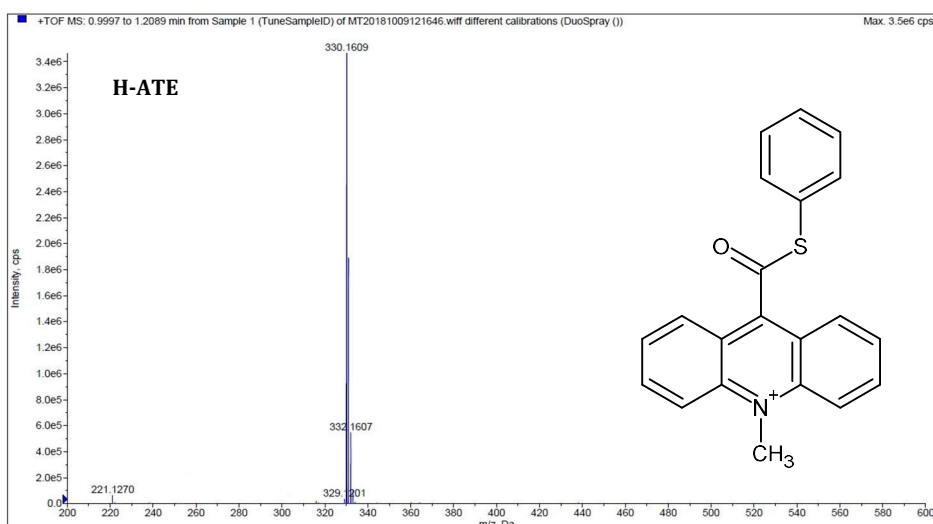
^1H NMR (CD_3CN , 700 MHz): δ = 8.53 (H1/8, d, J = 1.36), 8.15 (H2/7, t, J = 0.30), 8.51 (H3/6, t, J = 1.36), 8.68 (H4/5, d, J = 1.00), 7.67 (H18/20, d, J = 0.44), 7.48 (H19, m, J = 0.12), 7.85 (H21, d, J = 0.35), 3.59 (H22, m, J = 0.22), 4.87 (H22, s), 1.39 (H23, d, J = 2.49);

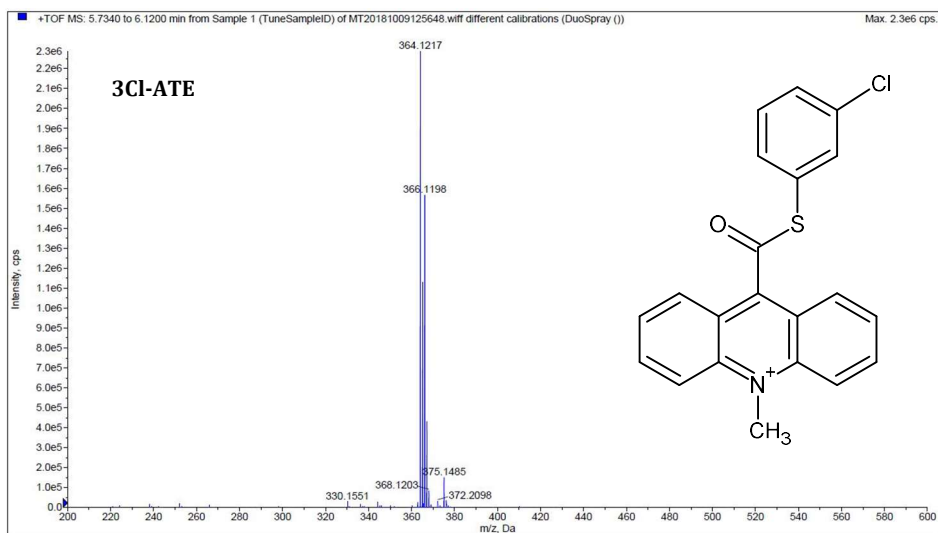
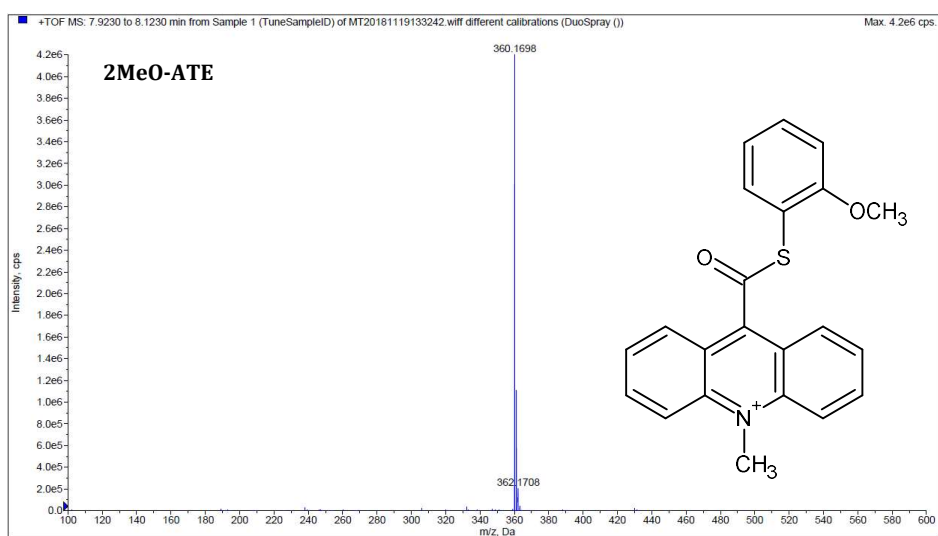
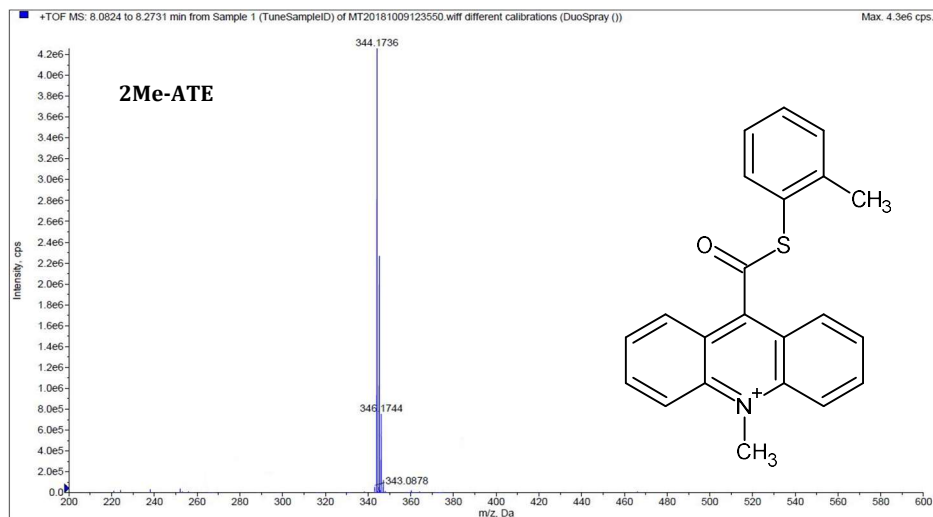
^{13}C NMR (CD_3CN , 700 MHz): δ 128.0 (C1/8), 123.25 (C2/7), 140.15 (C3/6), 119.86 (C4/5), 153.37 (C9), 127.88 (C11/14), 142.85 (C12/13), 192.34 (C15), 154.54 (C16), 137.44 (C17), 130.15 (C18), 123.72 (C19), 128.01 (C20), 132.78 (C21), 40.1 (C22), 32.40 (C23), 23.67 (C24);

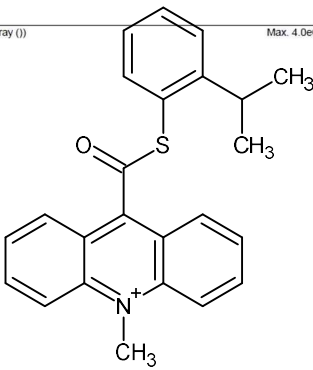
HRMS (ESI-QTOF): m/z [$\text{M} + \text{H}^+$] calcd for $\text{C}_{24}\text{H}_{22}\text{NOS}$: 372.50; found: 372.21;

IR (film, cm^{-1}): 1264.33, 1156.07, 1030.24, 758.30, 637.61.

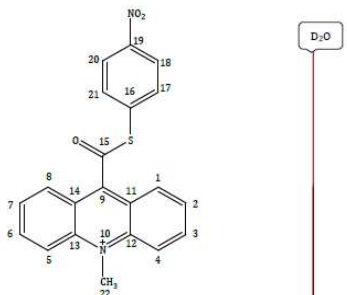
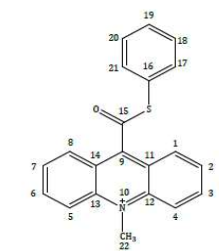
3. Mass spectra



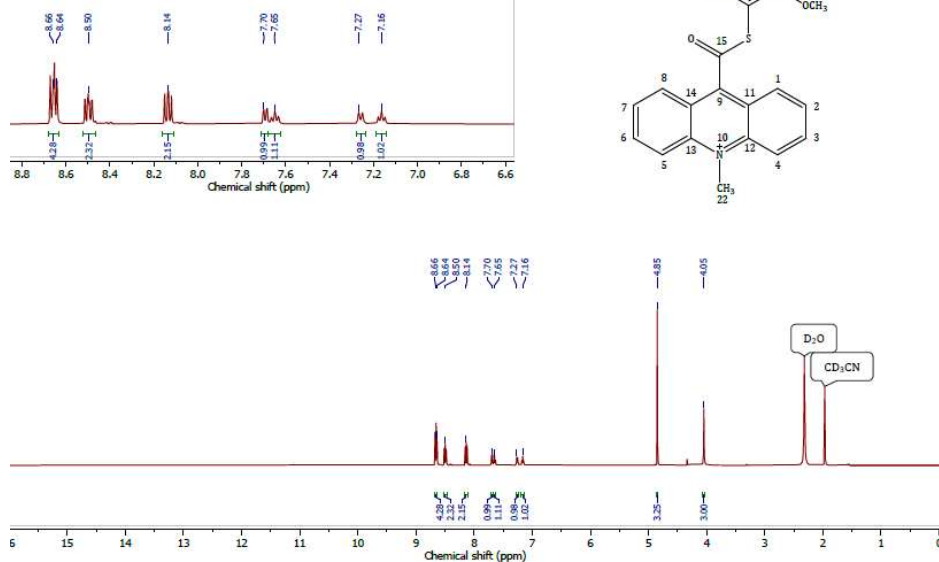




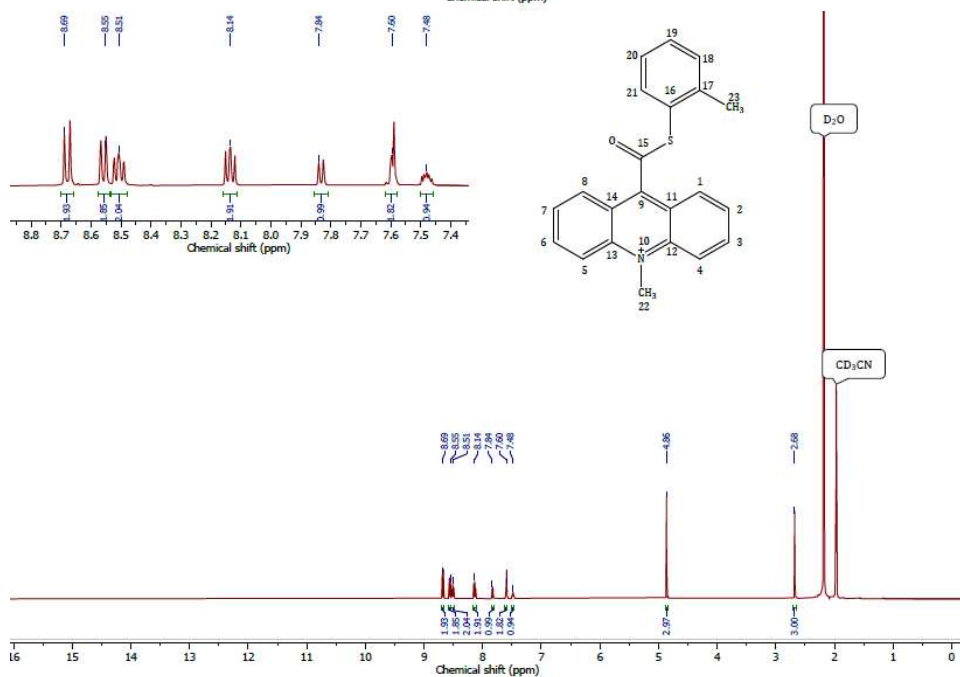
4. ^1H NMR spectra



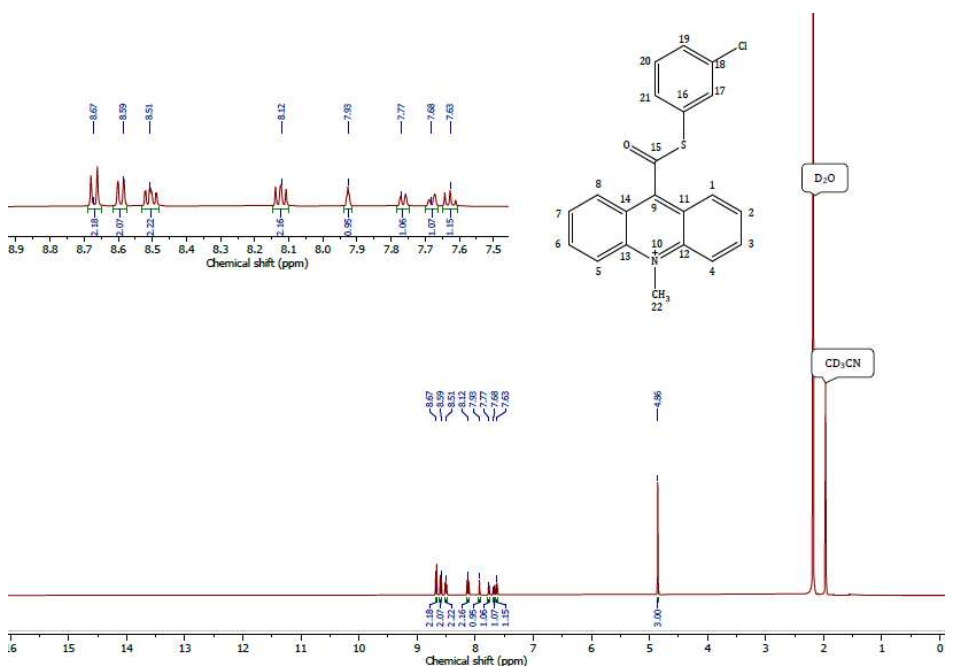
2MeO-ATE



2Me-ATE



3Cl-ATE



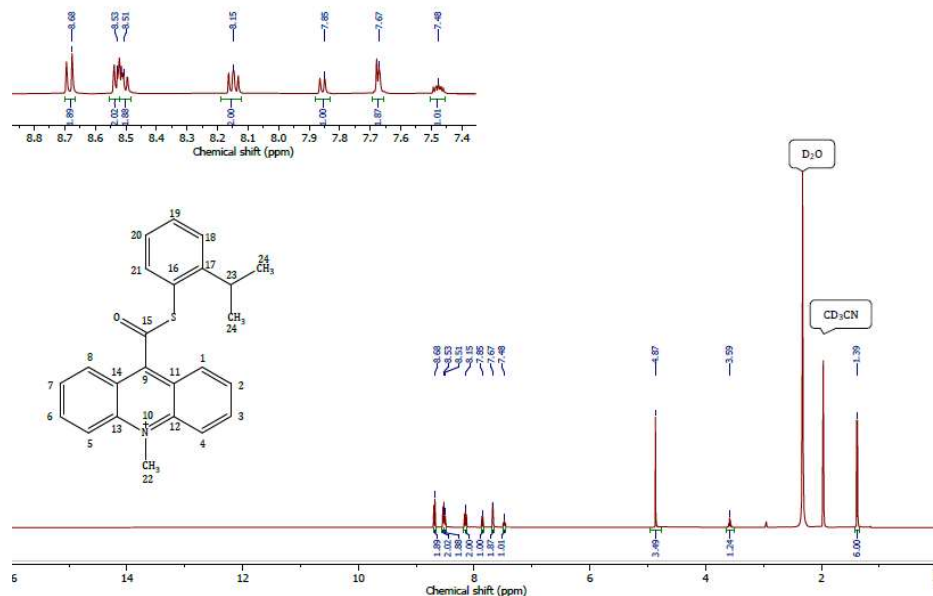
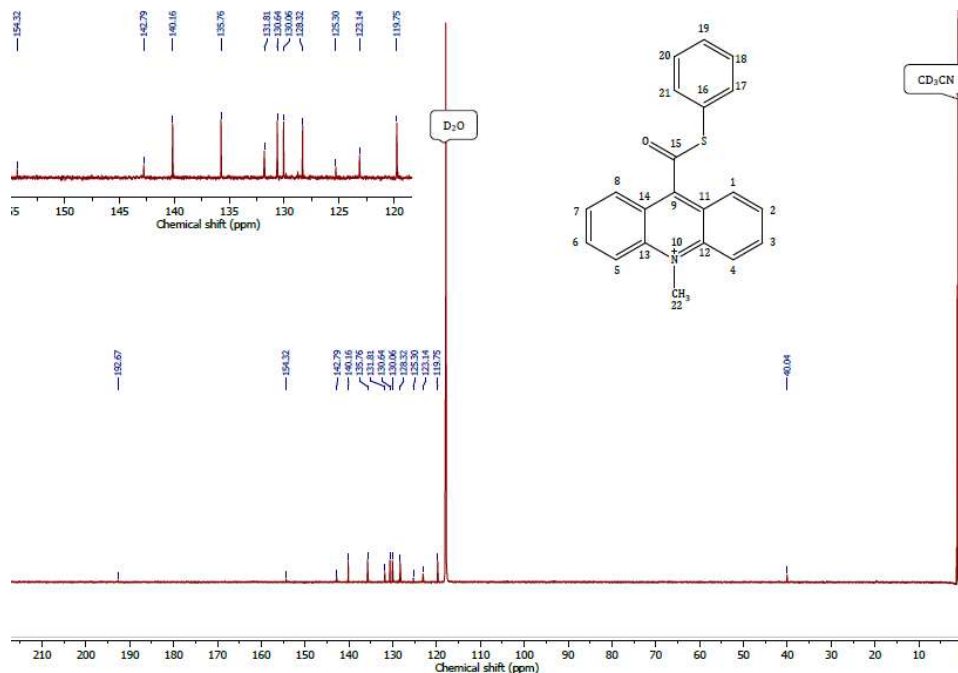


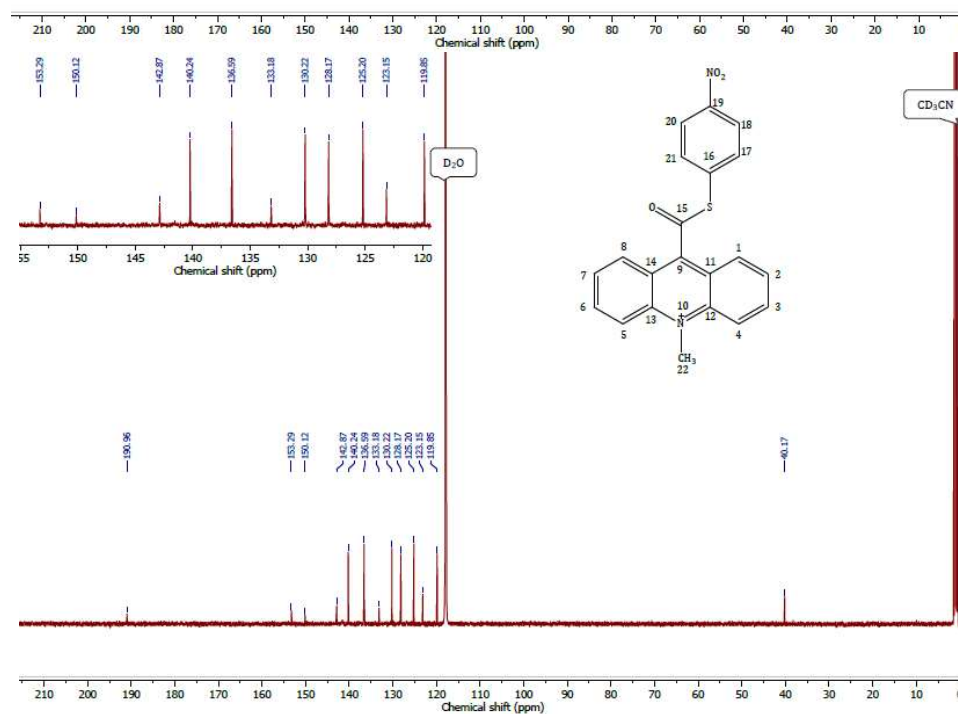
Fig. 2S. ^1H NMR spectra of 10-methyl-9-((phenylthio)carbonyl)acridin-10-ium triflates under study (ATEs, Table 1). For details see Materials and Methods section.

5. ^{13}C NMR spectra

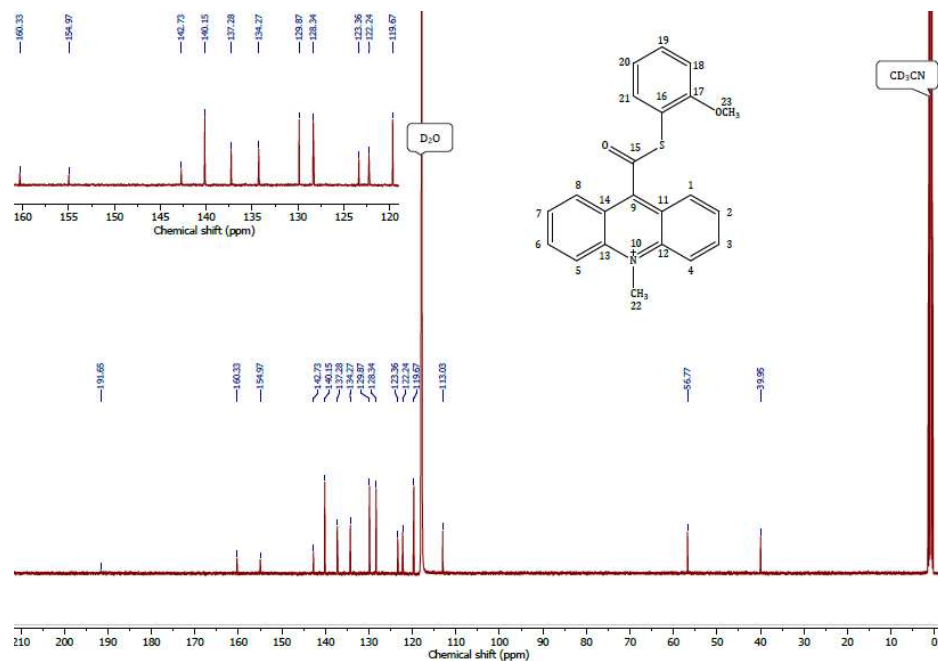
H-ATE



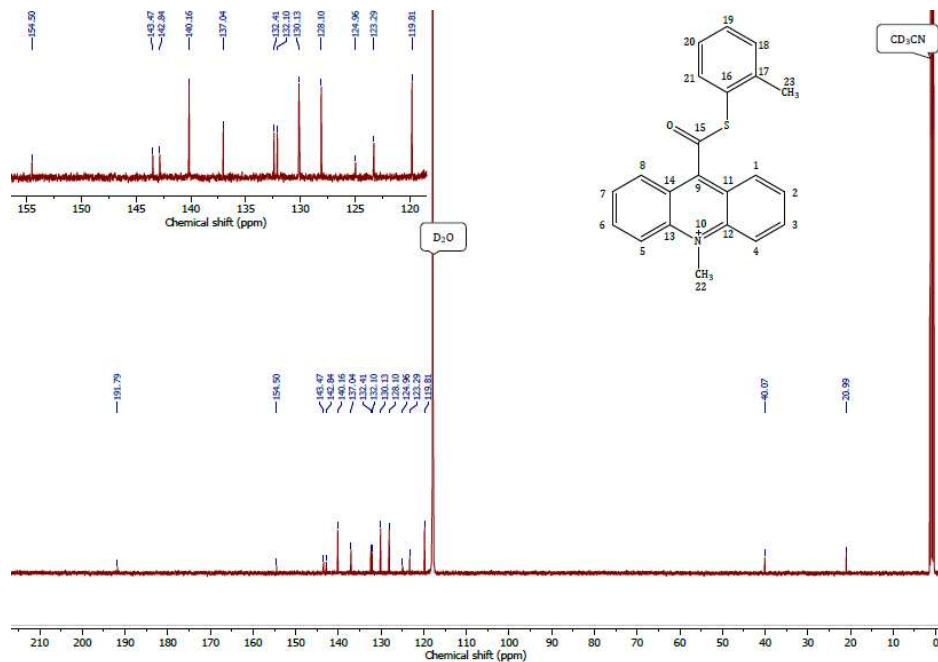
4NO₂-ATE



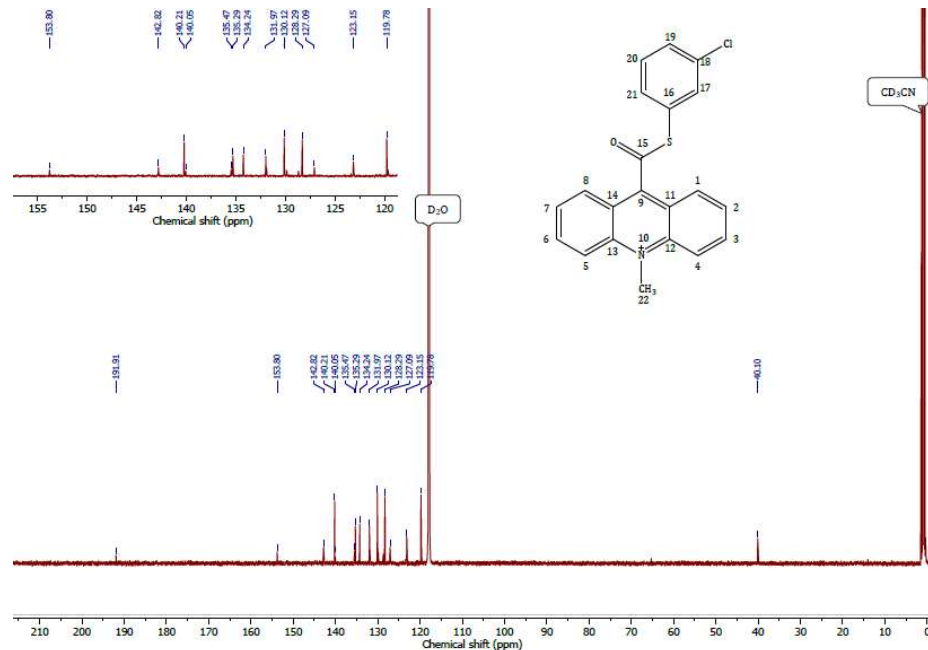
2MeO-ATE



2Me-ATE



3Cl-ATE



2iPr-ATE

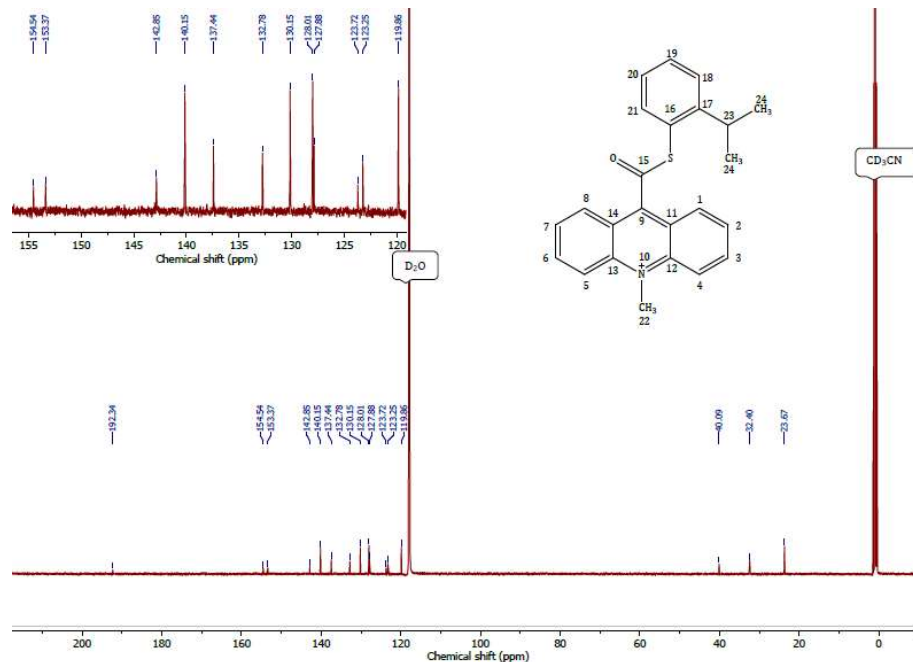
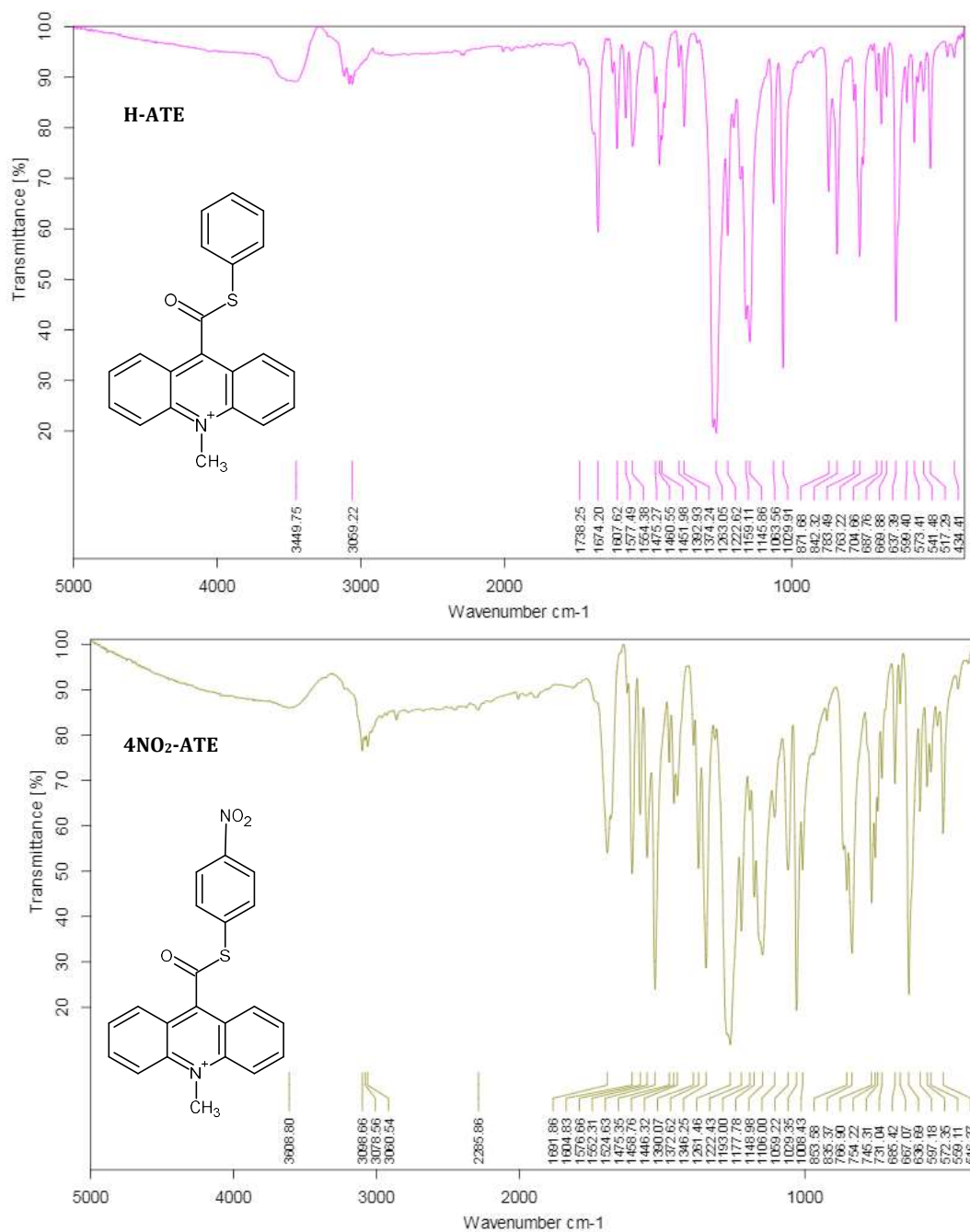
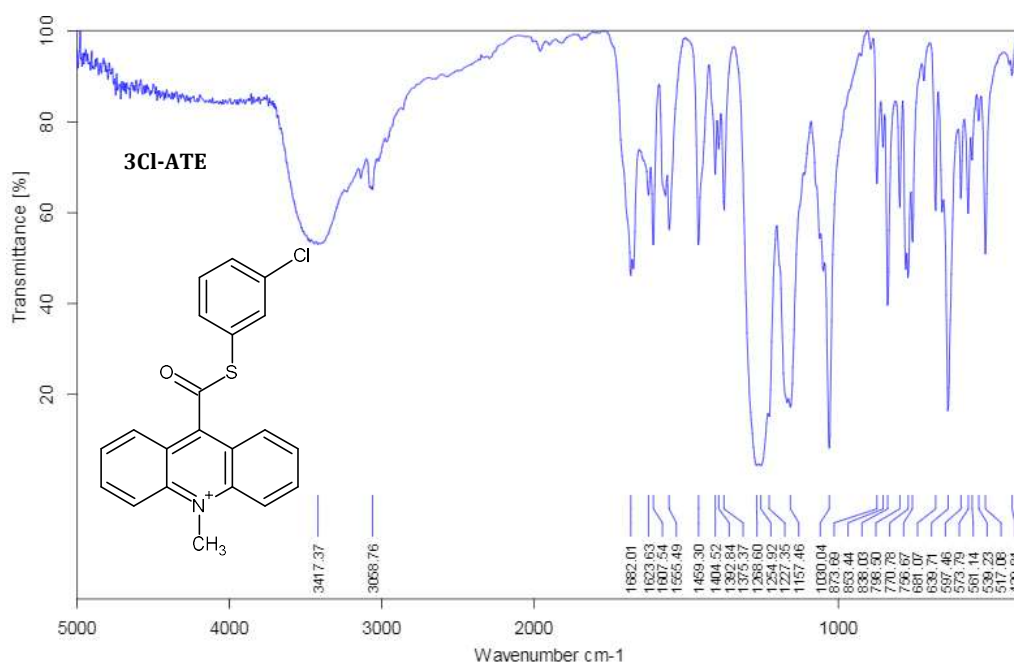
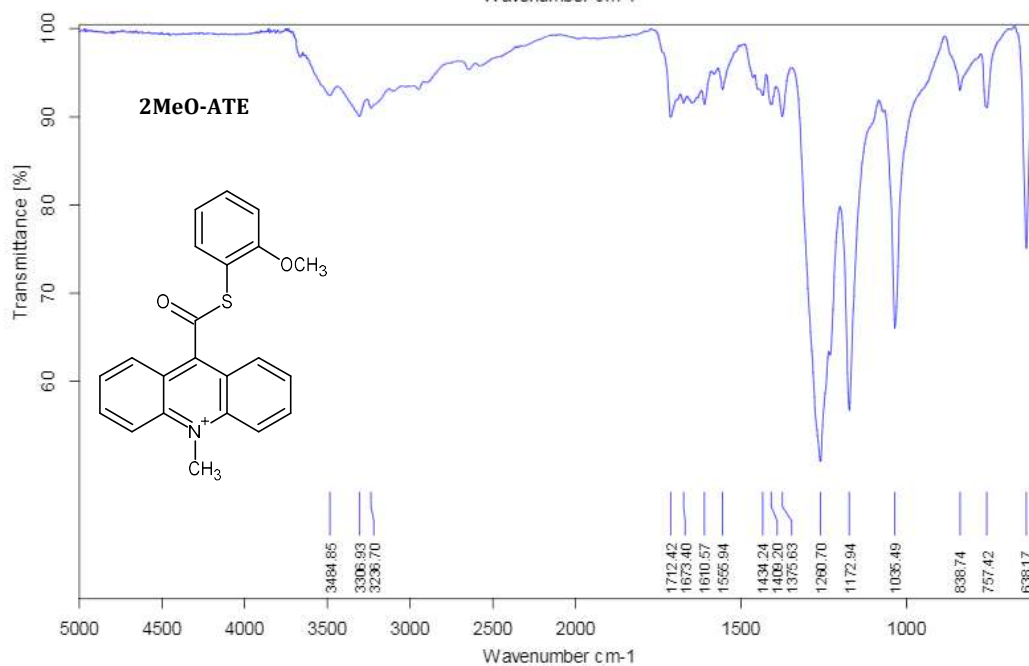
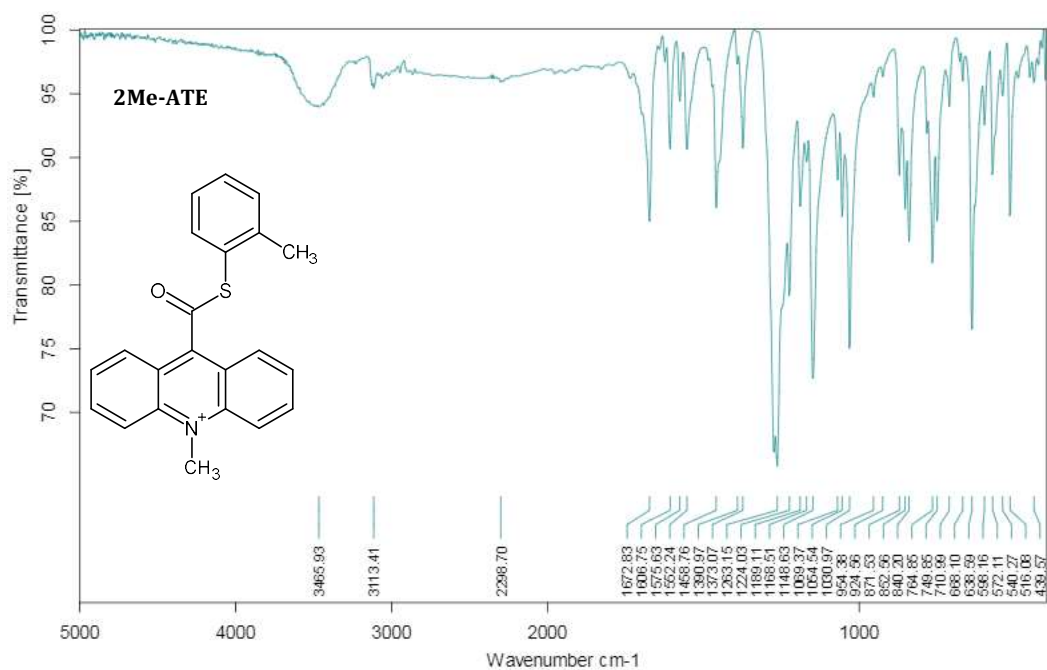


Fig. 3S. ¹³C NMR spectra of 10-methyl-9-((phenylthio)carbonyl)acridin-10-ium triflates under study (ATEs, Table 1). For details see Materials and Methods section.

6. IR spectra





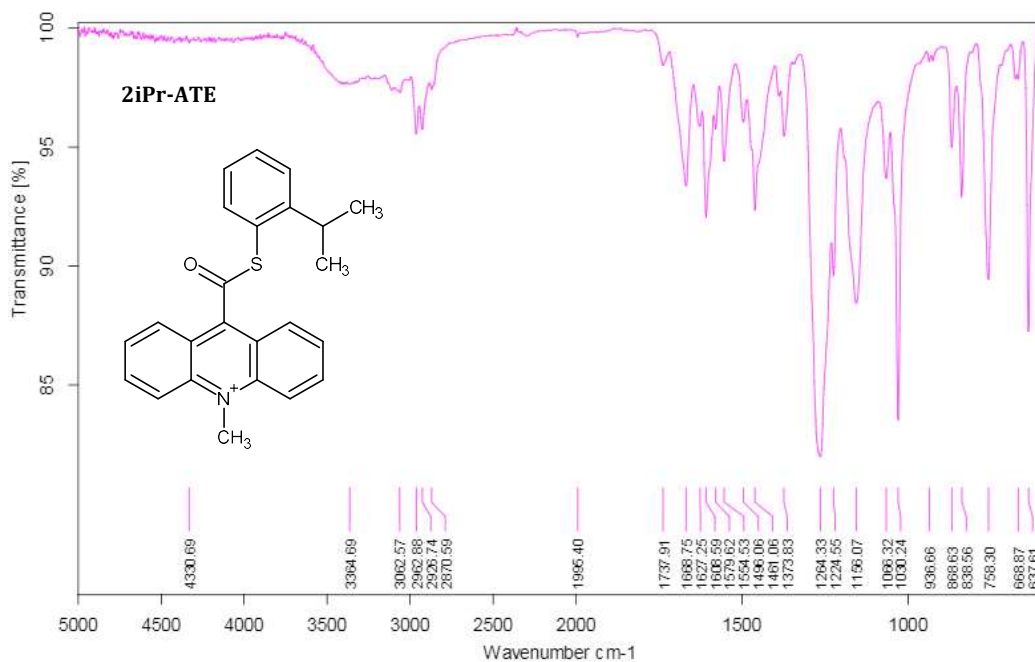


Fig. 4S. Infrared (FT-IR) spectra of 10-methyl-9-((phenylthio)carbonyl)acridin-10-ium triflates under study.

7. Chemiluminogenic properties

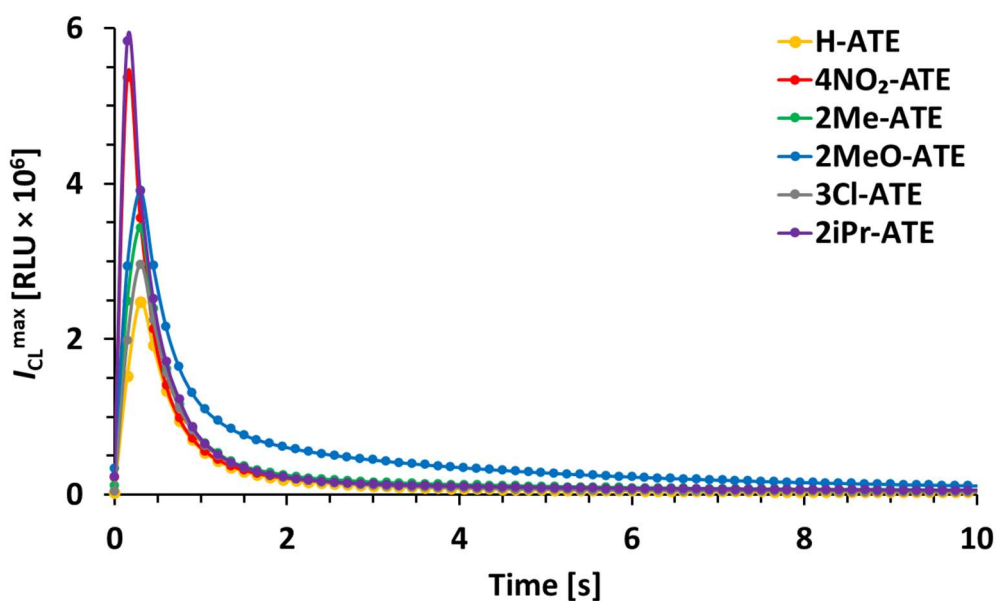


Fig. 5S. Time profiles of chemiluminescence of 10-methyl-9-((phenylthio)carbonyl)acridin-10-ium triflates under study (ATEs, Table 1). The concentration of CL substrate ($c = 1.0 \times 10^{-10}$ M) and triggering system (KOH/H₂O₂) were constant in all experiments. For details see Material and Methods section.

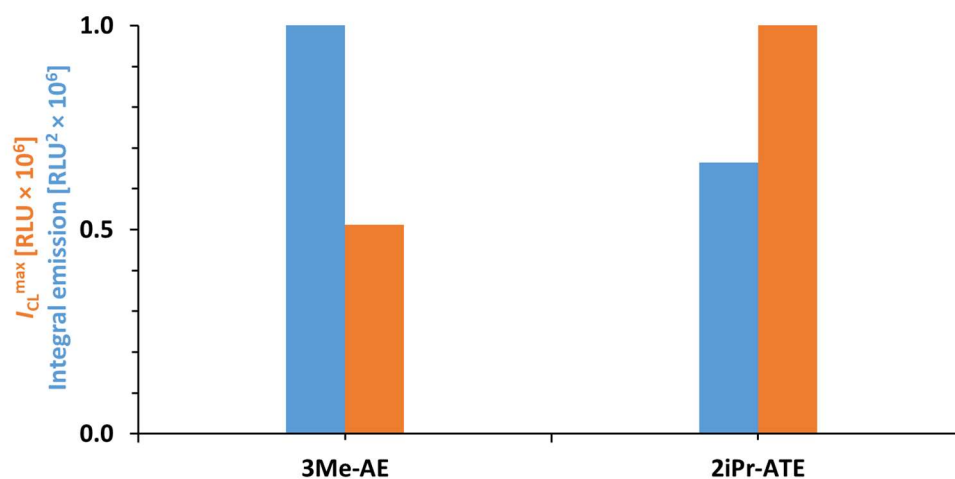


Fig. 6S. Comparison of CL efficiencies (intensity in maximum and integral emission) of 3Me-AE and 2iPr-ATE in the same experimental conditions. For details see Materials and Methods section.

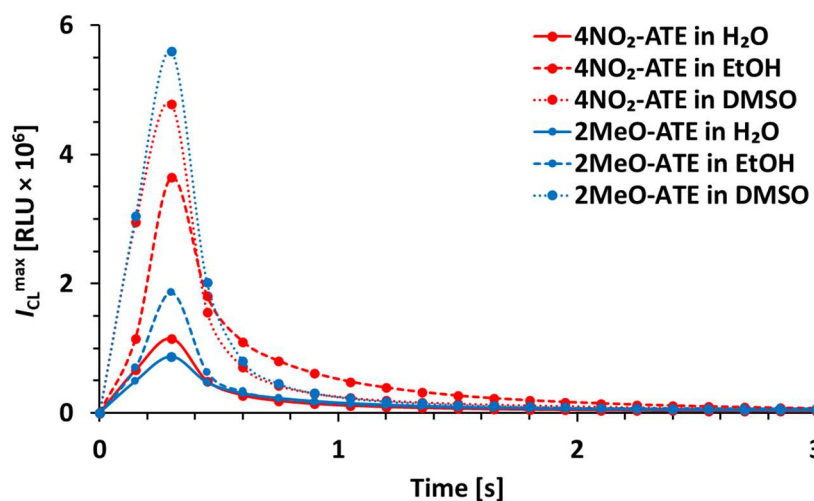


Fig. 7S. Time profiles of chemiluminescence of selected 10-methyl-9-(phenylthio)carbonyl)acridin-10-ium triflates in various liquid environments. The concentration of CL substrate was constant ($c = 1.0 \times 10^{-10}$ M) and typical triggering system (KOH/H₂O₂) was employed in each case. For details see Material and Methods section.

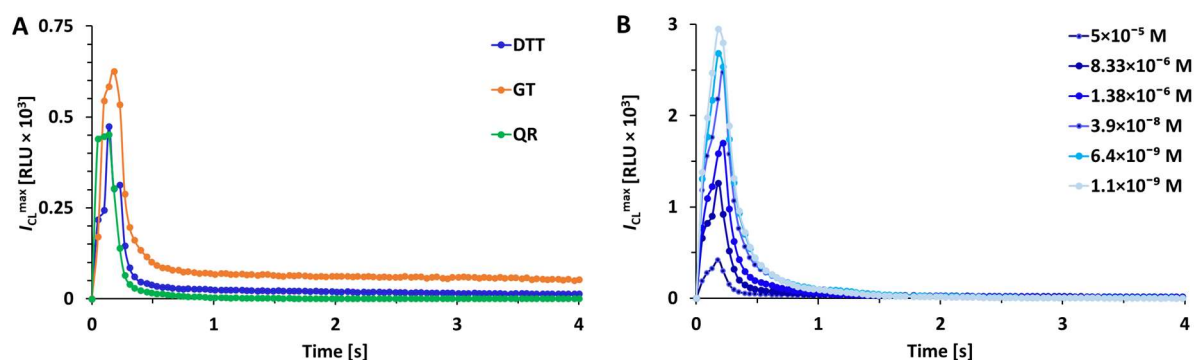


Fig. 8S. (A) Chemiluminescence profiles of 2MeO-ATE in water-ethanol mixtures in the presence of AOs (DTT, GT, QR, Fig. 1). The concentration of reagents were as follows: acridinium salt: $c = 1.25 \times 10^{-7}$ M, triggering system: 0.1 M KOH/0.1% H_2O_2 , $c(\text{AOs}) = 5.0 \times 10^{-5}$ M; (B) Changes in intensity of CL signal of 2MeO-ATE as a function of concentration of DTT in water-ethanol mixtures. The experimental conditions were identical as above-described.

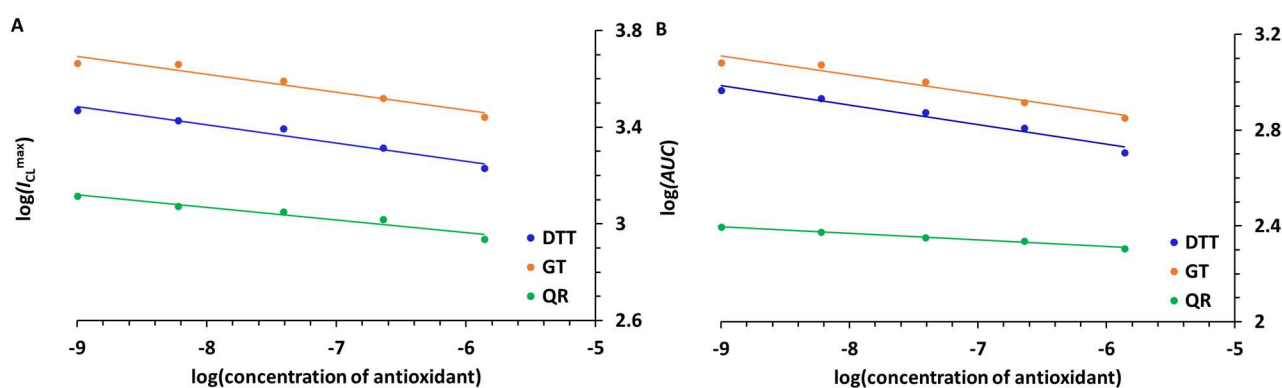


Fig. 9S. Log (CL intensity)–log(AO concentration) graphs for studied systems (2MeO-ATE (A) and 4NO₂-ATE (B) with AOs: DTT, GT, QR). Concentrations of other reagents were constant: $c(\text{ATE}) = 1.25 \times 10^{-7}$ M, triggering system: 0.1% H_2O_2 /0.1 M KOH. For details see Materials and Methods section.

Table 1S. Regression parameters of calibration graphs, obtained for ATE-AOs systems in water-ethanol environment. For details see Materials and Methods section.

Log-log ($I_{\text{CL}}^{\text{max}}$) vs. $c(\text{AO})$ interdependencies (Fig. 9S)			
ATE-AO system	Equation (R^2)	Linear range	LOD / LOQ
2MeO-ATE-DTT	$Y = -0.0755x + 2.807$ (0.962)	$1.0 \times 10^{-9} - 1.4 \times 10^{-6}$	$7.63 \times 10^{-7} / 2.31 \times 10^{-6}$
2MeO-ATE-GT	$Y = -0.0745x + 3.023$ (0.946)	$1.0 \times 10^{-9} - 1.4 \times 10^{-6}$	$7.95 \times 10^{-7} / 2.41 \times 10^{-6}$
2MeO-ATE-QR	$Y = -0.0519x + 2.653$ (0.937)	$1.0 \times 10^{-9} - 1.4 \times 10^{-6}$	$6.49 \times 10^{-7} / 1.95 \times 10^{-6}$
Log-log AUC vs. $c(\text{AO})$ interdependencies (Fig. 9S)			
2MeO-ATE-DTT	$Y = -0.0819x + 2.249$ (0.987)	$1.0 \times 10^{-9} - 1.4 \times 10^{-6}$	$7.48 \times 10^{-7} / 2.25 \times 10^{-6}$
2MeO-ATE-GT	$Y = -0.0789x + 2.399$ (0.954)	$1.0 \times 10^{-9} - 1.4 \times 10^{-6}$	$8.98 \times 10^{-7} / 2.70 \times 10^{-6}$
2MeO-ATE-QR	$Y = -0.0276x + 2.148$ (0.987)	$1.0 \times 10^{-9} - 1.4 \times 10^{-6}$	$8.21 \times 10^{-7} / 2.46 \times 10^{-6}$

8. UV-Vis electronic absorption spectra

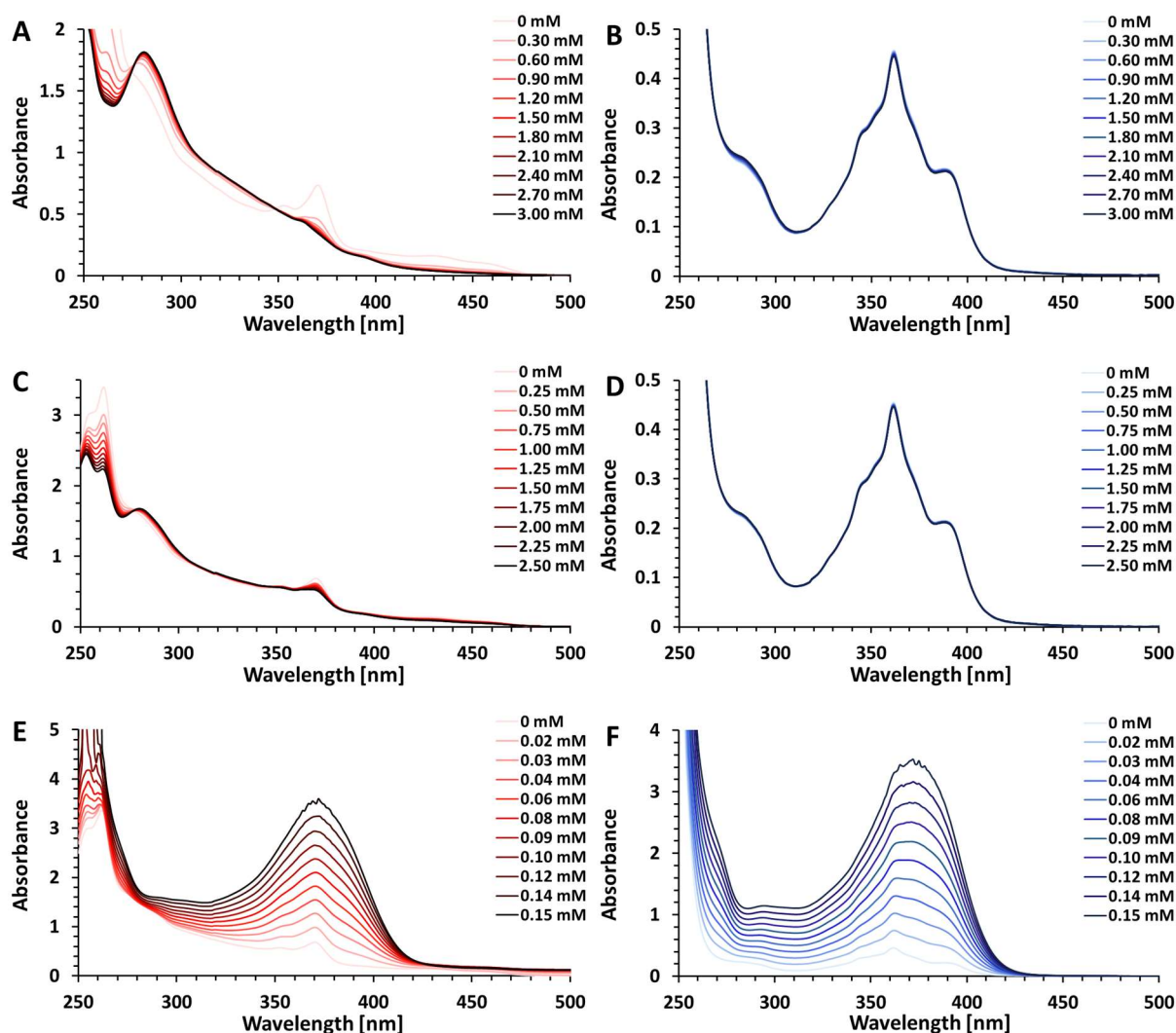


Fig. 10S. UV-Vis spectra for all studied ATE-AO systems in aqueous-ethanolic solutions (pH 3.5). 4NO₂-ATE-DTT (A), 2MeO-ATE-DTT (B), 4NO₂-ATE-GT (C), 2MeO-ATE-GT (D), 4NO₂-ATE-QR (E), 2MeO-ATE-QR (F). The concentration of 4NO₂-ATE and 2MeO-ATE was fixed and equal to 1.0×10^{-4} M.

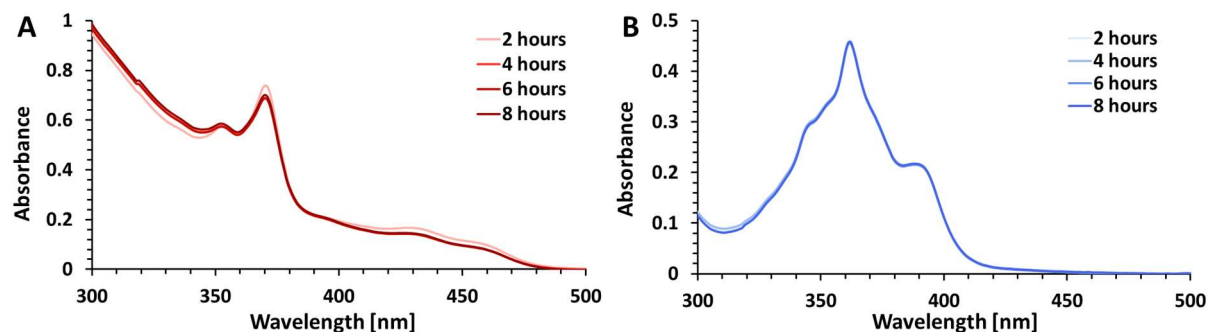


Figure 11S. Chemical stability of 4NO₂-ATE (A) and 2MeO-ATE (B) in aqueous-ethanolic solutions (pH 3.5), assessed by UV-Vis spectroscopy.

9. Computational data

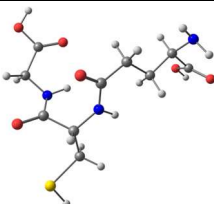
Table 2S. Thermodynamic and kinetic data obtained by quantum chemical calculations (DFT) for the additional studied systems (ATEs + AOs).

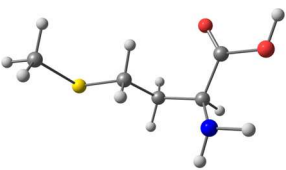
THERMODYNAMIC CHARACTERISTIC						
Step no.	Nucleophile (AO)	Gaseous phase			Aqueous phase	
		$\Delta_{r,298}H^0$	$\Delta_{r,298}G^0$		$\Delta_{r,298}H^0$	$\Delta_{r,298}G^0$
I	CYS	−100.6	−97.2		−65.0	−62.3
	MET	−77.1	−75.3		−51.4	−49.2
VI	–	−6.9	−18.7		−7.5	−19.0
H-ATE						
II	CYS	−120.5	−108.1		−33.8	−20.8
	MET	−134.7	−121.8		−36.6	−24.2
III	–	−176.4	−162.3		−65.7	−52.5
IV	CYS	−55.9	−54.1		−31.9	−31.7
	MET	−41.6	−40.4		−29.1	−28.3
V	–	−73.3	−85.5		−51.1	−63.0
4NO₂-ATE						
II	CYS	−126.2	−114.3		−34.7	−21.4
	MET	−140.2	−127.9		−37.4	−24.6
III	–	−181.3	−167.5		−66.4	−52.2
IV	CYS	−55.0	−53.2		−31.7	−30.8
	MET	−41.0	−39.5		−29.0	−27.6
V	–	−92.9	−105.4		−59.1	−71.4
2MeO-ATE						
II	CYS	−117.4	−104.8		−32.0	−18.3
	MET	−131.1	−117.9		−34.4	−21.2
III	–	−168.9	−155.3		−61.7	−47.7
IV	CYS	−51.6	−50.5		−29.8	−29.5
	MET	−37.8	−37.4		−27.3	−26.5
V	–	−75.6	−89.3		−49.6	−63.8
^a $\Delta_{r,298}H^0$ and $\Delta_{r,298}G^0$ (both in kcal mol ^{−1}), respectively, represent the enthalpy and Gibbs' free energy (gaseous phase) or free energy (aqueous phase) of the reaction corresponding to a given step number (Fig. 5) at standard temperature and pressure.						

Table 3S. Cartesian coordinates of the lowest energy structures of investigated molecules.

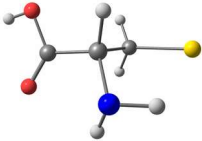
	CYS		
	X	Y	Z
C	0.001632000	0.007864000	0.000308000
S	-0.000150000	-0.016934000	1.820425000
C	1.425661000	0.001569000	-0.583242000
N	2.149468000	1.186140000	-0.167193000
C	1.331895000	-0.122855000	-2.102743000
O	1.604959000	0.757216000	-2.883373000
O	0.879333000	-1.327861000	-2.486897000
H	0.933685000	0.944123000	1.931807000
H	1.882205000	1.961281000	-0.768580000
H	3.145047000	1.054926000	-0.305906000
H	0.823761000	-1.310916000	-3.452587000
H	1.938534000	-0.888004000	-0.203638000
H	-0.538639000	0.888784000	-0.360937000
H	-0.542105000	-0.880810000	-0.325519000

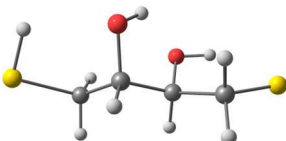
	DTT		
	X	Y	Z
C	-1.796795000	0.728293000	-0.210789000
S	-3.473192000	0.010690000	-0.098573000
C	-0.697521000	-0.335565000	-0.248984000
C	0.684336000	0.322355000	-0.303170000
C	1.785795000	-0.738966000	-0.240044000
S	3.466676000	-0.012576000	-0.221480000
O	-0.747202000	-1.180229000	0.871874000
O	0.779727000	1.243764000	0.756593000
H	-3.482455000	-0.567348000	-1.311904000
H	3.589270000	0.077635000	1.111414000
H	1.618812000	1.705019000	0.649167000
H	-1.666949000	-1.450388000	0.983602000
H	-1.734296000	1.388190000	-1.079393000
H	-1.671948000	1.334414000	0.687977000
H	-0.808102000	-0.919438000	-1.181617000
H	1.738256000	-1.385647000	-1.120073000
H	1.650835000	-1.360104000	0.645235000
H	0.755746000	0.842866000	-1.273375000

	GT 		
	X	Y	Z
C	2.516152000	0.267647000	-0.239882000
C	1.567200000	-0.558113000	-1.103246000
C	0.145342000	-0.051266000	-1.276818000
N	-0.294763000	0.903625000	-0.397617000
C	-1.662516000	1.387553000	-0.481006000
C	-2.672478000	0.255022000	-0.226336000
N	-2.255725000	-0.685692000	0.670100000
C	-2.899148000	-1.970770000	0.712704000
C	-1.852910000	-3.057091000	0.598479000
O	-0.657858000	-2.865153000	0.604400000
C	3.941697000	-0.339712000	-0.184206000
N	4.666338000	-0.411290000	-1.434623000
C	4.753890000	0.516435000	0.770404000
O	5.445403000	1.447198000	0.435419000
O	4.561690000	0.171056000	2.054573000
O	-0.599535000	-0.522000000	-2.117792000
C	-1.830760000	2.534978000	0.519142000
S	-3.508481000	3.260816000	0.425069000
O	-3.767302000	0.252088000	-0.754431000
O	-2.402486000	-4.272697000	0.524836000
H	5.074547000	0.795285000	2.587045000
H	3.865298000	-1.346159000	0.242249000
H	4.132029000	-0.888293000	-2.149768000
H	4.896126000	0.522923000	-1.757044000
H	2.136197000	0.321743000	0.788478000
H	2.596616000	1.292488000	-0.625930000
H	1.958647000	-0.673859000	-2.117735000
H	1.462320000	-1.568332000	-0.689309000
H	0.355786000	1.366959000	0.215939000
H	-1.879675000	1.735848000	-1.495050000
H	-1.641874000	2.166475000	1.532496000
H	-1.097494000	3.310360000	0.280701000
H	-3.195541000	4.348972000	1.146691000
H	-1.264039000	-0.708345000	0.868586000
H	-3.460866000	-2.132524000	1.640835000
H	-3.614757000	-2.045775000	-0.111854000
H	-1.676667000	-4.909361000	0.466100000

	MET 		
	X	Y	Z
C	3.468285000	-0.562024000	0.990255000
S	2.627657000	0.100925000	-0.470956000
C	0.915597000	0.070674000	0.149294000
C	-0.034540000	0.583648000	-0.929247000
C	-1.478109000	0.735096000	-0.440707000
C	-2.093495000	-0.614246000	-0.099845000

O	-3.193982000	-0.484891000	0.665398000
N	-1.551222000	1.626840000	0.710832000
O	-1.707590000	-1.685330000	-0.499864000
H	3.123419000	-1.574225000	1.215917000
H	3.310957000	0.080846000	1.860064000
H	4.535990000	-0.596262000	0.766439000
H	-3.534151000	-1.378759000	0.808313000
H	-2.505237000	1.690547000	1.047384000
H	-1.259435000	2.558023000	0.434018000
H	-0.025099000	-0.092391000	-1.788465000
H	0.303821000	1.564929000	-1.283764000
H	0.650790000	-0.956354000	0.416325000
H	0.838490000	0.696109000	1.042406000
H	-2.077356000	1.087742000	-1.301947000

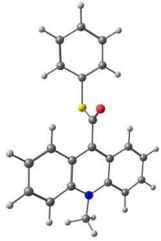
	CYS anion 		
	X	Y	Z
C	0.000312000	0.002008000	0.000844000
S	0.001716000	-0.014377000	1.822715000
C	1.448931000	0.000296000	-0.587170000
N	2.305192000	1.058369000	-0.069961000
C	1.351562000	0.118211000	-2.082902000
O	1.381399000	1.143555000	-2.732573000
O	1.129994000	-1.072890000	-2.695248000
H	2.066371000	1.072258000	0.929559000
H	1.939265000	1.933877000	-0.442520000
H	0.996297000	-0.844720000	-3.624796000
H	1.893039000	-0.970281000	-0.341159000
H	-0.505031000	0.900056000	-0.389083000
H	-0.528132000	-0.867927000	-0.412324000

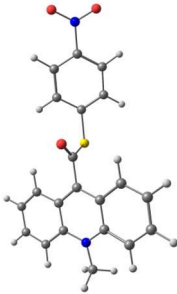
	DTT anion 		
	X	Y	Z
C	-1.845621000	0.595164000	-0.664839000
S	-3.460579000	-0.048614000	-0.096497000
C	-0.709313000	-0.367851000	-0.277583000
C	0.674888000	0.305175000	-0.295404000
C	1.783429000	-0.754741000	-0.299353000
S	3.458112000	-0.024542000	-0.177064000
O	-0.889448000	-0.829158000	1.047137000
O	0.791857000	1.138100000	0.839412000
H	0.207565000	0.688995000	1.477029000
H	-1.884145000	-0.798613000	1.126705000
H	-1.817040000	0.734696000	-1.753923000
H	-1.631599000	1.570022000	-0.206452000
H	-0.713325000	-1.219020000	-0.979852000
H	1.758187000	-1.325022000	-1.232151000
H	1.621709000	-1.444631000	0.532535000
H	0.774669000	0.934300000	-1.189358000
H	3.083876000	0.891749000	0.733122000

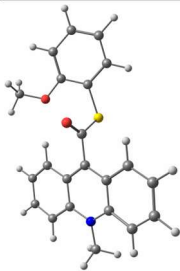
	GT anion		
	X	Y	Z
C	-2.867294000	-0.240916000	-0.066480000
C	-2.538953000	-1.727688000	-0.175866000
C	-1.066482000	-2.128776000	-0.338922000
N	-0.163128000	-1.146105000	-0.167464000
C	1.266447000	-1.303730000	-0.383930000
C	1.773037000	0.117163000	-0.670652000
N	3.107831000	0.240363000	-0.756665000
C	3.678421000	1.542038000	-0.877030000
C	3.554838000	2.393359000	0.376663000
O	3.152053000	2.054749000	1.457563000
C	-4.391602000	0.025926000	-0.023974000
N	-5.116962000	-0.540581000	1.100851000
C	-4.594478000	1.526693000	0.000702000
O	-4.798723000	2.184325000	0.993864000
O	-4.456752000	2.079811000	-1.217829000
O	-0.790708000	-3.296947000	-0.582468000
C	1.988528000	-1.982233000	0.803930000
S	3.728387000	-2.445749000	0.457805000
O	0.994838000	1.068826000	-0.811104000
O	3.996179000	3.655009000	0.135936000
H	-4.505924000	3.036392000	-1.086104000
H	-4.828322000	-0.355439000	-0.954854000
H	-4.862123000	-1.514375000	1.220706000
H	-4.850168000	-0.042234000	1.944978000
H	-2.444196000	0.296722000	-0.922918000
H	-2.416822000	0.183161000	0.839805000
H	-2.889742000	-2.267021000	0.711815000
H	-3.063707000	-2.171014000	-1.029479000
H	-0.445158000	-0.172926000	-0.159503000
H	1.435938000	-1.931566000	-1.267386000
H	1.918817000	-1.309563000	1.669211000
H	1.405645000	-2.879316000	1.030999000
H	3.662446000	-0.591489000	-0.409285000
H	4.744556000	1.452796000	-1.109116000
H	3.208201000	2.103774000	-1.691103000
H	3.892302000	4.121135000	0.975958000

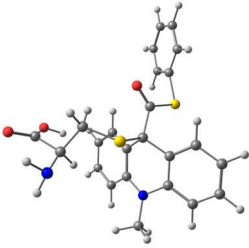
	MET anion		
	X	Y	Z
C	-1.81973000	-0.277781000	0.913693000
S	-2.59625300	-0.026909000	-0.722228000
C	-0.33653500	-0.687250000	0.846528000
C	0.46766700	0.254292000	-0.061999000
N	0.31615800	1.633207000	0.381955000
C	1.93574100	-0.094334000	-0.171338000
O	2.21230100	-1.412003000	-0.332311000
O	2.84213400	0.704853000	-0.189494000

H	1.37961500	-1.897273000	-0.280570000
H	-0.59980300	1.926456000	0.041827000
H	1.01717800	2.193310000	-0.093696000
H	0.03156100	0.097436000	-1.068826000
H	0.11059800	-0.702376000	1.851245000
H	-0.30804400	-1.711843000	0.440425000
H	-2.34523300	-1.055648000	1.484523000
H	-1.87727600	0.635663000	1.520163000

	H-ATE		
			
	X	Y	Z
C	4.022949000	-1.228986000	-0.108600000
C	3.399432000	-0.061630000	-0.547060000
C	4.079925000	1.155072000	-0.556244000
C	5.398750000	1.199981000	-0.117052000
C	6.025548000	0.039765000	0.328739000
C	5.339614000	-1.172019000	0.333394000
S	1.715720000	-0.121965000	-1.133932000
C	0.840641000	-0.040498000	0.407194000
O	1.325112000	-0.000602000	1.508684000
C	-0.664800000	-0.013419000	0.230666000
C	-1.381979000	-1.213400000	0.166359000
C	-2.794622000	-1.163351000	-0.033693000
N	-3.411418000	0.052116000	-0.195715000
C	-2.742137000	1.235068000	-0.001495000
C	-1.329356000	1.218319000	0.200607000
C	-0.740840000	-2.480494000	0.305183000
C	-1.464790000	-3.634993000	0.265869000
C	-2.867291000	-3.571711000	0.094909000
C	-3.524069000	-2.376467000	-0.053044000
C	-3.418089000	2.478862000	0.010205000
C	-2.709769000	3.640205000	0.187436000
C	-1.305851000	3.637590000	0.358420000
C	-0.632784000	2.451967000	0.369551000
C	-4.825372000	0.088297000	-0.600739000
H	-4.601193000	-2.381108000	-0.140534000
H	-3.444678000	-4.489887000	0.093268000
H	-0.977276000	-4.595478000	0.381312000
H	0.330727000	-2.508590000	0.465239000
H	0.438408000	2.428841000	0.533193000
H	-0.776720000	4.572653000	0.497136000
H	-3.246408000	4.582527000	0.209231000
H	-4.493977000	2.532426000	-0.076589000
H	-5.040829000	-0.770659000	-1.230184000
H	-5.481017000	0.088662000	0.272785000
H	-5.003881000	0.974855000	-1.202808000
H	3.586106000	2.054283000	-0.909060000
H	5.936236000	2.141882000	-0.124222000
H	7.054296000	0.078957000	0.670304000
H	5.831041000	-2.075403000	0.677566000
H	3.486013000	-2.171481000	-0.116826000

	4NO ₂ -ATE		
			
	X	Y	Z
C	-3.535396000	1.342447000	-0.086032000
C	-4.127267000	2.626853000	-0.150976000
C	-3.339696000	3.733677000	-0.340414000
C	-1.934757000	3.633848000	-0.470945000
C	-1.341256000	2.407231000	-0.431924000
C	-2.121929000	1.226490000	-0.250101000
H	-5.199136000	2.752884000	-0.095598000
H	-3.811869000	4.708055000	-0.403687000
H	-1.341187000	4.527818000	-0.619661000
H	-0.270302000	2.311767000	-0.566872000
C	-1.541961000	-0.047850000	-0.225158000
C	-2.337673000	-1.195823000	-0.143334000
C	-3.749479000	-1.044900000	0.014233000
N	-4.286561000	0.212742000	0.124228000
C	-0.036910000	-0.165067000	-0.355421000
C	-5.705268000	0.355225000	0.489634000
C	-1.782807000	-2.508173000	-0.228863000
C	-2.585128000	-3.608917000	-0.178583000
C	-3.984432000	-3.445778000	-0.050227000
C	-4.560658000	-2.204949000	0.045752000
H	-0.711842000	-2.616840000	-0.354107000
H	-2.161521000	-4.603166000	-0.253241000
H	-4.623199000	-4.322248000	-0.040604000
H	-5.637518000	-2.133339000	0.101514000
H	-5.837815000	1.267441000	1.064596000
H	-6.336261000	0.376706000	-0.401542000
H	-5.994828000	-0.470098000	1.134028000
S	0.770721000	-0.391781000	1.213487000
O	0.498016000	-0.082055000	-1.429879000
C	2.481697000	-0.258380000	0.725006000
C	3.228508000	0.809474000	1.222601000
C	4.571299000	0.922972000	0.885237000
C	5.125739000	-0.032036000	0.046816000
C	4.397647000	-1.099570000	-0.458581000
C	3.060219000	-1.216928000	-0.107250000
H	2.768062000	1.546274000	1.871245000
H	5.184177000	1.735156000	1.254628000
N	6.548979000	0.090968000	-0.322382000
H	4.881030000	-1.819277000	-1.106736000
H	2.474068000	-2.047233000	-0.482503000
O	7.010184000	-0.765010000	-1.056884000
O	7.162641000	1.040757000	0.131890000

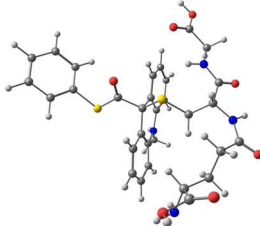
	2MeO-ATE		
			
	X	Y	Z
C	3.286770000	0.807793000	-0.639258000
C	4.228881000	1.750761000	-1.116809000
C	3.799313000	2.944280000	-1.638899000
C	2.425930000	3.270111000	-1.720199000
C	1.498845000	2.390888000	-1.244793000
C	1.899333000	1.143078000	-0.680486000
H	5.291358000	1.569601000	-1.040904000
H	4.537371000	3.659266000	-1.986069000
H	2.119251000	4.220046000	-2.141012000
H	0.443994000	2.637916000	-1.270157000
C	0.968099000	0.236641000	-0.160082000
C	1.389100000	-0.946785000	0.459248000
C	2.782716000	-1.252535000	0.485231000
N	3.673360000	-0.407971000	-0.131259000
C	-0.512025000	0.562260000	-0.186187000
C	5.074125000	-0.836051000	-0.266613000
C	0.460283000	-1.847996000	1.062842000
C	0.900891000	-2.980933000	1.681325000
C	2.286613000	-3.256472000	1.732837000
C	3.211104000	-2.425190000	1.152198000
H	-0.598865000	-1.612448000	1.025347000
H	0.198081000	-3.663976000	2.143234000
H	2.633981000	-4.143500000	2.251618000
H	4.260520000	-2.664090000	1.248393000
H	5.507224000	-0.386634000	-1.154873000
H	5.654110000	-0.557263000	0.615826000
H	5.105349000	-1.913397000	-0.409712000
S	-1.352571000	-0.135393000	-1.577985000
O	-1.002776000	1.206735000	0.705453000
C	-3.031367000	0.277591000	-1.181283000
C	-3.735831000	1.141600000	-2.014901000
C	-5.069833000	1.431643000	-1.755195000
C	-5.686103000	0.858498000	-0.649300000
C	-4.991883000	-0.002643000	0.195206000
C	-3.656152000	-0.307705000	-0.065228000
H	-3.233528000	1.581809000	-2.869772000
H	-5.618205000	2.101381000	-2.407030000
H	-6.725477000	1.080903000	-0.432819000
H	-5.498957000	-0.432416000	1.050163000
O	-2.906189000	-1.141959000	0.692499000
C	-3.494334000	-1.690384000	1.860245000
H	-2.717917000	-2.290631000	2.335051000
H	-3.812711000	-0.902949000	2.550869000
H	-4.344012000	-2.334929000	1.612341000

	H-ATE-CYS		
			
	X	Y	Z
C	0.391390000	3.003779000	-1.247351000
C	-0.380049000	2.159625000	-0.450460000
C	-1.458688000	2.693352000	0.272672000
C	-1.687671000	4.073610000	0.239874000
C	-0.889973000	4.899703000	-0.540714000
C	0.147868000	4.369982000	-1.297510000
C	-0.193203000	0.656728000	-0.468593000
C	-0.681033000	0.044102000	0.832570000
C	-1.780787000	0.636259000	1.481380000
N	-2.288595000	1.838473000	1.007159000
C	-2.339123000	-0.000587000	2.600549000
C	-1.803848000	-1.187017000	3.080184000
C	-0.685425000	-1.751700000	2.472762000
C	-0.137058000	-1.129749000	1.353448000
C	1.280550000	0.233372000	-0.666879000
O	1.624840000	-0.660074000	-1.391803000
S	-1.244097000	0.120567000	-1.905536000
C	-1.379142000	-1.679314000	-1.690793000
C	-2.669013000	-2.119318000	-0.973599000
N	-3.818898000	-1.818471000	-1.800160000
C	-3.585606000	2.303363000	1.453119000
S	2.440402000	1.106368000	0.415617000
C	3.844254000	0.018120000	0.278650000
C	4.179337000	-0.790018000	1.365000000
C	5.288669000	-1.626611000	1.287000000
C	6.052876000	-1.663788000	0.124577000
C	5.712333000	-0.860124000	-0.960445000
C	4.612420000	-0.013373000	-0.885085000
C	-2.546451000	-3.620450000	-0.659218000
O	-1.793938000	-3.947569000	0.403504000
O	-3.054455000	-4.471749000	-1.343639000
H	-2.481130000	4.510540000	0.833960000
H	-1.085601000	5.967052000	-0.553032000
H	0.760253000	5.009190000	-1.923034000
H	1.187962000	2.581121000	-1.850913000
H	0.727184000	-1.578944000	0.872954000
H	-0.236329000	-2.656449000	2.869118000
H	-2.247660000	-1.656709000	3.951647000
H	-3.177128000	0.447245000	3.120041000
H	-3.999627000	2.976553000	0.701724000
H	-4.265009000	1.453338000	1.537015000
H	-3.547816000	2.826202000	2.418162000
H	3.572290000	-0.760972000	2.264254000
H	5.551963000	-2.253015000	2.133095000
H	6.914651000	-2.320591000	0.063459000
H	6.305264000	-0.890393000	-1.868722000
H	4.342637000	0.616282000	-1.725561000
H	-2.754017000	-1.565767000	-0.031045000
H	-1.375978000	-2.104976000	-2.698706000
H	-0.478702000	-2.049478000	-1.197928000
H	-4.666596000	-1.888770000	-1.247439000

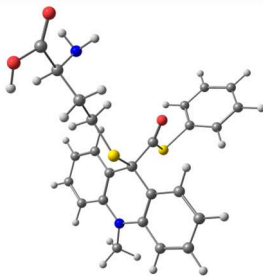
H	-1.510281000	-3.150109000	0.876644000
H	-3.892100000	-2.546868000	-2.507331000

	H-ATE-DTT		
	X	Y	Z
C	-0.566246000	3.198901000	0.918823000
C	-1.625328000	2.973903000	0.027753000
C	-2.442106000	4.047131000	-0.352898000
C	-2.205650000	5.330426000	0.149187000
C	-1.149232000	5.550357000	1.036874000
C	-0.330822000	4.484591000	1.420682000
S	-1.978344000	1.420090000	-0.632836000
C	-0.939255000	0.148145000	-0.126421000
O	0.027025000	0.607120000	0.749949000
C	-0.776237000	-1.297325000	-0.351825000
C	-1.911327000	-1.277669000	-1.269933000
C	-3.254543000	-1.500409000	-0.797100000
N	-3.493707000	-1.753112000	0.598078000
C	-2.391329000	-1.790968000	1.532700000
C	-1.025636000	-1.570003000	1.082736000
C	-4.364137000	-1.471562000	-1.722337000
C	-4.129851000	-1.220396000	-3.122725000
C	-2.786796000	-0.997958000	-3.599052000
C	-1.680545000	-1.026692000	-2.673725000
C	-2.672181000	-2.057171000	2.927038000
C	-1.604421000	-2.111242000	3.891392000
C	-0.250422000	-1.899601000	3.452720000
C	0.032210000	-1.633364000	2.064034000
S	0.789607000	-1.021450000	-1.067976000
C	2.301362000	-0.986885000	-0.020270000
C	3.452601000	-0.280901000	-0.746083000
O	3.631932000	-0.800151000	-2.048700000
C	-4.851528000	-1.974449000	1.058315000
C	4.772973000	-0.396201000	0.018342000
O	5.126732000	-1.764108000	0.138021000
C	5.873021000	0.394437000	-0.691921000
S	7.490415000	0.334227000	0.159011000
H	5.668863000	-1.855680000	0.926518000
H	2.720402000	-0.985807000	-2.341250000
H	2.124251000	-0.454810000	0.916362000
H	2.625534000	-2.003409000	0.222294000
H	3.209378000	0.796270000	-0.797238000
H	5.605982000	1.453689000	-0.733501000
H	5.992231000	0.031655000	-1.713780000
H	4.610667000	0.043617000	1.013497000
H	7.762289000	-0.953843000	-0.100733000
H	-4.850189000	-2.150794000	2.131539000
H	-5.458450000	-1.096849000	0.837498000
H	-5.271305000	-2.842327000	0.550445000
H	-0.667684000	-0.857701000	-3.034639000
H	-2.799112000	-0.826001000	-4.673802000
H	-4.965716000	-1.198962000	-3.819619000

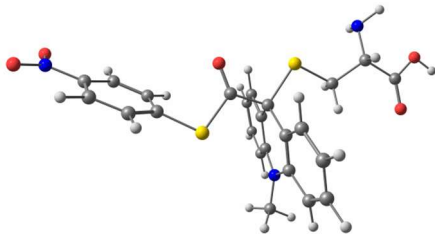
H	-5.294391000	-1.658866000	-1.189711000
H	-3.741964000	-2.192375000	3.066622000
H	-1.882850000	-3.050268000	4.369254000
H	0.564840000	-1.940743000	4.172922000
H	1.053277000	-1.484059000	1.761510000
H	-3.266563000	3.880776000	-1.044387000
H	-2.845138000	6.158325000	-0.151890000
H	-0.964568000	6.549431000	1.428234000
H	0.492621000	4.654365000	2.112268000
H	0.073716000	2.376803000	1.221866000

	H-ATE-GT		
			
	X	Y	Z
C	1.292727000	0.848761000	2.443468000
C	1.780586000	1.986868000	3.111484000
C	2.515883000	2.948253000	2.438808000
C	2.773405000	2.815029000	1.077035000
C	2.242307000	1.729948000	0.398786000
C	1.494052000	0.751193000	1.056872000
H	1.565201000	2.136216000	4.161601000
H	2.883080000	3.810814000	2.985425000
H	3.364514000	3.555806000	0.549519000
H	2.391450000	1.640089000	-0.673245000
C	0.883497000	-0.376134000	0.243830000
C	0.089024000	-1.344973000	1.091728000
C	-0.057965000	-1.166458000	2.476651000
N	0.619059000	-0.149709000	3.147510000
C	2.021378000	-1.088291000	-0.520464000
C	0.724615000	-0.197533000	4.595256000
C	-0.544696000	-2.422144000	0.466848000
C	-1.328482000	-3.317605000	1.173525000
C	-1.522208000	-3.105175000	2.537086000
C	-0.908271000	-2.042189000	3.177707000
H	-0.415414000	-2.545750000	-0.604417000
H	-1.795140000	-4.154637000	0.667061000
H	-2.159812000	-3.770468000	3.111296000
H	-1.107425000	-1.882923000	4.229521000
H	1.679416000	0.227718000	4.905022000
H	-0.086066000	0.342975000	5.098473000
H	0.718064000	-1.235961000	4.927730000
S	3.003765000	-2.157860000	0.541299000
O	2.256771000	-0.898085000	-1.683013000
C	4.341283000	-2.548172000	-0.569263000
C	4.482600000	-3.853995000	-1.034866000
C	5.550581000	-4.177307000	-1.866868000
C	6.464602000	-3.197753000	-2.241208000
C	6.316504000	-1.892070000	-1.779027000
C	5.260658000	-1.565166000	-0.937063000
H	3.758619000	-4.609642000	-0.748988000
H	5.662143000	-5.194412000	-2.227985000
H	7.293468000	-3.450648000	-2.894407000
H	7.027556000	-1.126576000	-2.071806000
H	5.141153000	-0.551637000	-0.568920000

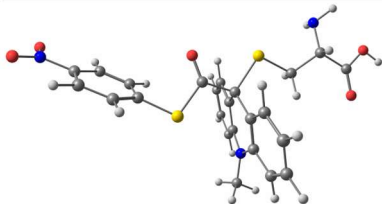
S	-0.218064000	0.332101000	-1.085926000
C	-1.459614000	1.082658000	0.015027000
C	-2.229323000	2.205335000	-0.723321000
H	-2.158105000	0.314822000	0.350978000
H	-0.964656000	1.494793000	0.899986000
N	-3.553471000	2.391874000	-0.192931000
C	-1.493075000	3.548412000	-0.546250000
H	-2.267418000	1.978427000	-1.797688000
O	-1.999480000	4.482825000	0.059070000
N	-0.255344000	3.613093000	-1.079659000
H	0.182730000	2.797451000	-1.495301000
C	0.560279000	4.776443000	-0.859960000
C	1.853676000	4.636122000	-1.619511000
H	0.043643000	5.685788000	-1.183650000
H	0.798830000	4.912288000	0.202720000
O	2.631514000	5.716188000	-1.463860000
O	2.177605000	3.674652000	-2.275251000
H	3.434583000	5.557862000	-1.979352000
H	-3.707558000	3.283441000	0.265236000
C	-4.643391000	1.577305000	-0.320371000
O	-5.718852000	1.892450000	0.162489000
C	-4.472415000	0.246554000	-1.035739000
H	-3.478292000	0.120989000	-1.476305000
C	-4.771966000	-0.897075000	-0.057634000
H	-5.196997000	0.215591000	-1.851773000
C	-4.373244000	-2.280403000	-0.561433000
H	-4.220248000	-0.730627000	0.877646000
H	-5.833212000	-0.888107000	0.199112000
N	-4.634866000	-3.271688000	0.481386000
C	-5.150108000	-2.699966000	-1.799708000
H	-3.309873000	-2.247713000	-0.869968000
O	-4.832327000	-3.961006000	-2.160719000
O	-5.941080000	-2.036052000	-2.422555000
H	-5.371949000	-4.165798000	-2.936594000
H	-4.357172000	-4.192983000	0.159689000
H	-4.064585000	-3.050638000	1.291427000

H-ATE-MET			
			
	X	Y	Z
C	-2.187065000	3.807667000	1.566815000
C	-2.397371000	2.871320000	0.556425000
C	-2.810652000	3.285761000	-0.710530000
C	-3.003985000	4.638048000	-0.964190000
C	-2.800163000	5.575685000	0.045925000
C	-2.395198000	5.160055000	1.310029000
S	-2.184940000	1.137451000	0.906277000
C	-0.700841000	0.812926000	-0.075079000
O	-0.066611000	1.683682000	-0.604408000
C	-0.411398000	-0.704207000	-0.216436000
C	-0.477337000	-1.403630000	1.121624000
C	-1.178254000	-2.612640000	1.282539000

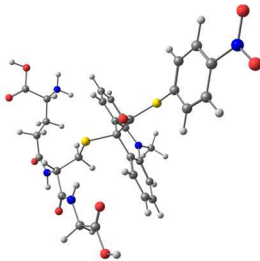
N	-2.018312000	-3.098916000	0.279033000
C	-2.104770000	-2.461216000	-0.960371000
C	-1.407727000	-1.269334000	-1.216632000
C	-1.024243000	-3.316976000	2.488796000
C	-0.286552000	-2.790841000	3.538063000
C	0.320759000	-1.546562000	3.418118000
C	0.225352000	-0.876910000	2.207935000
C	-2.895913000	-3.000942000	-1.989012000
C	-3.042281000	-2.343344000	-3.200757000
C	-2.393262000	-1.136531000	-3.433586000
C	-1.569169000	-0.623788000	-2.444048000
S	1.219981000	-0.995510000	-1.057668000
C	2.451261000	-0.226018000	0.036266000
C	3.771288000	-0.114114000	-0.721793000
C	4.897089000	0.416287000	0.186275000
N	4.520311000	1.689647000	0.761379000
C	-2.988845000	-4.129471000	0.606286000
C	6.214481000	0.482486000	-0.604749000
O	6.741642000	-0.701084000	-0.983295000
O	6.762178000	1.512563000	-0.893606000
H	-3.385972000	-3.956707000	-1.857398000
H	-3.664459000	-2.789247000	-3.970080000
H	-2.504190000	-0.616624000	-4.378389000
H	-1.016836000	0.294153000	-2.621242000
H	0.706705000	0.089938000	2.099315000
H	0.871849000	-1.111371000	4.243947000
H	-0.194271000	-3.361333000	4.456686000
H	-1.468073000	-4.296561000	2.609378000
H	-3.924988000	-3.934524000	0.082361000
H	-2.639593000	-5.136013000	0.347390000
H	-3.215606000	-4.097498000	1.671460000
H	-1.859565000	3.477236000	2.546880000
H	-2.233442000	5.888393000	2.098102000
H	-2.957391000	6.630767000	-0.153827000
H	-3.318633000	4.960751000	-1.951296000
H	-2.973027000	2.548165000	-1.489771000
H	6.199908000	-1.429503000	-0.660619000
H	4.468483000	2.378091000	0.014518000
H	5.261211000	2.017212000	1.372952000
H	4.051584000	-1.090258000	-1.136595000
H	3.651011000	0.562708000	-1.575760000
H	5.039689000	-0.298545000	1.010367000
H	2.118183000	0.771359000	0.325136000
H	2.583856000	-0.830294000	0.938850000

4NO₂-ATE-CYS 			
	X	Y	Z
C	1.203000000	1.171702000	2.007055000
C	1.326694000	1.198192000	3.406719000
C	1.061835000	0.070821000	4.167660000
C	0.682328000	-1.119326000	3.555388000
C	0.604826000	-1.164786000	2.172114000

C	0.873100000	-0.043484000	1.384283000
H	1.653150000	2.101564000	3.906303000
H	1.162612000	0.125626000	5.246918000
H	0.465088000	-2.003319000	4.144367000
H	0.338601000	-2.089228000	1.669950000
C	0.772474000	-0.156554000	-0.133980000
C	1.274314000	1.092486000	-0.835578000
C	1.596767000	2.258773000	-0.120667000
N	1.406056000	2.329661000	1.258242000
C	-0.716880000	-0.420927000	-0.444335000
C	1.398272000	3.620945000	1.917552000
C	1.414673000	1.086638000	-2.226070000
C	1.880090000	2.191391000	-2.919221000
C	2.245935000	3.326736000	-2.202596000
C	2.115211000	3.359823000	-0.824351000
H	1.159315000	0.178306000	-2.762178000
H	1.972314000	2.161628000	-3.998960000
H	2.648523000	4.193785000	-2.716378000
H	2.442844000	4.241840000	-0.288948000
H	0.719763000	3.588251000	2.771016000
H	2.391907000	3.930953000	2.265426000
H	1.013060000	4.376261000	1.231567000
S	-1.698424000	1.104306000	-0.493163000
O	-1.197978000	-1.512982000	-0.564320000
C	-3.336626000	0.414044000	-0.426522000
C	-4.246907000	0.748111000	-1.429781000
C	-5.552365000	0.277186000	-1.371904000
C	-5.916417000	-0.536766000	-0.309567000
C	-5.025569000	-0.889021000	0.696625000
C	-3.729333000	-0.401229000	0.638432000
H	-3.932191000	1.372372000	-2.258545000
H	-6.279302000	0.521983000	-2.135412000
N	-7.294018000	-1.042947000	-0.244784000
H	-5.356323000	-1.526232000	1.506514000
H	-3.018507000	-0.655794000	1.416243000
O	-7.591163000	-1.756902000	0.700316000
O	-8.059924000	-0.718101000	-1.138899000
S	1.662518000	-1.677643000	-0.734479000
C	3.332623000	-1.173436000	-0.218388000
C	4.374039000	-1.949556000	-1.022127000
H	3.475076000	-0.105523000	-0.393715000
H	3.456760000	-1.360504000	0.854148000
C	5.766428000	-1.426702000	-0.650241000
N	4.162671000	-3.376639000	-0.907625000
H	4.245466000	-1.677349000	-2.078953000
H	4.839765000	-3.887790000	-1.461469000
H	4.276225000	-3.677669000	0.054925000
O	6.692597000	-2.402356000	-0.606031000
O	6.038061000	-0.266146000	-0.456260000
H	7.533563000	-1.964767000	-0.412842000

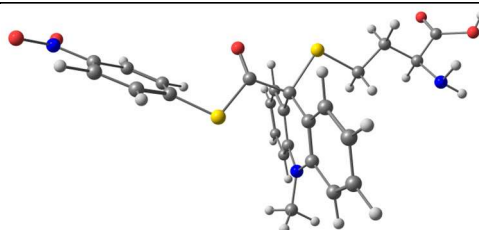
	4NO ₂ -ATE-DTT		
			
	X	Y	Z
C	1.095531000	-0.799104000	1.588095000
C	1.405491000	-1.929986000	2.363574000
C	1.070742000	-3.204570000	1.936118000
C	0.428146000	-3.392849000	0.716580000
C	0.164949000	-2.286203000	-0.076558000
C	0.506272000	-0.992586000	0.327827000
H	1.937708000	-1.817497000	3.299513000
H	1.324588000	-4.055395000	2.559755000
H	0.152847000	-4.385637000	0.379351000
H	-0.312727000	-2.412541000	-1.043328000
C	0.232057000	0.176564000	-0.612884000
C	0.755598000	1.488783000	-0.073775000
C	1.354016000	1.579938000	1.193448000
N	1.397644000	0.479857000	2.050930000
C	-1.299948000	0.199141000	-0.803202000
C	1.688205000	0.680951000	3.458317000
C	0.661058000	2.635350000	-0.867988000
C	1.164452000	3.855860000	-0.452423000
C	1.808920000	3.928792000	0.779105000
C	1.909412000	2.809429000	1.587577000
H	0.193980000	2.545060000	-1.844214000
H	1.074986000	4.730406000	-1.086546000
H	2.248383000	4.863065000	1.113097000
H	2.448256000	2.887982000	2.522981000
H	1.143859000	-0.054609000	4.051527000
H	2.757996000	0.602297000	3.688507000
H	1.332469000	1.664757000	3.765889000
S	-2.149295000	1.118378000	0.505108000
O	-1.876298000	-0.402766000	-1.666672000
C	-3.816889000	0.558508000	0.233794000
C	-4.815614000	1.506244000	0.009775000
C	-6.136802000	1.103788000	-0.139688000
C	-6.428065000	-0.250556000	-0.074998000
C	-5.449000000	-1.212722000	0.139112000
C	-4.135770000	-0.800270000	0.302224000
H	-4.559049000	2.557824000	-0.052616000
H	-6.932295000	1.816929000	-0.312926000
N	-7.823005000	-0.683277000	-0.236402000
H	-5.725019000	-2.258269000	0.182669000
H	-3.355269000	-1.531834000	0.477969000
O	-8.054980000	-1.880454000	-0.174686000
O	-8.666000000	0.180705000	-0.420827000
S	0.907239000	-0.173378000	-2.321542000
C	2.669146000	0.229373000	-2.104392000
C	3.428871000	-0.648544000	-1.106786000
H	3.082536000	0.077275000	-3.107351000
H	2.789162000	1.281284000	-1.839209000
C	4.921173000	-0.315114000	-1.119986000
H	3.068580000	-0.426669000	-0.091955000
O	3.320224000	-2.020217000	-1.397429000
H	2.391708000	-2.265190000	-1.311702000
C	5.678070000	-1.223285000	-0.149568000

H	5.308510000	-0.487044000	-2.136307000
O	5.034100000	1.046957000	-0.761856000
H	5.933118000	1.320139000	-0.968945000
S	7.449170000	-0.795692000	-0.000187000
H	5.218309000	-1.186374000	0.841596000
H	5.634713000	-2.254856000	-0.500229000
H	7.289870000	0.248505000	0.828675000

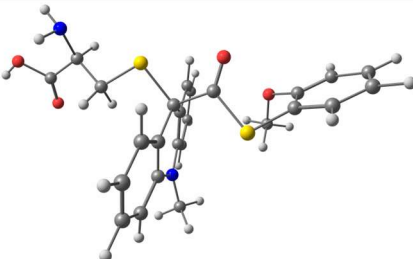
4NO ₂ -ATE-GT			
			
	X	Y	Z
C	0.264536000	1.208925000	2.694491000
C	0.403729000	2.416004000	3.402489000
C	0.947188000	3.537505000	2.798497000
C	1.352871000	3.493977000	1.467659000
C	1.163773000	2.326741000	0.745376000
C	0.611980000	1.186785000	1.334026000
H	0.060462000	2.486222000	4.426664000
H	1.044092000	4.453304000	3.372364000
H	1.797176000	4.362423000	0.993771000
H	1.432403000	2.297049000	-0.306083000
C	0.362653000	-0.043816000	0.472523000
C	-0.325276000	-1.158205000	1.231197000
C	-0.619184000	-1.046257000	2.600602000
N	-0.214129000	0.065760000	3.334827000
C	1.725977000	-0.487702000	-0.091809000
C	-0.236260000	0.009934000	4.785625000
C	-0.689810000	-2.319404000	0.544619000
C	-1.339414000	-3.366679000	1.175106000
C	-1.673192000	-3.233950000	2.521156000
C	-1.331426000	-2.089342000	3.221277000
H	-0.454377000	-2.389373000	-0.513060000
H	-1.596622000	-4.263409000	0.622817000
H	-2.208032000	-4.027101000	3.034485000
H	-1.635155000	-1.999085000	4.256058000
H	0.550048000	0.650258000	5.185022000
H	-1.198718000	0.321622000	5.209511000
H	-0.017301000	-1.007328000	5.113938000
S	2.701587000	-1.435630000	1.105915000
O	2.134643000	-0.181129000	-1.177749000
C	4.259559000	-1.468871000	0.247158000
C	4.798848000	-2.700178000	-0.125899000
C	6.039485000	-2.755665000	-0.748568000
C	6.709870000	-1.566997000	-0.995814000
C	6.187490000	-0.329560000	-0.642102000
C	4.954823000	-0.285230000	-0.008937000
H	4.246582000	-3.613069000	0.065854000
H	6.484704000	-3.695619000	-1.048188000
N	8.021783000	-1.618422000	-1.655814000
H	6.748650000	0.570392000	-0.858049000
H	4.526437000	0.667851000	0.279747000
O	8.593520000	-0.559290000	-1.860415000
O	8.459985000	-2.717182000	-1.958063000

S	-0.649926000	0.430750000	-1.019391000
C	-2.135932000	0.972664000	-0.120474000
C	-3.060606000	1.795482000	-1.050975000
H	-2.671328000	0.098857000	0.255387000
H	-1.838353000	1.579623000	0.740561000
N	-4.442119000	1.707083000	-0.658863000
C	-2.680114000	3.287444000	-0.983089000
H	-2.929207000	1.459030000	-2.089011000
O	-3.453710000	4.122928000	-0.537312000
N	-1.437968000	3.606748000	-1.408481000
H	-0.764487000	2.893217000	-1.667322000
C	-0.960231000	4.954180000	-1.246590000
C	0.494834000	5.026472000	-1.628989000
H	-1.526745000	5.659753000	-1.864562000
H	-1.070148000	5.293961000	-0.209727000
O	0.972282000	6.270605000	-1.500108000
O	1.165295000	4.093152000	-2.002736000
H	1.899227000	6.245672000	-1.775835000
H	-4.831251000	2.557729000	-0.266789000
C	-5.257389000	0.609344000	-0.668315000
O	-6.378400000	0.661321000	-0.189170000
C	-4.734941000	-0.675054000	-1.296805000
H	-3.678266000	-0.614047000	-1.575584000
C	-4.965735000	-1.851205000	-0.343628000
H	-5.300694000	-0.840773000	-2.217252000
C	-4.349335000	-3.168091000	-0.804466000
H	-4.518163000	-1.615710000	0.631608000
H	-6.036833000	-1.978394000	-0.175785000
N	-4.529911000	-4.179290000	0.235546000
C	-4.979339000	-3.696819000	-2.083287000
H	-3.284793000	-2.986771000	-1.052782000
O	-4.510091000	-4.926714000	-2.378559000
O	-5.777381000	-3.130232000	-2.788338000
H	-4.960837000	-5.202583000	-3.188457000
H	-4.100332000	-5.053431000	-0.048341000
H	-4.064033000	-3.867595000	1.081410000

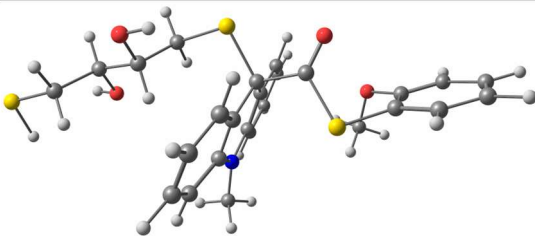
	4NO ₂ -ATE-MET		
	X	Y	Z
C	0.732138000	1.406758000	2.036782000
C	0.834786000	1.448670000	3.437810000
C	0.691471000	0.298528000	4.197284000
C	0.458087000	-0.926636000	3.581515000
C	0.402250000	-0.981956000	2.197339000
C	0.549594000	0.162290000	1.410859000
H	1.050143000	2.385197000	3.936915000
H	0.772361000	0.363383000	5.277641000
H	0.336750000	-1.829851000	4.168792000
H	0.248316000	-1.931768000	1.696653000
C	0.474491000	0.044712000	-0.110017000
C	0.862458000	1.338554000	-0.803778000
C	1.036993000	2.532971000	-0.084270000
N	0.810089000	2.581139000	1.289670000



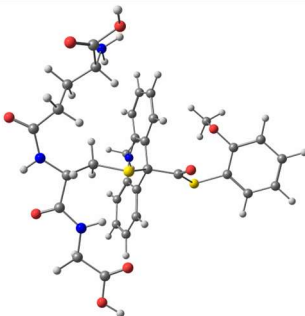
C	-0.980744000	-0.365044000	-0.432180000
C	0.634454000	3.862482000	1.944847000
C	1.038393000	1.349669000	-2.189843000
C	1.394174000	2.500657000	-2.873495000
C	1.609550000	3.670214000	-2.151296000
C	1.442716000	3.686552000	-0.776456000
H	0.901969000	0.418343000	-2.729879000
H	1.517107000	2.481942000	-3.950410000
H	1.921948000	4.578130000	-2.657282000
H	1.652570000	4.599907000	-0.233978000
H	-0.046633000	3.745362000	2.789064000
H	1.576856000	4.293590000	2.306581000
H	0.170363000	4.564064000	1.250085000
S	-2.101645000	1.054497000	-0.532680000
O	-1.351859000	-1.501341000	-0.528773000
C	-3.667824000	0.211260000	-0.482330000
C	-4.592467000	0.454788000	-1.497856000
C	-5.848630000	-0.136662000	-1.452093000
C	-6.147235000	-0.976209000	-0.389575000
C	-5.240051000	-1.238474000	0.629665000
C	-3.994971000	-0.631742000	0.583640000
H	-4.328955000	1.103147000	-2.325971000
H	-6.587179000	0.034188000	-2.224598000
N	-7.471648000	-1.609042000	-0.338180000
H	-5.520563000	-1.899667000	1.439329000
H	-3.272330000	-0.813388000	1.370971000
O	-7.713187000	-2.340635000	0.609499000
O	-8.253093000	-1.363142000	-1.244298000
S	1.511974000	-1.377959000	-0.706798000
C	3.140648000	-0.718933000	-0.237270000
C	4.220392000	-1.731459000	-0.603079000
H	3.324244000	0.227822000	-0.750252000
H	3.147331000	-0.533435000	0.842449000
C	5.620653000	-1.205559000	-0.253597000
H	4.064295000	-2.677648000	-0.079134000
H	4.181087000	-1.945753000	-1.679375000
C	6.625819000	-2.354196000	-0.379992000
N	5.919175000	0.004798000	-0.993737000
H	5.622762000	-0.954950000	0.816176000
O	7.709981000	-2.034204000	-1.110914000
O	6.489033000	-3.438481000	0.134215000
H	8.275800000	-2.819173000	-1.103479000
H	6.833088000	0.362070000	-0.738810000
H	5.960226000	-0.199379000	-1.987610000

2MeO-ATE-CYS			
			
	X	Y	Z
C	0.745732000	1.929880000	-1.331483000
C	1.123205000	3.241317000	-1.666084000
C	1.360060000	4.187482000	-0.681999000
C	1.244317000	3.849502000	0.662440000
C	0.916330000	2.545395000	0.997464000

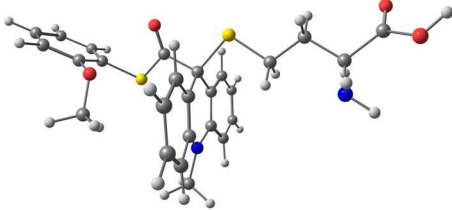
C	0.673218000	1.571913000	0.025677000
H	1.254320000	3.520484000	-2.704051000
H	1.646928000	5.193140000	-0.972590000
H	1.419588000	4.586246000	1.438332000
H	0.853481000	2.251514000	2.040529000
C	0.322065000	0.158813000	0.456593000
C	0.305166000	-0.812503000	-0.719598000
C	0.398294000	-0.357462000	-2.044989000
N	0.447067000	1.006478000	-2.331387000
C	-1.081583000	0.095606000	1.095300000
C	0.171246000	1.467200000	-3.676976000
C	0.173237000	-2.180438000	-0.477056000
C	0.177605000	-3.107279000	-1.508202000
C	0.336783000	-2.659108000	-2.815928000
C	0.447355000	-1.303332000	-3.083330000
H	0.062673000	-2.509102000	0.550129000
H	0.069457000	-4.164029000	-1.291633000
H	0.381335000	-3.366446000	-3.638081000
H	0.602641000	-0.980475000	-4.105207000
H	-0.300788000	2.449926000	-3.634443000
H	1.070706000	1.532778000	-4.303044000
H	-0.538277000	0.788400000	-4.152664000
S	-2.269349000	1.201165000	0.287010000
O	-1.377064000	-0.650122000	1.985432000
C	-3.779157000	0.395140000	0.760581000
C	-4.736177000	1.085890000	1.501751000
C	-5.947928000	0.483358000	1.824232000
C	-6.199163000	-0.824026000	1.420296000
C	-5.246470000	-1.524557000	0.688041000
C	-4.039346000	-0.920881000	0.350284000
H	-4.520983000	2.097568000	1.829533000
H	-6.685786000	1.030033000	2.401600000
H	-7.137451000	-1.303801000	1.679640000
H	-5.415597000	-2.549057000	0.373834000
O	-3.101195000	-1.637623000	-0.336689000
S	1.478665000	-0.440630000	1.785311000
C	3.022515000	-0.220697000	0.848317000
C	4.111443000	-1.116442000	1.435146000
H	2.861681000	-0.496421000	-0.196225000
H	3.333633000	0.829530000	0.875507000
C	5.358496000	-1.017008000	0.549811000
N	4.300074000	-0.847936000	2.845627000
H	3.774608000	-2.157211000	1.335637000
H	5.001316000	-1.464293000	3.239260000
H	4.625760000	0.103050000	2.985731000
O	6.502418000	-1.063567000	1.259389000
O	5.347961000	-0.940346000	-0.655253000
H	7.219948000	-1.033555000	0.611252000
C	-3.143228000	-1.467950000	-1.746259000
H	-2.337431000	-2.079956000	-2.152392000
H	-4.107303000	-1.801557000	-2.150868000
H	-2.974558000	-0.420730000	-2.023811000

	2MeO-ATE-DTT		
			
	X	Y	Z
C	0.878668000	-0.307924000	1.696499000
C	1.658949000	-1.019111000	2.625525000
C	1.925655000	-2.367337000	2.449743000
C	1.423578000	-3.048904000	1.344570000
C	0.700631000	-2.339779000	0.400556000
C	0.442622000	-0.973573000	0.539365000
H	2.085586000	-0.508745000	3.479706000
H	2.533905000	-2.886297000	3.183552000
H	1.612869000	-4.107652000	1.210318000
H	0.337158000	-2.842661000	-0.490967000
C	-0.250123000	-0.237626000	-0.588020000
C	-0.370217000	1.256097000	-0.322574000
C	0.069572000	1.825632000	0.883445000
N	0.560864000	1.029407000	1.917429000
C	-1.682576000	-0.770674000	-0.805730000
C	0.715160000	1.592504000	3.244057000
C	-0.920532000	2.077690000	-1.308007000
C	-1.010830000	3.450629000	-1.144012000
C	-0.521678000	4.020868000	0.027547000
C	0.012895000	3.223232000	1.026990000
H	-1.282318000	1.614330000	-2.219062000
H	-1.445205000	4.065682000	-1.923790000
H	-0.546947000	5.097023000	0.166949000
H	0.418857000	3.696447000	1.911850000
H	0.563298000	0.811848000	3.990218000
H	1.700080000	2.049801000	3.402530000
H	-0.054745000	2.347385000	3.409799000
S	-2.515305000	-1.160769000	0.756057000
O	-2.213511000	-0.859087000	-1.876290000
C	-4.203169000	-1.040535000	0.216438000
C	-5.042351000	-2.150631000	0.291114000
C	-6.380784000	-2.047157000	-0.073779000
C	-6.880525000	-0.832596000	-0.532846000
C	-6.048421000	0.278703000	-0.618552000
C	-4.712809000	0.183630000	-0.241190000
H	-4.636920000	-3.097676000	0.631511000
H	-7.025802000	-2.917061000	-0.012379000
H	-7.920822000	-0.749198000	-0.830398000
H	-6.413926000	1.231919000	-0.985417000
O	-3.900493000	1.274650000	-0.367512000
S	0.632207000	-0.518350000	-2.211433000
C	2.231235000	0.282759000	-1.859557000
C	3.238019000	-0.591470000	-1.105485000
H	2.634714000	0.519199000	-2.849509000
H	2.062833000	1.224894000	-1.332711000
C	4.597008000	0.098949000	-1.011255000
H	2.888924000	-0.748298000	-0.076784000
O	3.450226000	-1.823328000	-1.757410000
H	2.584746000	-2.239231000	-1.847223000
C	5.599873000	-0.802003000	-0.289326000
H	4.965460000	0.291314000	-2.031002000

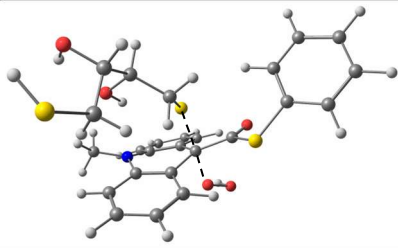
O	4.384803000	1.311350000	-0.315949000
H	5.183149000	1.838280000	-0.420307000
S	7.215767000	0.005577000	-0.003977000
H	5.191165000	-1.128933000	0.670422000
H	5.796735000	-1.690372000	-0.890534000
H	6.850788000	0.712502000	1.077470000
C	-3.782815000	2.061719000	0.809625000
H	-3.092473000	2.870912000	0.569575000
H	-4.756767000	2.474591000	1.101158000
H	-3.373480000	1.473600000	1.639115000

	2MeO-ATE-GT 		
	X	Y	Z
C	0.904866000	1.448178000	2.355791000
C	0.937473000	2.648863000	3.087966000
C	1.111180000	3.866641000	2.451838000
C	1.245117000	3.928005000	1.067357000
C	1.153820000	2.755452000	0.335721000
C	0.969752000	1.515979000	0.953982000
H	0.803017000	2.635365000	4.161967000
H	1.136076000	4.774186000	3.046265000
H	1.406293000	4.877127000	0.567418000
H	1.213488000	2.793850000	-0.747832000
C	0.813549000	0.283110000	0.090861000
C	0.542438000	-0.972719000	0.905280000
C	0.509437000	-0.943823000	2.308783000
N	0.807323000	0.222391000	3.012244000
C	2.073941000	0.015201000	-0.756890000
C	1.097953000	0.145968000	4.432199000
C	0.312388000	-2.175992000	0.236079000
C	0.021479000	-3.344684000	0.921456000
C	-0.071050000	-3.303726000	2.310898000
C	0.162167000	-2.121479000	2.995692000
H	0.378340000	-2.184124000	-0.846387000
H	-0.139685000	-4.268493000	0.377723000
H	-0.328284000	-4.197296000	2.871746000
H	0.049300000	-2.111160000	4.072163000
H	1.822620000	0.916364000	4.696946000
H	0.205111000	0.267225000	5.057767000
H	1.559405000	-0.816117000	4.658192000
O	3.600138000	0.325619000	0.158919000
O	2.044511000	-0.416355000	-1.875120000
C	4.709103000	-0.691149000	-0.785331000
C	5.790443000	-0.117735000	-1.451297000
C	6.692822000	-0.917732000	-2.144783000
C	6.504510000	-2.295558000	-2.188188000
C	5.422936000	-2.875498000	-1.533385000
C	4.525939000	-2.081011000	-0.827026000
H	5.915587000	0.959657000	-1.427719000
H	7.531523000	-0.462918000	-2.660646000

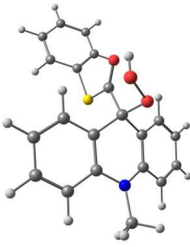
H	7.198689000	-2.922808000	-2.737996000
H	5.250439000	-3.946022000	-1.565341000
O	3.446967000	-2.659899000	-0.219841000
S	-0.567830000	0.521186000	-1.139251000
C	-1.915215000	0.787950000	0.055991000
C	-3.109090000	1.503033000	-0.624168000
H	-2.239370000	-0.177774000	0.447404000
H	-1.553433000	1.386774000	0.897380000
N	-4.363522000	1.172365000	-0.003307000
C	-2.941420000	3.028899000	-0.492487000
H	-3.125665000	1.253331000	-1.693932000
O	-3.719637000	3.707933000	0.162036000
N	-1.868870000	3.555351000	-1.120959000
H	-1.181825000	2.962192000	-1.574582000
C	-1.540160000	4.942534000	-0.933809000
C	-0.293377000	5.274301000	-1.711771000
H	-2.356883000	5.593081000	-1.264203000
H	-1.362249000	5.176756000	0.123379000
O	0.043627000	6.562709000	-1.570404000
O	0.346383000	4.489659000	-2.371720000
H	0.843471000	6.702151000	-2.096465000
H	-4.817275000	1.939578000	0.480180000
C	-5.050791000	-0.008028000	-0.053300000
O	-6.122904000	-0.130938000	0.516284000
C	-4.427537000	-1.176319000	-0.800809000
H	-3.491262000	-0.913736000	-1.303339000
C	-4.202138000	-2.341811000	0.170536000
H	-5.135179000	-1.488131000	-1.571730000
C	-3.356599000	-3.479223000	-0.393904000
H	-3.681159000	-1.974700000	1.065267000
H	-5.166624000	-2.727906000	0.506586000
N	-3.130230000	-4.480478000	0.647715000
C	-4.021969000	-4.175975000	-1.570374000
H	-2.415812000	-3.051945000	-0.793092000
O	-3.297679000	-5.242532000	-1.969279000
O	-5.044581000	-3.854441000	-2.123208000
H	-3.782241000	-5.640196000	-2.705565000
H	-2.567479000	-5.239454000	0.277826000
H	-2.597998000	-4.052402000	1.398699000
C	3.653817000	-3.000272000	1.144131000
H	2.712243000	-3.417455000	1.502812000
H	4.453804000	-3.744404000	1.243601000
H	3.904986000	-2.114249000	1.738711000

2MeO-ATE-MET			
			
	X	Y	Z
C	-0.208602000	-2.241114000	-1.061431000
C	-0.473347000	-3.615067000	-1.190526000
C	-0.702276000	-4.404219000	-0.074992000
C	-0.690290000	-3.844231000	1.198347000
C	-0.474367000	-2.481501000	1.326711000
C	-0.242921000	-1.662764000	0.218835000
H	-0.522287000	-4.068554000	-2.172645000

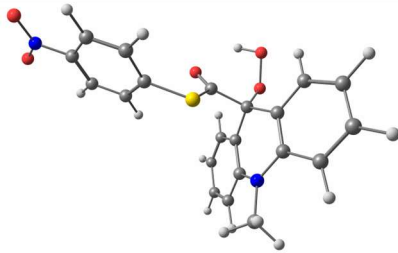
H	-0.901141000	-5.463020000	-0.207199000
H	-0.861037000	-4.456086000	2.076883000
H	-0.495649000	-2.018979000	2.308369000
C	-0.018734000	-0.175502000	0.424013000
C	0.006525000	0.589869000	-0.895491000
C	0.027510000	-0.080899000	-2.129145000
N	0.085707000	-1.472764000	-2.186181000
C	1.332557000	0.102014000	1.117429000
C	0.480610000	-2.124484000	-3.418444000
C	0.032957000	1.984840000	-0.878337000
C	0.033388000	2.728426000	-2.048659000
C	-0.011560000	2.062530000	-3.269675000
C	-0.016066000	0.676854000	-3.312021000
H	0.056042000	2.483947000	0.083785000
H	0.058630000	3.811440000	-2.006104000
H	-0.048036000	2.621102000	-4.199748000
H	-0.082869000	0.181009000	-4.272401000
H	1.011675000	-3.048716000	-3.186112000
H	-0.368603000	-2.359129000	-4.073507000
H	1.175046000	-1.481577000	-3.961503000
S	2.644091000	-1.019668000	0.564098000
O	1.516574000	1.001211000	1.887654000
C	4.060406000	-0.032497000	0.980758000
C	5.010695000	-0.519095000	1.876557000
C	6.153776000	0.220605000	2.162220000
C	6.340978000	1.462687000	1.564191000
C	5.393735000	1.960581000	0.675661000
C	4.256408000	1.217693000	0.375338000
H	4.844056000	-1.479362000	2.353355000
H	6.887023000	-0.167341000	2.861144000
H	7.224511000	2.049944000	1.792917000
H	5.512847000	2.932076000	0.207768000
O	3.319328000	1.739280000	-0.470626000
S	-1.301396000	0.541319000	1.563390000
C	-2.777085000	0.068312000	0.610535000
C	-4.003823000	0.760206000	1.193704000
H	-2.643911000	0.364958000	-0.432993000
H	-2.902289000	-1.018903000	0.642991000
C	-5.276236000	0.402468000	0.408525000
H	-4.153115000	0.477671000	2.239541000
H	-3.862626000	1.848550000	1.169599000
C	-6.484501000	0.949024000	1.171831000
N	-5.153624000	0.798545000	-0.980838000
H	-5.393363000	-0.688511000	0.442507000
O	-7.252880000	1.772297000	0.432070000
O	-6.743714000	0.680172000	2.320236000
H	-7.974692000	2.053097000	1.011896000
H	-5.984653000	0.537567000	-1.499598000
H	-5.080488000	1.809250000	-1.046468000
C	3.468221000	1.350602000	-1.828644000
H	2.649090000	1.820955000	-2.373274000
H	4.430493000	1.693842000	-2.229483000
H	3.395428000	0.262162000	-1.938804000

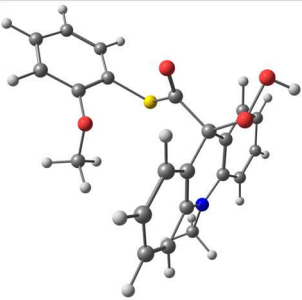
	TS-IV (DTT-H-ATE-OOH)		
			
	X	Y	Z
C	-3.479437000	-1.778328000	-1.084171000
C	-3.510034000	-1.811430000	0.313914000
C	-4.519903000	-2.524169000	0.962208000
C	-5.477942000	-3.214395000	0.224232000
C	-5.448155000	-3.179916000	-1.165818000
C	-4.449560000	-2.454639000	-1.813339000
S	-2.235324000	-1.056931000	1.292180000
C	-2.086557000	0.594350000	0.417258000
O	-3.060681000	1.008611000	-0.152299000
C	-0.669090000	1.282994000	0.481956000
C	-0.439111000	2.600884000	-0.317306000
C	0.880574000	3.070734000	-0.484222000
N	1.971996000	2.264666000	-0.127374000
C	1.872234000	1.343156000	0.923315000
C	0.613892000	0.850005000	1.309478000
C	-1.487384000	3.373983000	-0.816255000
C	-1.257084000	4.606307000	-1.429753000
C	0.035353000	5.092455000	-1.531874000
C	1.096579000	4.327480000	-1.055943000
C	3.022747000	0.902187000	1.587615000
C	2.944137000	-0.031529000	2.615083000
C	1.703167000	-0.493131000	3.025249000
C	0.555034000	-0.020844000	2.393052000
O	-1.015095000	2.048370000	1.784638000
O	-2.240537000	2.813990000	1.881222000
S	-0.279203000	0.287453000	-1.027807000
C	0.472180000	-1.362957000	-0.753787000
C	1.664817000	-1.560246000	-1.694347000
C	2.583857000	-2.735231000	-1.333061000
O	3.638575000	-2.774479000	-2.283933000
C	3.268443000	2.529811000	-0.708088000
O	2.511531000	-0.423392000	-1.738491000
C	3.140006000	-2.620527000	0.090026000
S	4.347202000	-3.937179000	0.475000000
H	3.993023000	1.299680000	1.315211000
H	3.854100000	-0.376114000	3.097034000
H	1.615051000	-1.197673000	3.846279000
H	-0.410584000	-0.326377000	2.771018000
H	2.104313000	4.721602000	-1.125364000
H	0.232711000	6.061493000	-1.981370000
H	-2.095937000	5.174316000	-1.820692000
H	-2.491707000	2.978425000	-0.746139000
H	3.133276000	2.919654000	-1.718858000
H	3.869823000	3.250486000	-0.132745000
H	3.819960000	1.590200000	-0.787648000
H	0.784934000	-1.414576000	0.291406000
H	-0.266498000	-2.153546000	-0.919293000
H	1.280091000	-1.761175000	-2.707214000
H	-1.981455000	3.630229000	1.429942000
H	-2.700913000	-1.211994000	-1.586846000
H	-4.420974000	-2.418247000	-2.898484000

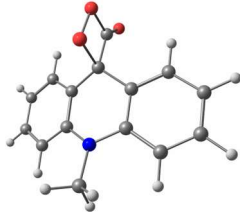
H	-6.200233000	-3.710438000	-1.742507000
H	-6.256031000	-3.769376000	0.740674000
H	-4.554263000	-2.531911000	2.047236000
H	1.908597000	0.340963000	-1.674321000
H	3.876695000	-1.846086000	-2.409293000
H	2.033044000	-3.677052000	-1.434091000
H	3.592608000	-1.636916000	0.230392000
H	2.344415000	-2.719720000	0.831267000
H	4.966272000	-3.868818000	-0.715570000

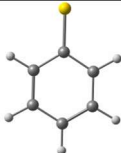
	H-ATE-OOH		
			
	X	Y	Z
C	0.006865000	0.058604000	-0.016894000
C	-0.006113000	0.029307000	1.377969000
C	1.202698000	-0.017052000	2.087428000
C	2.405021000	0.017620000	1.362494000
C	2.396914000	0.052987000	-0.022479000
C	1.196869000	0.065031000	-0.725680000
C	-1.344670000	0.009057000	2.092089000
C	-1.200449000	0.278913000	3.577346000
C	0.059852000	0.241015000	4.198784000
N	1.205227000	-0.092261000	3.475538000
C	0.150030000	0.542792000	5.566738000
C	-0.984897000	0.828452000	6.306861000
C	-2.236865000	0.832464000	5.703174000
C	-2.331259000	0.563400000	4.347476000
C	-1.963443000	-1.378704000	1.784521000
O	-2.652507000	-1.587183000	0.816257000
O	-2.093890000	1.020570000	1.404720000
O	-3.492155000	0.921530000	1.663641000
C	2.416252000	-0.470354000	4.173929000
S	-1.500845000	-2.645776000	2.964840000
C	-2.170148000	-4.086898000	2.159111000
C	-1.298149000	-4.979162000	1.538155000
C	-1.800735000	-6.127870000	0.935620000
C	-3.168806000	-6.378543000	0.944881000
C	-4.037313000	-5.482674000	1.561728000
C	-3.541104000	-4.339309000	2.176348000
H	3.354543000	0.046029000	1.882149000
H	3.342526000	0.080623000	-0.554585000
H	1.188717000	0.087048000	-1.809382000
H	-0.942775000	0.074682000	-0.538706000
H	-3.295606000	0.577424000	3.856789000
H	-3.129218000	1.049251000	6.279355000
H	-0.883898000	1.057306000	7.363011000
H	1.116303000	0.582658000	6.053621000
H	2.982078000	-1.173834000	3.561730000
H	3.058320000	0.386480000	4.415355000
H	2.155092000	-0.987971000	5.097677000
H	-0.233983000	-4.768768000	1.521979000
H	-1.121844000	-6.823147000	0.452936000
H	-3.559404000	-7.273379000	0.471342000

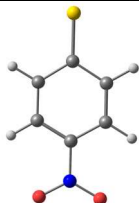
H	-5.104892000	-5.676131000	1.568684000
H	-4.211399000	-3.640043000	2.663187000
H	-3.737535000	0.214327000	1.046152000

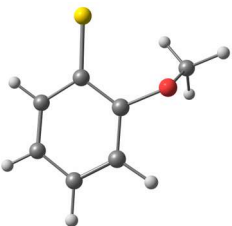
4NO ₂ -ATE-OOH			
			
	X	Y	Z
C	-2.620495000	0.711614000	-0.254385000
C	-2.127975000	-0.587521000	-0.401498000
C	-3.004455000	-1.667106000	-0.511625000
C	-4.376972000	-1.454526000	-0.482234000
C	-4.843026000	-0.157515000	-0.327902000
C	-3.988575000	0.931296000	-0.208628000
S	-0.378397000	-0.892326000	-0.526966000
C	0.174193000	-0.182537000	1.029630000
O	-0.576038000	0.191736000	1.896141000
N	-6.293989000	0.073553000	-0.291260000
O	-7.024531000	-0.898645000	-0.400690000
C	1.711443000	-0.000590000	1.118130000
C	1.978370000	1.382877000	0.550019000
C	2.496990000	1.539102000	-0.745506000
N	2.804879000	0.424272000	-1.518620000
C	3.013568000	-0.811335000	-0.902236000
C	2.494248000	-1.068170000	0.379111000
C	1.638422000	2.506507000	1.304847000
C	1.821188000	3.786911000	0.806351000
C	2.357530000	3.944046000	-0.468491000
C	2.696372000	2.839951000	-1.235137000
C	3.748646000	-1.815206000	-1.550939000
C	3.938413000	-3.050930000	-0.953119000
C	3.415102000	-3.311815000	0.308943000
C	2.703988000	-2.318691000	0.964831000
O	2.071972000	0.108958000	2.496028000
O	1.477130000	-0.932604000	3.267959000
C	3.028506000	0.570584000	-2.942273000
O	-6.680383000	1.223624000	-0.154859000
H	3.143488000	2.992067000	-2.209585000
H	2.525044000	4.937662000	-0.871815000
H	1.553955000	4.650003000	1.405422000
H	1.224235000	2.355183000	2.294302000
H	2.295955000	-2.501712000	1.950655000
H	3.563184000	-4.276742000	0.780648000
H	4.512253000	-3.809316000	-1.476129000
H	4.201594000	-1.621192000	-2.515272000
H	2.374017000	1.351761000	-3.331822000
H	4.067929000	0.821782000	-3.191400000
H	2.759489000	-0.358621000	-3.446364000
H	-2.613952000	-2.673263000	-0.615621000
H	-5.081203000	-2.272019000	-0.567198000
H	-4.399907000	1.925395000	-0.090751000
H	-1.934028000	1.546207000	-0.170298000
H	0.607995000	-0.540982000	3.451895000

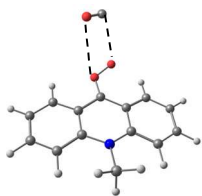
	2MeO-ATE-OOH		
			
	X	Y	Z
C	3.214472000	0.362159000	-0.338043000
C	2.720691000	-0.932708000	-0.556127000
C	3.614340000	-1.985786000	-0.742844000
C	4.986557000	-1.757821000	-0.726000000
C	5.471441000	-0.473022000	-0.503134000
C	4.587738000	0.583020000	-0.307190000
S	0.971099000	-1.222522000	-0.655668000
C	0.492960000	-0.697603000	1.017402000
O	1.260727000	-0.612545000	1.929385000
O	2.363221000	1.405390000	-0.105726000
C	1.899972000	2.063286000	-1.276251000
C	-0.990220000	-0.256189000	1.093431000
C	-1.894790000	-1.101623000	0.225827000
C	-2.700093000	-0.524058000	-0.773975000
N	-2.572755000	0.821313000	-1.113041000
C	-1.845541000	1.696018000	-0.307322000
C	-1.040375000	1.214879000	0.735538000
C	-1.953440000	-2.484899000	0.429283000
C	-2.838203000	-3.290785000	-0.271468000
C	-3.693807000	-2.700625000	-1.194684000
C	-3.627194000	-1.339241000	-1.445512000
C	-1.909917000	3.084773000	-0.514213000
C	-1.170251000	3.954620000	0.272843000
C	-0.350629000	3.471730000	1.288825000
C	-0.299824000	2.105315000	1.514241000
O	-1.409352000	-0.230548000	2.465876000
O	-1.280356000	-1.521057000	3.057637000
C	-3.115001000	1.296083000	-2.372375000
H	-4.317194000	-0.906249000	-2.158558000
H	-4.418846000	-3.302133000	-1.733755000
H	-2.860735000	-4.360389000	-0.095907000
H	-1.276763000	-2.928812000	1.150134000
H	0.326327000	1.700309000	2.300463000
H	0.233756000	4.148807000	1.901164000
H	-1.246248000	5.022286000	0.091642000
H	-2.568236000	3.495384000	-1.269194000
H	-3.113105000	0.483840000	-3.099921000
H	-4.136007000	1.686107000	-2.277622000
H	-2.473404000	2.082595000	-2.771521000
H	3.225549000	-2.987208000	-0.895040000
H	5.672960000	-2.584939000	-0.872251000
H	6.541004000	-0.291093000	-0.476318000
H	4.943375000	1.590505000	-0.118989000
H	-2.200839000	-1.818466000	3.040249000
H	1.213470000	2.840886000	-0.939069000
H	2.735246000	2.515217000	-1.826098000
H	1.364161000	1.369460000	-1.934316000

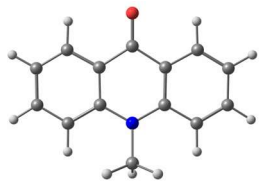
	[H-ATE-OO] _{cyclic}		
			
	X	Y	Z
C	2.394280000	-1.875155000	-0.178521000
C	1.205116000	-1.156394000	0.025682000
C	1.241237000	0.246766000	-0.054121000
C	2.446141000	0.894867000	-0.334987000
C	3.616100000	0.180686000	-0.529976000
C	3.579626000	-1.209689000	-0.445592000
N	0.000015000	-1.807902000	0.281670000
C	-1.205096000	-1.156412000	0.025682000
C	-1.241236000	0.246748000	-0.054122000
C	-0.000005000	1.016066000	0.250350000
C	-2.446148000	0.894833000	-0.334989000
C	-3.616098000	0.180638000	-0.529978000
C	-3.579606000	-1.209737000	-0.445593000
C	-2.394252000	-1.875188000	-0.178520000
C	-0.000011000	2.487897000	-0.144130000
O	-0.000045000	2.908341000	1.147519000
O	-0.000008000	1.535058000	1.647123000
C	0.000026000	-3.212988000	0.639326000
O	-0.000030000	3.158451000	-1.126722000
H	-2.390947000	-2.957837000	-0.161750000
H	-4.483580000	-1.788051000	-0.607642000
H	-4.543521000	0.697429000	-0.748258000
H	-2.461867000	1.978117000	-0.402887000
H	2.461846000	1.978151000	-0.402883000
H	4.543517000	0.697489000	-0.748253000
H	4.483607000	-1.787992000	-0.607641000
H	2.390986000	-2.957805000	-0.161751000
H	-0.877866000	-3.430027000	1.248981000
H	0.000023000	-3.876564000	-0.234995000
H	0.877933000	-3.430015000	1.248965000


	thiophenyl anion		
			
	X	Y	Z
C	0.000000000	0.595609000	0.000000000
C	1.196931000	-0.163396000	0.000000000
C	1.196253000	-1.552418000	0.000000000
C	0.000049000	-2.271410000	0.000000000
C	-1.196191000	-1.552466000	0.000000000
C	-1.196908000	-0.163450000	0.000000000
S	-0.000062000	2.338519000	0.000000000
H	2.146745000	-2.085150000	0.000000000
H	0.000081000	-3.358567000	0.000000000
H	-2.146664000	-2.085228000	0.000000000
H	-2.138619000	0.378883000	0.000000000
H	2.138638000	0.378943000	0.000000000


	4-nitrothiophenyl anion 		
	X	Y	Z
C	-0.000138000	1.745733000	0.000000000
C	1.207718000	0.984177000	0.000000000
C	1.213712000	-0.391223000	0.000000000
C	0.000000000	-1.094368000	0.000000000
C	-1.213845000	-0.391393000	0.000000000
C	-1.207993000	0.983982000	0.000000000
H	2.146247000	1.529102000	0.000000000
H	2.142040000	-0.950427000	0.000000000
N	0.000211000	-2.520832000	0.000000000
H	-2.142213000	-0.950511000	0.000000000
H	-2.146613000	1.528747000	0.000000000
S	-0.000190000	3.459370000	0.000000000
O	-1.081980000	-3.117888000	0.000000000
O	1.082653000	-3.117420000	0.000000000


	2-methoxythiophenyl anion 		
	X	Y	Z
C	-0.063029000	0.720327000	-0.051349000
C	1.183592000	1.348931000	0.183432000
C	2.392595000	0.666179000	0.214538000
C	2.428337000	-0.712584000	0.014782000
C	1.222755000	-1.374260000	-0.203666000
C	0.012183000	-0.687361000	-0.237848000
H	1.165427000	2.425091000	0.332187000
H	3.314471000	1.217386000	0.392181000
H	3.366199000	-1.261750000	0.033464000
H	1.191789000	-2.449449000	-0.363345000
O	-1.102590000	-1.458291000	-0.507908000
S	-1.540465000	1.649102000	-0.119821000
C	-1.990038000	-1.585955000	0.583231000
H	-2.829422000	-2.196777000	0.235527000
H	-1.501917000	-2.100656000	1.426924000
H	-2.356766000	-0.604801000	0.904738000

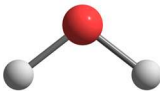
	TS-VI		
			
	X	Y	Z
C	-1.044176000	-2.347123000	0.515730000
C	-0.225953000	-1.215095000	0.276730000
C	1.137592000	-1.415262000	-0.109172000
C	1.628676000	-2.732282000	-0.202822000
C	0.800135000	-3.817867000	0.044739000
C	-0.539962000	-3.630905000	0.396470000
C	-0.697495000	0.138571000	0.418782000
C	0.249844000	1.233242000	0.327383000
C	1.586025000	0.968358000	-0.063972000
N	1.967574000	-0.331322000	-0.388457000
C	2.503915000	2.039697000	-0.110607000
C	2.096651000	3.330966000	0.186702000
C	0.768785000	3.600126000	0.546026000
C	-0.136683000	2.558087000	0.620694000
C	3.257551000	-0.561346000	-1.037244000
O	-1.913331000	0.520825000	0.660383000
O	-2.956931000	-0.379817000	0.809208000
C	-4.693348000	0.628397000	-1.081929000
O	-4.000710000	1.424993000	-1.516535000
H	-1.182897000	-4.484064000	0.585494000
H	-2.068912000	-2.145955000	0.794287000
H	1.211846000	-4.820324000	-0.029545000
H	2.669109000	-2.913749000	-0.436392000
H	3.544032000	1.861753000	-0.349584000
H	-1.165189000	2.737145000	0.908877000
H	0.456065000	4.613019000	0.776279000
H	2.824903000	4.135448000	0.149400000
H	3.517483000	0.306043000	-1.642271000
H	4.062124000	-0.749469000	-0.316233000
H	3.176849000	-1.413986000	-1.710632000


	[10-MA]* 		
	X	Y	Z
C	2.422326000	1.335981000	-0.162813000
C	1.216540000	0.653862000	0.003127000
C	1.241817000	-0.765991000	0.047805000
C	2.472273000	-1.444741000	-0.018842000
C	3.661374000	-0.742037000	-0.148701000
C	3.632266000	0.644453000	-0.229942000
N	-0.000034000	1.323176000	0.136744000
C	-1.216534000	0.653787000	0.003067000
C	-1.241762000	-0.766056000	0.047751000
C	0.000041000	-1.463995000	0.152757000
C	-2.472201000	-1.444832000	-0.018914000
C	-3.661317000	-0.742142000	-0.148747000
C	-3.632246000	0.644358000	-0.229903000
C	-2.422318000	1.335906000	-0.162768000
O	0.000071000	-2.769657000	0.254099000
C	-0.000207000	2.750697000	0.391286000
H	-2.430442000	2.414234000	-0.260584000
H	-4.552729000	1.204740000	-0.354720000
H	-4.603721000	-1.276601000	-0.198255000
H	-2.476193000	-2.527709000	0.026556000
H	2.476288000	-2.527616000	0.026642000
H	4.603787000	-1.276479000	-0.198216000
H	4.552733000	1.204843000	-0.354845000
H	2.430463000	2.414288000	-0.260776000
H	0.878418000	3.012301000	0.982044000
H	-0.879114000	3.012095000	0.981733000
H	-0.000125000	3.345433000	-0.530549000

	O₂ 		
	X	Y	Z
O	0.000000000	0.000000000	0.607334000
O	0.000000000	0.000000000	-0.607334000

	OH⁻ 		
	X	Y	Z
O	0.000000000	0.000000000	0.108368000
H	0.000000000	0.000000000	-0.866943000

	OOH⁻ 		
	X	Y	Z
O	0.055944000	-0.696157000	0.000000000
H	-0.895099000	-0.840854000	0.000000000
O	0.055944000	0.801263000	0.000000000

	H₂O 		
	X	Y	Z
O	0.000000000	0.000000000	0.117840000
H	0.000000000	0.757917000	-0.471359000
H	0.000000000	-0.757917000	-0.471359000

	CO₂ 		
	X	Y	Z
C	0.000000000	0.000000000	0.000000000
O	0.000000000	0.000000000	1.287745000
O	0.000000000	0.000000000	-1.287745000





[P2] V. Ievtukhov, B. Zadykowicz, M. Ye. Blazheyevski, K. Krzymiński.

New luminometric method for quantification of biological sulphur nucleophiles with the participation of 9-cyano-10-methylacridinium salt, *Luminescence*, 2021, 32, 208–219.

DOI: 10.1002/bio.4162.

RESEARCH ARTICLE

New luminometric method for quantification of biological sulfur nucleophiles with the participation of 9-cyano-10-methylacridinium salt

Vladyslav Ievtukhov¹  | Beata Zadykowicz¹  | Mykola Ye. Blazheyevskiy²  |
Karol Krzyminiński¹ 

¹Faculty of Chemistry, University of Gdańsk,
Wita Stwosza Str. 63, Gdańsk, Poland

²National University of Pharmacy,
Valentynivska Str.4, Kharkiv, Ukraine

Correspondence

Karol Krzyminiński, Faculty of Chemistry,
University of Gdańsk, Wita Stwosza Str.
63, 80-308, Gdańsk, Poland.
Email: karol.krzyminski@ug.edu.pl

Abstract

Biologically active compounds containing sulfhydryl groups (RSHs: *N*-acetyl-L-cysteine, D-penicillamine, glutathione and acetylthiocholine chloride) were used to develop a luminometric method for their quantification. The title substrate capable of chemiluminescence (CL) was isolated in a highly pure state as a chloride salt (99.9% using RP-HPLC) and identified using mass spectrometry (ESI Q-TOF) and ¹H NMR spectroscopy. The cation included in the salt, 9-CMA⁺, underwent oxidation in an alkaline environment containing RSHs by molecular oxygen, generating CL of various intensities, with no need for the use of hydrogen peroxide. The amount of produced light was linearly proportional to the content of investigated analytes in the system over the concentration range ~0.2–2 μM, with the detection limits in the range 0.19–1.73 μM. The mechanism of chemiluminogenic oxidation of 9-CMA⁺ in the presence of RSHs and molecular oxygen is proposed, using computational methods at the density-functional theory level. The presence of RSHs in an alkaline medium seems to be crucial to produce hydroperoxide anions (·OOH), which initiate the ‘light path’ of 9-CMA⁺ transformations, ending with the excretion of electronically excited molecules of 10-methyl-acridan-9-one.

Highlights

- The original chemiluminometric method for determination of biological analytes containing a thiol group (RSHs) has been developed.
- The integral emission from the proposed system is several times higher than that observed with the use of the classical CL emitter, Lucigenin under the experimental conditions.
- The method is based on the specific reaction of the 9-CMA⁺ with RSHs in an alkaline environment and does not require the addition of hydrogen peroxide.
- The most probable reaction path of chemiluminogenic oxidation of 9-CMA⁺ involves the production of OOH[·] ions *in situ* in the presence of molecular oxygen and RSHs, giving the rise for CL emission.
- The thermodynamic and kinetic studies also indicate the possibility of the formation of 9-CMA⁺ adducts with RS[·] and the subsequent emission with the participation of ·OOH ions as an alternative path.

KEYWORDS

9-cyano-10-methylacridinium cation, chemiluminescence analysis, DFT methods, MS and NMR spectroscopy, thiol nucleophiles

1 | INTRODUCTION

The research objects in this work [*N*-acetyl-L-cysteine (NAC), glutathione (GSH), D-penicillamine (DPA), and acetylthiocholine chloride (ATC)] have a common feature in that they contain the sulfhydryl group in their structures, eventually the latter appears as a result of hydrolysis of the analyte under experimental conditions.^[1,2] Due to the presence of -SH function, such substances make potent nucleophiles, can easily be deprotonated, and may undergo oxidation. This determines their specific interactions with other molecules present in the system, especially those experiencing electron deficiency. The above features make them highly biologically active substances, produced by living matter, and/or used as external drugs. Their brief characteristics are given in ESI.

According to the above, the accessible, reliable, and sensitive determination of such substrates is an important issue in modern biomedical analytics. Early quantification methods for thiol drugs involved redox titrations [i.e. iodine solutions, silver nitrate (V), and copper (II) salts].^[2,3] More advanced methods have been developed over time and these are at this time available for the analysis of such compounds in various matrices. The majority of these utilize derivatization steps to obtain compounds suitable for detection using ultraviolet-visible (UV-vis) light spectrophotometry, fluorimetry and various chromatographic methods, including tandem techniques.^[4]

Liquid chromatography coupled with mass spectrometry [electrospray ionization (ESI), liquid chromatography/ESI-tandem mass spectrometry (LC/ESI-MS/MS)] was used to analyze *N*-acetylcholine and choline from rat or mouse brains.^[5] Limits of detection (LOD) were 0.02 nM for NAC and 1 nM for choline and good linearity of calibration graph was obtained in the concentration range 0.1–50 nM for NAC and 100–3500 nM for choline. The repeatability of the method was good [relative significant difference (RSD) values in the range 3.1–3.5% between days] and recoveries were favourable, falling in the range 93–101%.

Zhang and colleagues developed a flow-injection analysis (FIA) for the assay of penicillamine in pharmaceutical preparations.^[6] The method was based on the assessment of the intensity of emission, resulting from the reaction of the drug with cerium (IV) ions in an acidic environment and in the presence of quinine, which was used as the target emitter in the energy transfer process. The authors obtained for the assayed thiol, LODs of 15 pM and the linearity range was 2–200 μ M.

Luminescence methods typically do not require time-consuming separations and expensive equipment such as chromatographic (HPLC, LC-MS) or FIA/sequential injection (SI) techniques, and their sensitivity is generally higher than that of other approaches. Classical chemiluminescence (CL), using standard luminol^[7] as well as

spectrophotometric methods^[8,9] were applied for analysis of biological thiols. A fast method of titration for NAC with hypochlorite ions (ClO^-) using CL measurements and using luminometric standard luminol has been described previously.^[10,11]

Sano and Nakamura developed an assay for the determination of physiological thiols (glutathione, cysteine) using the HPLC with CL detection.^[12] This approach was based on the precolumn derivatization of the aforementioned analytes with ortho-phthalaldehyde and isoluminol derivatives, giving a chemiluminogenic isoindole compound, the emission of which was measured after separation by oxidizing the latter in an H_2O_2 /hematin system. The authors obtained LOD of 1.5 nM for glutathione and 3.5 nM for cysteine (recovery 70%) and linearity of detector response was in the range 5–1000 nM. The physiological content of glutathione in human blood was determined to be 500–770 μ M. The method was sensitive, but quite complicated, as it required derivatization with the two components and post-column detection.

Suliman and colleagues developed an SI method for the determination of DPA and ephedrine (EP), using the reactions of these drugs with the $\text{Ru(II)(bpy)}_3^{2+}/\text{S}_2\text{O}_8^{2-}$ system in the presence of light.^[13] Derivatization of DPA and EP with aldehydes resulted in at least a 25-fold amplification of the CL emission signal for DPA and 12-fold for EP, leading to better sensitivity and lower LOD for both drugs. Under optimized conditions, linear calibration plots were obtained in the range 0.2–24 $\mu\text{g ml}^{-1}$ for DPA and 0.2–20 $\mu\text{g ml}^{-1}$ for EP. The LODs were 0.1 $\mu\text{g ml}^{-1}$ for DPA and 0.03 $\mu\text{g ml}^{-1}$ for EP in tested pharmaceutical products, and no interference from typical impurities was observed.

At this time, manufacturers offer sensitive and specific bioluminescence (BL) tests that can be used to detect some biological thiols under study. A BL assay based on the luciferin-luciferase system was developed, in which free luciferin, in the presence of the analyte (GSH) and a catalyst, is released from a coupled derivative; the resulting emission could be quantitated using luminometric techniques.^[14]

It has been known since the early 1980s that chemiluminogenic acridinium salts make an attractive substrate for ultrasensitive assays of wide sorts of biological analytes, including specific proteins (antibodies and antigens), drugs, and hormones.^[9] Weeks and colleagues for the first time proposed a new acridinium derivative that reacted with proteins under mild conditions to produce stable reagents capable of CL for high immunodiagnostic activity. The compound was used to label monoclonal antibodies directed at human α -fetoprotein, which enabled fast and sensitive determination of human α -fetoprotein (10^{-10} mol).^[15] In other studies the same authors assessed the concentration of α -fetoprotein in the serum of women at 14–20 weeks of gestation, using a different format of the

chemiluminescent immunoassay (CLIA) test using the same acridinium label. Obtained results were analytically consistent with the ones gained by a conventional radioimmunoassay and it was demonstrated that the sensitivity of the proposed test increased with increasing the specific activity of the substrate.^[16]

Acridinium chemiluminogenic salts express, in general, a wide sort of advantages over the luminol derivatives, as, among others, they did not require a catalyst to start the emission of light, they have generally a higher emission efficiency in the aqueous systems (reaching several per cent vs. ~1.3% obtained with luminol^[17]) and are characterized by an excellent dynamics of emission that could be relatively easily adopted to specific requirements.^[18-20] In his initial works, McCapra for the first time observed that 10-substituted-9-cyanoacridinium cations, such as other acridinium salts, may specifically react with an oxidant, producing molecules of 10-substituted-acridin-9-one in the excited electronic state. Relaxation of the latter to the ground state was accompanied by the emission of light in the blue range of the spectrum.^[21]

Wroblewska and colleagues investigated the mechanism of CL generated from 9-cyano-10-methylacridinium cations in alkaline solutions of hydrogen peroxide using quantum-chemical calculations at the density-functional theory (DFT) level.^[22] Based on these, the authors proposed a sensitive method for the assessment of simple nucleophiles (such as hydrazine, hydroxylamine, cysteine, and others) using CL of the above cations under carefully optimized conditions.^[23]

Other authors considered the oxidation of the 9-cyano-10-methylacridinium cation with molecular oxygen in the presence of sulfur-containing nucleophiles (RSH).^[24,25] It was postulated that in a highly alkaline environment, the respective anions derived from the nucleophiles (RS^-) could react with molecular oxygen, producing superoxide radicals ($O_2^{\cdot-}$). The above hypothesis (relying on the biradical nature of O_2) enabled them to postulate an alternative reaction path of chemiluminogenic oxidation of 9-CMA⁺; however, no adequate calculations were provided (Figure S1; ESI). The proposed pathway involved oxidation of 9-CMA⁺ by strong oxidants such as $O_2^{\cdot-}$ (generated as described above), producing 10-methyl-9-cyanoperoxyacridane radicals. Their reaction with excess RS^- produced 9-cyano-9-peroxide-acridane anions, which further reacted according to the path of transformations described previously.^[22]

The present work proposed a new adaptation of the chemiluminometric assay for a series of listed biologically active thiol derivatives and acetylcholine. The assays were thoroughly optimized, using substrates of confirmed purity and a modern tube luminometer, equipped with a high-class, sensitive detector. Experimental findings were supported by a well founded mechanism of assumed transformations that are likely to occur in the analytical systems, based on advanced quantum-chemical calculations at the DFT level of theory. The possibility of the oxidation of investigated thiols to disulfides was also taken into account in calculations. Literature reports indicated that the latter reaction did take place, however the use of various types of catalysts, such as maleic anhydride,^[26] $H_5PV_2Mo_{10}O_{41}$ ^[27] or nickel ferrite nanoparticles,^[28] were required.

Conversely, it is worth noting that the experiments described here additionally present another CL method for determination of hydrogen peroxide, which is in this approach generated *in situ* with the participation of the assessed substrates. As H_2O_2 creates a very important molecule, being the product of various types of transformations, the new possibility of its determination seems to be important.^[29]

2 | EXPERIMENTAL

2.1 | Synthesis and identity of the studied compounds

Crude 9-cyano-10-methylacridinium nitrate (V) was synthesized by adopting a known methodology, based on the oxidation of 9-cyano-10-methyl-acridan with nitric acid (V).^[23] The above product was purified, according to the original method described below. To a solution of red solid 9-CMA nitrate (V), a diluted aqueous solution of $NaHCO_3$ (5%) was added to attain a slightly alkaline pH ~8. The obtained yellowish amorphous solid of the resulting base was then extracted by $CHCl_3$ and the solution was dried over anhydrous $MgSO_4$. The crude 9-CMA (the base) was purified chromatographically (LC) using silica gel (40-63 mesh, Merck) as solid phase and cyclohexene-ethyl acetate mixture (2/1 v/v) as a mobile phase. The pure base obtained after chromatographic separation was then dissolved in dry $CHCl_3$ and to the obtained dark yellow mixture, saturated HCl solution in Et_2O (Sigma-Aldrich, USA) was added dropwise with stirring. Next, dry diethyl ether was added in excess, and the obtained yellow mixture was cooled (to approximately $-20^\circ C$) for the effective precipitation of the resulting acridinium salt. Fine yellow crystals of 9-cyano-10-methylacridinium chloride (9-CMACl) were then filtered, dried, and the purity of the final product was assessed by reverse phase (RP)-HPLC. The chromatographic set consisted of a Waters 600 E Multi-solvent Delivery System and a Waters 2487 Dual λ Absorbance Detector (UV-vis light detection was set at 254 and 384 nm and fluorescence detection at 540 nm). The wavelengths for optimal detection were established by recording the UV-vis absorption spectrum of the compound 9-CMACl in the range 280-550 nm (Lambda 40 UV-vis light spectrophotometer, Perkin Elmer, USA) and the fluorescence spectrum recorded at the excitation/emission wavelengths of 384 nm/538 nm respectively, using a Cary Eclipse spectrofluorometer (Varian, USA). The isocratic mobile phase consisted of acetonitrile/0.1% trifluoroacetic acid in ultrapure (UP) water (1/1 v/v), applied in isocratic mode at the flow rate of 0.7 ml/min. A Gemini C6-Phenyl 110A column (100 \times 4.60 mm, Phenomenex) was used in all RP-HPLC runs. The purities of the studied substances [*N*-acetyl-L-cysteine (NAC), glutathione, D-penicillamine and ATC] were also checked before the experiments, using the analogous chromatographic set, working at the flow rate of 1.0 ml/min with phosphate buffer [KH_2PO_4 (26 mM), $Na_2HPO_4 \times 2H_2O$ (40.8 mM), pH 7]/methanol (8/1 v/v) as the mobile phase and absorbance detection set at 227 nm.

The melting point of 9-CMAcI was established using melting point M-565 electronic apparatus, controlled by supported software (BUCHI, Switzerland). The chemical identity of 9-CMAcI was confirmed using high-resolution mass spectrometry (ESI-QTOF) by recording the molecular ions of this compound (positive mode, TripleTOF 5600+, AB SCIEX spectrometer, Canada), as well as its ^1H NMR spectrum, using an Advance III 500 MHz spectrometer, Bruker, USA).

The analysis data for 9-CMAcI were provided in the following manner: retention factor related to uracil (k), assessed using RP-HPLC; melting point (m.p.; Figure S2; ESI); molecular ion (M^+ , in m/z); ^1H NMR signals (in CD_3CN): chemical shift (δ) in ppm (integration, multiplicity, conjugation constant) (J): $k = 0.26$; m.p. = 424.15 K; $M^+ = 219.3$; ^1H NMR: 8.82 (2H, d, 8.5), 8.73 (2H, d, 9.3), 8.56 (2H, t, 8.5), 8.24 (2H, t, 7.6), and 4.92 (3H, s).

All the investigated substances were originally in the form of crystal powders. NAC, glutathione, and D-penicillamine were supplied by Ambeed (USA) and ATC by Sigma-Aldrich (USA). Their purity was established using RP-HPLC in the above-described setup before further experiments.

2.2 | Measurements of chemiluminescence

All solutions of used reagents were prepared at 298 K in UP (type 1) water (Synergy UV, Merck Millipore, USA), applying the volume-weight method. Accordingly, a 1.0×10^{-4} M working solution of the chemiluminogenic substrate, 9-cano-10-methylacridinium nitrate (V), was prepared by dissolving 1.1 mg of 9-CMAcI in 50 ml water (class A volumetric flask) and adding 50 μl of 1 M HNO_3 . Here, 1.0 mM solutions of the investigated analytes (RSHs) were prepared in the same manner. The solutions were kept in the fridge (at 4–5°C) for up to 3 days during the experiments. 5 M aqueous solution of KOH (p.a., POCH, Poland) was prepared from accurately weighed flakes that were dissolved in UP water.

Measurements of CL were conducted using a Lumat3 LB 9508 luminometer (Berthold Technologies, Germany), equipped with an ultrasensitive photon counting-type detector. All experiments were conducted in identical conditions, using freshly prepared solutions of the reagents. The intensity of light emission was measured in relative units (RLUs) with a total time of measurement of 25 sec and a counting time (resolution) of 0.15 sec. Before the measurements, the solution of 9-CMA salt was diluted 3.5 times in a 5 ml polystyrene tube (12 \times 75 mm), in which the measurements were taken. The exact volume of the solution of investigated substance was added to 5 M KOH (1 ml) and incubated in a glass flask with mixing. Next, 250 μl of 1.0×10^{-4} M 9-CMA in 1 mM HNO_3 were mixed with 650 μl of UP water and placed in the tube holder of the apparatus. Investigated solutions of each assayed substrate (1 ml) were incubated during the optimal time in 5 M KOH solution in a glass flask ($c = 1.0 \cdot 10 \times 10^{-6}$ M). The optimal incubation times for investigated substances were assessed individually by calculating the areas under the CL curves in 1 min. Periods over the total time of 15 min (the optimal times fell in the range 4–7 min). The next steps were performed

after incubation of researched substance in an alkaline environment (5 M KOH) over the specified period. After incubation, 100 μl of the researched solution was injected into the measuring tube and a reading of emission was carried out in real time.

Applying the optimal incubation times established for each investigated substance, calibration graphs were constructed by plotting dependences of the differences between the integral emissions (AUC) for each system (with RSH) and for the background (that is, an analogous system with no 9-CMA) against concentrations, $\Delta(\text{AUC})$ vs. c .

Measurements of CL with the use of 10,10'-dimethyl-9,9'-biacridinium nitrate (lucigenin) as the indicator^[30–32] were also performed in the presence of investigated analytes to obtain the comparison data. The experiments were conducted in the analogous experimental setup, such as that described above for the systems containing 9-CMA salt.

An experiment with lower concentrations of selected analyte, NAC, was carried out to compare the obtained LOD and limit of quantitation (LOQ) values based on areas under the curve.

The investigated solution of the assayed substrate (1 ml, $c = 1.0 \cdot 10 \times 10^{-8}$ M) was incubated for an optimal time (4 min) in 5 M KOH solution in a glass flask. Next, 250 μl of 1.0×10^{-5} M 9-CMA in 1 mM HNO_3 was mixed with 650 μl of UP water and placed in a tube holder on the apparatus. The differences between maximal intensities of emission, recorded for analytic systems with NAC and the background against concentration, were then plotted [ΔI_{CL} (max.) vs. c] and analytical data were derived based on the calibration graph.

2.3 | Calculations

The stationary-point structures of isolated molecules were obtained by applying the DFT^[33] or the time-dependent DFT (TD DFT)^[34] level to determine ground and excited states, respectively. Calculations were carried out with the CAM-B3LYP functional^[35] and the 6-31G (d,p) basis set.^[36] The intrinsic reaction coordinate (IRC)^[37] calculations at the same level of theory were made to connect the transition state to the reactants and products. The harmonic vibrational frequencies characterizing the stationary points were evaluated to ensure that the obtained structures correspond to true minima or first-order saddle points on the potential energy surface. Gas-phase geometries were optimized in an aqueous solution using the PCM^[38,39] solvation model. All the calculations were obtained using the Gaussian16^[40] program package. Visualization of the results of the calculations of equilibrium structures of all molecules was made using ChemCraft software.^[41]

3 | RESULTS AND DISCUSSION

3.1 | Preparation of reagents for the assays

The canonical structures of the objects this study for nucleophilic drugs containing the sulfhydryl group (or appearing under hydrolysis

at the experimental conditions, as is the case of NAC), are presented in Figure 1. The chemiluminogenic substrate used in all experiments, 9-cyano-10-methylacridinium chloride (9-CMACl) and its respective cation, 9-CMA⁺, is shown in Figure 2.

For this study, the compound 9-CMACl at ultrahigh purity was synthesized from its respective nitrate (V) salt, which was obtained by adopting known procedures.^[23] It should be mentioned that in previous reports concerning the use of 9-CMA nitrate (V) as the chemiluminogenic substrate, only basic preparative techniques, such as crystallization were used for its purification, without giving precise information on its final purity before measurements of emission. For this work, a chemiluminogenic compound was purified in the neutral form (9-CMA) by applying gravitational LC and, after isolation of chromatographically pure base and converting it to the chloride salt, its purity was assessed using RP-HPLC, obtaining a value exceeding 99.9% (Figure S2; ESI). The purity of the thiol-containing drugs (the commercial products) was also checked before assays and was always satisfactory, falling in the range 97.4–99.7% (Figure S2; ESI).

The chemical uniformity of the 9-CMACl salt was checked by determining its melting point, which fell in a narrow range (standard deviation <1.5 K), with a maximum at 424 K (Figure S3; ESI).

The results of the spectroscopic analysis fully confirmed the composition of the compound. The ESI-QTOF mass spectrum presented the parent ion (M⁺, m/z = 219.1) as well as the 10-methylacridinium cation (m/z = 194.1), typically appearing in the mass spectra of *N*-methylated acridinium salts (Figure S4; ESI).^[30] The ¹H NMR spectrum, presented in Figure S5 as ESI, expressed a simple and clear picture of a highly symmetrical molecular system containing four groups of signals in the aromatic range (~8.2–8.8 ppm) and a sharp singlet, derived from the methyl group attached to the endocyclic acridine nitrogen at ~4.9 ppm.

3.2 | Chemiluminescence assay systems

The results of the chemiluminometric measurements, making the basis for the development of the proposed assay, are presented in Tables 1 and 2 and in Figures 3–5. Before quantitative studies, the optimal conditions for the experiments were established. The preincubation studies on the analytes (RSHs) in an alkaline environment in the presence of molecular oxygen (vigorous mixing) enabled us to determine the optimal time to generate sufficiently high signals upon their reaction between 9-CMA⁺ and RS[−]. Results of the optimization experiments were as follows: for NAC: 4 min, for GSH: 5 min, for DPA: 6 min, and for ATC: 7 min.

Figure 3 presents time profiles of emission from the substrate used for CL, 9-CMA⁺ (at optimal conditions) in the presence of the studied biological substances containing sulfur. The curves showed that in all cases CL occurred quickly (flash-type), which enabled the measurement of the total energy corresponding to the entire emission time, falling in the range 5–15 sec. The maximal emission intensity

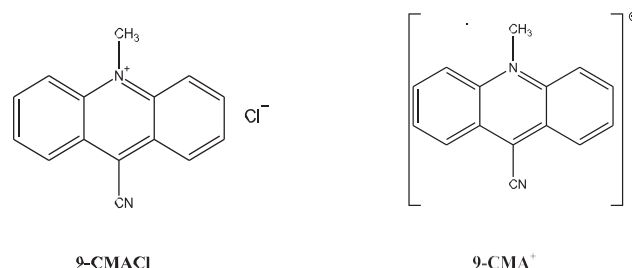


FIGURE 2 Structural formula of 9-cyano-10-methylacridinium chloride (9-CMACl), the substrate utilized in this work and the resulting monocation, the chemiluminogenic indicator used in the assays

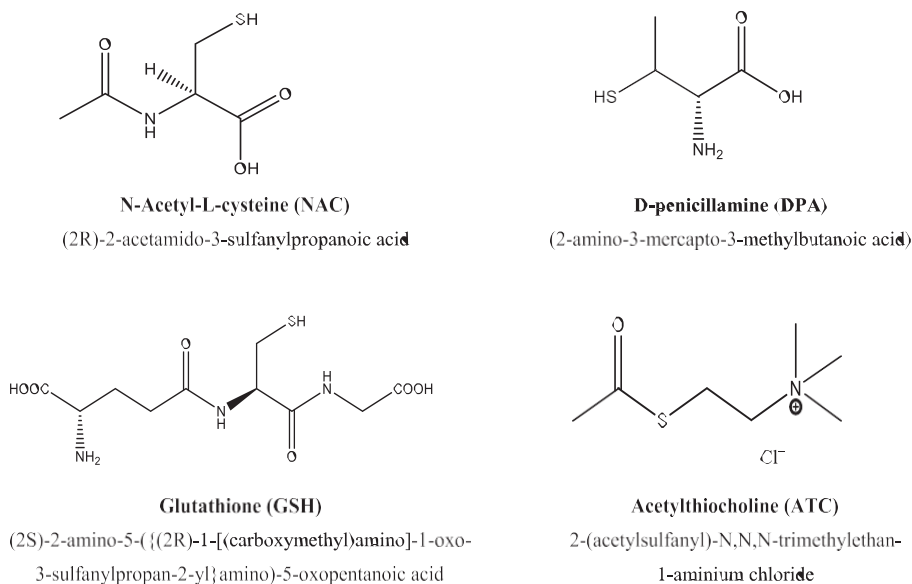


FIGURE 1 Structural formulas of D-penicillamine and three biologically active compounds containing a thiol moiety investigated in this work

TABLE 1 Results of the quantification of biologically active analytes containing a thiol group, based on the parameters of linear regression (integral emissions vs. concentrations, Figure 5b)

Parameter	<i>N</i> -Acetyl-L-cysteine	D-Penicillamine	Glutathione	Acetylthiocholine chloride
Slope (<i>a</i>)	$(1.73 \pm 0.17) \times 10^{12}$	$(1.32 \pm 0.36) \times 10^{12}$	$(1.37 \pm 0.05) \times 10^{12}$	$(1.01 \pm 0.24) \times 10^{12}$
Intercept (<i>b</i>)	1.12×10^7	1.40×10^7	1.44×10^7	1.88×10^7
Coef. of determ.	0.99	1.00	0.98	0.98
(<i>R</i> ²)	5.34-17.91	4.3-11.23	3.36-9.01	2.17-7.05
RSD (<i>n</i> = 3), % Average RSD (<i>n</i> = 3), %	9.75	7.31	6.79	4.05
Linearity range (M)	$(6.31-10) \times 10^{-7}$	$(1.73-10) \times 10^{-6}$	$(1.97-10) \times 10^{-7}$	$(1.50-10) \times 10^{-6}$
LOD (M)	6.31×10^{-7}	1.73×10^{-6}	1.97×10^{-7}	1.50×10^{-6}
LOQ (M)	1.89×10^{-6}	5.19×10^{-6}	5.90×10^{-7}	4.51×10^{-6}

TABLE 2 Comparison of efficiency of CL derived from compound such as 9-CMA⁺ and lucigenin based on the net areas under emission curves ($\Delta(\text{AUC})$) in the time frame of 25 sec. Final concentration of the reagents: C(RSHs) = 1.0×10^{-5} M, c(9-CMA⁺) = 2.5×10^{-5} M

Name of substance	$\Delta(\text{AUC})$ for 9-CMA ⁺ $\times 10^7$ (RLU ²)	$\Delta(\text{AUC})$ for lucigenin $\times 10^5$ (RLU ²)
D-Penicillamine	2.81	8.02
Glutathione	2.82	9.88
Acetylthiocholine	2.94	6.21
<i>N</i> -Acetyl-L-cysteine	2.90	9.99

was proportional to the nucleophile content in the sample, enabling its quantification after calibration. Comparing the relative intensities of the signal of maximal intensity for subsequent analytes, they could be ordered as follows: 1.0, 0.90, 0.64 and 0.50 for GSH, NAC, ATC, and DPA, respectively.

The linearized time profiles of chemiluminogenic oxidation of 9-CMA⁺ in the presence of RSHs are given in Figure 4. They enabled the assessment of kinetics constants of CL decays in all the investigated systems. According to luminometric analysis, all processes obey pseudo-first kinetic order, as was revealed by the high linearity of the interdependences of the logarithmic temporary intensities of emission ($\ln I_{\text{CL}}$) vs. time ($R^2 > 99\%$ in all cases). Kinetic constants derived graphically based on these were similar for each system and fell in the range 0.33-0.36 s⁻¹. The presence of thiol-containing analytes did not strongly influence the values of kinetic constants, as a small increase in this parameter was observed in all cases compared with the system containing no RSH, with the change of the latter within a few per cent (from -3.8% for ATC to ~6.1% for GSH).

By integrating the areas under the CL profiles, the interdependences of the integral emissions on the concentration of the investigated analyte were found. Linearization of the latter allowed determination of the calibration plots (Figure 5), and from them the analytical parameters of the assays, which are listed in Table 1. The slopes of the linear relationships (*a*) for the investigated systems were

characterized by high correlation coefficients (0.98-1.00) and fell in the range $\sim 1.0-1.7 \times 10^{12}$ RLU²/M. The slopes for DPA and GSH were comparable and assumed higher value than this, characterizing ATC. The highest value of this parameter was obtained for NAC. The intercepts characterizing the linear relationships assumed relatively high values (at a level of 10^7 RLU²), reflecting that CL emission also occurred when no thiol analytes were present in the system, although in the latter case this was much less intensive. This suggested that, in the absence of RSH, hydroperoxyl OOH⁻ ions were also likely to be formed, as their presence determined the occurrence of CL emission. The calculated LODs of the assayed biological thiols assumed sub-micromolar levels (10^{-7} to 10^{-6} M), falling in the lowest regions of the calibration graphs.

In addition, comparative studies were undertaken for ACC, in which the maximum of the CL profile was used instead of its area to prepare the calibration plot. The concentrations of the reagents were also slightly reduced, which enabled slightly better analytical results to be obtained exclusively for this compound (LOD ~8.3 nM), they are presented in ESI (Figures S7, S8 and Table S3).

The comparison of the emissive properties of 9-cyano-10-methylacridinium salt and well known acridinium compound capable of CL, lucigenin, is shown in Figure 6. It can be concluded that under experimental conditions lucigenin has a quite different emission profile than 9-CMA⁺ (glow vs. flash, respectively) (Figure 6a). Based on the above, it can be therefore concluded that in each case we dealt with glow-type emissions, but for the pairs of compounds GSH/DPA and ATC/NAC, significant differences in the efficiency and emission profiles were observed (low and steady vs. intense and slow increasing at longer times, >5 min.). Experiments revealed that lucigenin, when treated as the reference compound, was a less effective luminogenic substrate for assays of the studied analytes compared with the 9-CMA salt. These conclusions can be drawn when comparing the areas under curves for 25 sec for both CL indicators as this is the time interval needed for complete emission from 9-CMA⁺ (Figure 6b). According to this scenario, the intensity of CL emission generated by 9-CMA⁺ under optimal assay conditions was many times higher than the one found for lucigenin (Table 2). Moreover, using lucigenin as an CL indicator gave a less beneficial reaction

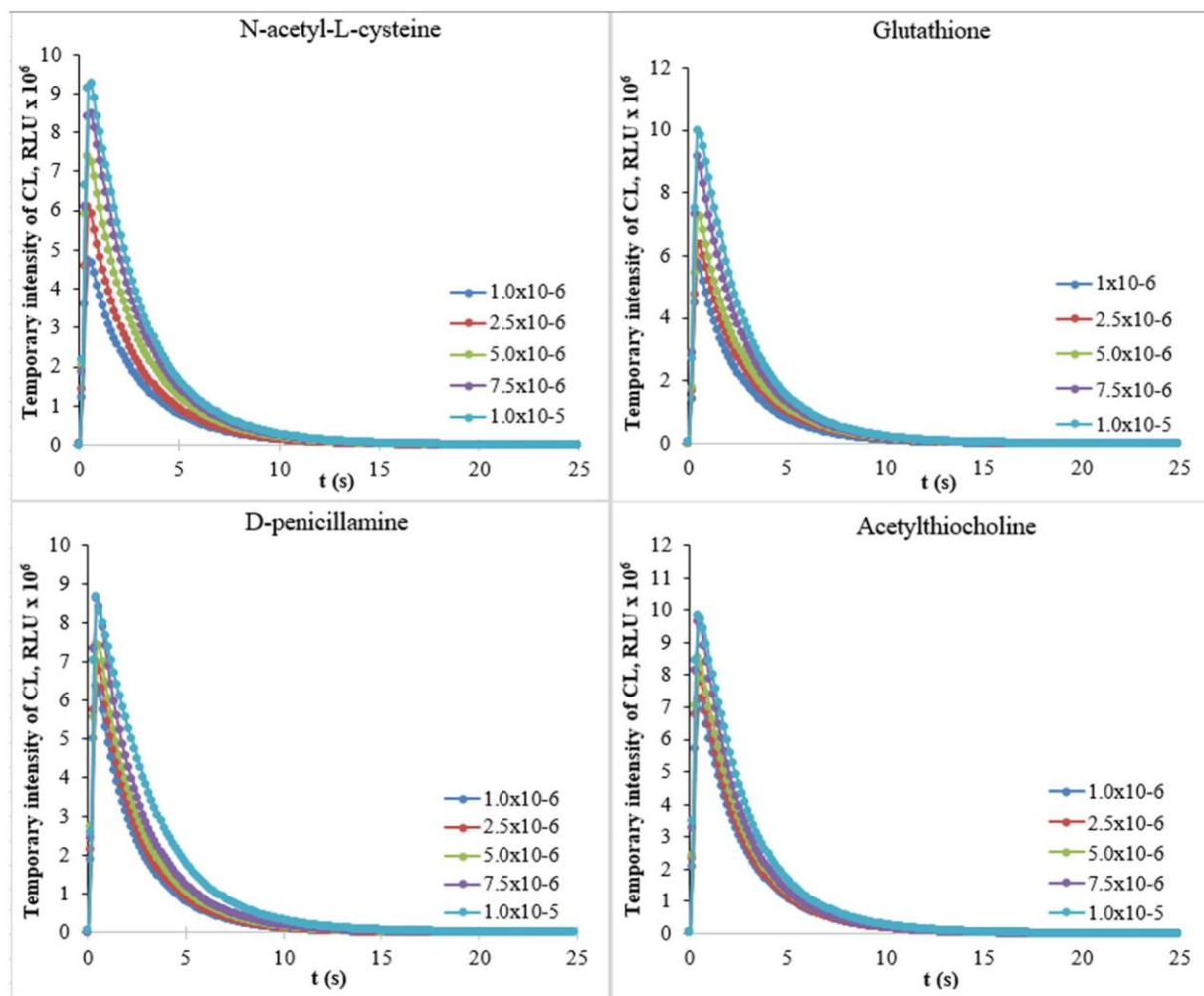


FIGURE 3 Temporary intensities of chemiluminescence of 9-CMA⁺ in alkaline medium in presence of various concentrations of thiol-containing compounds (the analytes). $C(9\text{-CMA}^+) = 2.5 \times 10^{-5} \text{ M}$, 0.5 M KOH. Concentration range of researched analytes was in the range $1\text{-}10 \times 10^{-6} \text{ M}$

profile, as more time was needed for effective emission (glow-type of kinetic curves) (Figure S6).

It should be remarked here that no hydrogen peroxide was needed to trigger light emission when applying the proposed method. Moreover, the analytes studied in this work were not simply model compounds of nucleophilic characteristics, but they encompassed molecular systems of great biological importance.

3.3 | Theoretical considerations

The data extracted from quantum-chemical calculations (DFT level) are shown in Tables 3, 4 and S2 in ESI and Figure 7 presents possible transformation steps. The thermodynamic data characterizing individual steps as well as the kinetics data for the steps, characterized by activation barriers, are provided in Tables 3 and 4, respectively.

According to the computational results, it can be concluded that sulfur nucleophilic drugs (RSHs) effectively facilitate the production of hydroperoxyl ions (HOO^-). Without the participation of the former

analytes, this process is of low feasibility in aqueous environments, and are characterized by small positive values for Gibbs free energy (Table 3, Paths 1 and 2). According to this, the presence of RSHs in the system seems to be crucial at this stage of the oxidation of 9-CMA⁺, giving rise to the occurrence of CL (Figure 7, step I and Table 3, equation 3).

Acridan hydroperoxy adduct (9-CMA-OOH) makes the precursor of the consecutive chemiluminogenic steps, initiating the 'light path' of transformations, marked in red (Figure 7, step II), as was formerly proposed similarly previously.^[22] However, the production of the above-mentioned adduct can be supplied, to some extent, by an alternative route (the paths marked in green) (Figure 7, steps II' and III), which is also thermodynamically probable, although less than the route marked in red. However, the kinetics of the reaction may be decisive in the considered problem. Indeed, it can be seen from the results of calculations (Table 4), that the activation barriers of process III of all sulfur nucleophilic drugs are extremely high, especially in the aqueous phase (the values of Gibbs free energy are in the range 49.4 and 59.2 kcal mol⁻¹). These results may exclude the paths marked in

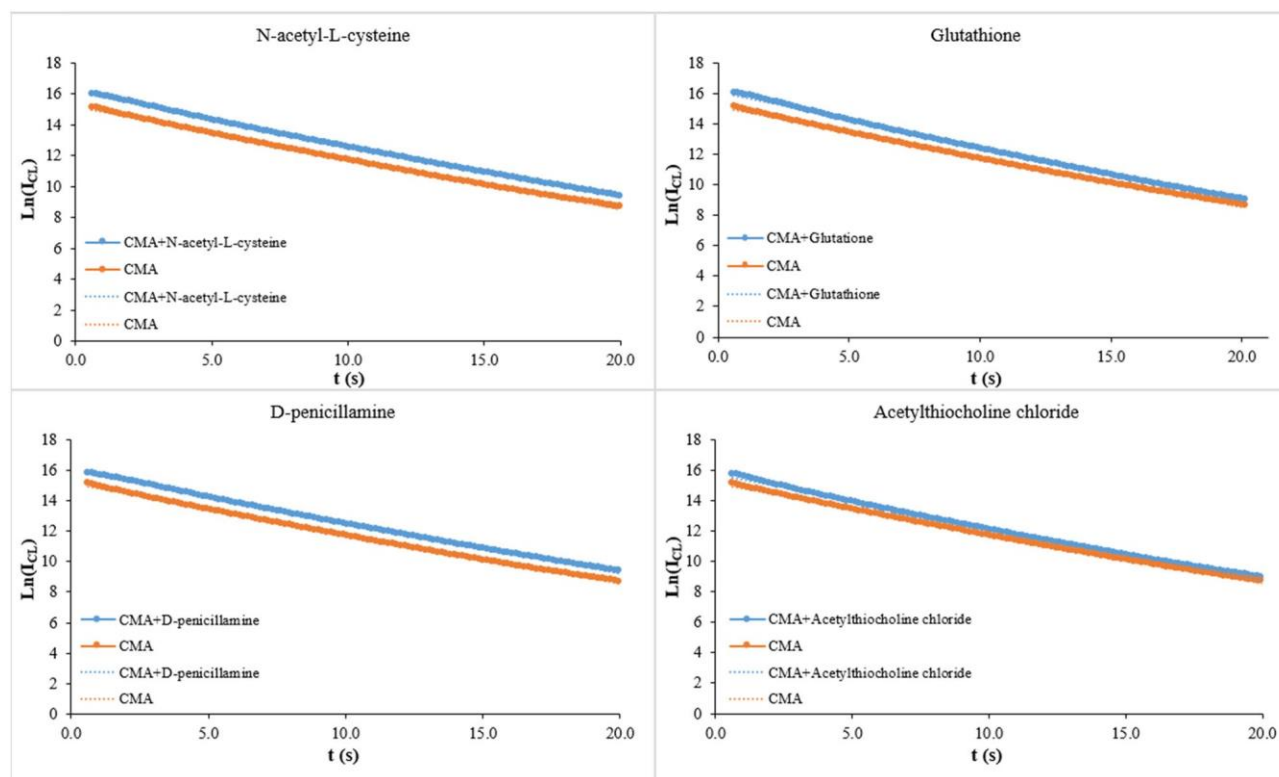


FIGURE 4 Plots of logarithms of temporary CL intensities $\ln(I_{CL})$ against time in systems that contain 9-CMA⁺ and researched analytes (RSHs). $C(9\text{-CMA}^+) = 2.5 \times 10^{-5}$ M, 0.5 M KOH, $c(\text{D-penicillamine}) = 1.0 \times 10^{-5}$ M. Regression equations for the natural logarithms of temporary CL intensities $\ln(I_{CL})$ against time: 9-CMA⁺: $Y = -0.331x + 15.14$, $R^2 = 0.997$; 9-CMA⁺/NAC: $Y = -0.342x + 16.09$, $R^2 = 0.998$; 9-CMA⁺/GSH: $Y = -0.362x + 16.13$, $R^2 = 0.997$; 9-CMA⁺/DPA: $Y = -0.336x + 15.96$, $R^2 = 0.998$; 9-CMA⁺/ATC: $Y = -0.349x + 15.73$, $R^2 = 0.997$

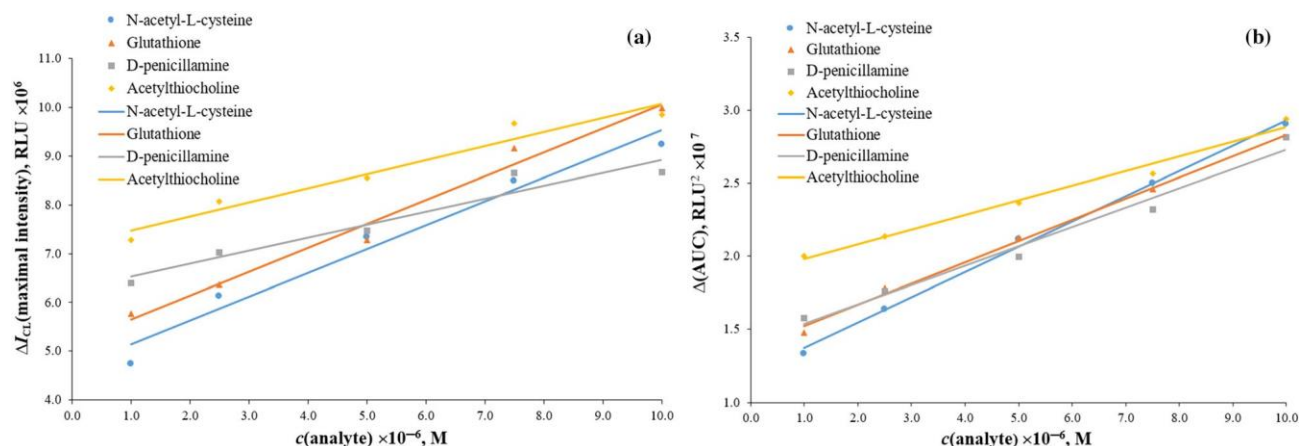


FIGURE 5 Calibration graphs for 9-CMA⁺ ($c = 2.5 \times 10^{-6}$ M) chemiluminescence in alkaline environment (0.5 M KOH) in the presence of investigated thiols. (a) Net signal of maximal intensity of CL at optimal conditions against concentration of the analyte. (b) Net signal of integral emission of CL, $\Delta(AUC)$, against concentration of the analyte. Regression equations for (b) NAC: $Y = 0.4595 \times 10^6x + 0.8651$, $R^2 = 0.968$; ATC: $Y = 0.2894 \times 10^6x + 1.1309$, $R^2 = 0.953$; GSH: $Y = 0.4862 \times 10^6x + 1.2980$, $R^2 = 0.982$; DPA: $Y = 0.2580 \times 10^6x + 0.9857$, $R^2 = 0.935$. Regression equations for (b) NAC: $Y = 0.1645 \times 10^6x + 0.0972$, $R^2 = 0.997$; ATC: $Y = 0.0877 \times 10^6x + 0.1687$, $R^2 = 0.984$; GSH: $Y = 0.1455 \times 10^6x + 0.2297$, $R^2 = 0.996$; DPA: $Y = 0.0934 \times 10^6x + 0.1712$, $R^2 = 0.979$

green (Figure 7, steps II' and III). Conversely, the simultaneous occurrence of both reactions (the paths marked in green, and this marked in red) may be a determinant of the success of the tested method. As a

result, we observed an enhancement of light emission from the chemiluminogenic substrate (9-CMA⁺) in the presence of sulfur nucleophiles, which created a principle for the proposed assay.

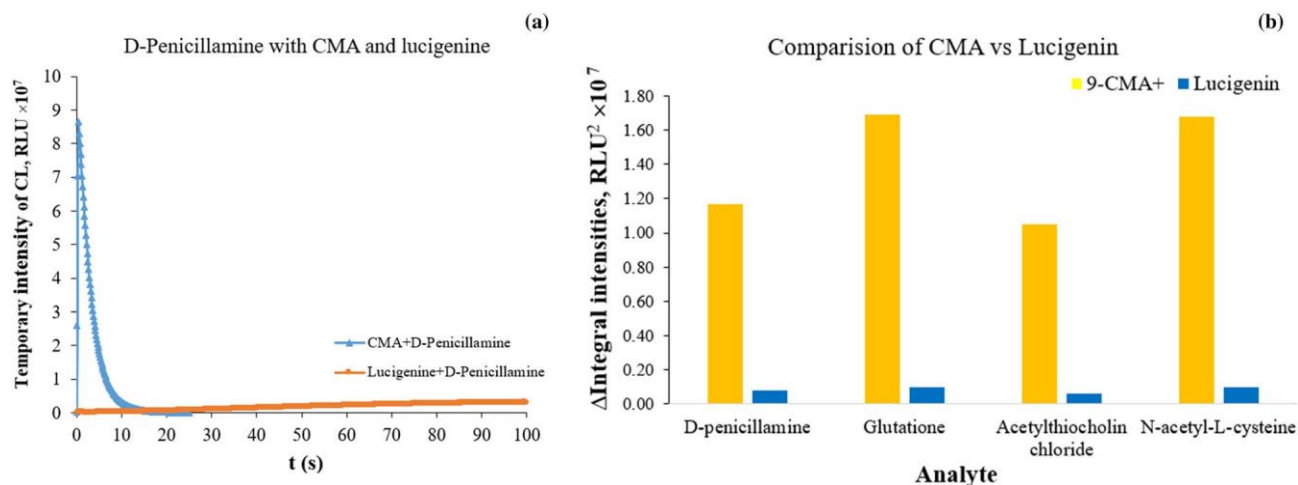


FIGURE 6 (a) Comparison of kinetic profiles denoting temporary CL intensities against time for 9-CMA⁺ ($c = 2.5 \times 10^{-5}$ M) and lucigenin ($c = 2.5 \times 10^{-5}$ M) in the presence of an exemplary analyte, D-penicillamine ($c = 1.0 \times 10^{-5}$ M) in 0.5 M KOH. (b) Comparison of the areas under CL curves within a time span of 25 sec (AUC) for 9-CMA⁺ and for lucigenin in the presence of the studied substances under optimal conditions. For details see Experimental

TABLE 3 Thermodynamical data concerning the elementary steps of chemiluminogenic transformations of 9-CMA⁺ cations in alkaline environments in the presence of biological nucleophiles containing sulfur

No.	Process	Gaseous phase		Aqueous phase	
		$\Delta_{r,298}H^0$	$\Delta_{r,298}G^0$	$\Delta_{r,298}H^0$	$\Delta_{r,298}G^0$
1.	$O_2 + H_2O + OH^- \rightarrow OOH^- + H_2O_2$	21.2	29.6	27.9	36.4
2.	$\frac{1}{2}O_2 + OH^- \rightarrow OOH^-$	-2.8	0.7	4.2	7.7
3.	$ATCh + H_2O \rightarrow TCh + MeCOOH$	-11.2	-12.8	-9.8	-11.5
4.	$RSH + \frac{1}{2}O_2 + 2OH^- \rightarrow RS^- + OOH^- + H_2O$ (NAC)	-82.0	-79.6	-49.3	-46.6
5.	$RSH + \frac{1}{2}O_2 + 2OH^- \rightarrow RS^- + OOH^- + H_2O$ (ATC)	-157.9	-154.4	-53.8	-50.3
6.	$RSH + \frac{1}{2}O_2 + 2OH^- \rightarrow RS^- + OOH^- + H_2O$ (DPA)	-70.5	-67.4	-44.0	-40.8
7.	$RSH + \frac{1}{2}O_2 + 2OH^- \rightarrow RS^- + OOH^- + H_2O$ (GSH)	-88.5	-85.5	-55.3	-52.0
8.	$9-CMA^+ + OOH^- \rightarrow 9-CMA-OOH$	-176.7	-164.0	-62.0	-49.4
9.	$9-CMA-OOH + OH^- \rightarrow 9-CMA-OO^- + H_2O$	-58.8	-60.6	-32.2	-33.7
10.	$9-CMA-OO^- \rightarrow 9-CMA-OO$ (cyclic form)	2.4	3.2	3.3	3.8
11.	$9-CMA-OO$ (cyclic) \rightarrow N-Me-9-acridone* + OCN^-	-10.2	-22.5	-20.7	-32.9
12.	$N-Me-9-acridone^* \rightarrow N-Me-9-acridone + h\nu$	-82.6	-82.4	-83.2	-83.0
13.	$9-CMA^+ + RS^- \rightarrow 9-CMA-SR$ (NAC)	-119.7	-108.5	-26.7	-16.1
14.	$9-CMA^+ + RS^- \rightarrow 9-CMA-SR$ (ATC)	-51.7	-37.6	-18.2	-5.2
15.	$9-CMA^+ + RS^- \rightarrow 9-CMA-SR$ (DPA)	-127.1	-113.8	-25.0	-12.4
16.	$9-CMA^+ + RS^- \rightarrow 9-CMA-SR$ (Glutathione)	-100.8	-85.4	-12.2	3.3
17.	$9-CMA-SR + OOH^- \rightarrow 9-CMA-OOH + RS^-$ (NAC)	-57.0	-55.5	-35.3	-33.3
18.	$9-CMA-SR + OOH^- \rightarrow 9-CMA-OOH + RS^-$ (ATC)	-124.9	-126.4	-43.8	-44.2
19.	$9-CMA-SR + OOH^- \rightarrow 9-CMA-OOH + RS^-$ (DPA)	-49.6	-50.2	-37.0	-37.0
20.	$9-CMA-SR + OOH^- \rightarrow 9-CMA-OOH + RS^-$ (GS)	-75.9	-78.6	-49.9	-52.7

$\Delta_{r,298}H^0$ and $\Delta_{r,298}G^0$ (both in kcal mol⁻¹), respectively, represent the enthalpy and Gibbs' free energy (gaseous phase) or free energy (aqueous phase) of the corresponding process at standard temperature and pressure.

Furthermore, the transformation of the substitution product (9-CMA-OOH) into excited molecules of 10-methyl-acridan-9-one ([9-MA]*) produces a complex, multistep process, the mechanism of

which has been proposed before.^[22] Some steps, which are those concerning the generation of light, have been confirmed in this work as the most thermodynamically probable (Figure 7, steps II-VII), while

TABLE 4 Transition states for the processes illustrated in Figure 7. For details see Experimental

Process	Step no.	Gaseous phase		Aqueous phase	
		$\Delta_{a,298}H^0$	$\Delta_{a,298}G^0$	$\Delta_{a,298}H^0$	$\Delta_{a,298}G^0$
9-CMA-OO (cyclic) \rightarrow N-Me-9-acridone* + OCN [−]	TS-VI	1.5	0.6	5.6	5.8
9-CMA-SR + OOH [−] \rightarrow 9-CMA-OOH + RS [−] (NAC)	TS-III	9.8	27.6	30.8	49.4
9-CMA-SR + OOH [−] \rightarrow 9-CMA-OOH + RS [−] (ATC)	TS-III	12.2	29.3	39.7	56.4
9-CMA-SR + OOH [−] \rightarrow 9-CMA-OOH + RS [−] (DPA)	TS-III	11.7	27.6	36.6	50.5
9-CMA-SR + OOH [−] \rightarrow 9-CMA-OOH + RS [−] (GSH)	TS-III	19.0	35.7	45.0	59.2

$\Delta_{a,298}H^0$ and $\Delta_{a,298}G^0$ (both in kcal mol^{−1}), respectively, represent the enthalpy and Gibbs' free energy (gaseous phase) or free energy (aqueous phase) of activation at standard temperature and pressure.

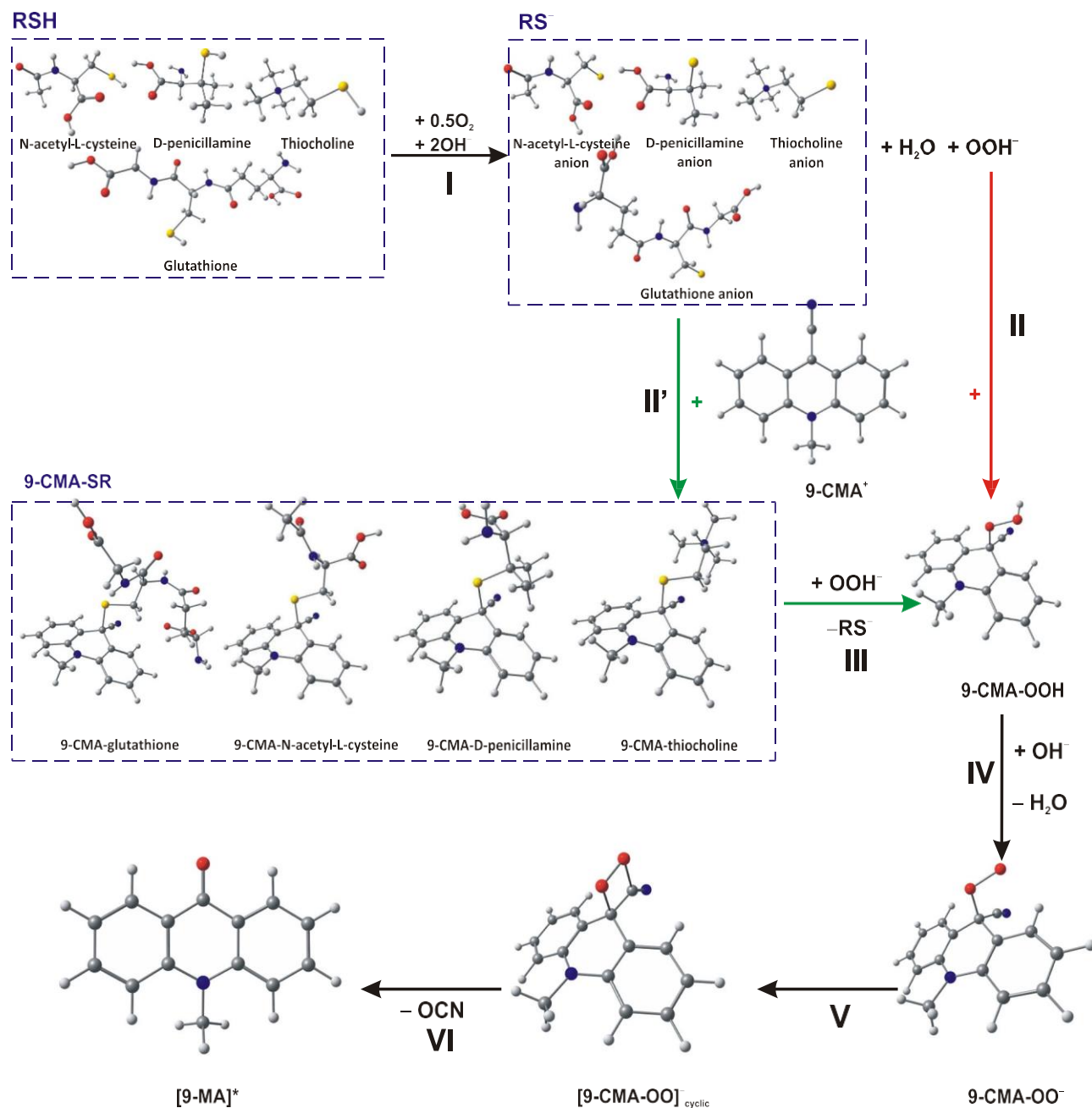


FIGURE 7 Pathways of transformations leading to chemiluminescence of 9-CMA⁺ in an alkaline medium in the presence of the studied analytes (RSHs, see Figure 1) and molecular oxygen, according to DFT calculations. See also Table 3. For details see Experimental

significant differences were observed at the initial stages of 9-CMA⁺ oxidation (Figure 7, steps II' and III). Also, from a kinetics perspective, the possibility of the proposed path enabling the luminometric assays seemed to be preferable. Most steps occurred without an activation barrier and only step VI (Figure 7) determined the kinetics of chemiluminogenic transformations involving 9-CMA⁺ and its derivatives. However, the activation barrier of this step was low, and the Gibbs free energy value was only 5.8 kcal mol⁻¹ in aqueous solution (Table 4).

The ionic mechanism of chemiluminogenic oxidation of 9-CMA⁺ in the presence of nucleophilic substances containing sulfhydryl groups, proposed in this study, should be related to previous attempts at this problem, which assumed the appearance of superoxide radicals (O₂^{•-}) at the initial stage of reaction.^[24,25] However, the calculations performed in this work suggested that, under standard conditions, the formation of the above-mentioned ROS-type entity, assuming the reaction between molecular oxygen and the anionic form of the nucleophile (RS⁻), was not thermodynamically feasible. This was indicated by the data gathered in Table S1 in ESI (the radical formation step), in which the formation of the superoxide radicals with the participation of RS⁻ and molecular oxygen in an aqueous environment was characterized using high positive Gibbs free energy changes in the range ~23–32 kcal mol⁻¹. It should be emphasized, however, that the addition of the hypothetically formed O^{•-} radical anions to 9-CMA⁺ should be, according to our calculations, a thermodynamically spontaneous process (step 3, Table S1 and Figure S1), which was not the case when considering the next hypothetical step, leading to the formation of complex anions of 10-methyl-9-cyano-9-peroxyacridan (step 4, Table S1 and Figure S1). It can be therefore concluded that the formerly proposed mechanism, based on general considerations and older reports on similar problems, is not likely to operate according to the presented DFT calculations.

Referring to the literature data, in the generated quantum-chemical calculations, we also decided to consider the two-stage oxidation reaction of the sulfur derivatives according to the following equations:

- i. $\text{H}_2\text{O}_2 + \text{RSH} \rightarrow \text{RSOH} + \text{H}_2\text{O}$
- ii. $\text{RSOH} + \text{RSH} \rightarrow \text{RSSR} + \text{H}_2\text{O}$

The results are presented in Table S2 in ESI. Thermodynamic data for both stages of the considered reaction indicated the possibility of free oxidation of the investigated thiol derivatives to disulfides in the presence of hydrogen peroxide (negative values for both $\Delta_r,298H$ and $\Delta_r,298G$ in the gas phase and in water). However, the kinetic data of the two consecutive processes under study turned out to be crucial, as both stages occurred with high activation barriers in analyzed media (Table S2 in ESI). The obtained kinetic data suggested that oxidation of the tested thiols to disulfides with hydrogen peroxide will not be the preferred reaction, and therefore should not affect the proposed method for the determination of investigated sulfur nucleophiles with the participation of the 9-cyano-10-methylacridinium cation.

4 | CONCLUSION

An original method for the quantification of biologically active substances such as NAC, glutathione, D-penicillamine, and ATC was developed and optimized. The proposed luminometric assay for the above nucleophilic analytes containing sulfhydryl groups assumed the use of a high purity 9-cyano-10-methylacridinium salt such as a chemiluminescent substrate. The advantages of the proposed method are that there was no need for the use of hydrogen peroxide to trigger light emission, as well as the simple experimental setup. The assay procedure differed from that previously described, making an original proposition in the field of luminescence analysis. The method was thoroughly optimized for the investigated problem and required strict adherence to the experimentally established conditions.

The emission from 9-cyano-10-methylacridinium cation represented flash-type kinetics under assay conditions, which distinguished it from glow-type kinetics, manifested in the same experimental setup by the classical CL system based on lucigenin. It was also revealed that lucigenin produced much less emission activity in the optimized systems than the cyanoacridinium salt used in the proposed assay. Flash-type kinetics enabled quantification of the total signal under the CL profiles and therefore precise determination of the studied analytes. Regression parameters of derived calibration curves were assessed for all the investigated systems, and were linear over the concentration range 0.2–1.7 μM. Accordingly, the proposed assay allowed the determination of the studied biological substances with LODs at the level of 10⁻⁷ to 10⁻⁶ M (LOD 0.19–1.73 μM, LOQ 0.59–5.19 μM).

Other approaches described in the literature for the analysis of biological thiols achieved even lower detection limits (at nM and even pM levels), but they usually required sophisticated methods such as FIA or tandem techniques (e.g. LC-MS). Therefore these approaches required the use of complicated equipment, and often the derivatization of samples with specific reagents prior to the experiments, which made them quite expensive and time consuming, and not always very highly sensitive, which is a crucial requirement in analyses.

Quantum-chemical calculations [DFT and time-dependent DFT (TDDFT) level of theory] indicated that the presence of the sulfhydryl-containing analytes strongly influenced the thermodynamics of the processes, especially at the stage of production of hydroperoxy ions (•OOH), initializing the 'light path' of transformations. The experimental data were supported by calculations and enabled us to propose an alternative mechanism for chemiluminogenic oxidation of 9-CMA⁺ in alkaline environments. This may therefore serve as a convenient basis for further use and investigation of emissive properties of the analytically useful substrate that is 9-cyano-10-methylacridinium salt. We hope that current studies open up prospects for the use of this reagent in modern luminescence analyses.

ACKNOWLEDGEMENTS

Calculations were carried out on the computers of the Wrocław Centre for Networking and Supercomputing (WCSS) (Grant No. 215).

DATA AVAILABILITY STATEMENT

The data included in the publication can be available for all readers.

ORCID

Vladyslav Ievtukhov  <https://orcid.org/0000-0002-2809-7524>

Beata Zadykowicz  <https://orcid.org/0000-0002-7125-5233>

Mykola Ye. Blazheyskiy  <https://orcid.org/0000-0002-8032-347X>

Karol Krzymin'ski  <https://orcid.org/0000-0003-4811-961X>

REFERENCES

- [1] N. Kardos, A. L. Demain, *Appl. Microbiol. Biotechnol.* 2011, 92, 677.
- [2] M. D. Mashkovsky, *Medicines* 1997, 1, 350.
- [3] The State Pharmacopoeia of Ukraine, *The Ukrainian Scientific Pharmacopoeial Center for Quality of Medicines*, 1st ed. State Enterprise "Ukrainian Scientific Pharmacopoeial Center for Drug Quality", Ukraine 2001, 556.
- [4] D. Tsikas, J. Sandmann, M. Ikic, J. Fauler, D. O. Stichenothe, J. C. Frölich, *J. Chromatogr., B* 1998, 708, 55.
- [5] P. Uutela, R. Reinila, P. Piepponen, R. A. Ketola, R. Kostiaainen, *Rapid Commun. Mass Spectrom.* 2005, 19, 2950.
- [6] Z. D. Zhang, W. R. G. Baeyens, X. R. Zhang, G. Van Der Weken, *The Analyst* 1996, 121(11), 1569. <https://doi.org/10.1039/an9962101569>
- [7] N. Costa, M. Mirjana, *Acta Pol. Pharm.* 1988, 45, 418.
- [8] T. S. Jovanović, B. S. Stanković, *Acta Pharm. Jugosl.* 1989, 39, 117.
- [9] N. Y. Bondarenko, M. Y. Blazheyskiy, *Methods Objects Chem. Anal.* 2018, 13, 110.
- [10] T. S. Jovanović, B. S. Stanković, *Analyst* 1989, 114, 401.
- [11] I. Lo'pez García, P. Viñas, J. A. Martínez Gil, *Fresenius' J. Anal. Chem.* 1993, 345(11), 723. <https://doi.org/10.1007/bf00325843>
- [12] A. Sano, H. Nakamura, *Anal. Sci.* 1998, 14(4), 731. <https://doi.org/10.2116/analsci.14.731>
- [13] F. E. O. Suliman, M. M. Al-Hinai, S. M. Z. Al-Kindy, S. B. Salama, *Talanta* 2008, 74, 1256.
- [14] https://pl.promega.com/products/cell-health-assays/oxidative-stress-assays/gsh_glo-glutathione-assay/?catNum=V6911 (accessed on Oct. 15, 2021).
- [15] I. Weeks, I. Beheshti, F. McCapra, A. K. Campbell, J. S. Woodhead, *Clin. Chem.* 1983, 29, 1474.
- [16] I. Weeks, A. K. Campbell, J. S. Woodhead, *Clin. Chem.* 1983, 29, 1480.
- [17] Y. Ando, K. Niwa, N. Yamada, T. Irie, T. Enomoto, H. Kubota, Y. Ohmiya, H. Akiyama, *Photochem. Photobiol.* 2007, 83, 1205.
- [18] C. Dodeigne, L. Thunus, R. Lejeune, *Talanta* 2000, 51, 415.
- [19] K. Krzymin'ski, A. Ożóg, P. Malecha, A. D. Roshal, A. Wroblewska, B. Zadykowicz, J. Błażejowski, *J. Organomet. Chem.* 2011, 76, 1072.
- [20] B. Zadykowicz, J. Czechowska, A. Ożóg, A. Renkevich, K. Krzymin'ski, *Org. Biomol. Chem.* 2016, 14, 652.
- [21] F. McCapra, D. G. Richardson, Y. C. Chang, *Photochem. Photobiol.* 1965, 4, 1111. <https://doi.org/10.1111/j.1751-1097.1965.tb09300.x>
- [22] A. Wroblewska, O. M. Huta, S. V. Midyanyj, I. O. Patsay, J. Rak, J. Błażejowski, *J. Organomet. Chem.* 2004, 69(5), 1607.
- [23] A. Wroblewska, O. M. Huta, I. O. Patsay, R. S. Petryshyn, J. Błażejowski, *Anal. Chim. Acta* 2004, 507(2), 229. <https://doi.org/10.1016/j.aca.2003.11.032>
- [24] J. Darkwa, C. Mundoma, R. H. Simoyi, *J. Chem. Soc., Faraday Trans.* 1998, 94(14), 1971. <https://doi.org/10.1039/a708863i>
- [25] M. Y. Blazheyskiy, N. Y. Bondarenko, *Methods Objects Chem. Anal.* 2011, 6, 124.
- [26] B. Karami, M. Montazerzohori, M. H. Habibi, *Molecules* 2005, 10, 1358.
- [27] S. Abdollah, R. Mohamad, H. Majid, *J. Serb. Chem. Soc.* 2011, 76(7), 955. <https://doi.org/10.2298/jsc100904086s>
- [28] A. M. Kulkarni, U. V. Desai, K. S. Pandit, M. A. Kulkarni, P. P. Wadgaonkar, *RSC Adv.* 2014, 4(69), 36702. <https://doi.org/10.1039/c4ra04095c>
- [29] Y. B. Tsaplev, *J. Anal. Chem.* 2012, 67, 506.
- [30] A. A. Al-Warthan, S. A. Al-Tamrah, A. A. Al-Akel, *Anal. Sci.* 1994, 10(3), 449. <https://doi.org/10.2116/analsci.10.449>
- [31] A. Larena, J. Martinez-Urreaga, *J. Mol. Struct.* 1986, 143, 521.
- [32] W. L. Hinze, T. E. Riehl, H. N. Singh, Y. Baba, *Anal. Chem.* 1984, 56(12), 2180. <https://doi.org/10.1021/ac00276a046>
- [33] J. K. Labanowski, J. W. Andzelm, *Density Functional Methods in Chemistry*, Springer, New York, NY, USA 1991.
- [34] G. Scalmani, M. J. Frisch, B. Mennucci, J. Tomasi, R. Cammi, V. Barone, *J. Chem. Phys.* 2006, 124, 094107.
- [35] T. Yanai, D. P. Tew, N. C. Handy, *Chem. Phys. Lett.* 2004, 393(1-3), 51. <https://doi.org/10.1016/j.cplett.2004.06.011>
- [36] P. C. Hariharan, J. A. Pople, *Theor. Chim. Acta* 1973, 28(3), 213. <https://doi.org/10.1007/bf00533485>
- [37] H. P. Hratchian, H. B. Schlegel, *J. Chem. Theory Comput.* 2005, 1, 61.
- [38] J. Tomasi, M. Persico, *Chem. Rev.* 1994, 94(7), 2027. <https://doi.org/10.1021/cr00031a013>
- [39] V. Barone, M. Cossi, J. Tomasi, *J. Chem. Phys.* 1997, 107(8), 3210. <https://doi.org/10.1063/1.474671>
- [40] M. J. Frisch, G. W. Trucks, H. B. Schlegel, G. E. Scuseria, M. A. Robb, J. R. Cheeseman, G. Scalmani, V. Barone, G. A. Petersson, H. Nakatsuji, X. Li, M. Caricato, A. V. Marenich, J. Bloino, B. G. Janesko, R. Gomperts, B. Mennucci, H. P. Hratchian, J. V. Ortiz, A. F. Izmaylov, J. L. Sonnenberg, D. Williams-Young, F. Ding, F. Lipparini, F. Egidi, J. Goings, B. Peng, A. Petrone, T. Henderson, D. Ranasinghe, V. G. Zakrzewski, J. Gao, N. Rega, G. Zheng, W. Liang, M. Hada, M. Ehara, K. Toyota, R. Fukuda, J. Hasegawa, M. Ishida, T. Nakajima, Y. Honda, O. Kitao, H. Nakai, T. Vreven, K. Throssell, J. A. Montgomery Jr., J. E. Peralta, F. Ogliaro, M. J. Bearpark, J. J. Heyd, E. N. Brothers, K. N. Kudin, V. N. Staroverov, T. A. Keith, R. Kobayashi, J. Normand, K. Raghavachari, A. P. Rendell, J. C. Burant, S. S. Iyengar, J. Tomasi, M. Cossi, J. M. Millam, M. Klene, C. Adamo, R. Cammi, J. W. Ochterski, R. L. Martin, K. Morokuma, O. Farkas, J. B. Foresman, D. J. Fox, *Gaussian 16, Revision C.01*, Gaussian, Inc, Wallingford CT 2019.
- [41] G. A. Zhurko, *Chemcraft - Graphical Program for Visualization of Quantum Chemistry Computations*. Available online: Ivanovo, Russia 2005, <https://chemcraftprog.com> (accessed on Apr. 20, 2021).

SUPPORTING INFORMATION

Additional supporting information may be found in the online version of the article at the publisher's website.

How to cite this article: V. Ievtukhov, B. Zadykowicz, M. Y. Blazheyskiy, K. Krzymin'ski, *Luminescence* 2021, 1. <https://doi.org/10.1002/bio.4162>

**New luminometric method for quantification of biological sulphur nucleophiles
with the participation of 9-cyano-10-methylacridinium salt**

Vladyslav Ievtukhov¹, Beata Zadykowicz¹, Mykola Ye. Blazheyevskiy²
and Karol Krzyński^{1*}

¹*Faculty of Chemistry, University of Gdańsk, Wita Stwosza Str. 63, 80–308 Gdańsk, Poland*

²*National University of Pharmacy, Valentynivska Str.4, 61168 Kharkiv, Ukraine*

**Corresponding author. E-mail address: karol.krzymski@ug.edu.pl*

Characteristics of the studied sulphur-containing analytes

N-Acetyl-L-cysteine (NAC) makes a substituted amino acid cysteine. Its wide medical usage involves, among others, the treatment of Paracetamol overdose, psychiatric disorders, relief of cognitive disorders including addiction, autism, compulsive and grooming disorders, schizophrenia, bipolar disorder, and the effects of psychedelic use.

Glutathione (GSH) is a tripeptide possessing a gamma peptide linkage between the carboxyl group of the glutamate side chain and cysteine, contained in plants, animals, fungi, some bacteria, and other living matter. Glutathione, being a strong natural antioxidant, expresses many physiological abilities, among others, can prevent damage to cellular components, caused by reactive oxygen species (ROSs).

D-penicillamine (DPAm) is a trifunctional amino acid, containing a thiol, an amine, and a carboxylic acid groups, structurally resembling the α -amino acid cysteine. It makes a chiral drug with one stereogenic center and exist as a pair of enantiomers. The (S) enantiomer is antiarthritic, while the distomer (R)-penicillamine is toxic. D-Penicillamine makes a medication used for treatment, among others, Wilson's disease (a rare genetic disorder of copper metabolism, cystine kidney stones, rheumatoid arthritis (it prevents collagen from cross-linking), scleroderma, as well as heavy metal poisonings.

Acetylthiocholine (ATCh), chemically a simple ester of tioacetic acid and choline, makes a sulphur analog of acetylcholine - biological compound of great physiological importance, acting in brain and body as the primary neurotransmitter of the parasympathetic nervous system as well as neurotransmitter at the neuromuscular junction, that trigger neurons of to activate muscles.

Table S1 Values of the enthalpies ($\Delta_{r,298}H^0$) and Gibbs' free energies ($\Delta_{r,298}G^0$) (aqueous phase, all values in kcal mol⁻¹) for deprotonation (step 1), radical formation (step 2) and O₂^{-·} conjugation (step 3). All calculations were performed for at the DFT level of theory using the CAM-B3LYP functional and the 6-31G(d,p) basis set.

The steps indicated in the Table are as follows:

1. $\text{RSH} + \text{OH}^- = \text{RS}^- + \text{H}_2\text{O}$ (deprotonation)
2. $\text{RS}^- + \text{O}_2 \rightleftharpoons \text{RS}^\cdot + \text{O}_2^{\cdot-}$ (radical formation)
3. $9\text{-CMA} + \text{O}_2^{\cdot-} \rightarrow 9\text{-CMA-OO}^\cdot$ conjugation (Fig. S1, the first step)
4. $9\text{-CMA-OO}^\cdot + \text{RS}^- \rightarrow 9\text{-CMA-OO}^- + \text{RS}^\cdot$ (Fig. S1, the second step)

Step No.	Investigated substance							
	N-acetyl-L-cysteine		D-Penicillamine		Glutathione		Acetylthiocholine	
	$\Delta_{r,298}H^0$	$\Delta_{r,298}G^0$	$\Delta_{r,298}H^0$	$\Delta_{r,298}G^0$	$\Delta_{r,298}H^0$	$\Delta_{r,298}G^0$	$\Delta_{r,298}H^0$	$\Delta_{r,298}G^0$
1.	-25.5	-26.6	-21.5	-21.6	-30.3	-31.0	-27.4	-28.7
2.	29.6	29.1	24.5	23.3	30.5	30.2	30.8	30.9
9-CMA-OO [·] conjugation								
3.	$\Delta_{r,298}H^0$				$\Delta_{r,298}G^0$			
	-20.8				-10.1			
4.	N-acetyl-L-cysteine		D-Penicillamine		Glutathione		Acetylthiocholine	
	$\Delta_{r,298}H^0$	$\Delta_{r,298}G^0$	$\Delta_{r,298}H^0$	$\Delta_{r,298}G^0$	$\Delta_{r,298}H^0$	$\Delta_{r,298}G^0$	$\Delta_{r,298}H^0$	$\Delta_{r,298}G^0$
	13.1	13.2	8.0	7.4	14.0	14.2	14.3	15.0

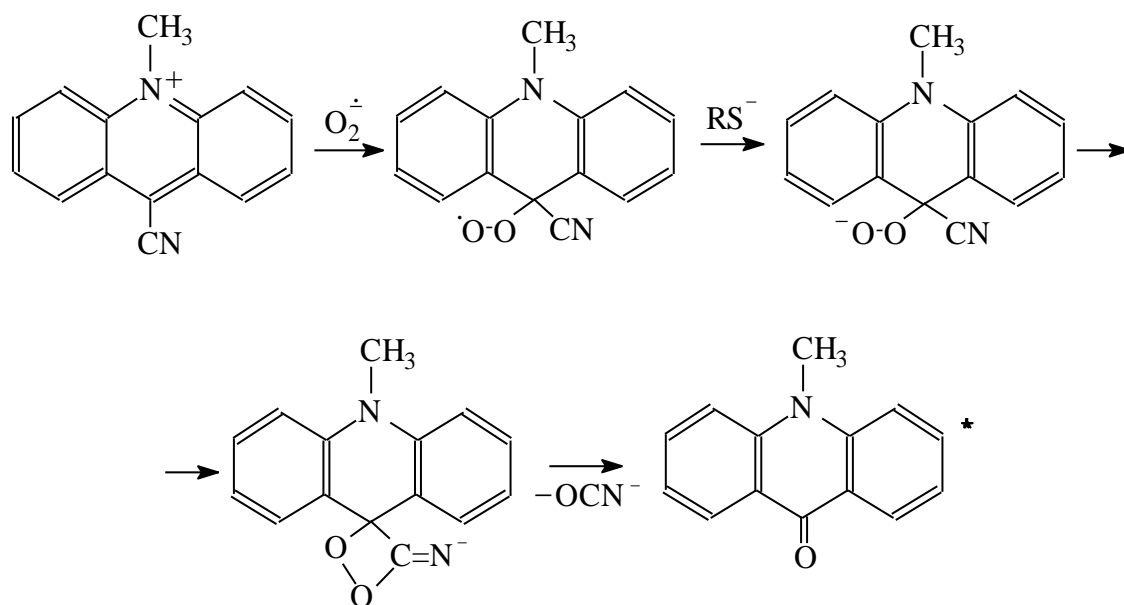
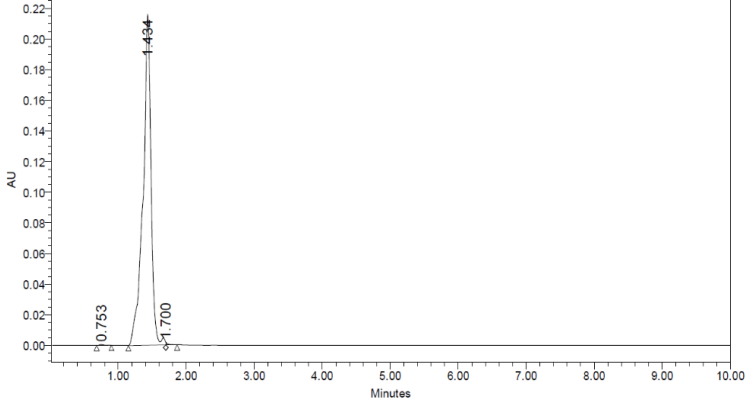
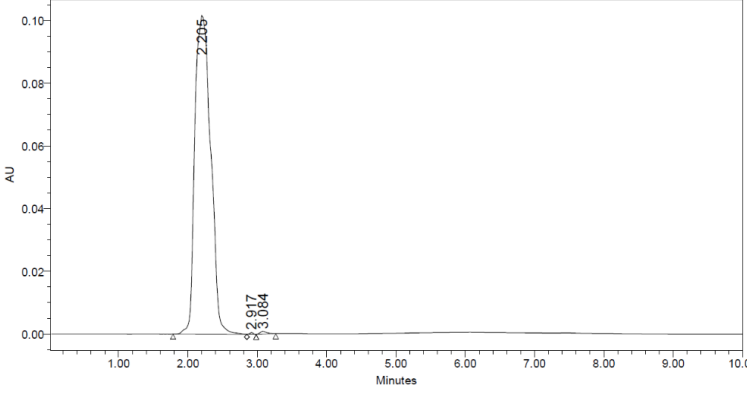
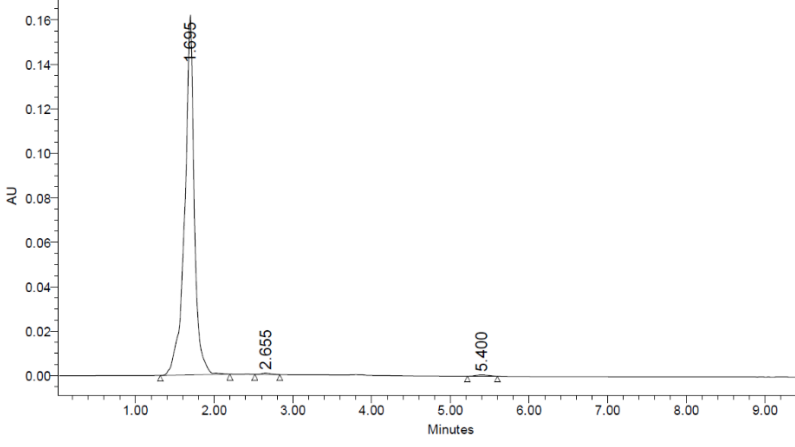
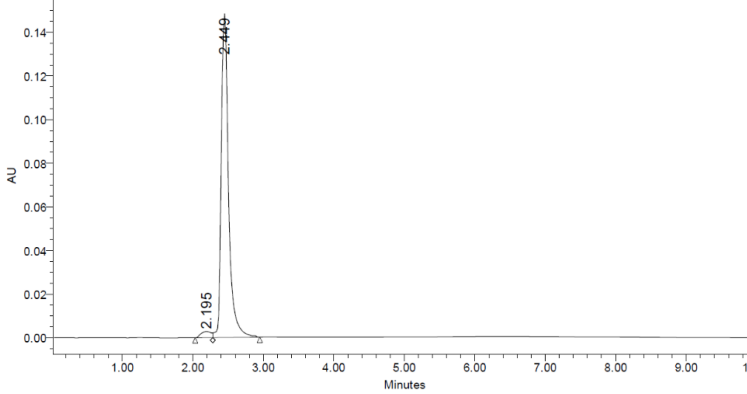


Fig. S1. Formerly proposed scheme of generation of chemiluminescence in the system containing 9-CMA-KOH-oxygen- RS^- [16,17].

Cpd. name/code, wavelength	Chromatogram	Purity (%)
N-acetyl-L-cysteine, (UV-Vis detection at 227 nm)		99.67
Glutathione (227 nm)		99.53
D-penicillamine (227 nm)		99.18
Acetylthiocholine chloride (227 nm)		97.43

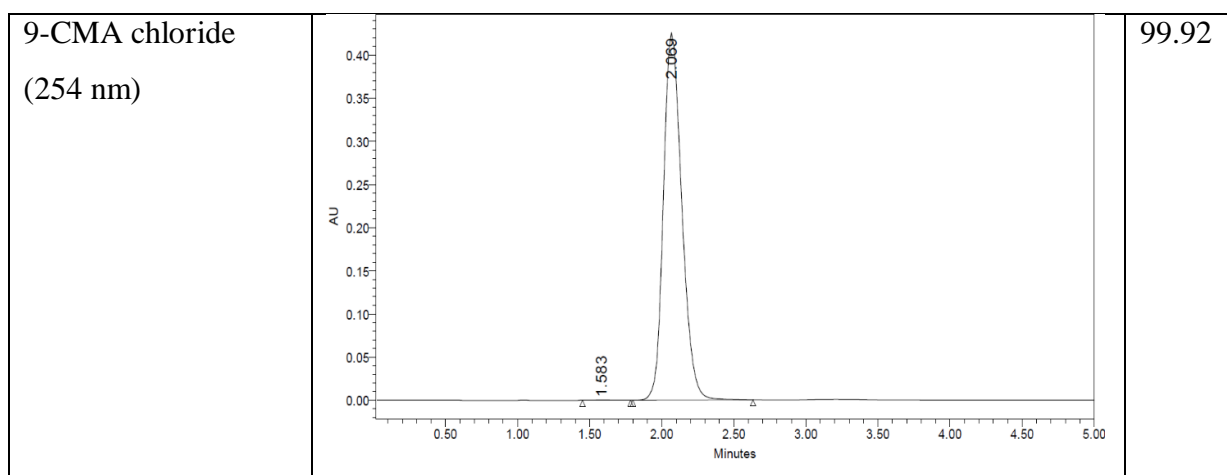


Fig. S2. RP-HPLC analyses of compounds investigated. Experimental conditions were kept constant in all analyses were as follows: stationary phase: Gemini 5 μ C6-Phenyl 110Å, 100×4.6 mm column (Phenomenex); mobile phase: isocratic, 0.7 mL/min, acetonitrile/0.1% TFA in water – 1/1 v/v and isocratic, 0.7 mL/min. (the substrate, 9-CMACl) and phosphate buffer (KH₂PO₄ (26 mM), Na₂HPO₄×2H₂O (40.8 mM), pH = 7)/methanol (8/1 v/v). Absorbance detection at 227 nm and 365 nm (all the analytes).

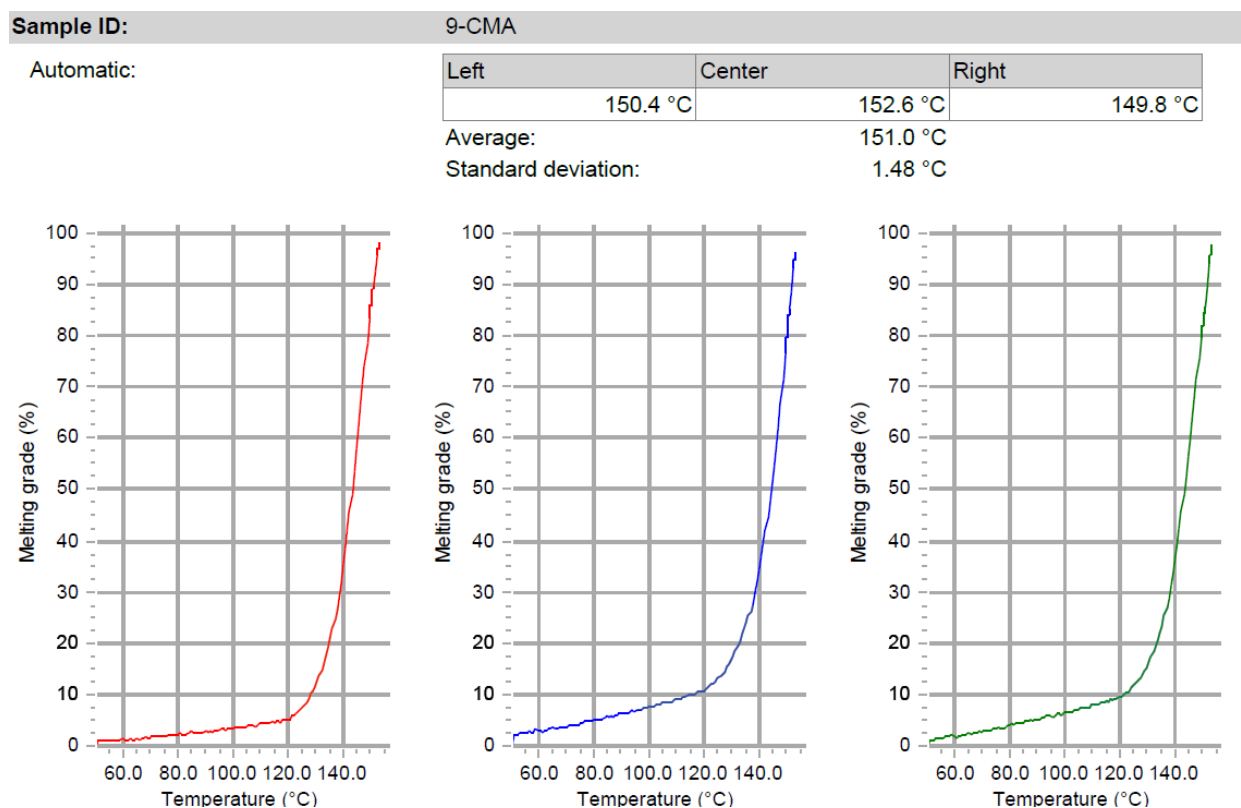


Fig. S3. Graph of dependence of the melting grade on the temperature of 9-CMACl.

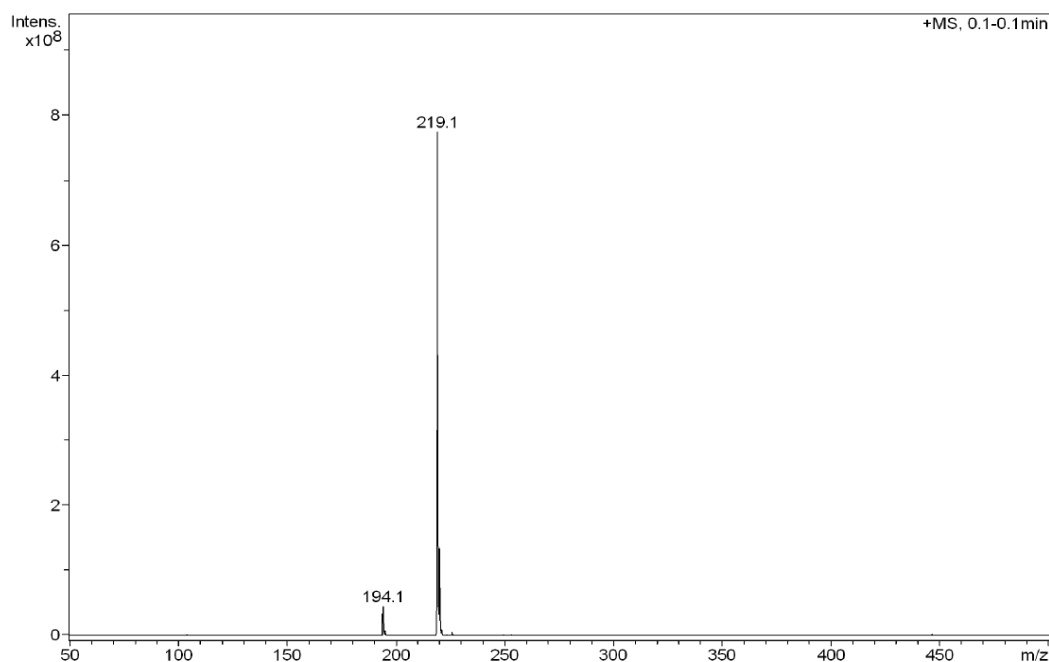


Fig. S4. ESI-QTOF MS spectra (positive mode of acquisition) of 9-CMAcI. Conditions: Triple TOF™ 5600+ MS spectrometer (AB Sciex, Canada), GS1 = GS2 = 30 psi, CUR = 25 psi, TEM = 300 °C, ISVF = 5500 V, CE = 10, DP = 100, V = 20 mL/min. Samples, dissolved in acetonitrile (MS grade, 20 µL) were introduced directly, using glass syringe (Hamilton, USA).

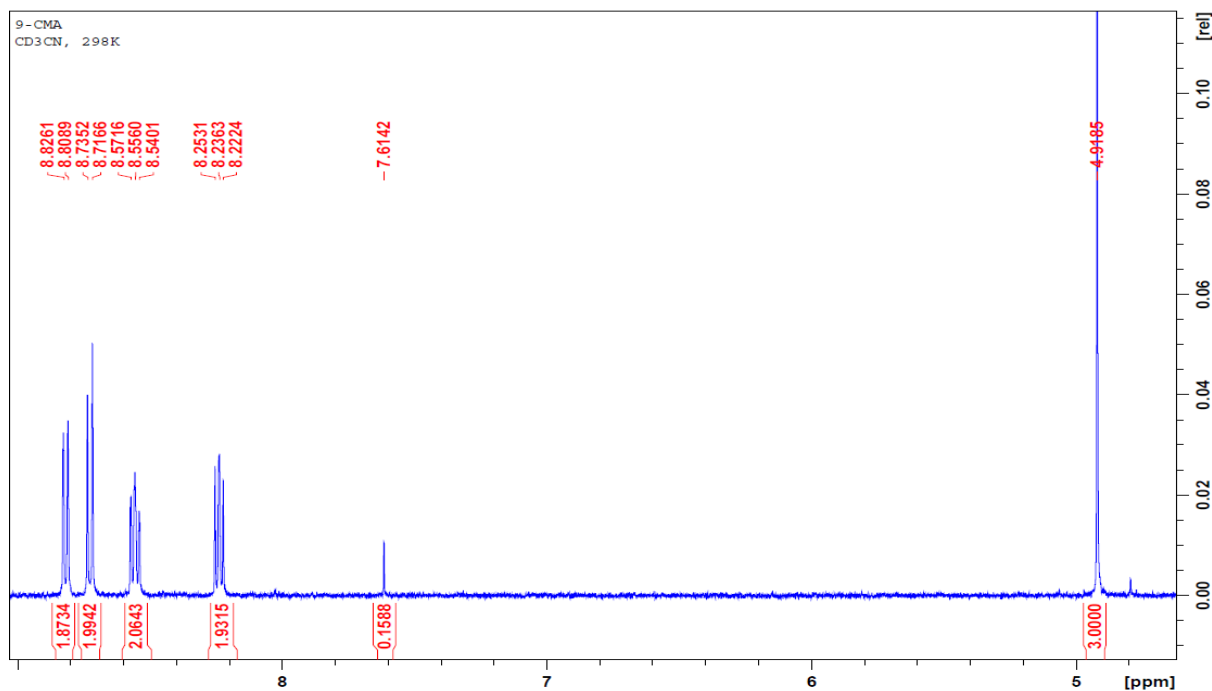


Fig. S5. ¹H NMR spectra of 9-CMAcI. Conditions: frequency 500 MHz, solvent: CD₃CN, room temperature. For details see the Experimental part.

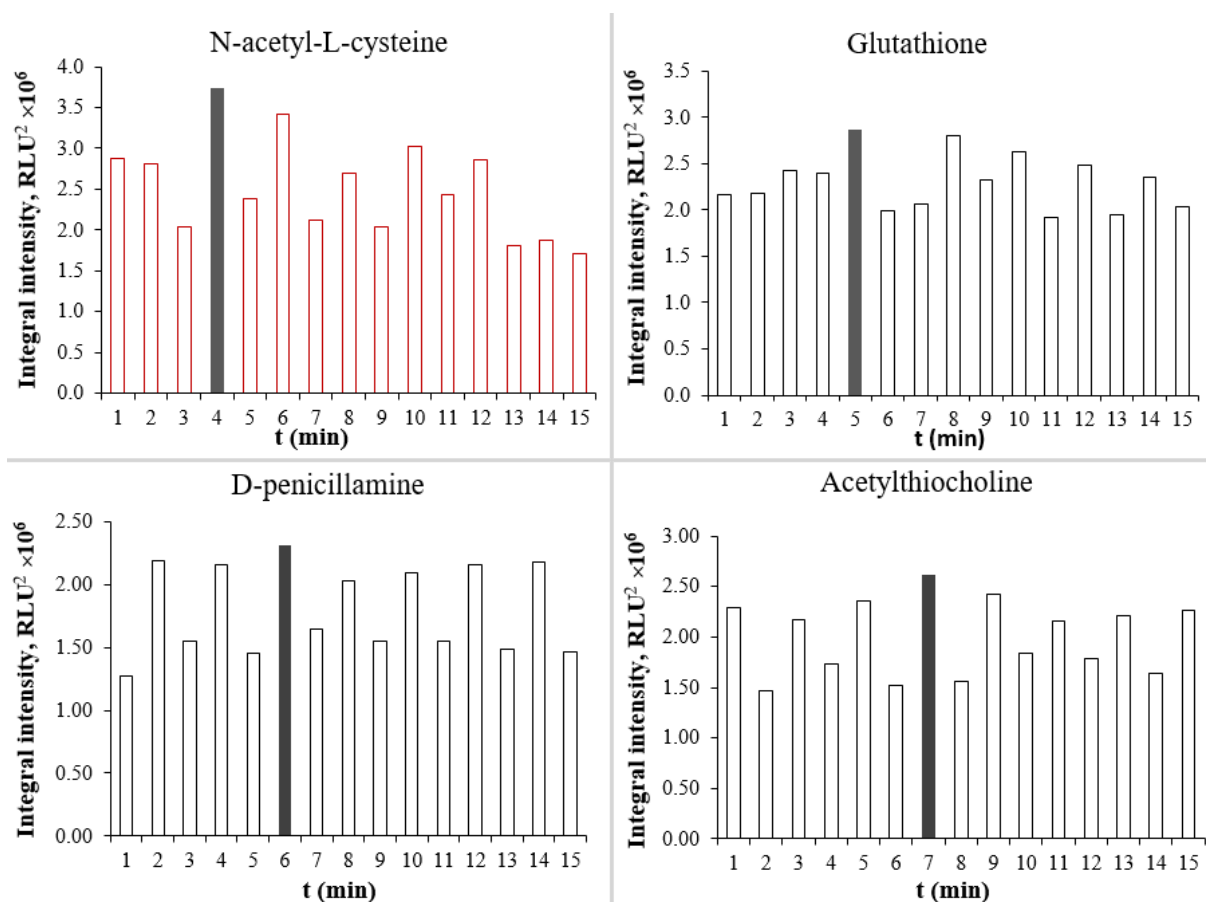


Fig. S6. Optimal efficiency (black marked bars) of emission (measured as areas under curves) vs. incubation time for investigated substances (for details see the Experimental).

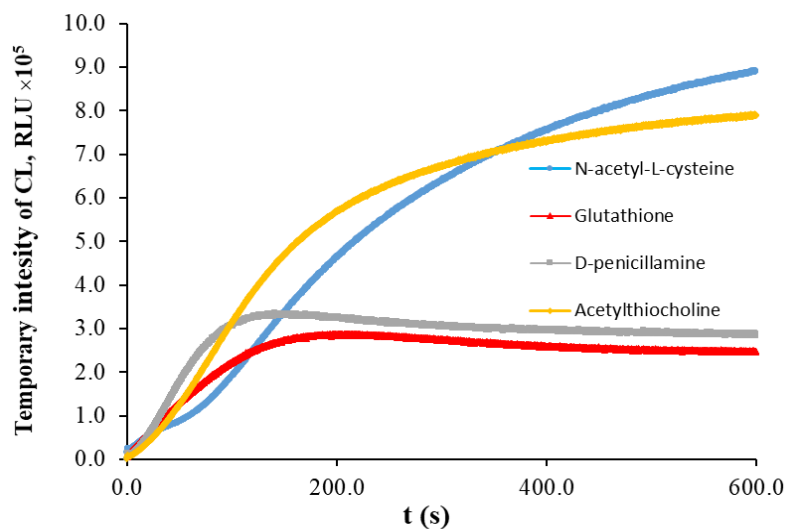


Fig. S7. Plots of temporary CL intensities of researched substances using Lucigenin as CL indicator. The areas under curves in the time frame of 600 s for Acetylthiocholine, N-acetyl-L-cysteine, D-Penicillamine and Glutathione remain in the proportion of 1.00: 0.97: 0.49: 0.42, respectively.

[P3] V. Ievtukhov, M. Mońka, O. Ciupak, I. Bylińska, P. Bojarski, K. Krzymiński, I. E. Serdiuk, Experimental evidences of the excited-state mixing in the blue emitter for organic light-emitting diodes, *Journal of Materials Chemistry C*, 2025, 13, 68-80. DOI: 10.1039/D4TC03925D

PAPER



Cite this: *J. Mater. Chem. C*, 2025, 13, 68

Experimental evidence of the excited-state mixing in the blue emitter for organic light-emitting diodes†

Vladyslav Ievtukhov,^{ab} Michał Mońka,^a Olga Ciupak,^c Irena Bylińska,^b Piotr Bojarski,^a Karol Krzymiński^{id}^b and Illia E. Serdiuk^{id}^{*a}

High hopes have been placed on organic emitters, which are supposed to solve the problem of low stability of blue OLEDs. A peculiar phenomenon of thermally activated delayed fluorescence (TADF), which brought such emitters to the range of the top-studied materials for organic optoelectronics within the last decade, remains poorly understood. Here, we report the results of comprehensive photophysical studies of one of the most successful candidates for blue TADF OLEDs, the TMCz-BO emitter (9-(5,9-dioxo-13*b*-boranaphtho[3,2,1-*de*]anthracen-7-yl)-1,3,6,8-tetramethyl-9*H*-carbazole) characterised by outstanding triplet-harvesting properties. One of the main aims of this work is to understand the reason for these unique properties. Steady-state and time-resolved spectroscopic investigations in media of various polarity, viscosity, and temperature reveal that at least five excited states of different characters and multiplicity are responsible for the emissive and spin-flip transitions in the TMCz-BO molecular systems. First of all, in contrast to typical donor-acceptor TADF emitters, the S_1 state of TMCz-BO does not have a pure charge-transfer character but shows a considerable contribution of the locally-excited state of the acceptor fragment, which provides a fast radiative rate. The T_1 state is a superposition of two locally excited and one charge-transfer states, providing reasonable spin-orbit coupling. Regarding the TADF mechanism in various media, reverse intersystem crossing follows the $T_1 \rightarrow S_1$ model, considering the excited-state mixing, a notion introduced here to explain the triple and dual nature of the respective states. Such a mixing is dynamic in low-viscosity solutions due to low barriers for molecular vibrations. In films with a host matrix, a static excited-state mixing occurs, assisted by the low-amplitude vibrations within the local energetic minimum of the emitting species. The high efficiency of the excited-state mixing in TMCz-BO is explained by the rigid structure of its donor and acceptor fragments and their limited but still active mutual rotations. This provides negligible structural differences between various electronic states, enabling low reorganisation energies favourable for radiative and spin-flip processes while maintaining vibrational activation of spin-orbit coupling. Despite a lower reverse intersystem crossing rate in media of high viscosity, TMCz-BO shows rare near-UV TADF in films with the non-polar host. Our results thus highlight the unique and intriguing properties of TMCz-BO, opening up new perspectives for further research and potential improvements in OLED applications.

Received 12th September 2024,
Accepted 23rd October 2024

DOI: 10.1039/d4tc03925d

rsc.li/materials-c

Introduction

Organic light-emitting diodes, commonly known as OLEDs, represent a cutting-edge technology that has revolutionised the display and lighting industries. OLEDs are a type of light-emitting diode (LED) in which most of the layers, including the emissive one, are composed of organic compounds. Unlike traditional LEDs or liquid crystal displays (LCDs), OLEDs are characterised by their self-emissive nature, allowing each pixel to emit light independently. The fundamental principle behind OLEDs lies in the emissive nature of the organic material used. The parameters of such organic compounds can be adjusted to

^a Faculty of Mathematics, Physics and Informatics, University of Gdańsk, Wita Stwosza 57, 80-308 Gdańsk, Poland. E-mail: illia.serdiuk@ug.edu.pl; Tel: +48 58 523 22 44

^b Faculty of Chemistry, University of Gdańsk, Wita Stwosza 63, 80-308 Gdańsk, Poland

^c Department of Organic Chemistry, Gdańsk University of Technology, Gabriela Narutowicza 11/12, 80-233 Gdańsk, Poland

† Electronic supplementary information (ESI) available. See DOI: <https://doi.org/10.1039/d4tc03925d>

emit light of different colours when an electric current is applied. This unique property enables OLED displays to achieve deeper blacks, higher contrast ratios, and a wider range of vibrant colours as compared to conventional display technologies.

Despite the accent on “organic” in the title, commercial OLEDs still rely on heavy metals as crucial components of the light-emitting layers. Heavy-metal organic complexes, or so-called OLED emitters of the second generation, apply the phosphorescence principle to convert triplet exciton energy from electric excitation to light, thus achieving quantitative internal quantum efficiency. Despite the high efficiency and stability of such emitters of different colours, environmental issues and especially low stability in the blue region stimulated great efforts in the research of all-organic emitters, specifically blue ones.

The key problem of all-organic emitters that should be solved is triplet harvesting. In the context of OLEDs and organic semiconductors, triplet excitons or states refer to a specific electronic configuration of the excited species. In organic materials, when a photon is absorbed, it can create an exciton, which is essentially an electron–hole pair bound together. This exciton can exist in the two spin states: singlet and triplet. Singlet excitons can pair electron and hole spins that are antiparallel. They are characterised by a total spin angular momentum of 0. On the other hand, triplet excitons have paired electron and hole spins that are parallel, giving a total spin angular momentum of 1. Typically, triplet excitons, or analogously triplet states of molecules, have longer lifetimes than singlet ones as their deactivation to the ground state requires spin change. Such long lifetimes above tens of microseconds cause a decrease in the efficiency and stability of OLED devices. Efficient harvesting and utilisation of both singlet and triplet states thus contribute to improved device performance, including enhanced external quantum efficiency and lower power consumption.

Thermally activated delayed fluorescence (TADF)¹ is one of the most promising solutions for the triplet harvesting problem, enabling 100% of internal quantum efficiency (IQE) and up to 40% of external quantum efficiency (EQE) in the TADF OLED devices.^{2,3} The latter feature brought organic emitters closer to their second-generation analogues and paved the way for their commercial applications. TADF is based on the reverse intersystem crossing (rISC) process, the “return” of excitons from T_1 to S_1 and further fluorescence. TADF molecules emit light in two regimes: prompt fluorescence (PF) and delayed fluorescence (DF). PF occurs from the S_1 state excited directly by photo- or electro-excitation. Delayed fluorescence also occurs from the S_1 state but is derived from T_1 produced by electroexcitation or photoexcitation to S_1 and further intersystem crossing (ISC). In TADF emitters, the rISC rate parameter is the most important for triplet harvesting. When other parameters are unchanged, the faster the rISC rate and the shorter the DF lifetime, the higher the TADF efficiency and – as a result – the OLED stability.⁴

The mechanism of rISC has been investigated extensively within the last decade. In general terms, rISC is a spin–forbidden process that occurs in the (milli)second-time domain, which is too

slow for OLED applications. To achieve fast rISC in the sub-microsecond domain, efficient TADF emitters have to meet the criteria of a minor (<0.2 eV) energy gap between S_1 and T_1 (ΔE_{ST}) and reasonable spin–orbital coupling (SOC). Several molecular design strategies developed recently enable rISC in micro- and even sub-microsecond time domains.^{5–8} The most efficient and reliable method combines strong donor (D) and strong acceptor (A) fragments that are connected orthogonally. Such strategy leads to (i) spatial separation of highest occupied and lowest unoccupied molecular orbitals (HOMO and LUMO, respectively), (ii) formation of singlet and triplet states of charge transfer character, 1CT and 3CT , respectively, and (iii) decrease in the exchange energy and thus reduction of the energy gap (ΔE_{ST}).

The origin of relatively high SOC in such organic D–A molecules is still debated. In the frames of the classic quantum physical approach, usually applied to describe electronic properties of molecules (referred further as a static quantum model), the excited states are regarded as single-configurational systems or, in other words, of fixed electronic character and energy values. The transition between two excited states with the same multiplicity, but different character occurs *via* internal conversion (IC). Due to the spin selection rule, the transition between two states with the same character but different multiplicity is forbidden. Therefore, in D–A emitters, SOC between 1CT and 3CT states of the same character should be zero. With the assumption that $^3CT \rightarrow ^1CT$ is forbidden, the three-state rISC model was developed. It relies on the presence of another energetically proximate triplet state of a different CT nature or, more often – a locally excited state involving a donor (3LE_D) or acceptor (3LE_A) fragment. According to this model, the highest rISC rate is achieved when the 3LE state aligns energetically^{9,10} and vibronically¹¹ with the 3CT or 1CT states. The distinguishing difference between the CT and LE states is the dipole moment. Significant dipole moments of the CT states cause high sensitivity to the polarity of the medium, which is not the case for weakly polarised LE states. Within the static quantum model, this means that the energy gaps ΔE_{CT-LE} can be altered by polarity. CT and LE states also have different geometry, affecting another important parameter – reorganisation energy (λ). Regarding Marcus’s theory, the smaller the λ , the faster the electronic transition.

Molecular vibrations are crucial for SOC in D–A emitters and are the basis of another, two-state rISC model. It was shown that in the emitters with strongly stabilised CT states, the $^3CT \rightarrow ^1CT$ transition is, in fact, not forbidden and can be highly efficient, playing a crucial role in the rISC process. In this case, the molecular motions activate SOC, which changes the dihedral angle (θ) between the D and A fragments. Together with the $\Delta E_{^1CT-^3CT}$ and $\lambda_{^1CT-^3CT}$ values of a few meV, this affords fast rISC up to the sub-microsecond domain in polar media¹² and/or in strong D–A emitters.¹³ In the media of low polarity or when $\Delta E_{^1CT-^3CT}$ is increased by weakened A and/or D, the $^3LE-^1CT$ transition can compete with $^3CT-^1CT$, affording a usually slower multichannel mechanism for rISC. The decrease of the rISC rate in weak DA systems is the main reason for the

continuous lack of fast-rISC deep-blue emitter and has been a persistent challenge in the field of organic electronics.

Some examples of the extensive studies on blue emitters are discussed briefly below. In the work¹⁴ authors report two deep-blue emitters based on the 2,12-di-*tert*-butyl-5-oxa-9-thia-13*b*-boranaphtho[3,2,1-*de*]anthracene acceptor and two weak donors for blue emission: carbazole (PhCz-TOSBA) and triphenylamine (TPA-TOSBA). The emitters showed PL_{max} of 454 and 467 nm, lifetimes of DF (τ_{DF}) of 47 μ s and 140 μ s and k_{rISC} values of 4×10^4 s⁻¹ and 1.9×10^4 s⁻¹, respectively, in the doped films. The EQE_{max} values for OLED devices did not exceed 17% in both cases. In the work of Niu *et al.*,¹⁵ authors combined a relatively weak but sterically hindered 1-methyl-carbazol donor with a triphenyl-*s*-triazine acceptor. The resulting 1-MeCz-TRZ emitter in 10 wt% DPEPO doped film showed PL_{max} of 449 nm and τ_{DF} value of 24.8 μ s. OLED devices showed EQE_{max} of 13.1%. In the work,¹⁶ authors introduced a series of indenocarbazole derivatives, featuring substitutions at the 2,3 and 3,4 positions on the carbazole moiety with various groups, and such donors were coupled with a triphenyl-*s*-triazine acceptor. The InCz34DPhtz emitter bearing diphenyl (DPH) groups performed best with a PL_{max} of 475 nm and high PLQY of 97.9% in 10 wt% DPEPO doped film. The τ_{DF} time was equal to 70.3 μ s and k_{rISC} value of 1.6×10^4 s⁻¹. In OLED devices, the InCz34DPhtz emitter enabled EQE_{max} of 25.9% with strong roll-off at 1000 cd m⁻² reaching 20.6%. Such examples illustrate the general problem mentioned above of blue TADF emitters: the decreased CT strength required for deep-blue emission causes long DF lifetime, low EQE and/or low operational stability of OLED due to slow rISC.

According to the photophysical and electroluminescent characteristics, the TMCz-BO (Fig. 1) molecule, consisting of 1,3,6,8-tetramethyl-9*H*-carbazole (TMCz) donor and 5,9-dioxo-13*b*-boranaphtho[3,2,1-*de*]anthracene (BO) acceptor (Fig. 1) described in ref. 17 by Adachi and coworkers remains one of the best deep-blue emitters up to date. Authors reported a short τ_{DF} lifetime of 0.75 μ s, a high k_{rISC} value of 1.9×10^{-6} s⁻¹ and EQE_{max} of 20.7%. The key parameter is the low-efficiency roll-off of the OLED device below 3.5%, measured at a high luminance of 1000 cd m⁻². Such a small roll-off indicates high stability and potential for commercialisation in blue OLEDs. Excellent exciton dynamics in 30 wt% PPF films were explained

by the small activation energy of rISC (13.4 meV) and an energetical proximity of the LE_A state localised on the BO acceptor. The latter attributed to a much larger SOC value for the 3LE \rightarrow 1CT transition, reaching 0.12 cm⁻¹, than the ³CT \rightarrow ¹CT one, equal to 0.001 cm⁻¹. The authors thus suggested the three-state rISC in TMCz-BO: ³CT \rightarrow ³LE \rightarrow ¹CT.

Taking into account the outstanding TADF features of the TMCz-BO emitter and the importance of understanding the mechanism of enhanced rISC for further progress in the blue OLED technology, we took a deeper look at the photophysics of this emitter in various media. Our results indicate that in TMCz-BO, the rISC rate can be increased substantially with the increase of polarity both in liquid and amorphous solid state. Moreover, a strong dependence on medium viscosity was also observed. The complex photophysical behaviour of this emitter is accomplished by the coexistence of the two singlets and three triplet excited states, which distinguish TMCz-BO from other D-A emitters with three or two key excited states. Our findings indicate that, in TMCz-BO, the TADF mechanism lies far beyond the three-state rISC model, and even the well-known bases of the static quantum model should be upgraded to explain the intense mixing of the excited states at room temperature.

Experimental and computational methods

Reagents and materials

TMCz-BO was synthesised according to the synthesis route described in ref. 17. A comparison of the results of the analyses confirmed the structural identity and purity of the above compound. Solvents of spectroscopic grade were used for all solvatochromic measurements. Solvents mentioned below were selected to enable gradual change of photoluminescence maximum of TMCz-BO. All reagents were purchased and used without further purification.

Sample preparation

Films were prepared on quartz glass using a solution-processing technique, applying the spin-coating method from the CHCl₃ solutions of the emitter and appropriate host. A ULTRON ultrasonic bath (TME Electronic Components, Poland) was used before spin-coating to facilitate the solubility of compounds.

Apparatus

UV-vis absorption spectra were recorded using a Shimadzu UV-1900 spectrophotometer. Steady-state photoluminescence (PL) spectra were recorded employing the FS5 spectrofluorometer (Edinburgh Instruments, UK) using front-face excitation geometry with a 1 nm spectral resolution. Absolute PL quantum yields (PLQYs) for films were measured using an integrating sphere included in the Quantaurus-QY Absolute PL quantum yield spectrometer. PLQYs for solutions were measured using the FS5 spectrofluorometer. Steady-state phosphorescence spectra in solvents were measured in liquid nitrogen (77 K) quartz dewar using a Varian spectrofluorometer with a 50 ms

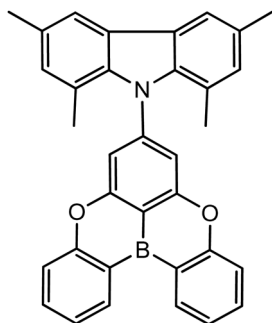


Fig. 1 Structure of the TMCz-BO molecule.

delay time and 0.5 s time gate. Time-resolved measurements were performed using a customised system consisting of a pulsed YAG:Nd laser (PL2251A, EKSPLA) coupled with an optical parametric generator (PG 401/SH) as the excitation light source and 2501S grating spectrometer (Bruker Optics) combined with a streak camera system (C4334-01 Hamamatsu) as (the detection unit).¹⁸ The system was equipped with a double-stage high vacuum pump (T-Station 85 Edwards). To reduce scattering, reflections and secondary order artefacts, a set of various high-performance optical bandpass (BP) and longpass (LP) filters were used in the excitation path 325/50BP, together with LP filter 375LP (Edmund Optics). Streak camera images were integrated over a constant specified wavelength interval to build PL intensity decay profiles. Phosphorescence measurements in films were recorded using a closed-cycle helium cryostat (APD DE-202) and a temperature controller (LakeShore 336). Photophysical constant rates k_r , k_{ISC} and k_{rISC} were calculated according to equations described in ESI,[†] Section 1. Fityk¹⁹ and Origin²⁰ programs were used for the plot building and fitting.

Quantum-chemical calculations

Quantum chemical calculations were conducted at the DFT/TD-DFT level of theory using the Gaussian 16 program package.²¹ The B3LYP,²² CamB3LYP,²³ M06,²⁴ M062X,²² PBE0²⁵ functionals were used with cc-pVDZ²⁶ basis set for geometry optimizations in various electronic states. Spin-orbit coupling (SOC) constants were computed using the ORCA 4.2 software package²⁷ with B3LYP functional and DEF2-TZVP²⁸ basis set with included relativistic zero-order regular approximation (ZORA).²⁹

Results and discussion

Steady-state absorption and PL in liquid solutions

We start the discussion of electronic properties with the absorption spectra analysis, which provides information on the properties of molecules in the ground state geometry. In nonpolar methylcyclohexane (MCH), the long-wavelength absorption of TMCz-BO is represented by a narrow and intense band (Fig. 2A) with the molar extinction coefficient ϵ of $15\,100\text{ L mol}^{-1}\text{ cm}^{-1}$ at the peak maximum of 378 nm. This feature is somewhat unusual for the D-A type TADF emitters, whose long-wavelength absorption band is broad, structureless, and has much lower ϵ below $2000\text{ L mol}^{-1}\text{ cm}^{-1}$.³⁰ Such a low-intensity absorption is typically ascribed to the charge-transfer (CT) band. It evidences the formation of the CT state, which has crucial importance for TADF, as was mentioned above. On the contrary, TMCz-BO shows absorption similar to that of the isolated BO acceptor unit. This indicates the locally excited nature of its $S_0 \rightarrow S_1$ transition, which involves the electronic density on the BO fragment: the $S_0 \rightarrow {}^1\text{LE}_A$ transition. Slightly broadened absorption of TMCz-BO in the blue edge indicates that the $S_0 \rightarrow {}^1\text{CT}$ transition is characterised by higher energy and strongly overlaps with more intense $S_0 \rightarrow {}^1\text{LE}_A$. Moreover, absorption spectra of TMCz-BO are identical in non-polar methylcyclohexane (MCH) and other solvents, including

polar dimethyl sulfoxide (DMSO). The lack of solvatochromism led us to the conclusion that independently of the polarity of the medium in the ground state geometry, the $S_0 \rightarrow S_1$ transition in TMCz-BO leads to the formation of the singlet locally-excited state ${}^1\text{LE}_A$ localised on the acceptor fragment.

On the other hand, strong changes are observed in the photoluminescence (PL) spectra under the solvent change. In nonpolar MCH, fluorescence and absorption spectra follow the mirror image rule, preserving vibrational structure in liquid solution at room temperature (RT, Fig. 2D) and in frozen glass at 77 K (Fig. 2B), where solvent relaxation is blocked due to high viscosity. Absorption and PL spectra overlap substantially (Fig. S1, ESI[†]), showing a small Stokes shift value of 0.06 eV (77 K) and 0.20 eV (RT). Under such conditions, the emission of TMCz-BO is very similar to that of the isolated acceptor molecule (Fig. S2, ESI[†]), revealing its ${}^1\text{LE}_A$ -state origin. At 77 K, when moving from MCH to more polar benzene, the fluorescence maximum shifts from 385 nm to 416 nm, whilst its band shape maintains the narrow shape and vibronic structure of the ${}^1\text{LE}_A$ fluorescence (Fig. 2B and 3A). With further growing polarity in frozen chlorobenzene, 1,2-dichloroethane (DCE), and especially DMSO, the fluorescence band gradually becomes broad and structureless, and its maximum wavelength reaches 445 nm in DMSO. Thus, one can suggest that the ${}^1\text{CT}$ character plays an important role in the S_1 state under the increase of polarity and becomes dominant in DMSO.

At room temperature, the polarity effect is much more pronounced (Fig. 2D): the fluorescence maximum shifts from 403 nm (MCH) to 557 nm (DMSO), while the PL band becomes broad and structureless. Such a strong positive solvatofluorochromism and shape changes indicate that the ${}^1\text{CT}$ state is dominant in most of the discussed solvents, except for MCH. The observed temperature effect indicates the importance of solvent relaxation in the formation and stabilisation of the ${}^1\text{CT}$ state. For example, according to the comparison of fluorescence maxima at 77 K and RT in DMSO, solvent relaxation is responsible for more than 0.55 eV decrease of the S_1 -state energy, most likely *via* efficient ${}^1\text{CT}$ stabilisation.

The discussed temperature-dependent solvatofluorochromic investigations led us to conclude that, at room temperature, the S_1 state of TMCz-BO has a dual nature. Depending on the medium, ${}^1\text{LE}_A$ or ${}^1\text{CT}$ characters can dominate, or both can contribute. In this context, the radiative rate constant (k_r) can serve as an adequate measure of the contribution of the ${}^1\text{LE}_A$ character. The ${}^1\text{LE}_A \rightarrow S_0$ transition in BO analogues is usually more intense³¹ than the ${}^1\text{CT} \rightarrow S_0$ one, which is “forbidden” by the selection rule due to non-overlapping transition molecular orbitals. In fact in MCH, where the ${}^1\text{LE}_A$ character dominates, the k_r value is the highest reaching $1.7 \times 10^7\text{ s}^{-1}$, and decreases to $3.5 \times 10^6\text{ s}^{-1}$ in the most polar DMSO where ${}^1\text{CT}$ dominates (Table 1). The k_r value shows strong logarithmic dependence on the energy of the S_1 state (E_{S_1}), an effective internal measure of medium polarity in D-A emitters (Fig. 3B). This illustrates the effect of increasing contribution of the CT character in the S_1 state with the increasing polarity due to more efficient separation of frontier molecular orbitals, reduction of the oscillator strength and consequent decrease of k_r .

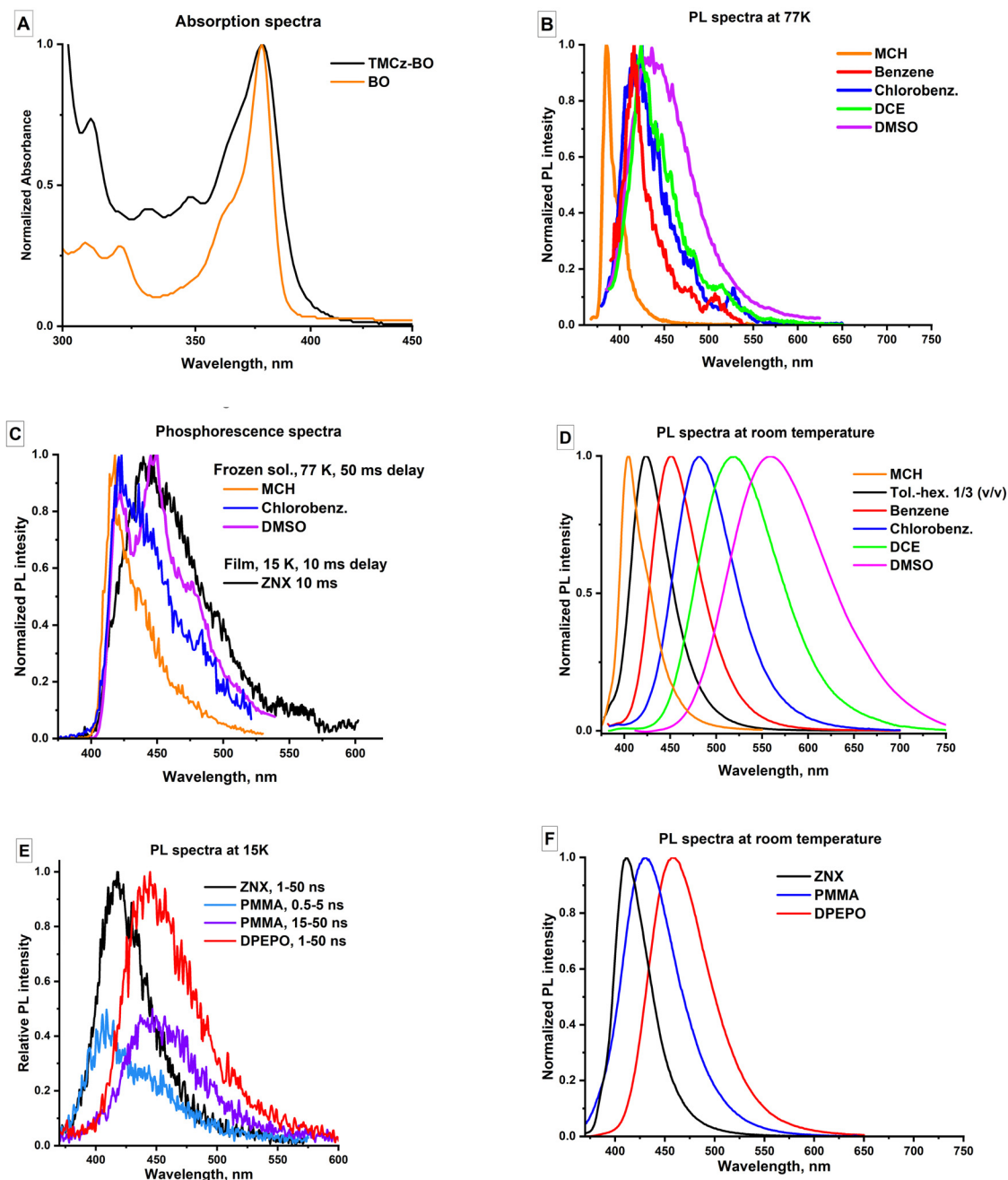


Fig. 2 Absorption spectra of TMCz-BO and the isolated acceptor (BO) in MCH (A). Emission spectra of TMCz-BO in various solvents: PL at 77 K (B), phosphorescence at 77 K (C), and fluorescence at room temperature (D). Films: time-resolved emission spectra at 15 K (E) and stationary PL spectra at RT (F).

Next, the nature of the triplet excited state was analysed based on phosphorescence spectra at 77 K. In MCH, the phosphorescence spectra of TMCz-BO and BO are very similar (Fig. S3, ESI[†]), indicating the $^3\text{LE}_\text{A}$ character of T_1 . In the row benzene, chlorobenzene, and DCE, the increase of polarity causes bathochromic shift and broadening of the spectra, which may indicate the growing contribution of ^3CT (Fig. 2C and Fig. S4, ESI[†]). A peculiar behaviour is observed for DMSO, where TMCz-BO unexpectedly exhibits phosphorescence similar to the donor fragment TMCz (Fig. S5, ESI[†]). This may

indicate the effect of specific intermolecular interactions on the triplet state character: DMSO has high basicity and nucleophilicity, which causes selective stabilisation of the triplet state localised on the donor fragment ($^3\text{LE}_\text{D}$).

Following a so-called static quantum model, which assumes the lack of electronic state mixing, a qualitative alignment of the lowest excited states at 77 K is presented in Fig. 3A. The energies of ^1CT and $^1\text{LE}_\text{A}$ states were estimated by deconvolution of fluorescence spectra in benzene solution of TMCz-BO at 77 K, respective values for triplets $E_{^3\text{LE}_\text{A}}$, $E_{^3\text{CT}}$, and $E_{^3\text{LE}_\text{D}}$

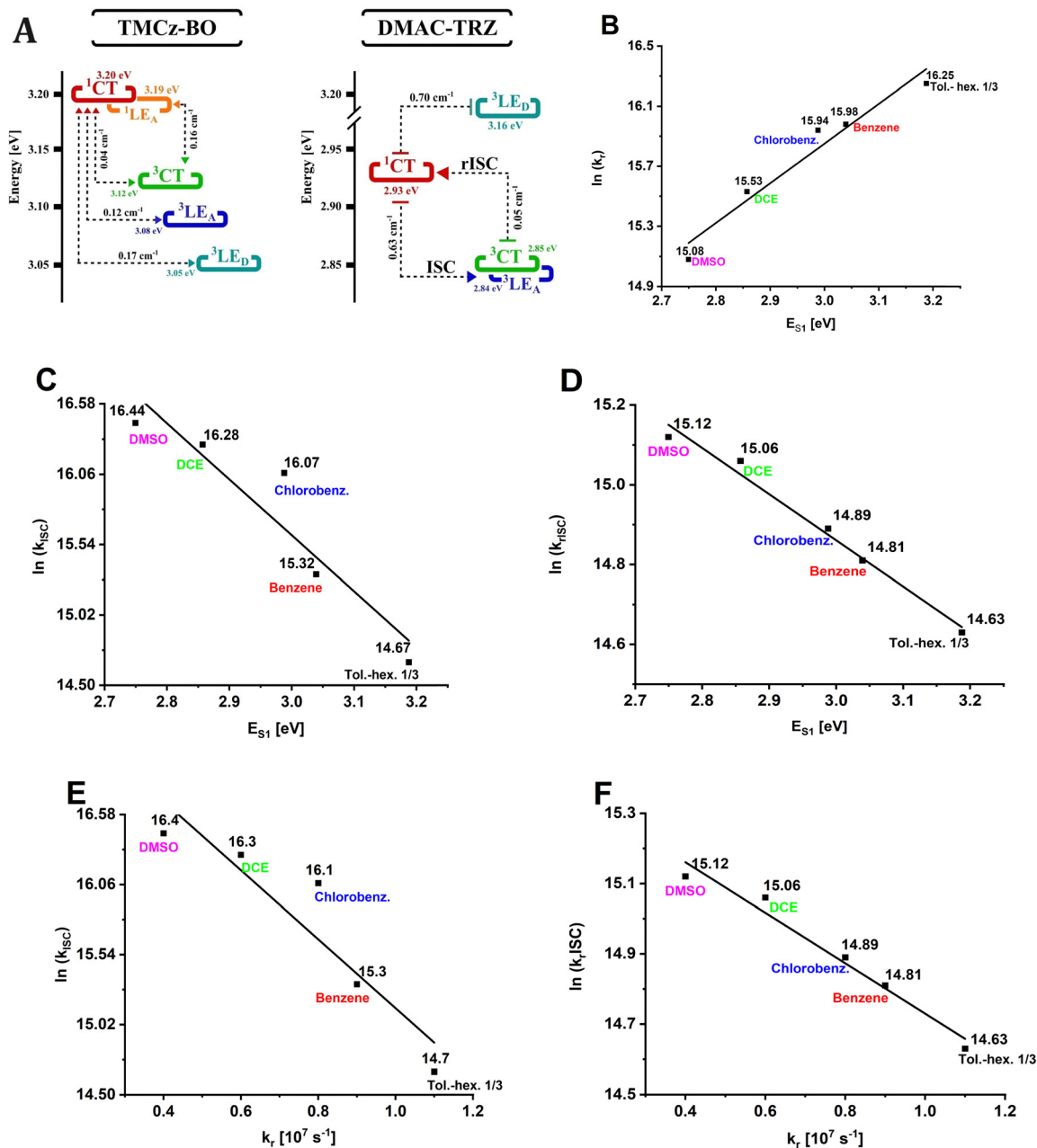


Fig. 3 An illustrative energy diagram of the lowest excited states of TMCz-BO at 77 K with the TDDFT-predicted SOC values showed (A). The dependencies of the natural logarithm of k_r (B), k_{ISC} (C), and k_{rISC} (D) on the energy of S_1 state (E_{S1}) in solutions. The dependencies of $\ln(k_{rISC})$ (E) and k_{ISC} (F) on k_r in solutions. For fitted equations and R^2 parameters see Table S1 (ESI†).

estimated from the phosphorescence spectra in MCH, benzene, and DMSO solutions, respectively. At room temperature, under polarity variations, solvent relaxation and specific medium effects, the alignment of states can be different. However, it is important to notice that there are at least five excited states of close energy: 1LE_A , 1CT , 3LE_A , 3CT , and 3LE_D , which can participate in photophysical processes.

Calculations on various levels of theory support these experimental findings. Whilst the predicted energy of a selected state differs depending on the computational method, the analysis of the transition molecular orbitals confirms the coexistence of

the five lowest excited states 1LE_A , 1CT , 3LE_A , 3CT , and 3LE_D (Fig. S6, ESI†). The excited singlet localised on the TMCz donor, 1LE_D , has sufficiently higher energy above 3.8 eV and is relatively inactive in terms of optical and photophysical properties.

PL in films

As was reported previously,¹⁷ TMCz-BO has a specific potential in OLED applications, where it can be used as a dopant dispersed in a solid host material. For this reason, we further analysed the electronic states in films of different hosts: nonpolar Zeonex® (ZNX), polar bis[2-(diphenylphosphino)phenyl]ether oxide (DPEPO),

Table 1 Photophysical properties in liquid solutions and amorphous films

Medium	λ_{abs} [nm]	PL_{max} [nm]	$\text{PL}_{\text{onset}}/E_{\text{S}_1}$ [nm]/[eV]	PLQY [%]	τ_{PF}^a [ns]	τ_{DF}^a [μs]	k_{r}	k_{nr}	k_{ISC}	k_{rISC}
							[10^6 s^{-1}]			
Solutions										
MCH	378	405	386/3.21	12	7	—	17	—	—	—
Tol.-hex. 1/3 (v/v)		424	389/3.19	20	17	0.46	11	46	2.4	2.3
Benzene		450	408/3.04	37	36	0.44	8.7	15	4.5	2.7
Chlorobenzene		482	415/2.99	66	45	0.60	8.4	4.3	9.5	2.9
DCE		519	434/2.86	57	46	0.64	5.5	4.2	12	3.5
DMSO		557	451/2.75	45	46	0.75	3.5	4.3	14	3.7
Films										
ZNX	378	411	377/3.31	50	8.6	149	14	29	73	1.8×10^{-2}
PMMA		430	381/3.25	53	19	52	14	15	21	3.1×10^{-2}
DPEPO		459	411/3.02	69	21	9.0	22	11	10	0.14

^a Average PF and DF lifetimes. For details see ESI, Section 1.

and medium polarity polymethyl methacrylate (PMMA), which helps to differentiate the emitting species.³⁰

As depicted in Fig. 1E and F, in ZNX at both 15 K and RT, TMCz-BO shows blue-UV emission with PL_{max} at 411 nm and full width at half maximum (FWHM) of 40 nm (0.29 eV). Time-resolved emission spectra (TRES) at RT evidence a 7 nm red-shift within the first 10 ns of prompt fluorescence and reverse blue-shift after the 10 μs of the delayed fluorescence (Fig. S7, ESI†). In polar DPEPO films, the PL spectrum is sufficiently red-shifted and broader with PL_{max} at 459 nm and FWHM of 70 nm (0.40 eV); at 15 K, TRES show negligible changes in time, whilst at RT, a relatively small 7 nm (40 meV) red-shift is observed within the first 10 ns of prompt fluorescence, with further stable PL_{max} of the delayed fluorescence at >200 ns (Fig. S8, ESI†). In films of D-A TADF emitters, strong spectral dependence on the delay time after excitation is usually caused by the rotational isomerism of the emitter involving the dihedral angle θ between the donor and acceptor fragment.^{13,32} For example, under the same conditions, the DPEPO film of popular TADF emitter, DMAC-TRZ, shows more than twice as much shift of 35 nm (160 meV), indicating much higher conformational disorder and inhomogeneity of the emitting species as compared to TMCz-BO.

On the other hand, in a medium-polar PMMA at 15 K, TMCz-BO exhibits dual fluorescence resembling the bands observed in both ZNX and DPEPO. The transformation of two spectral bands is well distinguished in TRES: within the first few nanoseconds, the 410 nm band transforms into the broad 450 nm band (Fig. 2E). At higher temperatures, such spectral changes are faster and more intense. During the first 50 ns, the PL_{max} shifts from 420 nm to 455 nm, and the reverse shift occurs in the delayed fluorescence region from 1 μs to 1 ms (Fig. S9, ESI†). As was concluded from absorption spectra, excitation provides the $^1\text{LE}_\text{A}$ state. Thus, the observed spectral changes indicate its transformation to the ^1CT one. Considering the conclusions made for the liquid solutions, we suggest that the contributions of $^1\text{LE}_\text{A}$ and ^1CT characters are decisive in the S_1 state in ZNX and DPEPO films, respectively, but in PMMA, their contributions are comparable.

At 15 K, the phosphorescence spectra in films differ from those in frozen solutions by their almost identical shape and

maximum in all types of studied solid hosts (Fig. S10, ESI†). This indicates that under such conditions, the nature and energy of the T_1 state are negligibly affected by medium parameters. There is no reliable information on the contribution of $^3\text{LE}_\text{A}$, $^3\text{LE}_\text{D}$, or ^3CT characters, but the complex and broad shape of the phosphorescence spectra indicates that these characters can be strongly mixed. At this point, we assume that when moving from liquid solutions to solid matrices, the high viscosity of the medium plays a key role in the nature of triplet states.

PL kinetics

In all the investigated media except for MCH solutions, TMCz-BO shows TADF. In the PL decay profile, there are well-defined regions of PF until 100 ns and DF up to 10 μs in solutions (Fig. 4A) and up to 10 ms in films (Fig. 4B). The polarity increase leads to the elongation of the PF lifetime rise of the DF plateau (in solutions) and/or shortening of the DF lifetime (in films).

The gradual change of polarity in liquid solvents without strong specific intermolecular interactions enables the analysis of the trends of ISC and rISC change. According to the correlations in Fig. 3C and D, natural logarithms of the ISC (k_{ISC}) and rISC (k_{rISC}) rate constants grow linearly with the increase of polarity described by the decrease of E_{S_1} . This indicates the acceleration of the spin-flip transitions: in the most polar DMSO solution, k_{ISC} and k_{rISC} reach $1.4 \times 10^7 \text{ s}^{-1}$ and $3.7 \times 10^6 \text{ s}^{-1}$, respectively (Table 1). Moreover, both ISC and rISC rate constants rise linearly with the decrease of k_{r} , which, as was mentioned above, indicates the reduction of the $^1\text{LE}_\text{A}$ character in favour of the ^1CT one (Fig. 3E and F).

Together with a strong solvatochromic effect, the decrease of k_{r} with E_{S_1} (Fig. 3B) indicates (i) stabilisation of the ^1CT character, (ii) decrease of the $^1\text{LE}_\text{A}$ contribution to S_1 , and (iii) more efficient separation of HOMO and LUMO. On the other hand, such a separation of the frontier molecular orbitals decreases the exchange energy and the energy gap between the S_1 and T_1 states. This explains the correlations observed for the rISC rate (Fig. 3D) following the exponential dependence on $\Delta E_{\text{S}_1-\text{T}_1}$ (eq. 1) and also provides a meaningful conclusion on

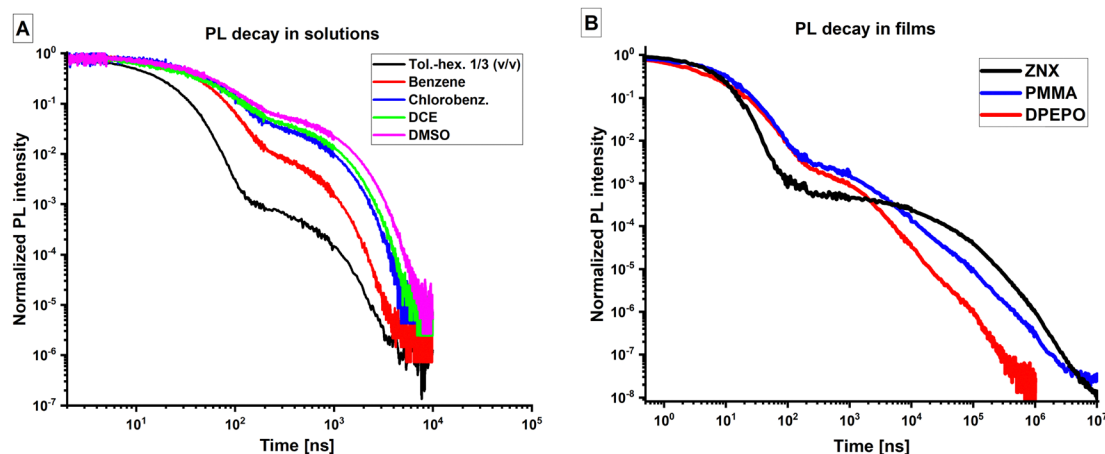


Fig. 4 PL decay curves in solutions (A) and films (B) at room temperature, vacuum.

the two-state T_1 - S_1 mechanism of rISC in TMCz-BO because (i) rISC increases with the decrease of E_{S_1} ($\Delta E_{S_1-T_1}$) and (ii) these correlations are linear without any local maxima, which indicates that rISC is not mediated by a higher-energy triplet state of different sensitivity to medium polarity.

In films, TMCz-BO shows several differences in the PL kinetics. Most importantly, whilst the τ_{PF} , k_r , and k_{ISC} remain in a similar range as in solutions, DF lifetimes are two orders longer, and the k_{rISC} values are two orders smaller. Regarding the polarity effect, the τ_{DF} is shortened, and k_{rISC} is increased with the growing polarity (decreasing E_{S_1}) in the row ZNX-PMMA-DPEPO, similar to the liquid phase. This is in agreement with the decrease of the $\Delta E_{S_1-T_1}$ in polar media, as was mentioned above, but according to much slower rISC, the energy gap value should be much larger than in solutions. Another difference is that the k_{ISC} dependence on polarity is inversed in films: k_{ISC} decreases with E_{S_1} , indicating different ISC mechanisms. Considering that the most crucial difference between solutions and films is viscosity, we suggest that the change in rotational freedom is the reason for the lower rISC rate and different ISC mechanisms in films.

The largest difference between the liquid and solid hosts for TMCz-BO is observed in the MCH solution and ZNX film. In spite of very similar polarity, in ZNX, both S_1 and T_1 emissions are broader (Table S2, ESI†) and red-shifted (Fig. S12, ESI†). Specifically, phosphorescence in ZNX at 15 K, differs strongly from that in MCH frozen glass, showing similar onset value, but no longer resembling pure 3LE_A emission by shape. What is more, despite similar E_{S_1} values, only in the MCH solution, TMCz-BO lacks TADF. Under such low-viscosity, low-polarity conditions, TMCz-BO thus behaves like a LE emitter, but not a CT one. We suggest that considerable role of 1LE_A character in the S_1 state is the reason of slow ISC which occur *via* the ${}^1LE_A \rightarrow T_n$ mechanism. When 1CT is stabilised in more polar media, the ${}^1CT \rightarrow T_n$ mechanism affords higher ISC rates (Fig. 3C).

To explain the inversed $k_{ISC}(E_{S_1})$ dependence in films *vs.* solutions (Table 1) and the $k_{ISC}(k_r)$ dependence in general

(Fig. 3E), it is useful to compare TMCz-BO with another blue TADF emitter, DMAC-TRZ and its analogues, whose S_1 states are of pure 1CT character.^{12,33} In the solutions of such CT-emitters, the ISC rate, remains relatively constant, because the $\Delta E_{S_1-T_1}$ value as well as its change with polarity is small. In films, where the statistical $\Delta E_{S_1-T_1}$ value and its change with E_{S_1} are larger, k_{ISC} decreases with E_{S_1} , just like in films doped with TMCz-BO (Table 1). In fact, in terms of Marcus theory, the decrease of the $\Delta E_{S_1-T_1}$ energy gap is equal to the decrease of the driving force of ISC. Hence, if SOC of the $S_1 \rightarrow T_n$ transition remains constant, which is the case when S_1 has pure character (like 1CT as in DMAC-TRZ), the ISC rate should either (1) remain relatively constant, if the change of $\Delta E_{S_1-T_1}$ is small (as in DMAC-TRZ solutions)¹² or (2) decrease, if the reduction of $\Delta E_{S_1-T_1}$ is substantial (as for DMAC-TRZ emitters in films).³³ The latter case correlates very well with the ISC rate of TMCz-BO in films. Therefore, in high-viscosity media regardless of polarity, TMCzBO behaves more as a CT emitter.

Last but not least experimental peculiarity is the following. In ZNX, TMCz-BO represents one of very rare examples of UV-blue TADF with a reasonable rISC rate and microsecond DF lifetime. In such a medium, the large portion of the 1LE state enables narrow-band emission. On the other hand, thanks to the discussed viscosity effect, both S_1 and T_1 states bear a considerable portion of the CT character thus serving as mediators for rISC. One can consider this as an atypical case of inversed three-state rISC model *via* ${}^3LE_i \rightleftharpoons {}^3CT \rightleftharpoons {}^1CT \rightleftharpoons {}^1LE_A$. In contrast, D-A emitters usually take advantage of the 3LE state as a mediator for the ${}^3CT \rightleftharpoons {}^1CT$ transition, *via* the ${}^3CT \rightleftharpoons {}^3LE_i \rightleftharpoons {}^1CT$ model.¹¹

The role of rotational isomerism and excited-state mixing. Whilst the effect of medium polarity on the CT states of DA emitters is well-known, the described effects of medium viscosity is rather unexpected and needs to be explained. To do so, we rely on the key role of molecular vibrations for the photophysical properties.

As was mentioned above, from the point of view of the TADF mechanism, the molecular vibrations which change the

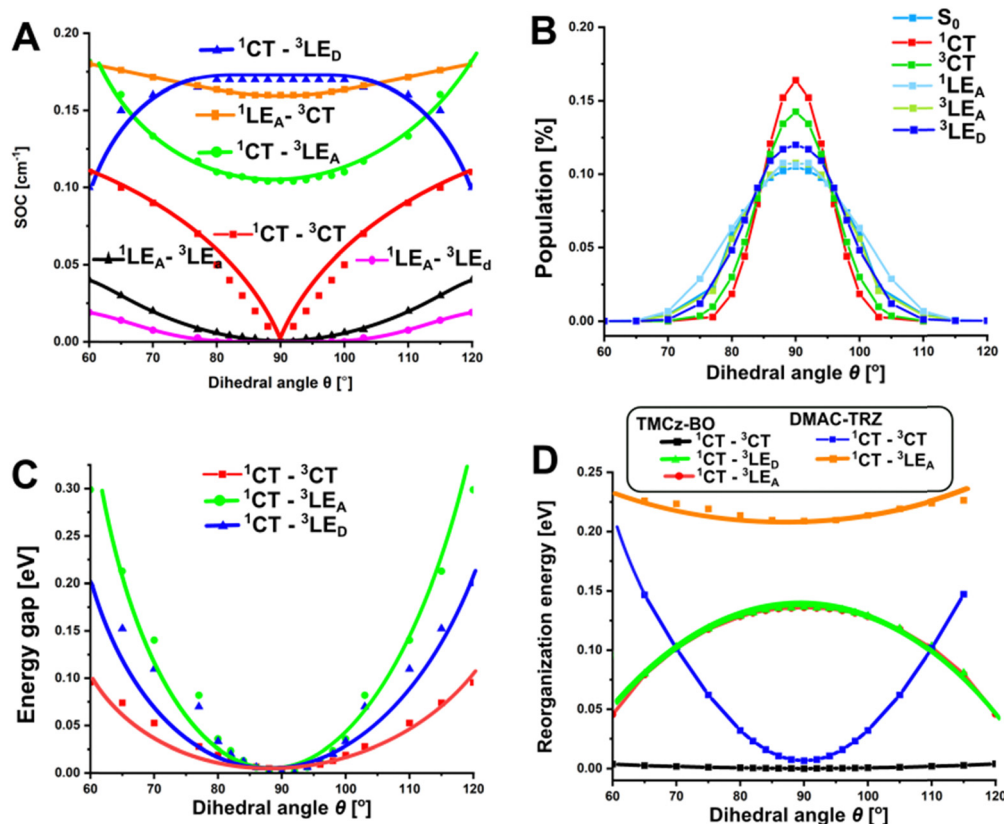


Fig. 5 Dependences of SOC (A), θ -rotamer distribution at room temperature (B), relative singlet–triplet energy gaps (C) reorganisation energy (D) on the θ value.

dihedral angle θ between D and A are of key importance for TADF. Such θ -rotations have the strongest effect on the $^1\text{CT} \rightleftharpoons ^3\text{CT}$ transition in TMCz-BO (Fig. S5A, ESI†) affording SOC increase from zero ($\theta = 90^\circ$) to 0.12 ($\theta = 60^\circ$). With other triplet states, the ^1CT state shows comparable SOC constants: 0.12 cm^{-1} for $^1\text{CT} \rightleftharpoons ^3\text{LE}_A$ and 0.17 cm^{-1} for $^1\text{CT} \rightleftharpoons ^3\text{LE}_D$, but these transitions are weakly affected by the change of θ . Regarding the spin-flip transitions involving another excited singlet state, $^1\text{LE}_A$, only $^1\text{LE}_A \rightleftharpoons ^3\text{CT}$ shows nonzero SOC constant of 0.16 cm^{-1} and weak θ -rotational activation (Fig. 5A). Other transitions, namely $^1\text{LE}_A \rightleftharpoons ^3\text{LE}_A$ and $^1\text{LE}_A \rightleftharpoons ^3\text{LE}_D$, are almost completely forbidden (Fig. 5A). This leads to an important conclusion that the contribution of $^1\text{LE}_A$ should thus decrease total SOC constant of the $S_1 \rightleftharpoons T_1$ transitions.

As the experimental data support the two-state rISC mechanism, we calculated the rotationally enhanced rISC rate for the $^3\text{CT} \rightarrow ^1\text{CT}$ transition, because only in this case the triplet–singlet energy gap should decrease with the increase of medium polarity due to stabilisation of charge transfer. Following the procedure described previously,¹² for various E_{S_1} corresponding to each solvent the $\Delta E_{^3\text{CT} \rightarrow ^1\text{CT}}$ values were estimated from the $k_r(E_{S_1})$ dependence and the $k_{^3\text{CT} \rightarrow ^1\text{CT}}$ rate constants were calculated for all θ -rotamers available at room temperature using Marcus–Hush equation (for details see ESI†, Section 4 and Tables S3–S8). In this case, the DFT-predicted SOC constants for the $^3\text{CT} \rightarrow ^1\text{CT}$ transition ($V_{T_1 \rightarrow S_1} = V_{^3\text{CT} \rightarrow ^1\text{CT}}$) were used (Approach 1

in Section 4, ESI†). The obtained statistically weighted $k_{^3\text{CT} \rightarrow ^1\text{CT}}$ follow the experimental linear dependence of the k_{rISC} value on E_{S_1} (Fig. 6): rISC rate increases gradually with polarity as the ^3CT and ^1CT states become energetically closer indicating that in fact the $^3\text{CT} \rightarrow ^1\text{CT}$ channel is realized in TMCz-BO. However, the calculated values of $k_{^3\text{CT} \rightarrow ^1\text{CT}}$ are 3–5 times lower than the experimental k_{rISC} , which means that the applied SOC of pure $^3\text{CT} \rightarrow ^1\text{CT}$ transition is too low.

Apparently, rISC in TMCz-BO can be described by the two-state $T_1 \rightarrow S_1$ model with the key role of CT states. On the other hand, SOC of the real system is substantially higher than that of the $^1\text{CT} \rightleftharpoons ^3\text{CT}$ transition itself. In fact, under the assumption that SOC is constant, the predicted rISC rates become close to the experimental ones when the statistically weighted $V_{T_1 \rightarrow S_1}$ exceeds twice that predicted for $V_{^3\text{CT} \rightarrow ^1\text{CT}}$ and reaches 0.044 cm^{-1} (Fig. 6, and Approach 2 in Section 4, ESI†). However, even in this case, the experimental $k_{\text{rISC}}(E_{S_1})$ dependence is not described properly due to different slopes of fitted linear equations. Finally, the numerical solution of the system of k_{rISC} equations using $\Delta E_{^3\text{CT} \rightarrow ^1\text{CT}}$ yielded different SOC constants for each solution (Fig. 6 and Approach 3 in Section 4, ESI†) varying from 0.051 cm^{-1} (the toluene–hexane mixture) to 0.038 cm^{-1} (DMSO) (Table S3, ESI†). This provides a conclusion that SOC is a function of the excited state energy. Importantly, this means that the nature of S_1 and T_1 changes with medium polarity.

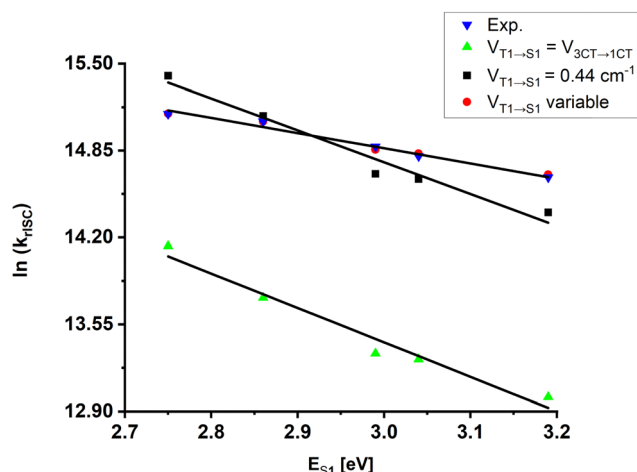


Fig. 6 Summary of k_{rISC} calculations using various approaches and comparison with experimental values; V values for the “ $V_{\text{T}_1 \rightarrow \text{S}_1}$ variable” set are given in Table S9 (ESI†).

What is more, as was mentioned above, high k_{r} values indicate the decreasing contribution of the ^1LE character in S_1 with growing polarity, and the phosphorescence spectra differentiate various triplet-state characters $^3\text{LE}_\text{A}$, $^3\text{LE}_\text{D}$, and ^3CT which prevail or coexist in T_1 depending on the medium features. All these observations cannot be explained within the static quantum model which assumes different polarity dependence of the CT and LE states' energies. Namely, in polar media at room temperature, as the energy gaps between LE and CT states should be too high to afford thermally activated internal conversion (IC) (Fig. S12, ESI†). To explain such contradictions, we suggest the occurrence of vibrationally assisted excited-state mixing (Fig. 7A) which is required to modify the notion of IC typically used for the description of the interaction of the excited states of the same multiplicity. The excited-state mixing will be further used as a basis of a semiempirical model beyond the θ -rotamer model to explain complex deviation of the real TMCz-BO system from the Born-Oppenheimer approximation.

With this in mind and taking into account the bases of the θ -rotamer model, we suggest the following. In solutions of low viscosity, molecular vibrations, specifically θ -rotations, occur barrierlessly within the amplitudes accessible at given temperature (Fig. 7B). The emitter can thus be described as a single individual with averaged electronic parameters of all contributing species with varying portions of different characters of the S_1 and T_1 states. That is in accordance with the monoexponential decays and identical TRES of PF and DF in solutions at RT. One can thus consider such a system as a dynamic mixture of coexisting species with various θ values which contribute collectively to the emissive and spin-flip processes *via* averaged single channel. Taking into account the observations of multiple nature of S_1 and T_1 states for TMCz-BO in low-viscosity media at room temperature, we introduce the notion of dynamic excited-state mixing (DESM), an electronic effect which affords dual ^1CT - $^1\text{LE}_\text{A}$ nature of S_1 state and triple ^3CT - $^3\text{LE}_\text{A}$ - $^3\text{LE}_\text{D}$ nature of T_1 state (Fig. 7C). DESM is activated

by the vibrations within the energetic minima of S_1 or T_1 and is affected mostly by the θ -rotations, solvation (polarity/polarizability of the medium) and solvent relaxation.

In an attempt to understand the scale of DESM and its evolution with solvent, we estimated the contribution of each of the spin-flip transition by fitting empirical SOC constants with the TD-DFT predicted $V_{\text{T}_n \rightarrow \text{S}_i}$ (Fig. 7D). It was taken into account that the contribution of LE characters decreases with polarity, and assumed that contributions of transitions involving $^3\text{LE}_\text{A}$ and $^3\text{LE}_\text{D}$ states is equal. According to such estimations, the rotationally-activated $^3\text{CT} \rightarrow ^1\text{CT}$ channel dominates in all media, with its contribution growing from 50% to over 85% with the increasing polarity. The transitions involving the $^1\text{LE}_\text{A}$ state have noticeable contributions in low to medium polarity solvents up to chlorobenzene, where $E_{\text{S}_1} < 3.0$ eV. In more polar media, $^3\text{LE}_\text{A} \rightarrow ^1\text{CT}$ and $^3\text{LE}_\text{D} \rightarrow ^1\text{CT}$ contribute from 20% to 15% in rISC. Note that such contributions are estimated using the $\Delta E_{^3\text{CT} \rightarrow ^1\text{CT}}$ energy gaps and may vary if actual $\Delta E_{\text{T}_1-\text{S}_1}$ is higher.

In amorphous films, the excited-state relaxation and solvent reorganisation are strongly inhibited. The species with various θ are formed during the film preparation and remain trapped in their non-equilibrium geometries with θ as in the S_0 state due to high energetic barrier for rotation of large molecular fragments A and D caused by high viscosity of the medium. Such θ -rotamers should be thus regarded as individual species with different electronic and spectral features. Under such conditions, emitter represents highly heterogeneous mixture of species with different characters of S_1 and T_1 coexisting within the same sample. This is supported by the above-mentioned spectral shifts in TRES, especially in PMMA, and polyexponential PL decays in films. To describe the electronic properties of such a system, we introduce the notion of static excited-state mixing (SESM) (Fig. 7B). Vibrations which enable SESM occur within a local energetic minima corresponding to each individual, namely a θ -rotamer. In this case, in a group of rotamers with the same θ value, emission, ISC, and rISC can occur *via* its own unique mechanism. However, as such group coexists in a macroscopic system with the respective measurable values of k_{r} , k_{ISC} , and k_{rISC} appear as averaged complex functions. With the θ value being constrained, regarding actual state-mixing, SESM is much less effective than DESM, and thus S_1 and T_1 states have more defined characters.

The differences in the θ -rotamer distribution and occurrence of DESM or SESM explain different behavior of TMCz-BO in film and solutions. According to the (TD)DFT calculations, the energy of θ -rotamers differs for various electronic states of TMCz-BO (Fig. S13 and Table S4, ESI†). For this reason the distribution of rotamers in the ground and LE states, is substantially broader than in the excited CT states (Fig. 5B and Table S5, ESI†): in S_0 , the deviation of the θ angle can reach $\pm 30^\circ$, whilst in $\text{T}_1(^3\text{CT})$, and especially $\text{S}_1(^1\text{CT})$, it can hardly exceed $\pm 15^\circ$. Such a variation of rotamer distribution in S_0 and CT states explains global effect of medium viscosity. Specifically, the singlet-triplet energy gaps increase with the θ -deviation (Fig. 5C). In films, where the θ -distribution remains as in the

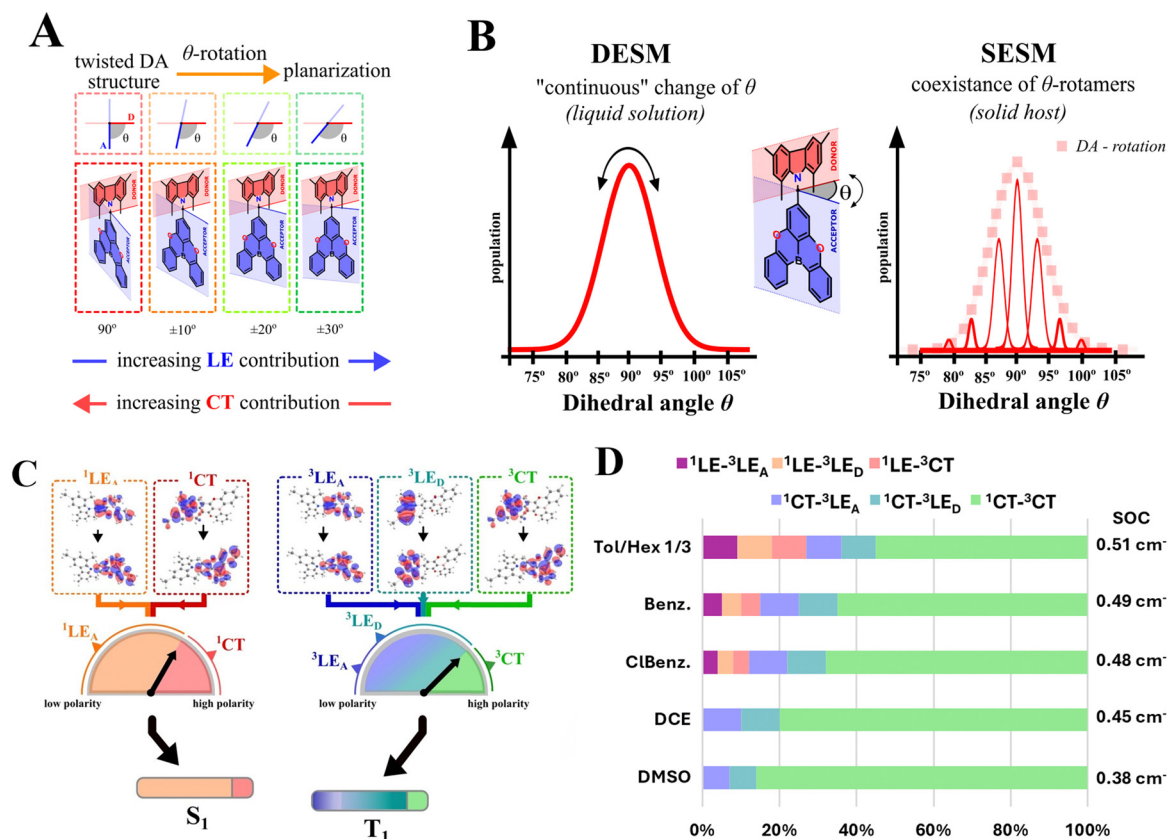


Fig. 7 Illustration of the vibrationally-assisted excited state mixing (A) with the qualitative distribution of θ angle in solutions and films (B). The resulting dual and triple characters of S_1 and T_1 states (C) and contributions of various electronic transitions in rISC in various solutions estimated from empirical SOC (D).

S_0 -state geometry at the moment of sample preparation, considerable contribution of the rotamers with large θ -deviation results in larger $\Delta E_{S_1-T_1}$ and insufficiently higher SOC. On the example of the rotationally activated $^3\text{CT} \rightarrow ^1\text{CT}$ transition, the statistically weighted $\Delta E_{^1\text{CT}-^3\text{CT}}$ and SOC for S_0 geometry, reach 10.4 meV and 0.027 cm^{-1} , respectively, causing faster ISC and slower rISC in films. The respective values predicted for S_1 and T_1 (CT) geometries and attributed to solutions are 7.8 meV and 0.021 cm^{-1} . As was mentioned above, at similar E_{S_1} in solutions (benzene, toluene-hexane mixture) SOC reaches 0.051 cm^{-1} , thus such an increase of SOC is rather negligible.

One should take into account that due to SESM, contribution of LE states should be considerable in all types of solid hosts, what causes much larger average energy gaps in films, where the portion of rotamers with pure CT states is low. On the other hand, constrained geometry in films, affords reasonable CT contribution to S_1 and T_1 states even at low polarities and enhances reasonable SOC *via* SESM. This affords rISC even at very low polarities, but the limiting factor is still large $\Delta E_{S_1-T_1}$. In solutions, sufficient stabilisation of the CT states with polarity narrows the distribution of θ -rotamers, causing the decrease of the $\Delta E_{S_1-T_1}$ energy gap, whilst efficient DESM maintains high SOC values. All together, these factors result in fast ISC and rISC rates in media with low viscosity and

medium-high polarity, whilst relatively fast emission from S_1 is facilitated by the $^1\text{LE}_A-S_0$ contribution *via* DESM.

Conclusions and outlook

TMCz-BO is an example of a complex polyelectronic molecular system with five strongly interacting excited states of different nature and multiplicity. Its fluorescent, phosphorescent, and triplet-harvesting properties strongly depend on the polarity and/or viscosity of medium due to its rich rotational isomerism and vibronic activation of spin-orbit coupling.

According to the experimental evidence, rISC is described by the two-state $T_1 \rightarrow S_1$ model, where S_1 and T_1 states are represented by a superposition of two and three states, respectively, of different nature: charge-transfer states and locally-excited states localised on the acceptor and donor fragments.

Due to the efficient dynamic excited-state mixing and free θ -rotations under the conditions of low-viscosity, TMCz-BO achieves its highest rISC rates in liquid solutions. In low polarity solutions, the LE_A character dominates in T_1 and specifically S_1 , which is less favourable for the spin-flip transitions (Fig. 5A). The increase of polarity stabilises CT states *via* solvent reorganisation, thus growing portion of ^1CT in S_1

favours the spin-flip channels with relatively high SOC, which yields higher rates of ISC and rISC.

Under the conditions of high-viscosity, in films, the θ -rotamer distribution is fixed during the film preparation and is negligibly affected by external or internal factors. The CT-state formation and static excited-state mixing are ensured by such a fixed θ -distribution. For this reason, CT character is present in S_1 and T_1 even in the ZNX films of the lowest polarity, enabling near-UV TADF. Such a static θ -rotamer distribution has favourable effect on SOC what is confirmed by the increased ISC rates. On the other hand, the species with large deviation of θ from 90° have increased $\Delta E_{S_1-T_1}$ which results in long DF lifetimes and overall decrease of rISC rate. In the case of solid hosts, the enriched distribution of the $\Delta E_{S_1-T_1}$ energy gap has bigger influence on TADF than the SOC activation *via* state-mixing.

The obtained results of relatively simple experiments with changing polarity and viscosity show how complex a single-molecular emissive system can be. Whilst the conclusions on the static and dynamic excited-state mixing were drawn mainly on the basis of the experimental data and only partly supported by DFT calculations, these findings indicate sharp need in more advanced theoretical approaches beyond the vibronic models developed recently to explain deviations from the Born-Oppenheimer approximation.

From the point of view of molecular design principles for deep-blue emitters we can confirm that:

- The control of the distribution of θ -rotamers in various electronic states is important, as was mentioned previously in ref. 13. Small θ -deviations observed for S_1 and T_1 states of TMCz-BO in solutions enable fast rISC, but larger θ -deviations in films are unfavourable for rISC.

- Low S_1 - T_1 energy gap and reorganisation energy are very important. In TMCz-BO, the λ values between the LE, and CT states are below 0.13 eV, which is almost twice smaller than in DMAC-TRZ (Fig. 5D) and other blue DA emitters like DMAC-DPS.¹³ In the case of 3CT - 1CT transition, internal λ is negligibly small. Another favourable factor in TMCz-BO, is that λ decreases with the increase of θ -deviation. These factors facilitate the excited-state mixing.

- Evidence of strong CT-LE mixing in the excited states of TMCz-BO even in polar media indicate that the energy gap between the states of the same multiplicity, but different characters is not that important as assumed by static quantum model. In the case of TMCz-BO, the 1CT - 1LE_A mixing occurs even in the S_1 state, but it is not favourable for spin-flip transitions. Most likely efficient mixing of three characters occurs in the T_1 state even when IC should be blocked by high energy barrier inaccessible by thermal activation at RT. We assume that the above-mentioned low reorganisation energy between LE and CT states achieved by the rigidification of donor and acceptor structure is the key to efficient excited-state mixing.

Data availability

The data supporting this article have been included as part of the ESI.†

Conflicts of interest

There are no conflicts to declare.

Acknowledgements

Financial support within the National Science Centre, Poland for financial support within the Sonata 16 project No. UMO-2020/39/D/ST5/03094 is gratefully acknowledged. Quantum chemical calculations were performed on the computers of the Wroclaw Centre for Networking and Supercomputing (WCSS), Poland.

References

- 1 H. Uoyama, K. Goushi, K. Shizu, H. Nomura and C. Adachi, *Nature*, 2012, **492**, 234.
- 2 Z. Yang, Z. Mao, Z. Xie, Y. Zhang, S. Liu, J. Zhao, J. Xu, Z. Chi and M. P. Aldred, *Chem. Soc. Rev.*, 2017, **46**, 915–1016.
- 3 Y. Liu, C. Li, Z. Ren, S. Yan and M. R. Bryce, *Nat. Rev. Mater.*, 2018, **3**, 18020.
- 4 S. Diesing, L. Zhang and E. Zysman-Colman, *et al.*, *Nature*, 2024, **627**, 747–753.
- 5 Y. X. Hu, J. Miao, T. Hua, Z. Huang, Y. Qi, Y. Zou, Y. Qui, H. Xia, H. Liu and X. Cao, *et al.*, *Nat. Photonics*, 2022, **16**, 803–810.
- 6 L. S. Cui, A. J. Gillett, S. F. Zhang, H. Ye, Y. Liu, X. K. Chen, Z. S. Lin, E. W. Evans, W. K. Myers and T. K. Ronson Hajime, *et al.*, *Nat. Photonics*, 2020, **14**, 636–642.
- 7 Y. Wada, H. Nakagawa, S. Matsumoto, Y. Wakisaka and H. Kaji, *Nat. Photonics*, 2020, **14**, 643–649.
- 8 Y. Yu, S. Mallick, M. Wang and K. Börjesson, *Nat. Commun.*, 2021, **12**, 3255.
- 9 A. Endo, M. Ogasawara, A. Takahashi, D. Yokoyama, Y. Kato and C. Adachi, *Adv. Mater.*, 2009, **21**, 4802–4806.
- 10 A. Endo, K. Sato, K. Yoshimura, T. Kai, A. Kawada, H. Miyazaki and C. Adachi, *Appl. Phys. Lett.*, 2011, **98**, 083302.
- 11 T. Penfold, F. Dias and A. Monkman, *Chem. Commun.*, 2018, **54**(32), 3926–3935.
- 12 I. E. Serdiuk, M. Monka, K. Kozakiewicz, B. Liberek, P. Bojarski and S. Y. Park, *J. Phys. Chem. B*, 2021, **125**(10), 2696–2706.
- 13 C. H. Ryoo, J. Han, J.-H. Yang, K. Yang, I. Cho, S. Jung, S. Kim, H. Jeong, C. Lee and J. E. Kwon, *et al.*, *Adv. Opt. Mater.*, 2022, **10**, 2201622.
- 14 H. Gao, S. Shen, Y. Qin, G. Liu, T. Gao, X. Dong, Z. Pang, X. Xie, P. Wang and Y. Wang, *J. Phys. Chem. Lett.*, 2022, **13**(32), 7561–7567.
- 15 R. Niu, J. Li, D. Liu, R. Dong, W. Wei, H. Tian and C. Shi, *Dyes Pigm.*, 2021, **194**, 109581.
- 16 X. Lv, R. Huang, S. Sun, Q. Zhang, S. Xiang, S. Ye, P. Leng, F. B. Dias and L. Wang, *ACS Appl. Mater. Interfaces*, 2019, **11**, 10758–10767.
- 17 J. U. Kim, I. S. Park, C.-Y. Chan, M. Tanaka, Y. Tsuchiya, H. Nakanotani and C. Adachi, *Nat. Commun.*, 2020, 1765.

- 18 A. A. Kubicki, P. Bojarski, M. Grinberg, M. Sadownik and B. Kukliński, *Opt. Commun.*, 2006, **269**, 275–280.
- 19 M. Wojdyr, *J. Appl. Crystallogr.*, 2010, **43**, 1126–1128.
- 20 *Origin. Origin 7.5*, OriginLab Corp., Northampton, MA, 2003.
- 21 M. J. Frisch, G. W. Trucks, H. B. Schlegel, G. E. Scuseria, M. A. Robb, J. R. Cheeseman, G. Scalmani, V. Barone, G. A. Petersson and H. Nakatsuji, *et al.*, *Gaussian 16, Revision C.01*, Gaussian, Inc., Wallingford, CT, 2016.
- 22 A. D. Becke, *J. Chem. Phys.*, 1993, **98**, 1372–1377.
- 23 T. Yanai, D. Tew and N. Handy, *Chem. Phys. Lett.*, 2004, **393**, 51–57.
- 24 Y. Zhao and D. G. Truhlar, *Theor. Chem. Acc.*, 2008, **120**, 215–241.
- 25 J. P. Perdew, K. Burke and M. Ernzerhof, *Phys. Rev. Lett.*, 1997, **78**, 1396.
- 26 T. H. Dunning Jr., *J. Chem. Phys.*, 1989, **90**, 1007–1023.
- 27 F. Neese, *Wiley Interdiscip. Rev.: Comput. Mol. Sci.*, 2012, **2**, 73–78.
- 28 F. Weigend and R. Ahlrichs, *Phys. Chem. Chem. Phys.*, 2005, **7**, 3297–3305.
- 29 E. van Lenthe, J. G. Snijders and E. J. Baerends, *J. Chem. Phys.*, 1996, 105.
- 30 I. E. Serdiuk, C. H. Ryoo, K. Kozakiewicz, M. Mońka, B. Liberek and S. Y. Park, *J. Mater. Chem. C*, 2020, **8**, 6052–6062.
- 31 J. Ochi, Y. Yamasaki, K. Tanaka, Y. Kondo, K. Isayama, S. Oda, M. Kondo and T. Hatakeyama, *Nat. Commun.*, 2024, **15**, 2361.
- 32 K. Stavrou, L. G. Franca and A. P. Monkman, *ASC Appl. Electron. Mater.*, 2020, **2**, 2868–2881.
- 33 M. Mońka, I. E. Serdiuk, K. Kozakiewicz, E. Hoffman, J. Szumilas, A. Kubicki, S. Y. Park and P. Bojarski, *J. Mater. Chem. C*, 2022, **10**, 7925–7934.

SUPPORTING INFORMATION

Experimental evidences of the excited-state mixing in the blue emitter

for organic light emitting diodes

Vladyslav Ievtukhov,^{1,2} Michał Mońka,¹ Olga Ciupak,³ Irena Bylińska,² Piotr Bojarski,¹ Karol Krzymiński,² Illia E. Serdiuk^{1*}

¹ Faculty of Mathematics, Physics and Informatics, University of Gdańsk, Wita Stwosza 57, 80-308 Gdańsk, Poland

² Faculty of Chemistry, University of Gdańsk, Wita Stwosza 63, 80-308 Gdańsk, Poland

³ Department of Organic Chemistry, Gdańsk University of Technology, Gabriela Narutowicza 11/12, 80-233 Gdańsk, Poland

Contents

Section 1. Determination of photophysical parameters

Section 2. Computational determination of the nature of excited states

Section 3. Additional spectroscopic data

Section 4. Time-resolved emission spectra

Section 5. Quantum chemical calculations

Section 1. Determination of photophysical parameters

The parameters of photophysical processes were calculated using equations described in the literature[S1,S2].

PL decay curves showed in Figure 4 (main text) were fitted with the multiexponential equation:

$$I(t) = A_0 + \sum_{i=1}^n A_i \exp(-t/\tau_i), \quad (S1)$$

where A_i is the pre-exponential factor, τ_i is the decay time and $I(t)$ is emission intensity. Average lifetimes of prompt (τ_{PF}) and delayed fluorescence (τ_{DF}) were determined using formula:

$$\tau_{PF, DF} = \sum_{i=1}^n f_i \tau_i, \quad (S2)$$

where f_i is fractional contribution of i -th component expressed as:

$$f_i = \frac{A_i \tau_i}{\sum_{i=1}^n A_i \tau_i}. \quad (S3)$$

The ratio of DF and PF quantum yields $\varphi_{DF}/\varphi_{PF}$ was determined as following:

$$\frac{\varphi_{DF}}{\varphi_{PF}} = \frac{A_{DF} \tau_{DF}}{A_{PF} \tau_{PF}}, \quad (S4)$$

where A_{DF} and A_{PF} are pre-exponential factors of delayed and prompt fluorescence, respectively. Rate constants of radiative (k_r) and nonradiative (k_{nr}) decay and intersystem crossing (k_{ISC}) were given by equations:

$$k_r = \frac{\varphi_{PF}}{\tau_{PF}}, \quad (S5)$$

$$k_{ISC} = \frac{\varphi_{DF}}{\varphi \tau_{PF}}, \quad (S6)$$

$$k_{nr} = \frac{1}{\tau_{PF}} - (k_r + k_{ISC}), \quad (S7)$$

where φ is PLQY ($\varphi_{DF} + \varphi_{PF}$). Further, the quantum yields for ISC and rISC were calculated as

$$\varphi_{ISC} = k_{ISC} \tau_{PF}, \quad (S8)$$

$$\varphi_{rISC} = \frac{1 - \varphi_{PF}/\varphi}{\varphi_{ISC}}. \quad (S9)$$

Finally, rate constant for rISC (k_{rISC}) was calculated as

$$k_{rISC} = \frac{\varphi_{rISC}}{\tau_{DF}} \left(\frac{\varphi}{\varphi_{PF}} \right). \quad (S10)$$

Thus obtained photophysical parameters are presented in **Table 1**, main text.

Section 2. Additional spectroscopic data

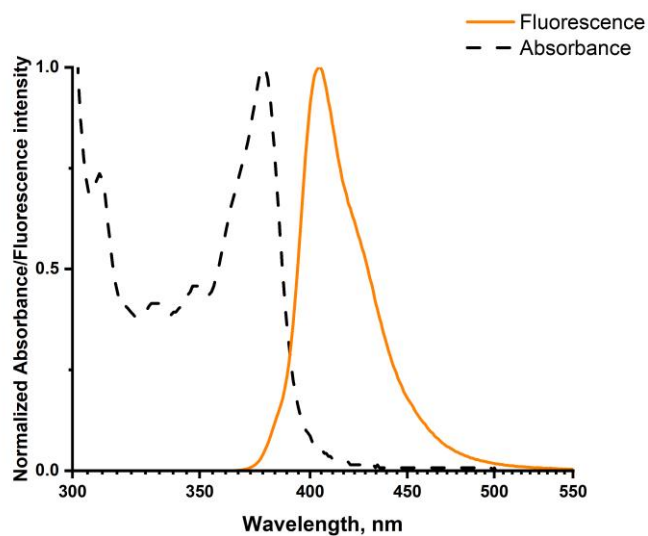


Figure S1. Absorbance and fluorescence spectra of TMCz-BO in methylcyclohexane (MCH) solution.

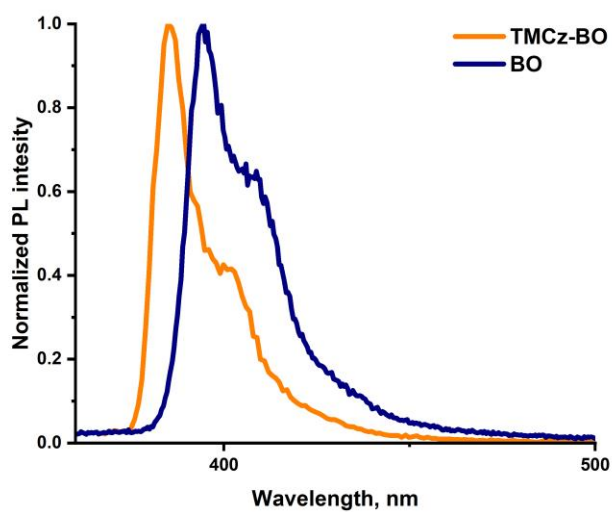


Figure S2. Fluorescence spectra of TMCz-BO and acceptor fragment BO in MCH solution at room temperature

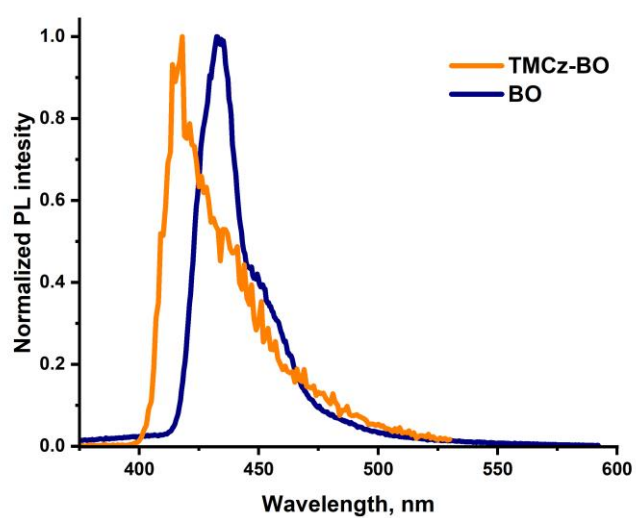


Figure S3. Phosphorescence spectra of **TMCz-BO** and the acceptor molecule **BO** in MCH frozen glass at 77K.

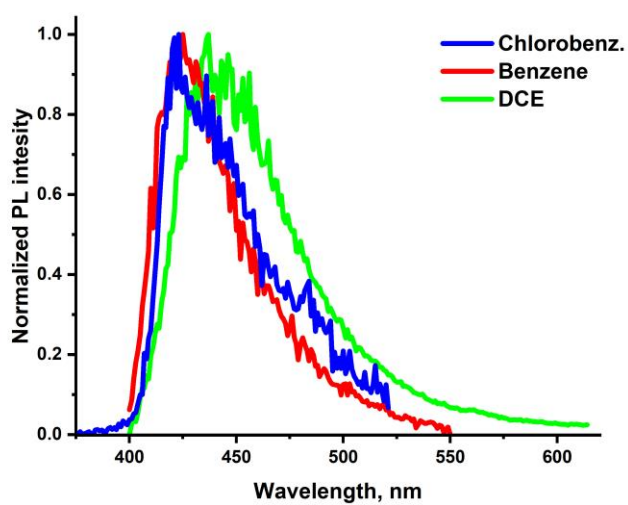


Figure S4. Phosphorescence spectra of TMCz-BO in chlorobenzene, benzene and DCE frozen solutions at 77K

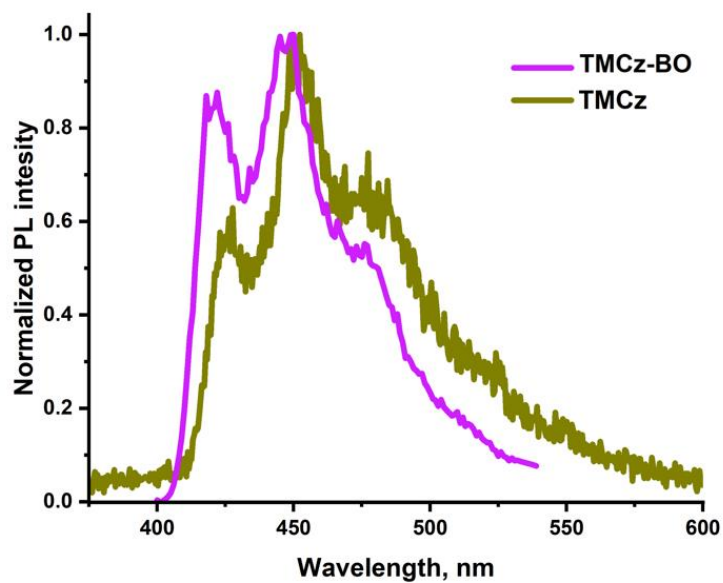


Figure S5. Phosphorescence spectra of **TMCz-BO** in frozen DMSO and the TMCz donor at 77K.

Table S1. Linear regression parameters for the fitted linear dependencies Figure 3, main text.

Parameter	Plot B $\ln k_r$ vs. E_{SI}	Plot D $\ln k_{rISC}$ vs. E_{SI}	Plot C $\ln k_{ISC}$ vs. E_{SI}	Plot E $\ln k_{rISC}$ vs. k_r	Plot F k_{ISC} vs. k_r
Slope	2.65 ± 0.34	-1.16 ± 0.09	-4.14 ± 0.87	-0.72 ± 0.07	-1.76 ± 0.27
Intercept	7.91 ± 1.01	18.34 ± 0.26	28.03 ± 2.59	15.45 ± 0.06	21.84 ± 2.16
R^2	0.953	0.984	0.882	0.97	0.933

Section 3. Computational determination of the nature of excited states

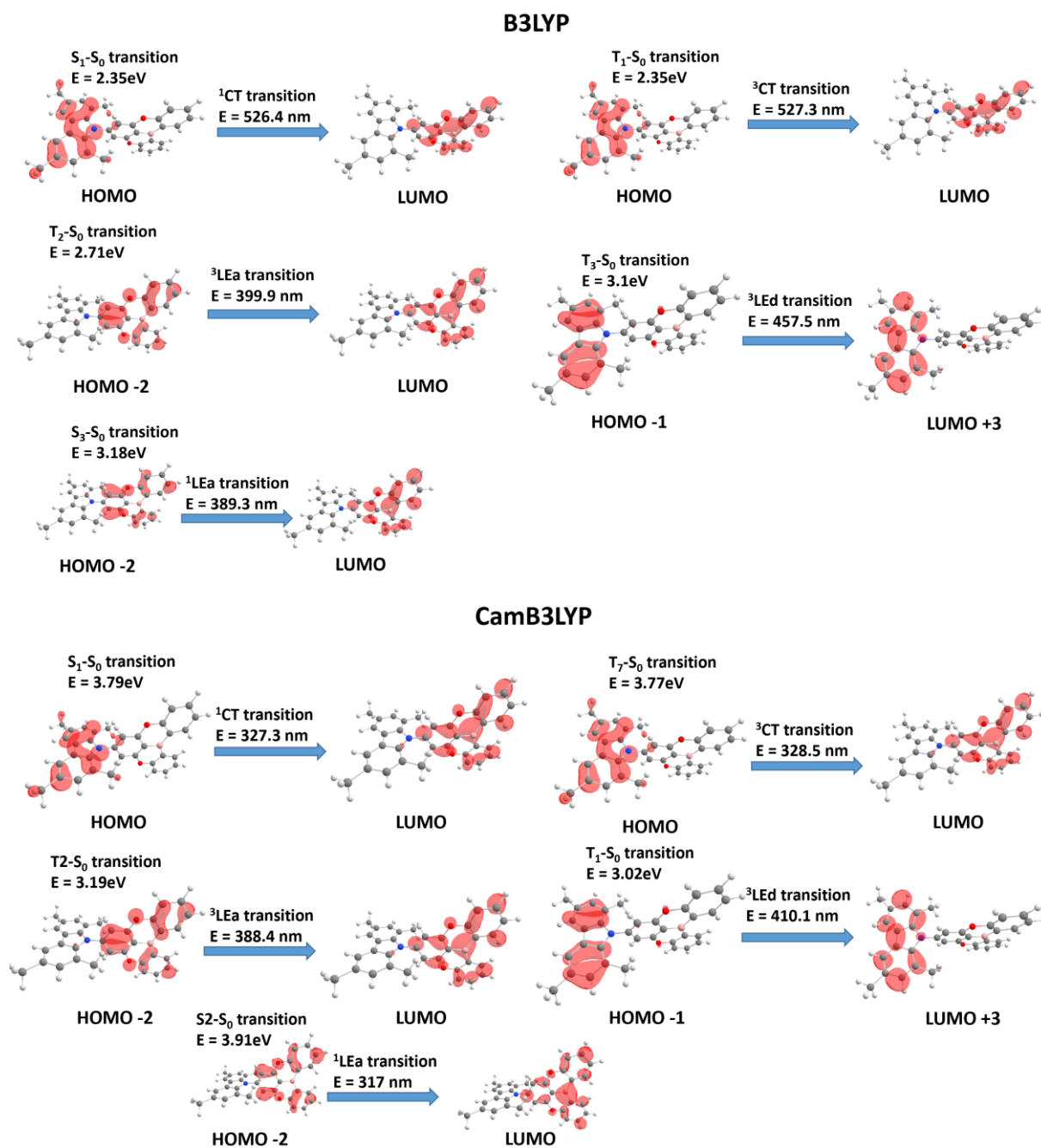
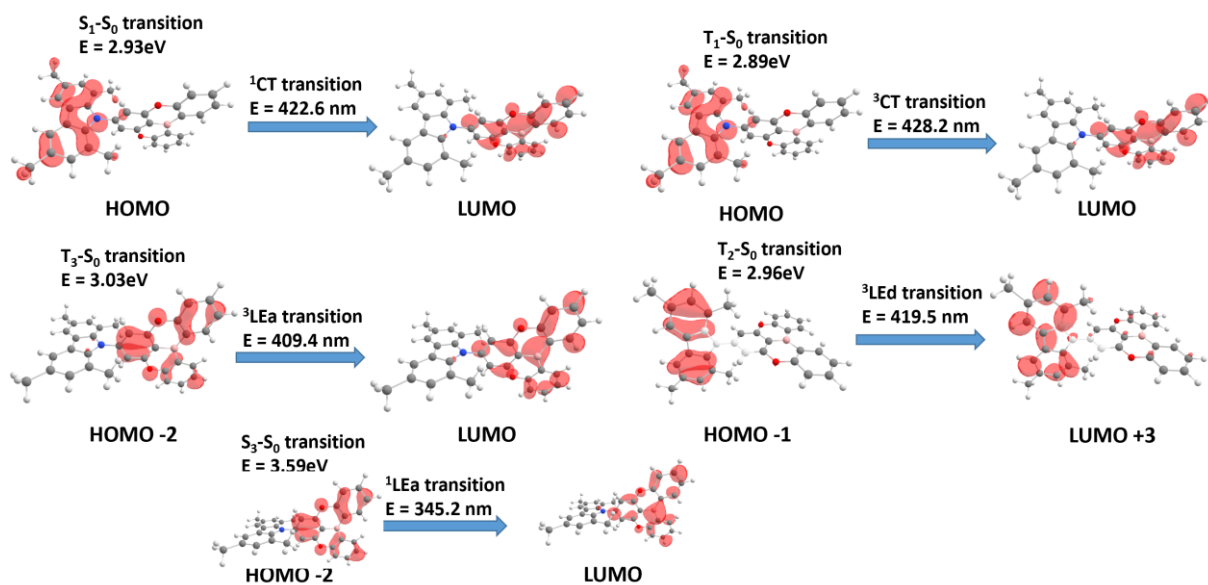


Figure S6. Profiles of molecular orbitals calculated using various levels of theory; for clarity only one sign of wave function is shown.

M06



M062X

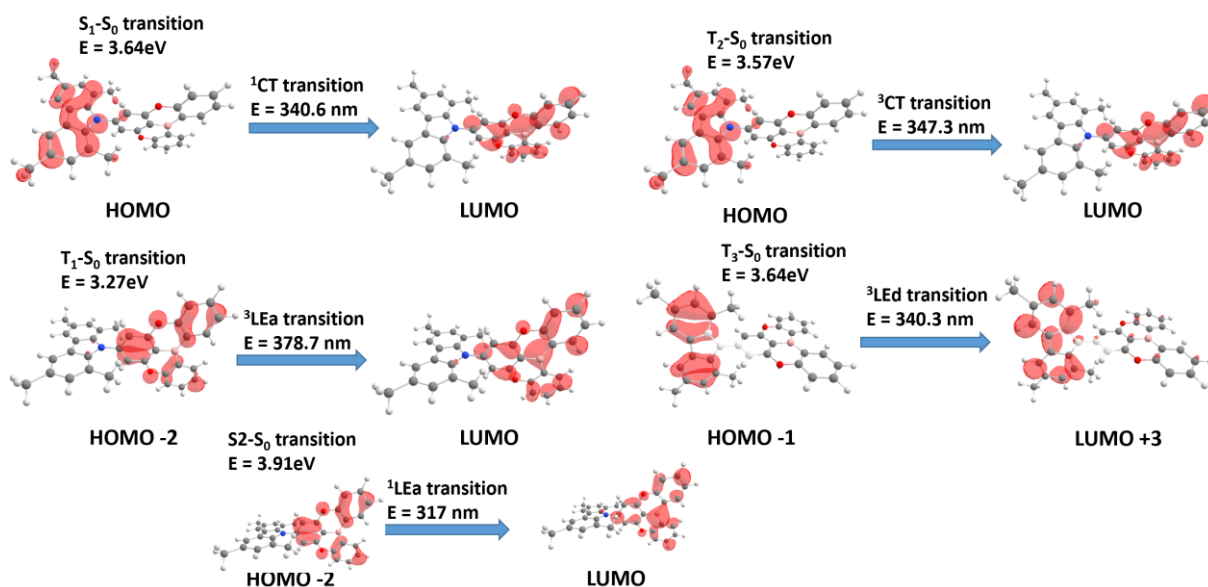


Figure S6. continued

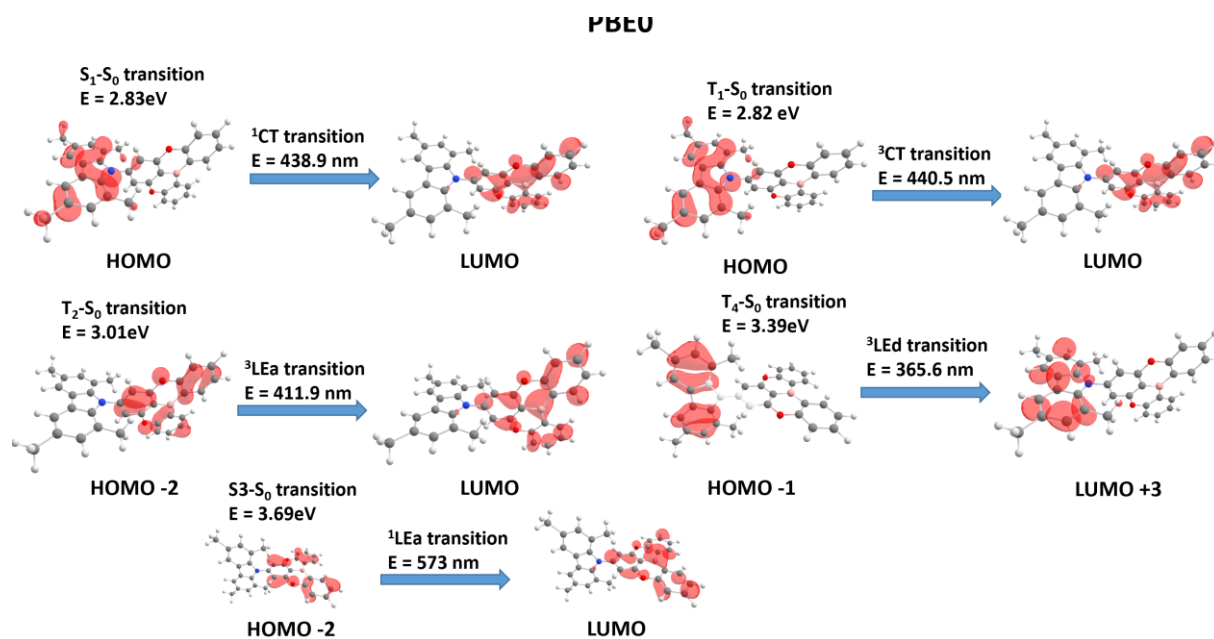


Figure S6. continued

Section 4. Time-resolved emission spectra

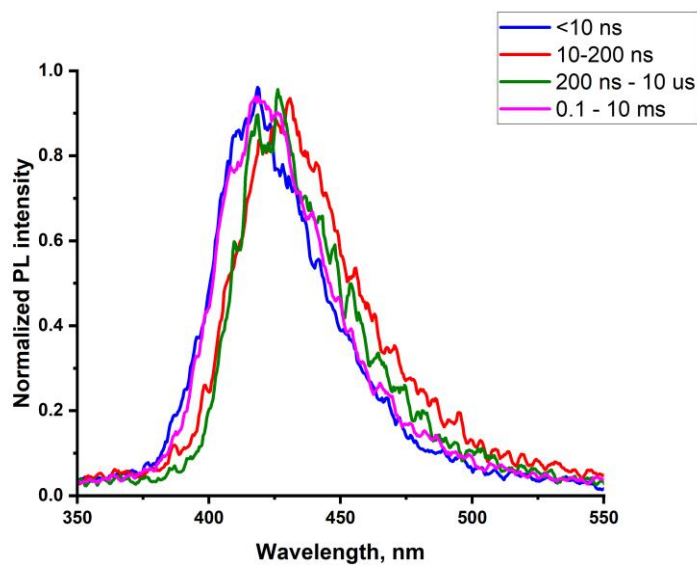


Figure S7. TRES of TMCz-BO in ZNX film (0.1%, w/w) at RT, vacuum.

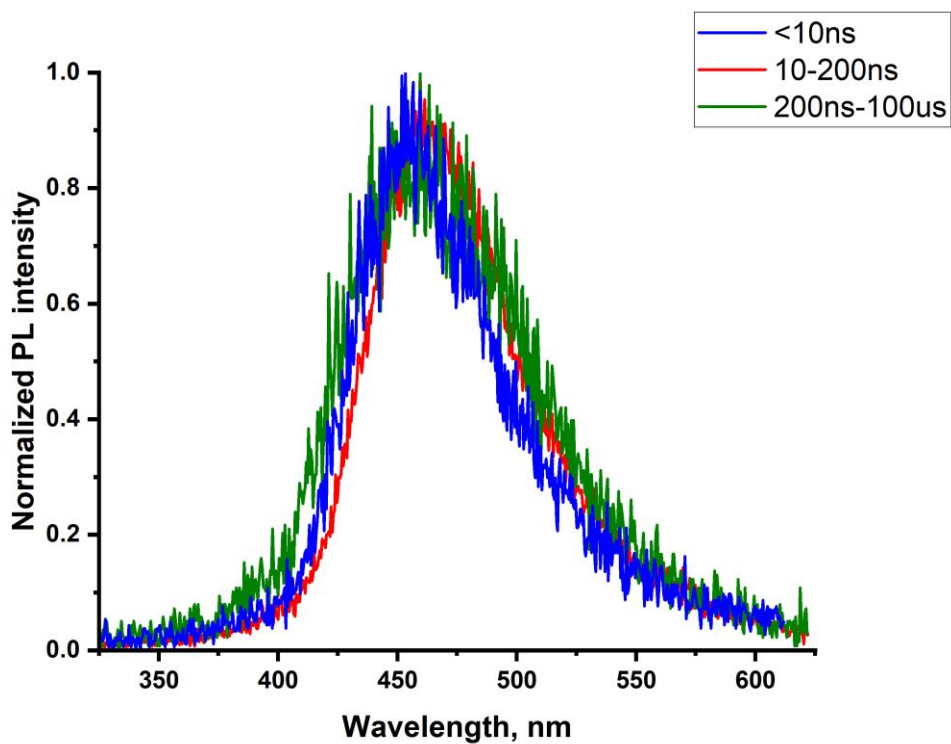


Figure S8. TRES of TMCz-BO in DPEPO film (10%, w/w) at RT, vacuum

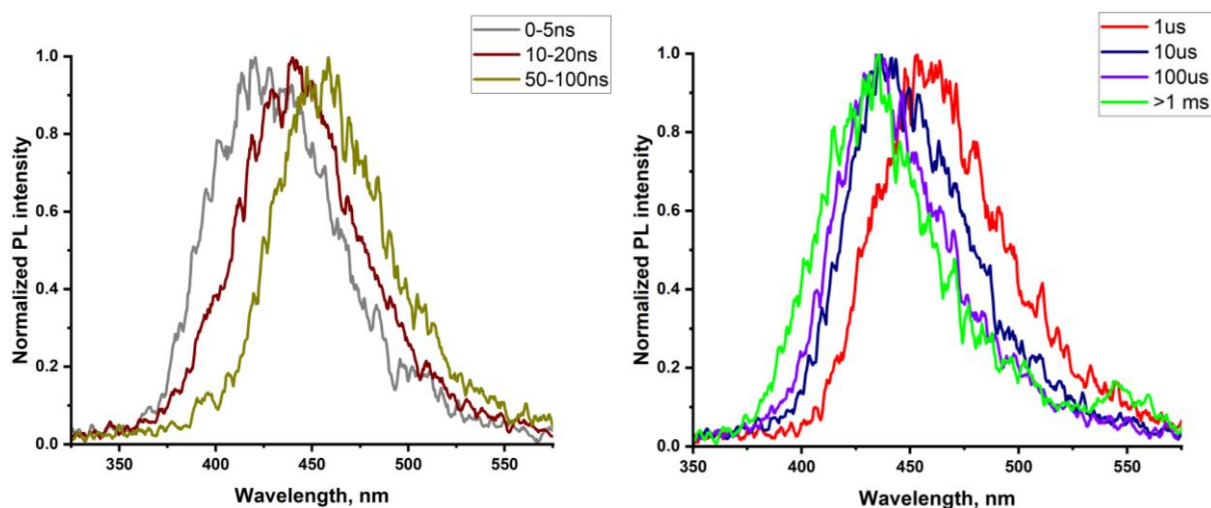


Figure S9. TRES of TMCz-BO in PMMA film (0.1%, *w/w*) at RT, vacuum.

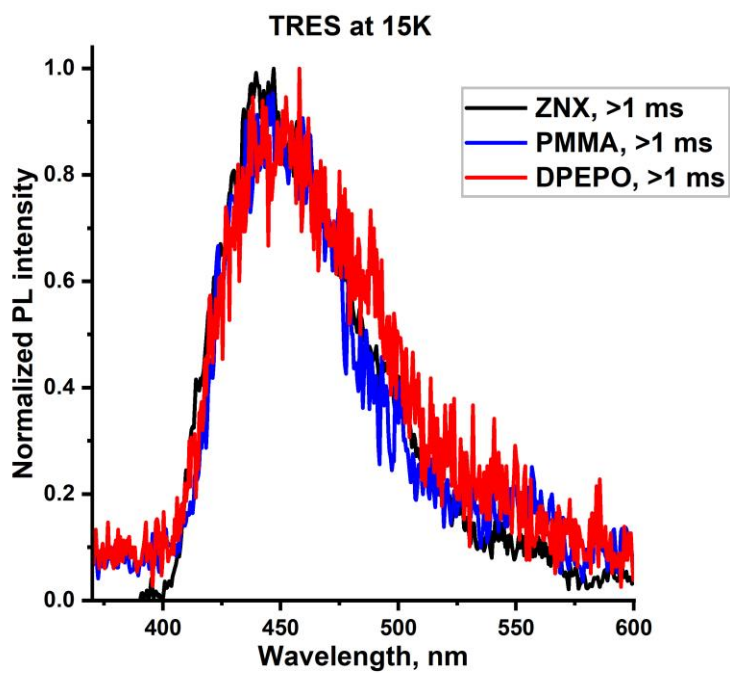


Figure S10. PL spectra of TMCz-BO in doped films at 15 K with a delay time of 1 ms.

Comparison of TMCz-BO spectra in the MCH solvent and ZNX host

Table S2. Full-width at half-maximum (FWHM) values in MCH solution and ZNX film

	Fluorescence		Phosphorescence	
	[nm]	[eV]	[nm]	[eV]
MCH	35	0.26	34	0.23
ZNX	41	0.29	66	0.41

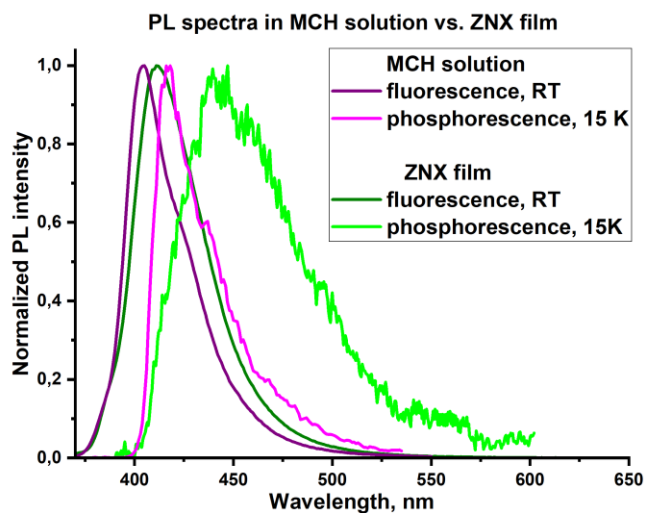


Figure S11. Fluorescence (RT) and phosphorescence (15K) spectra in MCH solution and ZNX film.

Section 5. Quantum Chemical Calculations

Calculations of electronic parameters and rISC values

For the calculations of k_{rISC} values Marcus-Hush equation [S3] was used

$$k = \frac{V^2}{\hbar} \sqrt{\frac{\pi}{k_{\text{B}} T \lambda}} \exp \left[-\frac{(\Delta E_{\text{ST}} + \lambda)^2}{4 k_{\text{B}} T \lambda} \right] \quad (1)$$

where:

k is a rate constant

V is the SOC constant

λ is the sum of internal and external (λ_{solv}) reorganization energies for the respective transition

ΔE_{ST} is an energy gap between singlet and triplet state

k_{B} is the Boltzmann constant

\hbar is the reduced Planck's constant

T is the temperature (298.15 K).

On the B3LYP/cc-pVDZ level of theory, the value of the $\Delta E_{3\text{CT} \rightarrow 1\text{CT}}$ energy gap was predicted of 4.5 meV for the 90° rotamer. Deviation of θ from the optimal value causes the increase of $\Delta E_{3\text{CT} \rightarrow 1\text{CT}}$ values as shown in Table S6. To take this into account, the statistically weighted $\Delta E_{3\text{CT} \rightarrow 1\text{CT}}$ was calculated using population of each θ -rotamer given by Boltzmann distribution at room temperature using respective energies of species (Table S4, S5). To describe the rISC dynamics in solutions, θ -rotamer population in the T_1 (^3CT) state geometry was used. The statistically weighted $\Delta E_{(3\text{CT} \rightarrow 1\text{CT})_{\text{w}}}$ value of 7.8 meV was obtained as described below. The calculated reorganization energies (Table S7) and SOC constants (Table S8) at various θ are presented below.

The $\Delta E_{3\text{CT} \rightarrow 1\text{CT}}$ values in various solvents were estimated using the $k_{\text{r}}(E_{\text{S}1})$ dependence as described in [S2]. Specifically, DFT calculations predicted PL_{max} of 526 nm matching well the experimental value of 519 nm obtained for the DCE solution (Table 1, main text). The abovementioned $\Delta E_{3\text{CT} \rightarrow 1\text{CT}}$ value of 7.8 meV was thus ascribed to the DCE medium. Taking into account linear dependence of k_{r} on the S_1 energy (Figure 3B) and $\ln(k_{\text{rISC}})$ on k_{r} (Figure 3D), linear correlation between k_{r} and $\Delta E_{3\text{CT} \rightarrow 1\text{CT}}$ was assumed. Therefore, $\Delta E_{3\text{CT} \rightarrow 1\text{CT}}$ for other solvents were estimated by proportion using experimental k_{r} values (Table S3).

For each medium, statistically weighted $k_{3CT \rightarrow 1CT}$ rate constants were obtained (Table S3) using Marcus-Hush equation (1) for each θ -rotamer via three approaches. As described below, these approaches use different SOC constants, and the same set of $\Delta E_{(3CT \rightarrow 1CT)}(\theta)$ and $\lambda(\theta)$ for each medium.

Table S3. Summary of estimation of $\Delta E_{(3CT \rightarrow 1CT)w}$, $\ln(k_{T1-S1})_w$, and V_w for different media.

	E_{S1} [eV]	k_r [10^{-6} s^{-1}]	$\Delta E_{(3CT \rightarrow 1CT)w}$, meV	$\ln(k_{T1-S1})_w^a$			
				$V_w = V_{3CT-1CT}$	$V_w = 0.44 \text{ cm}^{-1}$	exper. (V_w is a variable)	V_w variable, ^d [cm^{-1}]
Tol/Hex	3.19	11.0	15.6	13.01	14.39	14.7	0.051
Benz.	3.04	8.7	12.3	13.29	14.64	14.8	0.049
ClBenz.	2.99	8.4	11.9	13.33	14.68	14.9	0.048
DCE	2.86	5.5	7.8	13.75	15.11	15.1	0.045
DMSO	2.75	3.5	5.0	14.14	15.41	15.1	0.038

E_{S1} – energy of the S_1 state obtained experimentally from PL_{onset} ;

$\Delta E_{(3CT \rightarrow 1CT)w}$ – statistically weighted energy gap between 3CT and 1CT states obtained by DFT calculations (for DCM) or using proportion:

$$\Delta E_{(3CT \rightarrow 1CT)w}(i\text{-solvent}) = k_r(i) * \Delta E_{(3CT \rightarrow 1CT)w}(\text{DCM}) / k_r(\text{DCM});$$

^a statistically weighted rISC constants calculated using 1) $V_{3CT-1CT}$ predicted for each θ -rotamer (Approach 1); 2) V values giving a statistically weighted V_w value of 0.44 cm^{-1} (Approach 2), or 3) variable V values obtained from the reconstruction of experimental k_{rISC} values (Approach 3);

^b statistically weighted variable V values obtained from the reconstruction of experimental k_{rISC} values using $\Delta E_{(3CT \rightarrow 1CT)w}$;

note that in all calculations, the external reorganization energy was equal to $\Delta E_{(3CT \rightarrow 1CT)}$ for each θ -rotamer.

Dependence of electronic parameters on the dihedral angle between donor and acceptor fragments (θ)

Table S4. Relative energies of the species with various θ value in various electronic states.

θ [°]	Energies of electronic states relative to the optimal geometry in the same state [eV]					
	S ₀	¹ CT	¹ LE _A	³ CT	³ LE _A	³ LE _D
60	0.27	0.57	0.26	0.48	0.28	0.20
65	0.15	0.37	0.14	0.30	0.16	0.21
70	0.082	0.23	0.071	0.18	0.086	0.14
75	-	-	0.034	0.094	0.042	0.059
77	0.039	0.10	-	0.069	-	-
80	0.015	0.056	0.014	0.040	0.017	0.026
82	0.0091	0.034	-	0.025	0.010	0.013
84	0.0048	0.019	-	0.014	0.0054	0.0076
85	-	-	0.0036	-	-	-
86	0.0020	0.0078	-	0.0058	0.0020	0.0038
88	0.0008	0.0019	0.0	0.00	0.00019	0.0015
90	0.0000	0.0000	0.00030	0.0058	0.0	0.00
92	0.0008	0.0019	0.0	0.014	0.00019	0.0015
94	0.0020	0.0078	-	0.025	0.0020	0.0038
95	-	-	0.0036	-	-	-
96	0.0048	0.019	-	0.040	0.0054	0.0076
98	0.0091	0.034	-	0.069	0.010	0.013
100	0.015	0.056	0.014	0.094	0.017	0.026
103	0.039	0.10	-	0.18	-	-
105	-	-	0.034	0.30	0.042	0.059
110	0.082	0.23	0.071	0.48	0.086	0.14
115	0.15	-	0.14	-	0.16	0.21
120	0.27	-	0.26	-	0.28	0.20

Table S5. Population (p) of species with various θ value

	Population of rotamers, p [%]					
θ [°]	S ₀	¹ CT	¹ LE _A	³ CT	³ LE _A	³ LE _D
60	2.39×10 ⁻⁶	3.14×10 ⁻¹¹	6.55×10 ⁻⁶	9.54×10 ⁻¹⁰	2.30×10 ⁻⁶	5.46×10 ⁻⁵
65	2.67×10 ⁻⁴	9.03×10 ⁻⁸	4.90×10 ⁻⁴	1.18×10 ⁻⁶	2.35×10 ⁻⁴	2.44×10 ⁻⁵
70	4.41×10 ⁻³	2.47×10 ⁻⁵	6.69×10 ⁻³	1.40×10 ⁻⁴	3.82×10 ⁻³	1.08×10 ⁻³
75	-	-	2.89×10 ⁻²	3.63×10 ⁻³	2.08×10 ⁻²	1.19×10 ⁻²
77	2.31×10 ⁻²	2.76×10 ⁻³	-	9.87×10 ⁻³	-	-
80	5.85×10 ⁻²	1.85×10 ⁻²	6.33×10 ⁻²	3.00×10 ⁻²	5.58×10 ⁻²	4.82×10 ⁻²
82	7.38×10 ⁻²	4.42×10 ⁻²	-	5.36×10 ⁻²	7.20×10 ⁻²	6.86×10 ⁻²
84	8.74×10 ⁻²	7.97×10 ⁻²	9.37×10 ⁻²	8.35×10 ⁻²	8.72×10 ⁻²	9.06×10 ⁻²
86	9.76×10 ⁻²	1.21×10 ⁻¹	-	1.14×10 ⁻¹	9.95×10 ⁻²	1.09×10 ⁻¹
88	0.1×10 ⁻¹	1.52×10 ⁻¹	1.08×10 ⁻¹	1.34×10 ⁻¹	1.07×10 ⁻¹	1.17×10 ⁻¹
90	1.05×10 ⁻¹	1.64×10 ⁻¹	1.06×10 ⁻¹	1.43×10 ⁻¹	1.08×10 ⁻¹	1.20×10 ⁻¹
92	1.02×10 ⁻¹	1.52×10 ⁻¹	1.08×10 ⁻¹	1.34×10 ⁻¹	1.07×10 ⁻¹	1.17×10 ⁻¹
94	9.76×10 ⁻²	1.21×10 ⁻¹	9.37×10 ⁻²	1.14×10 ⁻¹	9.95×10 ⁻²	1.09×10 ⁻¹
96	8.74×10 ⁻²	7.97×10 ⁻²	-	8.35×10 ⁻²	8.72×10 ⁻²	9.06×10 ⁻²
98	7.38×10 ⁻²	4.42×10 ⁻²	-	5.36×10 ⁻²	7.20×10 ⁻²	6.86×10 ⁻²
100	5.85×10 ⁻²	1.85×10 ⁻²	6.33×10 ⁻²	3.00×10 ⁻²	5.58×10 ⁻²	4.82×10 ⁻²
103	2.31×10 ⁻²	2.76×10 ⁻³	-	9.87×10 ⁻³	-	-
105	-	-	2.89×10 ⁻²	3.63×10 ⁻³	2.08×10 ⁻²	1.19×10 ⁻²
110	4.41×10 ⁻³	2.47×10 ⁻⁵	6.69×10 ⁻³	1.40×10 ⁻⁴	3.82×10 ⁻³	1.08×10 ⁻³
115	2.67×10 ⁻⁴	-	4.90×10 ⁻⁴	-	2.35×10 ⁻⁴	2.44×10 ⁻⁵
120	2.39×10 ⁻⁶	-	4.64×10 ⁻⁶	-	2.30×10 ⁻⁶	5.46×10 ⁻⁵

Table S6. Calculated singlet-triplet energy gaps between selected states as a function of θ .

	Energy gap [eV]		
θ [°]	¹ CT- ³ CT	¹ CT- ³ LE _A	¹ CT- ³ LE _D
60	0.10	0.30	0.20
65	0.074	0.21	0.15
70	0.053	0.14	0.11
77	0.028	0.082	0.070
80	0.019	0.036	0.033
82	0.013	0.023	0.020
84	0.0092	0.013	0.012
86	0.0065	0.0059	0.006
88	0.0048	0.0018	0.00017
90	0.0045	0.000074	0.0013
92	0.0048	0.0018	0.00017
94	0.0065	0.0059	0.0061
96	0.0092	0.013	0.012
98	0.013	0.023	0.020
100	0.019	0.036	0.033
103	0.028	0.082	0.070
110	0.053	0.14	0.11
115	0.074	0.21	0.15
120	0.10	0.30	0.20

Table S7. Calculated internal reorganization energies for selected spin-flip transitions in TMCz-BO and DMAC-TRZ as a function of θ .

	Internal reorganization energy [eV]				
θ [°]	TMCz-BO			DMAC-TRZ	
	$^1\text{CT}-^3\text{CT}$	$^1\text{CT}-^3\text{LE}_\text{A}$	$^1\text{CT}-^3\text{LE}_\text{D}$	$^1\text{CT}-^3\text{CT}$	$^1\text{CT}-^3\text{LE}_\text{A}$
60	0.0038	0.046	0.095	-	-
65	0.0025	0.079	0.080	0.15	0.23
70	0.0018	0.10	0.10	0.10	0.22
75	0.0011	0.12	0.12	0.062	0.22
80	0.00063	0.13	0.13	0.032	0.21
82	0.00047	0.13	0.13	0.023	0.21
84	0.00033	0.13	0.13	0.016	0.21
86	0.00021	0.14	0.14	0.011	0.21
88	0.00014	0.14	0.14	0.0076	0.21
90	0.0	0.14	0.14	0.0066	0.21
92	0.00014	0.14	0.14	0.0076	0.21
94	0.00021	0.14	0.14	0.011	0.21
96	0.00033	0.13	0.13	0.016	0.21
98	0.00047	0.13	0.13	0.023	0.21
100	0.00063	0.13	0.13	0.032	0.21
105	0.0011	0.12	0.12	0.062	0.22
110	0.0018	0.10	0.10	0.10	0.22
115	0.0025	0.079	0.080	0.15	0.23
120	0.0038	0.046	0.095	-	-

Table S8. Calculated SOC constants for various transitions and values.

	SOC [cm^{-1}]					
θ [$^\circ$]	$^1\text{CT} \rightleftharpoons ^3\text{CT}$	$^1\text{CT} \rightleftharpoons ^3\text{LE}_\text{A}$	$^1\text{CT} \rightleftharpoons ^3\text{LE}_\text{D}$	$^1\text{LE}_\text{A} \rightleftharpoons ^3\text{CT}$	$^1\text{LE}_\text{A} \rightleftharpoons ^3\text{LE}_\text{A}$	$^1\text{LE}_\text{A} \rightleftharpoons ^3\text{LE}_\text{D}$
60	0.11	0.18	0.10	0.18	0.019	0.040
65	0.10	0.16	0.15	0.18	0.014	0.030
70	0.090	0.13	0.16	0.17	0.0075	0.020
77	0.070	0.12	0.17	0.17	0.0025	0.0080
80	0.050	0.11	0.17	0.16	0.0	0.0060
82	0.040	0.11	0.17	0.16	0.0	0.0040
84	0.030	0.11	0.17	0.16	0.0	0.0030
86	0.020	0.11	0.17	0.16	0.0	0.0020
88	0.010	0.10	0.17	0.16	0.0	0.0
90	0.0	0.10	0.17	0.16	0.0	0.0
92	0.010	0.10	0.17	0.16	0.0	0.0
94	0.020	0.11	0.17	0.16	0.0	0.0020
96	0.030	0.11	0.17	0.16	0.0	0.0030
98	0.040	0.11	0.17	0.16	0.0	0.0040
100	0.050	0.11	0.17	0.16	0.0	0.0060
103	0.070	0.12	0.17	0.17	0.0025	0.0080
110	0.090	0.13	0.16	0.17	0.0075	0.020
115	0.10	0.16	0.15	0.18	0.014	0.030
120	0.11	0.18	0.10	0.18	0.019	0.040

Approach 1. V_w is constant equal to $V_{3CT \rightarrow 1CT_w}$; $V_w = 0.02 \text{ cm}^{-1}$ (selected examples)

Medium: DCE. $\Delta E_{3CT \rightarrow 1CT}(\theta)$ as calculated. $V = V_{3CT-1CT}$

θ°		$\Delta E_{3CT \rightarrow 1CT}$		λ_{in}	λ_{sum}			V	
deviation	p_{T1}	[eV]	$\Delta E_{3CT \rightarrow 1CT} * p_{T1}$	[eV]	[eV]	$k_{HSC} [s^{-1}]$	$k_{HSC} * p_{T1}$	[cm $^{-1}$]	$V * p_{T1}$
± 30	1.95×10^{-9}	0.096	1.9×10^{-10}	0.004	0.096	2.27×10^{-5}	4.41×10^{-4}	0.11	2.1×10^{-10}
± 25	2.41×10^{-6}	0.074	1.8×10^{-7}	0.003	0.074	4.95×10^{-5}	1.19	0.10	2.4×10^{-7}
± 20	2.87×10^{-4}	0.053	1.5×10^{-5}	0.002	0.053	1.09×10^{-6}	3.13×10^{-2}	0.09	2.6×10^{-5}
± 15	7.40×10^{-3}	0.033	2.5×10^{-4}	0.001	0.033	1.76×10^{-6}	1.30×10^{-4}	0.07	5.2×10^{-4}
± 10	6.1×10^{-2}	0.018	1.1×10^{-3}	0.001	0.018	2.26×10^{-6}	1.38×10^{-5}	0.05	3.1×10^{-3}
± 8	0.11	0.013	1.4×10^{-3}	0.000	0.013	2.04×10^{-6}	2.23×10^{-5}	0.04	4.4×10^{-3}
± 6	0.17	0.009	1.6×10^{-3}	0.000	0.009	1.58×10^{-6}	2.68×10^{-5}	0.03	5.1×10^{-3}
± 4	0.23	0.006	1.5×10^{-3}	0.000	0.006	9.30×10^{-5}	2.16×10^{-5}	0.02	4.6×10^{-3}
± 2	0.27	0.005	1.3×10^{-3}	0.000	0.005	2.87×10^{-5}	7.87×10^{-4}	0.01	2.7×10^{-3}
0	0.15	0.004	6.5×10^{-4}	0.000	0.004	0	0	0	0
SUM	1.000		0.0078				9.37×10^{-5}		0.020

Medium: Tol/Hex. Each $\Delta E_{3CT \rightarrow 1CT}(\theta)$ is divided by constant $b = 0.502$ to attain $\Delta E_{(3CT \rightarrow 1CT)_w} = 15.6 \text{ meV}$. $V = V_{3CT-1CT}$

θ°		$\Delta E_{3CT \rightarrow 1CT}$		λ_{in}	λ_{sum}			V	
deviation	p_{T1}	[eV]	$\Delta E_{3CT \rightarrow 1CT} * p_{T1}$	[eV]	[eV]	$k_{HSC} [s^{-1}]$	$k_{HSC} * p_{T1}$	[cm $^{-1}$]	$V * p_{T1}$
± 30	1.95×10^{-9}	0.191	3.7×10^{-10}	0.004	0.191	3.98×10^{-3}	7.74×10^{-6}	0.11	2.1×10^{-10}
± 25	2.41×10^{-6}	0.148	3.6×10^{-7}	0.003	0.148	2.00×10^{-4}	4.83×10^{-2}	0.10	2.4×10^{-7}
± 20	2.87×10^{-4}	0.105	3.0×10^{-5}	0.002	0.105	1.01×10^{-5}	0.3	0.09	2.6×10^{-5}
± 15	7.40×10^{-3}	0.067	4.9×10^{-4}	0.001	0.067	3.44×10^{-5}	2.54×10^{-3}	0.07	5.2×10^{-4}
± 10	6.1×10^{-2}	0.035	2.2×10^{-3}	0.001	0.035	8.05×10^{-5}	4.93×10^{-4}	0.05	3.1×10^{-3}
± 8	0.11	0.026	2.8×10^{-3}	0.000	0.026	8.72×10^{-5}	9.54×10^{-4}	0.04	4.4×10^{-3}
± 6	0.17	0.018	3.1×10^{-3}	0.000	0.018	7.82×10^{-5}	1.33×10^{-5}	0.03	5.1×10^{-3}
± 4	0.23	0.013	3.0×10^{-3}	0.000	0.013	5.13×10^{-5}	1.19×10^{-5}	0.02	4.6×10^{-3}
± 2	0.27	0.010	2.6×10^{-3}	0.000	0.010	1.69×10^{-5}	4.63×10^{-4}	0.01	2.7×10^{-3}
0	0.15	0.009	1.3×10^{-3}	0.000	0.009	0	0	0.00	0
SUM	1.000		0.0156				4.46×10^{-5}		0.0205

Medium: DMSO. Each $\Delta E_{3CT \rightarrow 1CT}(\theta)$ is divided by constant $b = 1.58$ to attain $\Delta E_{(3CT \rightarrow 1CT)_w} = 5.0 \text{ meV}$. $V = V_{3CT-1CT}$

θ°		$\Delta E_{3CT \rightarrow 1CT}$		λ_{in}	λ_{sum}			V	
deviation	p_{T1}	[eV]	$\Delta E_{3CT \rightarrow 1CT} * p_{T1}$	[eV]	[eV]	$k_{HSC} [s^{-1}]$	$k_{HSC} * p_{T1}$	[cm $^{-1}$]	$V * p_{T1}$
± 30	1.95×10^{-9}	0.061	1.2×10^{-10}	0.004	0.061	1.12×10^{-6}	2.18×10^{-3}	0.11	2.1×10^{-10}
± 25	2.41×10^{-6}	0.047	1.1×10^{-7}	0.003	0.047	1.79×10^{-6}	4.33	0.10	2.4×10^{-7}
± 20	2.87×10^{-4}	0.033	9.6×10^{-6}	0.002	0.033	2.92×10^{-6}	8.36×10^{-2}	0.09	2.6×10^{-5}
± 15	7.40×10^{-3}	0.021	1.6×10^{-4}	0.001	0.021	3.57×10^{-6}	2.64×10^{-4}	0.07	5.2×10^{-4}
± 10	6.1×10^{-2}	0.011	6.9×10^{-4}	0.001	0.011	3.66×10^{-6}	2.24×10^{-5}	0.05	3.1×10^{-3}
± 8	0.11	0.008	9.0×10^{-4}	0.000	0.008	3.08×10^{-6}	3.37×10^{-5}	0.04	4.4×10^{-3}
± 6	0.17	0.006	1.0×10^{-3}	0.000	0.006	2.26×10^{-6}	3.85×10^{-5}	0.03	5.1×10^{-3}
± 4	0.23	0.004	9.5×10^{-4}	0.000	0.004	1.28×10^{-6}	2.97×10^{-5}	0.02	4.6×10^{-3}
± 2	0.27	0.003	8.4×10^{-4}	0.000	0.003	3.87×10^{-5}	1.06×10^{-5}	0.01	2.7×10^{-3}
0	0.15	0.003	4.1×10^{-4}	0.000	0.003	0	0	0.00	0
SUM	1.000		0.0050				1.38×10^{-6}		0.0205

Approach 2. V_w is constant and higher than $V_{3CT \rightarrow 1CT}$; $V_w = 0.044 \text{ cm}^{-1}$ (selected examples)

Medium: DCE. $\Delta E_{3CT \rightarrow 1CT}(\theta)$ as calculated. To each $V_{3CT-1CT}(\theta)$ a constant value $c = 0.021$ is added to attain $V_w = 0.044 \text{ cm}^{-1}$

θ° deviation	p_{T1}	$\Delta E_{3CT \rightarrow 1CT}$ [eV]	$\Delta E_{3CT \rightarrow 1CT} * p_{T1}$	λ_{in} [eV]	λ_{sum} [eV]	k_{HSC} [s ⁻¹]	$k_{HSC} * p_{T1}$	V [cm ⁻¹]	$V * p_{T1}$
±30	1.95×10 ⁻⁹	0.096	1.9×10 ⁻¹⁰	0.004	0.096	3.22×10 ⁻⁵	6.26×10 ⁻⁴	0.13	2.5×10 ⁻¹⁰
±25	2.41×10 ⁻⁶	0.074	1.8×10 ⁻⁷	0.003	0.074	7.24×10 ⁻⁵	1.75	0.12	2.9×10 ⁻⁷
±20	2.87×10 ⁻⁴	0.053	1.5×10 ⁻⁵	0.002	0.053	1.66×10 ⁻⁶	4.76×10 ⁻²	0.11	3.2×10 ⁻⁵
±15	7.40×10 ⁻³	0.033	2.5×10 ⁻⁴	0.001	0.033	2.98×10 ⁻⁶	2.20×10 ⁻⁴	0.09	6.7×10 ⁻⁴
±10	6.1×10 ⁻²	0.018	1.1×10 ⁻³	0.001	0.018	4.56×10 ⁻⁶	2.79×10 ⁻⁵	0.07	4.3×10 ⁻³
±8	0.11	0.013	1.4×10 ⁻³	0.000	0.013	4.74×10 ⁻⁶	5.18×10 ⁻⁵	0.06	6.7×10 ⁻³
±6	0.17	0.009	1.6×10 ⁻³	0.000	0.009	4.56×10 ⁻⁶	7.76×10 ⁻⁵	0.05	8.7×10 ⁻³
±4	0.23	0.006	1.5×10 ⁻³	0.000	0.006	3.91×10 ⁻⁶	9.06×10 ⁻⁵	0.04	9.5×10 ⁻³
±2	0.27	0.005	1.3×10 ⁻³	0.000	0.005	2.76×10 ⁻⁶	7.56×10 ⁻⁵	0.03	8.5×10 ⁻³
0	0.15	0.004	6.5×10 ⁻⁴	0.000	0.004	1.34×10 ⁻⁶	1.94×10 ⁻⁵	0.02	5.8×10 ⁻³
SUM	1.000		0.0078				3.45×10⁻⁶		0.044

Medium: Tol/Hex. Each $\Delta E_{3CT \rightarrow 1CT}(\theta)$ divided by constant $b = 0.502$ to attain $\Delta E_{(3CT \rightarrow 1CT)w} = 15.6 \text{ meV}$. To each $V_{3CT-1CT}(\theta)$ a constant value $c = 0.021$ is added to attain $V_w = 0.044 \text{ cm}^{-1}$

θ° deviation	p_{T1}	$\Delta E_{3CT \rightarrow 1CT}$ [eV]	$\Delta E_{3CT \rightarrow 1CT} * p_{T1}$	λ_{in} [eV]	λ_{sum} [eV]	k_{HSC} [s ⁻¹]	$k_{HSC} * p_{T1}$	V [cm ⁻¹]	$V * p_{T1}$
±30	1.95×10 ⁻⁹	0.191	3.7×10 ⁻¹⁰	0.004	0.191	5.64×10 ⁻³	1.10×10 ⁻⁵	0.13	2.5×10 ⁻¹⁰
±25	2.41×10 ⁻⁶	0.148	3.6×10 ⁻⁷	0.003	0.148	2.93×10 ⁻⁴	7.07×10 ⁻²	0.12	2.9×10 ⁻⁷
±20	2.87×10 ⁻⁴	0.105	3.0×10 ⁻⁵	0.002	0.105	1.54×10 ⁻⁵	4.41×10 ⁻¹	0.11	3.2×10 ⁻⁵
±15	7.40×10 ⁻³	0.067	4.9×10 ⁻⁴	0.001	0.067	5.81×10 ⁻⁵	4.30×10 ⁻³	0.09	6.7×10 ⁻⁴
±10	6.1×10 ⁻²	0.035	2.2×10 ⁻³	0.001	0.035	1.62×10 ⁻⁶	9.94×10 ⁻⁴	0.07	4.3×10 ⁻³
±8	0.11	0.026	2.8×10 ⁻³	0.000	0.026	2.03×10 ⁻⁶	2.22×10 ⁻⁵	0.06	6.7×10 ⁻³
±6	0.17	0.018	3.1×10 ⁻³	0.000	0.018	2.26×10 ⁻⁶	3.85×10 ⁻⁵	0.05	8.7×10 ⁻³
±4	0.23	0.013	3.0×10 ⁻³	0.000	0.013	2.15×10 ⁻⁶	5.00×10 ⁻⁵	0.04	9.5×10 ⁻³
±2	0.27	0.010	2.6×10 ⁻³	0.000	0.010	1.62×10 ⁻⁶	4.45×10 ⁻⁵	0.03	8.5×10 ⁻³
0	0.15	0.009	1.3×10 ⁻³	0.000	0.009	7.97×10 ⁻⁵	1.16×10 ⁻⁵	0.02	5.8×10 ⁻³
SUM	1.000		0.0156				1.77×10⁻⁶		0.044

Medium: DMSO. Each $\Delta E_{3CT \rightarrow 1CT}(\theta)$ is divided by constant $b = 1.58$ to attain $\Delta E_{(3CT \rightarrow 1CT)w} = 5.0 \text{ meV}$. To each $V_{3CT-1CT}(\theta)$ a constant value $c = 0.021$ is added to attain $V_w = 0.044 \text{ cm}^{-1}$

θ° deviation	p_{T1}	$\Delta E_{3CT \rightarrow 1CT}$ [eV]	$\Delta E_{3CT \rightarrow 1CT} * p_{T1}$	λ_{in} [eV]	λ_{sum} [eV]	k_{HSC} [s ⁻¹]	$k_{HSC} * p_{T1}$	V [cm ⁻¹]	$V * p_{T1}$
±30	1.95×10 ⁻⁹	0.061	1.2×10 ⁻¹⁰	0.004	0.061	1.59×10 ⁻⁶	3.09×10 ⁻³	0.13	2.5×10 ⁻¹⁰
±25	2.41×10 ⁻⁶	0.047	1.1×10 ⁻⁷	0.003	0.047	2.63×10 ⁻⁶	6.33	0.12	2.9×10 ⁻⁷
±20	2.87×10 ⁻⁴	0.033	9.6×10 ⁻⁶	0.002	0.033	4.44×10 ⁻⁶	1.27×10 ⁻³	0.11	3.2×10 ⁻⁵
±15	7.40×10 ⁻³	0.021	1.6×10 ⁻⁴	0.001	0.021	6.03×10 ⁻⁶	4.46×10 ⁻⁴	0.09	6.7×10 ⁻⁴
±10	6.1×10 ⁻²	0.011	6.9×10 ⁻⁴	0.001	0.011	7.39×10 ⁻⁶	4.52×10 ⁻⁵	0.07	4.3×10 ⁻³
±8	0.11	0.008	9.0×10 ⁻⁴	0.000	0.008	7.17×10 ⁻⁶	7.84×10 ⁻⁵	0.06	6.7×10 ⁻³
±6	0.17	0.006	1.0×10 ⁻³	0.000	0.006	6.54×10 ⁻⁶	1.11×10 ⁻⁶	0.05	8.7×10 ⁻³
±4	0.23	0.004	9.5×10 ⁻⁴	0.000	0.004	5.39×10 ⁻⁶	1.25×10 ⁻⁶	0.04	9.5×10 ⁻³
±2	0.27	0.003	8.4×10 ⁻⁴	0.000	0.003	3.72×10 ⁻⁶	1.02×10 ⁻⁶	0.03	8.5×10 ⁻³
0	0.15	0.003	4.1×10 ⁻⁴	0.000	0.003	1.79×10 ⁻⁶	2.60×10 ⁻⁵	0.02	5.8×10 ⁻³
SUM	1.000		0.0050				4.92×10⁻⁶		0.044

Approach 3. V_w is dependent on the medium. variable. (selected examples)

Medium: DCE. $\Delta E_{3CT \rightarrow 1CT}(\theta)$ as calculated. To each $V_{3CT-1CT}(\theta)$ a constant value $c = 0.0213$ is added to attain $V_w = 0.045 \text{ cm}^{-1}$

θ° deviation	p_{T1}	$\Delta E_{3CT \rightarrow 1CT}$ [eV]	$\Delta E_{3CT \rightarrow 1CT} * p_{T1}$	λ_{in} [eV]	λ_{sum} [eV]	k_{HSC} [s ⁻¹]	$k_{HSC} * p_{T1}$	V [cm ⁻¹]	$V * p_{T1}$
±30	1.95×10^{-9}	0.096	1.9×10^{-10}	0.004	0.096	3.23×10^{-5}	6.29×10^{-4}	0.13	2.6×10^{-10}
±25	2.41×10^{-6}	0.074	1.8×10^{-7}	0.003	0.074	7.28×10^{-5}	1.76	0.12	2.9×10^{-7}
±20	2.87×10^{-4}	0.053	1.5×10^{-5}	0.002	0.053	1.67×10^{-6}	4.79×10^{-2}	0.11	3.2×10^{-5}
±15	7.40×10^{-3}	0.033	2.5×10^{-4}	0.001	0.033	3.00×10^{-6}	2.22×10^{-4}	0.09	6.8×10^{-4}
±10	6.1×10^{-2}	0.018	1.1×10^{-3}	0.001	0.018	4.60×10^{-6}	2.81×10^{-5}	0.07	4.4×10^{-3}
±8	0.11	0.013	1.4×10^{-3}	0.000	0.013	4.78×10^{-6}	5.23×10^{-5}	0.06	6.7×10^{-3}
±6	0.17	0.009	1.6×10^{-3}	0.000	0.009	4.61×10^{-6}	7.85×10^{-5}	0.05	8.7×10^{-3}
±4	0.23	0.006	1.5×10^{-3}	0.000	0.006	3.96×10^{-6}	9.19×10^{-5}	0.04	9.6×10^{-3}
±2	0.27	0.005	1.3×10^{-3}	0.000	0.005	2.81×10^{-6}	7.71×10^{-5}	0.03	8.6×10^{-3}
0	0.15	0.004	6.5×10^{-4}	0.000	0.004	1.37×10^{-6}	2.00×10^{-5}	0.02	5.8×10^{-3}
SUM	1.000		0.0078				3.50×10^{-6}		0.045

Medium: Tol/Hex. Each $\Delta E_{3CT \rightarrow 1CT}(\theta)$ divided by constant $b = 0.502$ to attain $\Delta E_{(3CT \rightarrow 1CT)w} = 15.6 \text{ meV}$. To each $V_{3CT-1CT}(\theta)$ a constant value $c = 0.027$ is added to attain $V_w = 0.051 \text{ cm}^{-1}$

θ° deviation	p_{T1}	$\Delta E_{3CT \rightarrow 1CT}$ [eV]	$\Delta E_{3CT \rightarrow 1CT} * p_{T1}$	λ_{in} [eV]	λ_{sum} [eV]	k_{HSC} [s ⁻¹]	$k_{HSC} * p_{T1}$	V [cm ⁻¹]	$V * p_{T1}$
±30	1.95×10^{-9}	0.191	3.7×10^{-10}	0.004	0.191	6.17×10^{-3}	1.20×10^{-5}	0.14	2.7×10^{-10}
±25	2.41×10^{-6}	0.148	3.6×10^{-7}	0.003	0.148	3.23×10^{-4}	7.79×10^{-2}	0.13	3.1×10^{-7}
±20	2.87×10^{-4}	0.105	3.0×10^{-5}	0.002	0.105	1.71×10^{-5}	4.90×10^{-1}	0.12	3.4×10^{-5}
±15	7.40×10^{-3}	0.067	4.9×10^{-4}	0.001	0.067	6.60×10^{-5}	4.88×10^{-3}	0.10	7.2×10^{-4}
±10	6.1×10^{-2}	0.035	2.2×10^{-3}	0.001	0.035	1.91×10^{-6}	1.17×10^{-5}	0.08	4.7×10^{-3}
±8	0.11	0.026	2.8×10^{-3}	0.000	0.026	2.45×10^{-6}	2.68×10^{-5}	0.07	7.3×10^{-3}
±6	0.17	0.018	3.1×10^{-3}	0.000	0.018	2.82×10^{-6}	4.81×10^{-5}	0.06	9.7×10^{-3}
±4	0.23	0.013	3.0×10^{-3}	0.000	0.013	2.83×10^{-6}	6.57×10^{-5}	0.05	1.1×10^{-2}
±2	0.27	0.010	2.6×10^{-3}	0.000	0.010	2.31×10^{-6}	6.33×10^{-5}	0.04	1.0×10^{-2}
0	0.15	0.009	1.3×10^{-3}	0.000	0.009	1.32×10^{-6}	1.92×10^{-5}	0.03	7.4×10^{-3}
SUM	1.000		0.0156				2.35×10^{-6}		0.051

Medium: DMSO. Each $\Delta E_{3CT \rightarrow 1CT}(\theta)$ is divided by constant $b = 1.58$ to attain $\Delta E_{(3CT \rightarrow 1CT)w} = 5.0 \text{ meV}$. To each $V_{3CT-1CT}(\theta)$ a constant value $c = 0.0154$ is added to attain $V_w = 0.038 \text{ cm}^{-1}$

θ° deviation	p_{T1}	$\Delta E_{3CT \rightarrow 1CT}$ [eV]	$\Delta E_{3CT \rightarrow 1CT} * p_{T1}$	λ_{in} [eV]	λ_{sum} [eV]	k_{HSC} [s ⁻¹]	$k_{HSC} * p_{T1}$	V [cm ⁻¹]	$V * p_{T1}$
±30	1.95×10^{-9}	0.061	1.2×10^{-10}	0.004	0.061	1.46×10^{-6}	2.83×10^{-3}	0.13	2.4×10^{-10}
±25	2.41×10^{-6}	0.047	1.1×10^{-7}	0.003	0.047	2.39×10^{-6}	5.76	0.12	2.8×10^{-7}
±20	2.87×10^{-4}	0.033	9.6×10^{-6}	0.002	0.033	4.00×10^{-6}	1.15×10^{-3}	0.11	3.0×10^{-5}
±15	7.40×10^{-3}	0.021	1.6×10^{-4}	0.001	0.021	5.31×10^{-6}	3.93×10^{-4}	0.09	6.3×10^{-4}
±10	6.1×10^{-2}	0.011	6.9×10^{-4}	0.001	0.011	6.27×10^{-6}	3.84×10^{-5}	0.07	4.0×10^{-3}
±8	0.11	0.008	9.0×10^{-4}	0.000	0.008	5.91×10^{-6}	6.47×10^{-5}	0.06	6.1×10^{-3}
±6	0.17	0.006	1.0×10^{-3}	0.000	0.006	5.18×10^{-6}	8.82×10^{-5}	0.05	7.7×10^{-3}
±4	0.23	0.004	9.5×10^{-4}	0.000	0.004	4.02×10^{-6}	9.32×10^{-5}	0.04	8.2×10^{-3}
±2	0.27	0.003	8.4×10^{-4}	0.000	0.003	2.50×10^{-6}	6.84×10^{-5}	0.03	7.0×10^{-3}
0	0.15	0.003	4.1×10^{-4}	0.000	0.003	9.63×10^{-5}	1.40×10^{-5}	0.02	4.2×10^{-3}
SUM	1.000		0.0050				3.71×10^{-6}		0.038

Table S9. Linear regression parameters for the fitted dependencies Figure 6 main text.

Parameter	Plot Exp.	Plot $V = V_{3CT \rightarrow 1CT}$	Plot $V = 0.44 \text{ cm}^{-1}$	Plot $V \text{ variable}$
Slope	-1.14 ± 0.09	-2.58 ± 0.27	-2.39 ± 0.25	-1.09 ± 0.09
Intercept	18.28 ± 0.26	21.14 ± 0.81	21.92 ± 0.75	18.15 ± 0.28
R^2	0.98	0.97	0.97	0.98

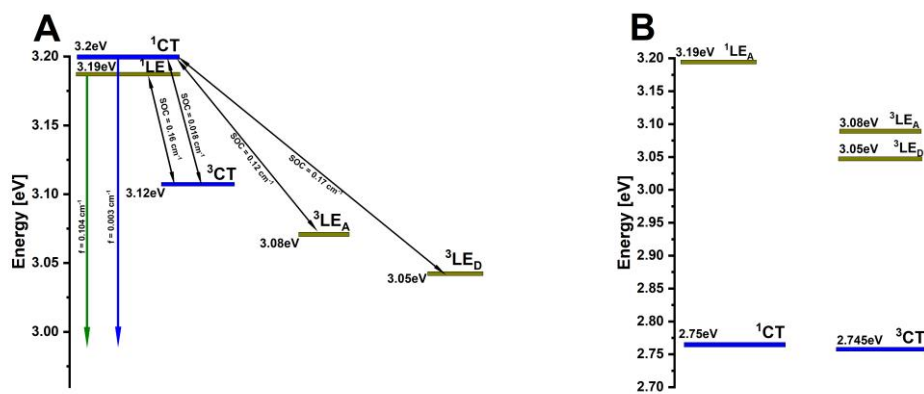


Figure S12. Energy diagram for TMCz-BO in (A) Benzene in 77K, (B) in DMSO in RT .

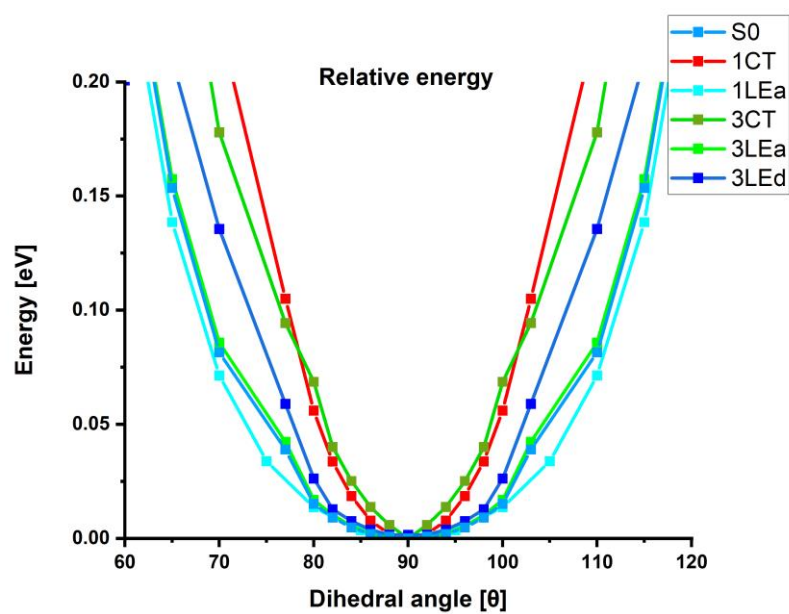


Figure S13. The dependence of relative energy of electronic state on dihedral angle θ

REFERENCES

- [S1] Y. Tao, K. Yuan, T. Chen, P. Xu, H. Li, R. Chen, C. Zheng, L. Zhang, W. Huang, *Adv. Mater.*, 2014, 26, 7931–7958.
- [S2] I. E. Serdiuk, M. Monka, K. Kozakiewicz, B. Liberek, P. Bojarski, S. O. Park, *J. Phys. Chem. B.*, 2021, 125, 2696–2706.
- [S3] P. K. Samanta, D. Kim, V. Coropceanu, J. L. Brédas, *J. Am. Chem. Soc.*, 2017, 139, 4042–4051.